Programa de Doctorado en Biotecnología Sanitaria

Desarrollo de nuevos materiales poliméricos nanocompuestos con capacidad antimicrobiana

Rocío Díaz Puertas

Director de la tesis

Dr. Ricardo Mallavia Marín

Codirector de la tesis

Dr. Juan Alberto Falcó Graciá

Universidad Miguel Hernández de Elche

- 2025 -

La presente Tesis Doctoral, titulada "Desarrollo de nuevos materiales poliméricos nanocompuestos con capacidad antimicrobiana", se presenta bajo la modalidad de **tesis por compendio** de las siguientes **publicaciones**:

- **Díaz-Puertas R,** Álvarez-Martínez FJ, Falco A, Barrajón-Catalán E, Mallavia R. Phytochemical-Based Nanomaterials against Antibiotic-Resistant Bacteria: An Updated Review. Polymers. 2023; 15(6):1392. https://doi.org/10.3390/polym15061392. **IF (2023): 4.7 (Q1).**
- **Díaz-Puertas R,** Adamek M, Mallavia R, Falco A. Fish Skin Mucus Extracts: An Underexplored Source of Antimicrobial Agents. Marine Drugs. 2023; 21(6):350. https://doi.org/10.3390/md21060350. **IF (2023): 4.9 (Q1).**
- **Díaz-Puertas R,** Rodríguez-Cañas E, Bello-Perez M, Fernández-Oliver M, Mallavia R, Falco A. Viricidal Activity of Thermoplastic Polyurethane Materials with Silver Nanoparticles. Nanomaterials. 2023; 13(9):1467. https://doi.org/10.3390/nano13091467. **IF (2023): 4.4 (Q2).**
- **Díaz-Puertas R**, Rodríguez-Cañas E, Lozoya-Agulló MJ, Badía-Hernández PV, Álvarez-Martínez FJ, Falcó A, Mallavia R. Bovine serum albumin and lysozyme nanofibers as versatile platforms for preserving loaded bioactive compounds. Int J Biol Macromol. 2024; 26;280:136019. https://doi.org/10.1016/j.ijbiomac.2024.136019. **IF (2023): 7.7 (Q1).**

En el marco de esta Tesis Doctoral, titulada "Desarrollo de nuevos materiales poliméricos nanocompuestos con capacidad antimicrobiana", se realizaron otros trabajos que forman parte de este documento pero que aún no han sido publicados y, por tanto, no constan como indicio de calidad:

- **Díaz-Puertas R**, Álvarez-Martínez FJ, Rodríguez-Cañas E, Borrás F, Valente AJM, Paixao JM, Falcó A, Mallavia R. An innovative approach based on the green synthesis of silver nanoparticles using pomegranate extract for antibacterial purposes. (Enviado a Bioinorg. Chem. Appl., revisado el 29 de noviembre de 2024).

El *Dr. Ricardo Mallavia Marín,* director, y el *Dr. Juan Alberto Falcó Graciá*, codirector de la tesis doctoral titulada "Desarrollo de nuevos materiales poliméricos nanocompuestos con capacidad antimicrobiana"

INFORMA/N:

Que Dña. *Rocío Díaz Puertas* ha realizado bajo nuestra supervisión el trabajo titulado "Desarrollo de nuevos materiales poliméricos nanocompuestos" conforme a los términos y condiciones definidos en su Plan de Investigación y de acuerdo al Código de Buenas Prácticas de la Universidad Miguel Hernández de Elche, cumpliendo los objetivos previstos de forma satisfactoria para su defensa pública como tesis doctoral.

Lo que firmo/firmamos para los efectos oportunos, en ……..…….…… a ……..
de …….. de 202….

Director de la tesis	**Codirector de la tesis**
Ricardo Mallavia Marín	**Juan Alberto Falcó Graciá**

El Dr. *Gregorio Fernández Ballester*, Coordinador del Programa de Doctorado en **Biotecnología Sanitaria**

INFORMA:

Que Dña. *Rocío Díaz Puertas* ha realizado bajo la supervisión de nuestro Programa de Doctorado el trabajo titulado "Desarrollo de nuevos materiales poliméricos nanocompuestos con capacidad antimicrobiana" conforme a los términos y condiciones definidos en su Plan de Investigación y de acuerdo al Código de Buenas Prácticas de la Universidad Miguel Hernández de Elche, cumpliendo los objetivos previstos de forma satisfactoria para su defensa pública como tesis doctoral.

Lo que firmo para los efectos oportunos, en …… a ……. de …….. de 202….

Prof. Dr. *Gregorio Fernández Ballester*

Coordinador del Programa de Doctorado en Biotecnología Sanitaria

FINANCIACIÓN

La presente Tesis Doctoral ha sido financiada por los siguientes proyectos:

- **RTI2018-101969-J-I00**, financiado por el Fondo Europeo de Desarrollo Regional (FEDER, "Una forma de hacer Europa") y el Ministerio de Ciencia, Innovación y Universidades (MICIU) – Agencia Estatal de Investigación (AEI) (MCIN/AEI/ 10.13039/501100011033).
- **MetDisFish**, del Ministerio de Agricultura, Pesca y Alimentación (MAPA) y Fondo europeo Marítimo, de Pesca y de Acuicultura (FEMPA).
- **PDI2021-123253OB-C21,** de la AEI y del MICIU.
- **GVA-IDIFEDER_2018/020,** de la Generalitat Valenciana y cofinanciado con fondos FEDER ("Una forma de hacer Europa").

Además, se obtuvo la ayuda de movilidad para la obtención de la Mención de Doctorado Internacional de la Universidad Miguel Hernández.

AGRADECIMIENTOS

El desarrollo de esta Tesis no habría sido posible sin el apoyo de muchas personas. En primer lugar, quiero agradecer a **Javi**, mi compañero de vida y de ciencia, por ser mi apoyo más grande dentro y fuera de los laboratorios y por ayudarme en cada etapa del doctorado.

A mis **padres**, Dulce y Enrique, por estar siempre ahí, celebrar todos mis logros, darme ánimos en todas mis etapas académicas y profesionales y ayudar a levantarme cuando más lo necesitaba. A mis **gatos**, Diluc y Jojo, por apoyarme inconscientemente tumbándose en mi regazo mientras escribía esta Tesis.

Por supuesto, a mis dos tutores de Tesis, por darme la oportunidad de realizar esta investigación con ellos y enseñarme todo lo relativo a los nanobiomateiales. A **Ricardo**, por permitirme realizar esta Tesis en su grupo, por abrirme paso al mundo de los nanomateriales y ser un gran mentor en química. A **Alberto**, por su guía y sus grandes consejos, por aportar ese bio a los nanobiomateriales y por enseñarme la importancia de nunca parar de formarse.

En general, a todos los componentes del grupo de Diseño y Validación de Nanobiomateriales, en especial a **Pedro**, por ser mi compañero de escritorio y dar esa chispa de alegría al laboratorio. También a todos **TFGs** y **TFMs** que han pasado por el laboratorio durante la realización de mi Tesis, no solo por su granito de arena en cuanto a investigación, sino por todas las experiencias vividas juntos: David, María Jesús, Miguel, Marta, Joan, Paula. A **Kike**, por hacer visible lo que a nuestro ojo es invisible y por estar tan involucrado con nuestro grupo de investigación. A **Salomé**, por ser mi compañera de doctorado desde el día uno que entré al IDiBE y por nuestra amistad, que permanece a pesar de la distancia.

A todas las personas que me han abierto los brazos recibiéndome en sus centros de investigación durante mis estancias. A **Artur** y **Dina** por recibirme en su grupo de investigación, formar parte no solo de esta Tesis sino de futuros trabajos y colaboraciones, y por enseñarme síntesis química. A **Sara** y **Mariette**, por su amabilidad y hospitalidad y por los futuros trabajos en conjunto. A **Juan Carlos** por darme la bienvenida en el hospital, permitiéndome finalizar experimentos importantes para esta Tesis.

A todos los **investigadores** que han formado parte de los trabajos que conforman esta Tesis: Melissa Belló, Enrique Barrajón, Mikolaj Adamek, Fernando Borrás, José Antonio Paixao. A la coordinación del **Programa de Doctorado**, por su ayuda en todas las gestiones relativas a esta Tesis Doctoral. A todo el personal del **IDiBE** que hace que el trabajo aquí sea más fácil: investigadores, personal técnico, de secretaría, de limpieza.

Y, por último, a mis **amigas**, por ser mis confidentes y las personas con las que puedo ser yo misma fuera del laboratorio.

Muchas gracias a todos.

«Lo importante en la ciencia no es tanto obtener nuevos datos, sino descubrir nuevas formas de pensar sobre ellos»

- William Lawrence Bragg

INDEX

ABSTRACT 1

RESUMEN 3

ABBREVIATIONS AND ACRONYMS 5

1. INTRODUCTION 11

1.1. Nanomaterials 11

1.2. Nanofibers 13

1.3. Materials for nanofiber synthesis: polymers 14

1.4. Nanofiber synthesis techniques: electrospinning 16

1.5. Nanofiber applications: delivery of antimicrobial agents 17

1.6. Antimicrobial agents incorporated into nanofibers 19

1.7. Metal nanoparticles: fundamentals, synthesis and antimicrobial activity 20

2. INTEGRATION AND CONTRIBUTION OF RESEARCH PAPERS TO THESIS THEMATIC FIELD 25

3. OBJECTIVES 29

4. MATERIALS AND METHODS 33

4.1. Materials 33

4.1.1. TPU materials with AgNPs 33

4.1.2. Preparation of solutions 33

4.1.3. Extract characterization 33

4.1.4. AgNPs synthesis 33

4.1.5. Antimicrobial assays 33

4.1.6. Cellular assays 34

4.1.7. Viricidal assays 34

4.1.8. Manufacturers 33

4.2. Methods 34

4.2.1. Bibliographic search 34

4.2.2. Preparation of samples 34

4.2.3. Synthesis techniques 35

4.2.4. Characterization techniques 36

4.2.5. Biological properties 41

5. RESULTS 47

CHAPTER 1: FISH SKIN MUCUS EXTRACTS: AN UNDEREXPLORED SOURCE OF ANTIMICROBIAL AGENTS 47

CHAPTER 2: BOVINE SERUM ALBUMIN AND LYSOZYME NANOFIBERS AS VERSATILE PLATFORMS FOR PRESERVING LOADED BIOACTIVE COMPOUNDS.....81

CHAPTER 3: VIRICIDAL ACTIVITY OF THERMOPLASTIC POLYURETHANE MATERIALS WITH SILVER NANOPARTICLES.....101

CHAPTER 4: PHYTOCHEMICAL-BASED NANOMATERIALS AGAINST ANTIBIOTIC-RESISTANT BACTERIA: AN UPDATED REVIEW.....119

CHAPTER 5: OPTIMIZING THE GREEN SYNTHESIS OF SILVER NANOPARTICLES WITH POMEGRANATE EXTRACT FOR ANTIBACTERIAL PURPOSES: AN INNOVATIVE APPROACH.....139

6. DISCUSSION.....165

7. CONCLUSIONS.....177

8. LIMITATIONS AND FUTURE RESEARCH.....183

9. BIBLIOGRAPHY.....187

ABSTRACT

This Thesis, entitled "*Development of new polymeric nanocomposite materials with antimicrobial activity*" represents a comprehensive effort to develop novel antimicrobial nanomaterials, focusing on the incorporation of bioactive compounds into polymeric matrices and eco-friendly synthesis techniques. The research spans several interconnected studies that explore both natural and synthetic antimicrobial agents, advancing our understanding of their applications in materials science and biomedicine.

This work begins by investigating fish skin mucus as an untapped resource for antimicrobial agents, highlighting the presence of antimicrobial peptides (AMPs) and other bioactive compounds within the mucus that exhibit potent activity against a range of pathogens. The research assesses various extraction methods to isolate these compounds and discusses their activity. The initial findings underscore the potential of marine-derived compounds for their use in antimicrobial applications, contributing valuable insights to the field.

Following this, the synthesis of protein-based nanofibers using bovine serum albumin (BSA) and lysozyme (LYZ) is explored as a strategy for encapsulating bioactive agents. The electrospun nanofibers, featuring proteins with different molecular weights, serve as biocompatible carriers for bioactive agents, including an AMP and an antibody. The study confirms that these proteins maintain their structural integrity post-electrospinning and that the bioactive agents embedded within them retain partial to full activity, indicating the promise of protein nanofibers for bioactive drug administration and protection.

In a move toward real-world applications, the third section of this Thesis assesses thermoplastic polyurethane (TPU) materials embedded with silver nanoparticles (AgNPs) for antiviral efficacy. Collaborating with an industry partner, the study evaluates the viricidal properties of AgNP-TPU materials against pathogens such as SARS-CoV-2 and SVCV, showing a substantial reduction in viral infectivity without cytotoxic effects in cell culture models. These results position AgNP-TPU composites as promising candidates for antiviral surface coatings in various settings.

The Thesis then transitions to greener synthesis approaches, using phytochemical-based methods to produce antibacterial nanomaterials. A review of plant-derived compounds and their applications reveals how natural extracts, rich in antioxidants and other bioactive compounds, can serve as both antimicrobial agents and reducing agents for NP synthesis. This study encourages sustainable production practices that reduce reliance on synthetic chemicals, aligning with global goals for environmentally responsible material development.

Finally, the research culminates in the synthesis of AgNPs using pomegranate peel extract, a byproduct of Mediterranean agriculture. Employing the Box-Behnken response surface model, the synthesis is optimized for particle stability and antibacterial efficacy. When incorporated into the protein-based nanofibers developed earlier in the Thesis, these AgNPs demonstrate effective, antibacterial properties, paving the way for their application in novel and greener antimicrobial materials.

These studies collectively push the boundaries of antimicrobial nanomaterials, offering practical strategies to tackle urgent global health issues like antibiotic resistance and viral infections. In turn, by focusing on cutting-edge nanomaterials and sustainable approaches, this research provides important insights for developing safer, more effective, and eco-friendly solutions.

RESUMEN

Esta Tesis, titulada "*Desarrollo de nuevos materiales poliméricos nanocompuestos con capacidad antimicrobiana*" representa un esfuerzo exhaustivo para desarrollar nuevos nanomateriales antimicrobianos, centrándose en la incorporación de compuestos bioactivos en matrices poliméricas y en técnicas de síntesis ecológicas. La investigación abarca varios estudios interrelacionados que exploran tanto agentes antimicrobianos naturales como sintéticos, avanzando en la comprensión de sus aplicaciones en ciencia de materiales y biomedicina.

Este trabajo comienza investigando el moco de la piel de peces como un recurso inexplorado para agentes antimicrobianos, destacando la presencia de péptidos antimicrobianos (AMPs) y otros compuestos bioactivos dentro del moco que muestran una actividad potente contra una variedad de patógenos. La investigación evalúa varios métodos de extracción para aislar estos compuestos y analiza su actividad. Los hallazgos iniciales subrayan el potencial de los compuestos de origen marino para su utilización en aplicaciones antimicrobianas, aportando conocimientos valiosos a este campo.

A continuación, se explora la síntesis de nanofibras a base de proteínas utilizando albúmina de suero bovina (BSA) y lisozima (LYZ) como estrategia para encapsular agentes bioactivos. Las nanofibras electrohiladas sirven como portadoras biocompatibles de agentes bioactivos, incluidos un AMP y un anticuerpo. El estudio confirma que estas proteínas mantienen su integridad estructural después del proceso de electrohilado y que los agentes bioactivos cargados dentro de ellas retienen su actividad parcial o total, indicando el potencial de las nanofibras de proteínas para la administración y protección de fármacos bioactivos.

En una orientación hacia aplicaciones en el mundo real, la tercera sección de esta tesis evalúa la eficacia antiviral de materiales de poliuretano termoplástico (TPU) con nanopartículas de plata (AgNPs). En colaboración con un socio industrial, el estudio evalúa las propiedades viricidas de los materiales AgNP-TPU contra patógenos como el SARS-CoV-2 y el SVCV, mostrando una reducción sustancial en la infectividad viral sin efectos citotóxicos en modelos de cultivo celular. Estos resultados posicionan a los compuestos AgNP-TPU como candidatos potenciales para recubrimientos antivirales en diversas aplicaciones.

La Tesis transita más adelante hacia enfoques de síntesis más ecológicos, utilizando métodos basados en fitoquímicos para producir nanomateriales antibacterianos. Una revisión de los compuestos derivados de plantas y sus aplicaciones revela cómo los extractos naturales, ricos en antioxidantes y otros compuestos bioactivos, pueden servir tanto como agentes antimicrobianos como agentes reductores para la síntesis de nanopartículas. Este estudio fomenta prácticas de producción sostenible que reducen la dependencia de productos químicos sintéticos, alineándose con los objetivos globales para el desarrollo responsable de materiales.

Finalmente, la investigación culmina en la síntesis de AgNPs utilizando extracto de piel de granada, un subproducto de la agricultura mediterránea. Empleando el modelo de superficie de respuesta de Box-Behnken, se optimiza la síntesis para lograr estabilidad de partículas y eficacia antibacteriana. Cuando se incorporan en las nanofibras a base de proteínas desarrolladas anteriormente en la Tesis, estas AgNPs demuestran propiedades antibacterianas efectivas, abriendo el camino para su aplicación en materiales antimicrobianos novedosos y más ecológicos.

Estos estudios amplían colectivamente los límites de los nanomateriales antimicrobianos, ofreciendo estrategias prácticas para abordar problemas urgentes de salud global, como la resistencia a los antibióticos y las infecciones virales. A su vez, al centrarse en nanomateriales innovadores y enfoques sostenibles, esta investigación aporta conocimientos importantes para desarrollar soluciones más seguras, eficaces y respetuosas con el medio ambiente.

ABBREVIATIONS AND ACRONYMS

ABTS	2,2'-azinobis(3-ethylbenzothiazoline)-6-sulfonic acid
AgNP	Silver nanoparticle
AMP	Antimicrobial peptide
AMR	Antimicrobial resistance
ARB	Antibiotic-resistant bacteria
BBD	Box-Behnken design
BSA	Bovine serum albumin
BSL-3	Biosafety level 3
CV	Coefficient of variation
CuNP	Copper nanoparticle
DLS	Dynamic light scattering
DMEM	Dulbecco's modified eagle medium
DMSO	Dimethyl sulfoxide
DNS	3,5-dinitrosalicylic acid
EHT	Electron high tension
EPC	Epithelioma papulosum cyprinid
FBS	Fetal bovine serum
FESEM	Field emission scanning electron microscopy
Ffu	Focus-forming units
FTIR	Fourier transform infrared
HDD	Hydrodynamic diameter
HRP	Horseradish peroxidase
HRP-IgG	HRP-conjugated goat anti-mouse IgG
HPLC	High-performance liquid chromatography
ICP-MS	Inductively coupled plasma mass spectrometry
INT	p-iodonitrotetrazolium chloride
LSPR	Localized surface plasmon resonance
LYZ	Lysozyme

MBC	Minimum bactericidal concentration
MH	Mueller-Hinton
MIC	Minimum inhibitory concentration
MNP	Metal nanoparticle
MTT	3-(4,5-dimethylthiazol-2-yl)-2,5-diphenyltetrazolium bromide
NFs	Nanofibers
NPs	Nanoparticles
PA	Polyamides
PAN	Polyacrylonitrile
PBS	Phosphate-buffered saline
PCL	Polycaprolactone
PDI	Polydispersity index
PEG	Poly(ethylene glycol)
PEO	Polyethylene oxide
Pfu	Plaque-forming units
PGE	*Punica granatum* (pomegranate) extract
PI	Polyimide
PIS	Piscidin-1
PLA	Poly(lactic acid)
PMMA	Poly(methyl methacrylate)
PS	Polystyrene
PU	Polyurethane
PVA	Poly(vinyl alcohol)
ROS	Reactive oxygen species
RPMI	Roswell park memorial institute
SARS-CoV-2	Severe acute respiratory syndrome coronavirus-2
SD	Standard deviation
SDG	Sustainable development goal
SVCV	Spring viremia of carp virus

TBS	Tris-buffered saline
TMB	Tetramethylbenzidine
TPC	Total phenolic content
TPU	Thermoplastic polyurethane
TTBS	Tween-Tris-buffered saline
WHO	World health organization
XRD	X-ray diffraction
ZnONP	Zinc oxide nanoparticle
ZP	Zeta potential

INTRODUCTION

1. INTRODUCTION

1.1. Nanomaterials

Nanomaterials are defined as those materials whose structure exists on the nanoscale in at least one dimension. Due to their incredibly small size, nanomaterials exhibit unique and often enhanced properties compared to their bulk counterparts, including increased surface area, reactivity, and distinctive mechanical, optical and magnetic characteristics [1]. These attributes arise largely from quantum effects and the high surface-to-volume ratio associated with nanoscale dimension [2].

The high surface-to-volume ratio of nanomaterials indicates that as the size of materials decreases, its surface area per unit volume increases substantially. This amplified surface-to-volume ratio profoundly affects the properties of the material, notably enhancing its chemical reactivity [3]. In terms of mechanical properties, certain nanomaterials, particularly nanoparticles (NPs), display unique mechanical behaviors compared to their macroscopic counterparts due to pronounced relative surface and quantum effects, the latter becoming significant at sizes within the lower nanometer range. For example, many nanomaterials exhibit significantly enhanced hardness, ductility, and plasticity compared to their bulk forms [4]. The optical properties of nanomaterials, such as light absorption, transmission, reflection, and emission, are also variable and can differ significantly from those of the same material in its macroscopic form [5]. The magnetic properties of nanomaterials, such as metal nanoparticles (MNPs), arise from uneven electronic distribution and are of great interest across a wide range of applications, including heterogeneous and homogeneous catalysis, biomedicine, magnetic fluids, data storage, magnetic resonance imaging, and environmental remediation [6].

Even though American physicist and Nobel laureate Richard Feynman introduced the concept of nanotechnology in 1959 during a lecture at the California Institute of Technology (Caltech) titled "There's Plenty of Room at the Bottom", the use of nanotechnology and nanomaterials predates his ideas by centuries [7]. Ancient civilizations unknowingly exploited nanoscale properties in various materials, as seen in the Roman Lycurgus Cup from the 4th century AD (Figure 1A), which changes color due to embedded NPs of gold and silver [8]. Similarly, artisans in medieval Europe used nanoscale particles in stained glass windows to achieve vibrant and durable colors (Figure 1B). In Asia, Damascus steel swords were crafted with carbon nanotube-like structures that contributed to their renowned strength and sharpness (Figure 1C) [9]. While the talk by Feynman is credited with sparking modern interest in nanotechnology, these early examples highlight humanity's longstanding, if unintentional, interaction with nanomaterials. Since the conceptual introduction by Feynman, however, nanotechnology has evolved into a field of rigorous scientific exploration, leading to precise manipulation of materials at the atomic level and expanding applications across diverse practical sectors, from electronics to medicine.

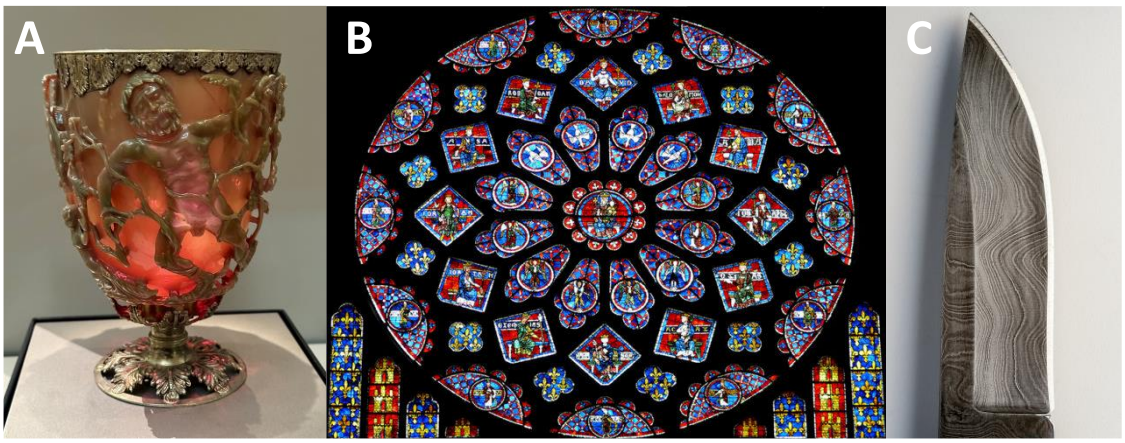

Figure 1. (A) Front of 4th century CE Roman Lycurgus Cup, British Museum (Source: Wikimedia Commons) (B) Colored stained glass on the rose window of the north façade of Notre Dame Cathedral, located in Paris (Source: Ruggero Vanni/CORBIS), (C) Damascus knife blade (Source: Wikimedia Commons).

Nanomaterials are classified according to multiple criteria, such as their dimensions, source materials, and field of application (Figure 2). In terms of dimensions, nanomaterials can be classified as zero-dimensional, one-dimensional, two-dimensional, or three-dimensional [10]. Zero-dimensional nanomaterials, or 0D, are those whose dimensions are entirely within the nanoscale range. Examples include NPs, quantum dots, carbon dots, and fullerenes. One-dimensional nanomaterials, or 1D, possess one dimension at the macro or micro scale, while the other two dimensions are in the nanoscale range. This category includes nanofibers (NFs), carbon nanotubes, and nanorods. Two-dimensional nanomaterials, or 2D, have only one dimension at the nanoscale. Common examples include graphene and MXenes, which are a family of transition metal carbides and nitrides in 2D discovered in 2011 [11]. Lastly, three-dimensional nanomaterials, or 3D, can be constructed based on the arrangement and organization of a collection of 0D, 1D, or 2D nanostructures. Although the dimensions of 3D nanomaterials exceed the nanoscale, their properties differ from those of their bulk counterparts due to the quantum confinement effect arising from the constituent nanostructures [12].

Nanomaterials can also be classified based on the materials from which they are composed. According to their origin, they are distinguished between natural and synthetic nanomaterials. Natural nanomaterials include those materials that occur in nature and can be extracted from natural resources, such as proteins or polysaccharides. In contrast, synthetic nanomaterials are intentionally produced through mechanical processes and precise manufacturing techniques. Within the category of synthetic nanomaterials, there are those based on carbon, metals, and synthetic polymers [13].

Nanomaterials have applications across diverse fields, including nanomedicine, where they are utilized in the development of nanodrugs, medical devices, and tissue engineering [14]. In materials science, they are employed in formulating paints and coatings [15]. Additionally, in the electronics sector, nanomaterials serve as contrast agents and play an important role in improving battery performance [16]. In agriculture, they are applied in the production of nanofertilizers and nanopesticides [17], while in the food industry, they are used in enhanced packaging functionalized by incorporating antimicrobial nanomaterials in order to improve food preservation.[18].

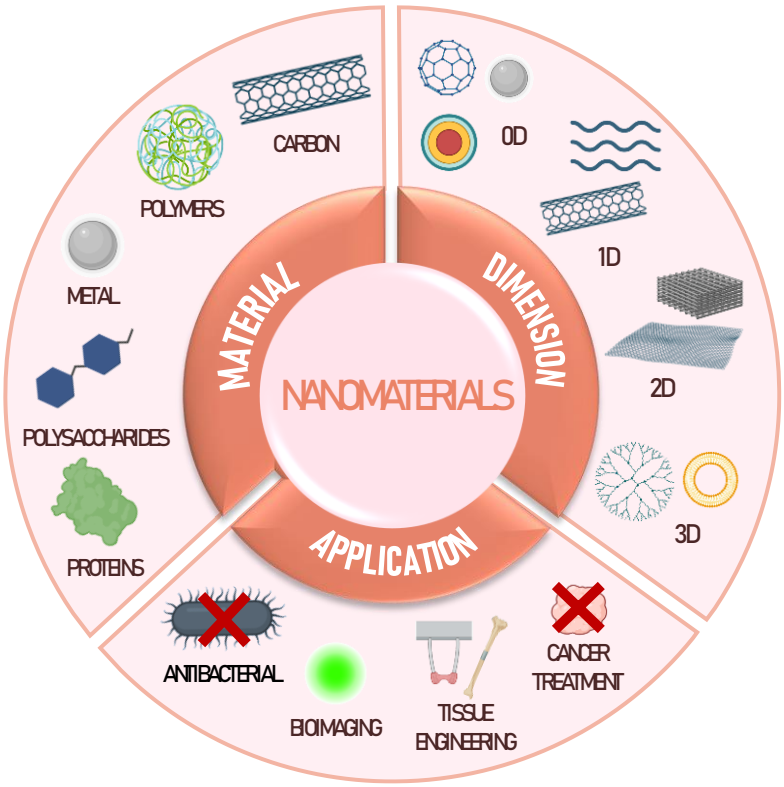

Figure 2. Graphical representation of the classification of nanomaterials according to different criteria, including dimensions, materials and applications.

1.2. Nanofibers

As previously mentioned, NFs are one-dimensional nanomaterials. These specific materials have garnered significant attention due to their remarkable properties. In comparison to conventional macroscopic fibrous materials, NFs are characterized by their lightweight and reduced diameter, which result in a high surface-to-volume ratio [19]. This feature is associated with notable tensile strength of the fibrous matrix, attributed to the increased length of the NFs, which contributes to the mechanical integrity of the structure. Furthermore, the high specific surface area offers substantial advantages in applications such as controlled drug release, catalysis, sensors, and mass transfer processes, as it facilitates enhanced efficiency in surface interactions [20].

The ability to modify characteristics such as the porosity of nanofibrous structures allows for the tailoring of NFs to specific applications. For instance, high porosity is particularly beneficial in tissue engineering, as it promotes cell infiltration and, consequently, interactions among cells as well as between cells and the matrix, resulting in a favorable cellular response [21]. Additionally, greater porosity in NFs is associated with improved drug loading capacity, as porous materials can protect the drug from the surrounding environment, regulate its release rate, and enhance its solubility [22]. However, it is important to note that tensile strength exhibits an inverse relationship with porosity. Thus, achieving a balance between high porosity and mechanical strength presents a challenge, indicating that these properties must be adapted to the desired fields of application [23].

Nonetheless, the characteristics of NFs, such as diameter, morphology, porosity, and flexibility, are largely dependent on the material properties and the parameters employed during their synthesis. These characteristics can be adjusted according to the specific requirements of the intended application.

1.3. Materials for nanofiber synthesis: polymers

NFs can be fabricated from various materials, including carbon, metals, ceramics, polymers, or combinations thereof. Carbon NFs are composed of graphene layers forming cylindrical structures with various orientations. These layers are typically arranged as stacked cones, in contrast to carbon nanotubes, where the graphene layers are wrapped into hollow cylinders [24]. Metal NFs are typically synthesized in conjunction with a polymer matrix, which facilitates their formation. The resulting fibers are then calcined and reduced to degrade the polymer and obtain NFs of the desired metal from its precursors. These NFs exhibit remarkable properties, such as thermal stability and conductivity, and have potential applications in fields such as photoelectricity, sensors, high-temperature filtration, and others [25]. Similarly, ceramic NFs can be synthesized from a ceramic precursor solution combined with a polymer solution through various methods, followed by calcination or thermal treatment. These NFs are particularly utilized in tissue engineering, as catalytic supports, in sensors, and for water purification [26]. However, polymers are among the most commonly studied materials due to their ease of processing, structural flexibility, functionalization capabilities, diversity, and mechanical properties, among other advantages [27]. A wide range of polymers, both natural and synthetic, have been utilized for NFs synthesis. The most commonly used polymers for NF synthesis are summarized in Table 1.

Although the use of natural polymers is of great interest due to their typically biodegradable, non-toxic, and biocompatible properties, certain polysaccharides, such as alginate and chitosan, present challenges in forming NFs. These difficulties arise from their polyelectrolytic nature [28], lack of chain entanglement due to their rigid and extended chain conformation in aqueous solutions [28,29], or their tendency to undergo gelation at relatively low concentrations [30]. Other natural polymers, such as proteins, are also highly attractive for NF fabrication due to their ease of synthesis and purification, scalability, exquisite tunability, and intrinsic functions [31]. However, their secondary and tertiary structures complicate the formation of NFs. For all these reasons, various strategies are often necessary to fabricate NFs from natural polymers, such as blending with electrospinnable polymers, using surfactants, or applying chemical modifications to reduce hydrogen bonding density [32].

Table 1. Commonly used polymers in electrospinning, along with their solvents, resulting nanofiber sizes, and potential applications.

Polymer	Solvent	Size (nm)	Applications	Ref.
Synthetic				
Polyamides (PA)	Acetic acid, chloroform, formic acid	88-259	Drug loading, filtration	[33-37]
Polyacrylonitrile (PAN)	DMF	183-400	Carbon NFs precursor, filtration, sensing	[38-40]
Polycaprolactone (PCL)	Acetone, chloroform, DCM, DMF	55-876	Drug release, tissue engineering, wound healing	[41-43]
Poly(ethylene glycol)/Poly(ethylene oxide) (PEG/PEO)	Water	36-405	Drug release, food preservation	[44-46]
Poly(lactic acid) (PLA)	Acetone, chloroform, DMF	144-444	Biosensing, drug release, food preservation	[47-49]
Poly(methyl methacrylate) (PMMA)	Chloroform, DMF	250-900	Drug release, sensing, tissue engineering	[50-52]
Polyimide (PI)	DMAc, DMF	80-700	Carbon NFs precursor, LIBs, sensing	[53-55]
Polystyrene (PS)	DMF, THF	300-400	Filtration, sorbent	[56-58]
Polyurethane (PU)	DMF	75-723	Drug release, filtration	[59-61]
Poly(vinyl alcohol) (PVA)	PBS, water	133-324	Drug release, filtration, wound healing,	[62-64]
Natural				
Alginate	Water	109-313	Drug release, filtration, wound healing	[65-67]
Cellulose	DMAc, GAA, TFA	200-800	Filtration, sorbent, wound healing	[68-70]
Chitosan	Acetic acid	41-823	Food preservation, tissue engineering, wound healing	[71-73]
Collagen	HFIP	203-1200	Tissue engineering, wound healing	[74,75]
Gelatin	TFP, HFIP	100-803	Drug release, tissue engineering	[76,77]
Silk fibroin	Formic acid, water	80-500	Drug release, tissue engineering, wound healing	[78-80]

DCM: dichloromethane; DMAc: dimethylacetamide; DMF: dimethylformamide; GAA: glacial acetic acid; HFIP: hexafluoroisopropanol; LIBs: lithium-ion batteries; NFs: nanofibers; PBS: phosphate-buffered saline; TFP: trifluoropropanol; THF: tetrahydrofuran.

1.4. Nanofiber synthesis techniques: electrospinning

NFs can be synthesized using a variety of techniques, including self-assembly, phase separation, template synthesis, centrifugal spinning and drawing [81]. However, the most widely used method is electrospinning, due to its efficiency, low cost, simplicity, scalability, and ability to produce NFs with high surface-area-to-volume ratios and good porosity. Electrospinning has gained significant attention in both academic and industrial settings because it allows the fabrication of different types of NFs, including polymeric NFs, which can be produced directly, as well as carbon, ceramic, and metal NFs that often require further post-treatment processes [82].

Electrospinning dates back to the early 20th century, with its origins attributed to Zeleny in 1914, who first described the behavior of liquid droplets under an electric field. The technique was further developed in the 1930s by Formhals, who filed patents on fiber formation from polymer solutions using electrostatic forces [83]. However, the study of electrospinning technology began gaining popularity in the early 1990s, driven by the growing interest in nanotechnology. Since then, electrospinning has evolved into a versatile process for producing continuous NFs.

The basic principle of electrospinning involves applying a high-voltage electric field to a polymer solution or melt. As the electrostatic forces overcome the surface tension of the solution, a charged jet is ejected from the tip of a nozzle. The electric discharged of the polymer droplet, induces a conically-shaped geometry referred to as the Taylor cone. The jet elongates and undergoes thinning as it travels toward a grounded collector, where solid NFs are deposited. This process is governed by the balance between electrostatic repulsion and viscoelastic forces in the polymer solution. A typical laboratory-scale setup consists of five main components: a high-voltage power supply, a syringe charged with a polymeric solution, a syringe pump, a nozzle (usually a metallic syringe needle) and a collector (which can be a metallic foil, plate, or disc) [84]. Figure 3 shows a schematic representation of the components of an electrospinning device.

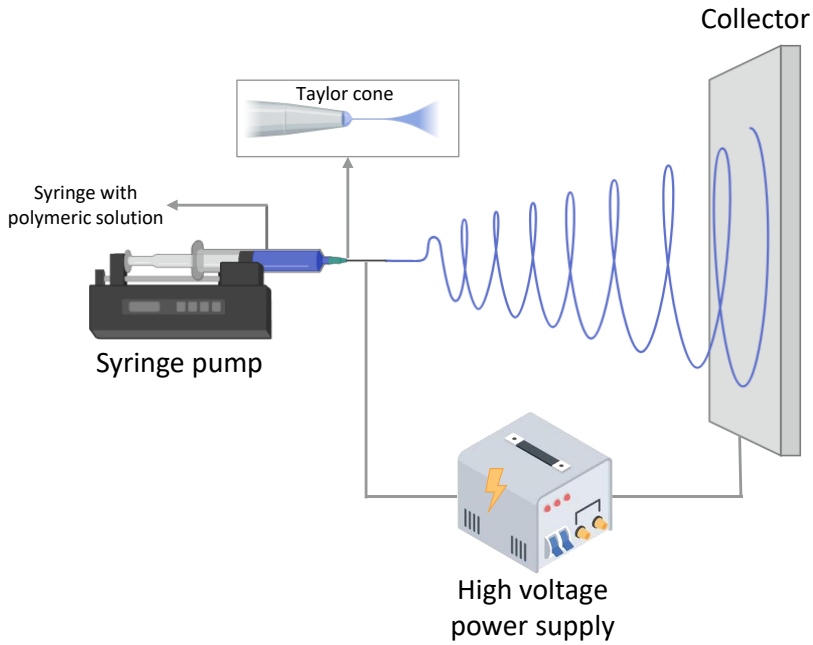

Figure 3. Schematic representation of a typical electrospinning setup, including a syringe loaded with a polymer solution, a syringe pump, a high-voltage power supply, and a collector. The formation of the Taylor cone at the tip of the metallic needle attached to the syringe is also shown.

The electrospinning process is influenced by several critical parameters, which can be divided into three main categories: equipment settings, solution properties, and environmental conditions. These parameters are detailed in Table 2, along with their effects on the morphology and diameter of the NFs.

Table 2. Influence of various parameters on the electrospinning process and resulting effect on nanofiber formation.

Parameters	Effects on nanofibers
Solution properties	
Viscosity	Low viscosity leads to jet breakup and droplet formation; excessive viscosity limits charge-induced stretching, preventing fiber formation.
Conductivity	High solution conductivity enhances jet stretching and fiber quality but may also increase jet count.
Surface tension	Surface tension, largely determined by the solvent, must be low for fiber formation. Higher surface tension increases the minimum voltage needed for nanofiber production.
Equipment settings	
Applied voltage	High voltage reduces nanofiber diameter, but excessive voltage shortens flight time, leading to thicker fibers.
Tip-to-collector distance	Short distances can cause fused fibers due to incomplete solvent evaporation, while excessive distances weaken the electrostatic field, reducing fiber stretching.
Feed rate	Excessive feed rate causes solution dripping, while insufficient feed rate disrupts spinning, leading to intermittent Taylor cone formation and greater fiber diameter variation.
Environmental conditions	
Humidity	High humidity increases fiber diameter due to surface condensation on the jet and reduced evaporation rate.
Temperature	Elevated temperatures lower solution viscosity, promoting stretching and smaller fiber diameters, but excessive heat can accelerate solvent evaporation, limiting benefits.

1.5. Nanofiber applications: delivery of antimicrobial agents

NFs, with their unique properties, have become valuable in diverse applications, including tissue engineering, drug delivery, wound dressings, air and water filtration, energy storage, sensors, and textiles [85]. Their functional characteristics—such as mechanical strength, structural integrity, surface morphology, porosity, and chemical functionalities—can be specifically tailored to suit each application by adjusting fiber alignment, orientation, dimension, or material composition [86].

An application growing in significance in recent years is the development of antimicrobial NFs, driven by the urgent need to control infections and curb the spread of pathogens, particularly those resistant to antibiotics. Antimicrobial resistance (AMR) arises when bacteria, viruses, fungi, and parasites evolve and become unresponsive to treatments, making infections more difficult to manage and increasing the risks of disease transmission, severe illness, and mortality. Today, AMR ranks among the most critical global public health and development challenges. In 2019, bacterial AMR was estimated to be directly responsible for 1.27 million deaths worldwide, with

an additional 4.95 million deaths associated with resistant infections [87]. As represented in Figure 4, the number of deaths associated with AMR is expected to reach 10 million per year worldwide by 2050 with global economic losses estimated to reach approximately $100 trillion [88]. The main drivers of drug-resistant pathogens are the misuse and overuse of antimicrobial agents in humans, animals, and agriculture.

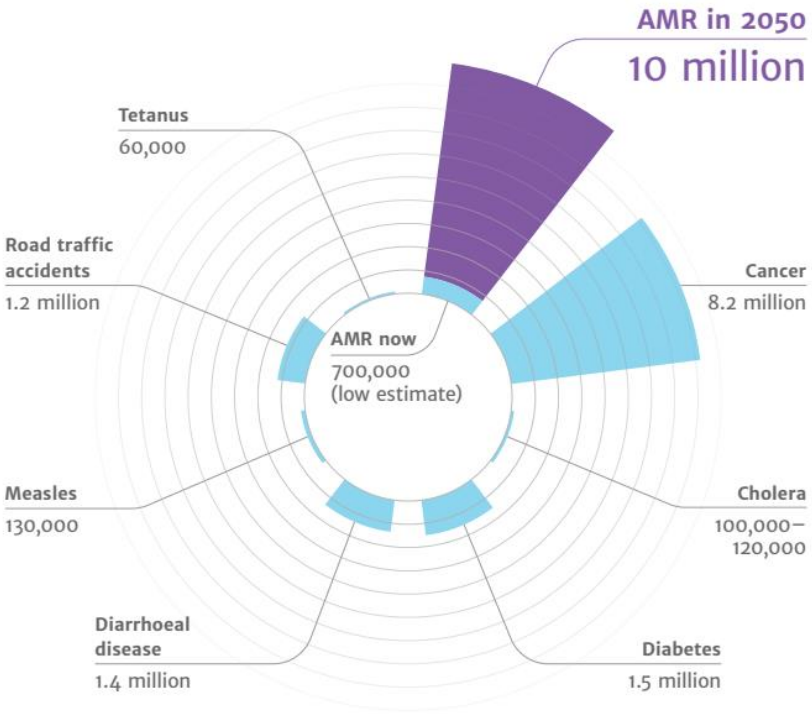

Figure 4. Predicted mortality from AMR compared with common causes of current deaths. Source: O'Neill, 2016 [89].

This urgent issue underscores the critical need for innovative antimicrobial delivery strategies. Traditional antibiotic treatments are prone to rapid release and subsequent degradation, which can accelerate resistance development. NFs offer a promising alternative by enabling sustained, controlled release of antimicrobial agents, along with passive and active targeting capabilities [90]. This technology enhances antimicrobial effectiveness through targeted drug delivery, reducing both the required dosage and frequency of administration, which can also minimize side effects. Importantly, NF encapsulation protects antimicrobials from premature degradation, improving their stability and bioactivity and potentially lowering the risk of resistance.

Various antimicrobial agents—including antibiotics, antimicrobial peptides (AMPs), MNPs, and natural extracts—have been extensively studied for encapsulation within NFs using diverse electrospinning techniques. The most common methods to encapsulate drugs into NFs include blend electrospinning, coaxial electrospinning and emulsion electrospinning. In blend electrospinning, antimicrobial agents are mixed directly into the polymer solution, creating a straightforward method for uniformly distributing the agents within NFs. This approach dissolves or disperses the drug within the polymeric matrix, resulting in a formulation that offers a sustained release profile under optimal conditions. The release mechanism from polymeric matrices is typically governed by desorption and diffusion, or by the dissolution and erosion of the polymer matrix [91]. Coaxial electrospinning, on the other hand, utilizes a core-shell structure created by two coaxially aligned needles. This spinneret configuration allows for the formation of a composite polymeric droplet, where the inner (core) liquid is pumped through an inner needle and

the outer (shell) material is fed through an outer needle. Key advantages of coaxial electrospinning include the ability to fabricate core-shell NFs from both miscible and immiscible polymers, a high loading capacity for bioactive molecules, and the flexibility to use non-spinnable liquids in the core [91]. Finally, emulsion electrospinning is especially advantageous for encapsulating both hydrophilic and hydrophobic antimicrobial agents within NFs. This technique employs emulsions in which the dispersed phase contains the active agent. These emulsions consist of two or more immiscible phases, stabilized by an emulsifier. During the electrospinning process, core-shell NFs are formed, with the continuous phase transforming into the shell of the fibers while the droplet phase forms the core. This approach not only facilitates the effective encapsulation of diverse antimicrobial agents but also enhances their release profiles and bioactivity within the NF matrix [92].

1.6. Antimicrobial agents incorporated into nanofibers

Incorporating antimicrobial agents into NFs has emerged as a promising strategy for enhancing their efficacy in combating infections and controlling microbial growth. These agents can be classified into several categories, each with distinct mechanisms of action and advantages. The most commonly used antimicrobial agents include antibiotics, metal oxides and NPs, AMPs and natural compounds, among others. Table 3 presents examples of these antibacterial agents used in various studies in combination with polymeric NFs, as well as their observed effects.

These antimicrobial agents originate from a wide array of natural and synthetic sources, each contributing distinct mechanisms of action against pathogens. Many antibiotics were initially discovered as natural products from fungi and soil bacteria; however, modern antibiotics are largely semisynthetic, derived from modifications of natural compounds and manufactured in laboratory settings [93]. Their mechanisms of action include disruption of bacterial cell wall synthesis or interference with protein production or inhibition of DNA replication, among others, effectively targeting a broad spectrum of bacterial infections. Metal oxides and NPs, such as silver, zinc oxide, and copper oxide, are synthesized through chemical, physical, or biological methods, with potent antimicrobial activity driven by oxidative stress and cell membrane disruption [94]. AMPs are naturally present in all organisms; many exhibit not only antibacterial activity but also antiviral, antifungal, antiparasitic, and antitumor properties [95]. Plant-derived compounds—including crude extracts, essential oils, and specific constituents like flavonoids, alkaloids, and tannins—have demonstrated broad-spectrum efficacy by disrupting microbial cell structures and interfering with cellular processes [96].

Table 3. Examples of antibacterial agents incorporated into nanofibers and their effect.

Antimicrobial agent	Polymers	Microorganisms	Effect	Ref.
Antibiotics				
Amoxicilin	Pullulan, PLGA	*Escherichia coli, Staphylococcus aureus*	Antimicrobial activity, extended storage time, wound healing	[97]
Ciprofloxacin	Alginate, PVA	*Pseudomonas aeruginosa, S. aureus*	Antimicrobial activity equivalent to free drug	[98]
Gentamicin	Alginate, chitosan	*E. coli, S. aureus*	Antimicrobial activity, rapid wound healing	[99]
Antimicrobial peptides				
CAMP	Silk fibroin	*E. coli, P. aeruginosa, Staphylococcus epidermidis, S. aureus*	No bacterial survival, biofilm inhibition, long-term storage	[100]
Nisin	PDLLA, PEO	*S. aureus*	Bacterial inhibition, wound closure time reduction	[101]
ε-poly-L-lysine	PAA, PVA	*E. coli, S. aureus, S. epidermidis*	Antibiofilm effect, cell membrane disruption	[102]
Metal oxide NPs				
CuO NPs	PLGA	*E. coli, S. aureus*	Inhibition governed by release of Cu^{2+} ions	[103]
Fe_3O_4 NPs	Chitosan, gelatin	*E. coli, S. aureus*	Combined antibacterial action of chitosan and Fe_3O_4 NPs	[104]
ZnO NPs	PCL	*E. coli, S. aureus*	Bacterial growth inhibition	[105]
Metal NPs				
AgNPs	Gelatin, PCL	*E. coli*	Bacterial growth inhibition, rapid wound healing	[106]
CuNPs	PAN	*S. aureus*	Bacterial growth inhibition	[107]
AuNPs	Cellulose	*Enterococcus faecalis, E. coli, P. aeruginosa, S. aureus*	Bacterial growth inhibition and cell damage	[108]
Natural compounds				
Aloe vera	Chitosan, PCL, PEO	*E. coli, S. aureus*	Antibacterial activity, biofilm inhibition	[109]
Oregano essential oil	Chitosan, PCL	*E. coli, Lysteria monocytogenes, S. aureus, Salmonella enteritidis*	Bacterial growth inhibition	[110]
Pomegranate flowers extract	Chitosan, PCL, PVA	*P. aeruginosa, S. aureus*	Bacterial growth inhibition, accelerated tissue regeneration	[111]

CAMP: cathelicidin antimicrobial peptide; PAA: polyacrylic acid; PAN: polyacrylonitrile; PCL: polycaprolactone; PDLLA: poly(DL-lactide); PEO: polyethylene oxide; PLGA: poly(lactic-co-glycolic acid); PVA: Poly(Vinyl Alcohol).

1.7. Metal nanoparticles: fundamentals, synthesis and antimicrobial activity

MNPs are particles of metals with dimensions typically below 100 nm. This nanoscale size confers unique characteristics such as high electrical properties, high mechanical, chemical and thermal stability, high surface area, and high optical and magnetic properties [112]. These traits arise due to quantum effects and increased surface energy, making MNPs highly effective in various technological and biomedical applications. Commonly used MNPs include silver (AgNPs), copper (CuNPs), and zinc oxide NPs (ZnONPs), each selected for specific attributes: AgNPs are noted for their strong bioactivity [113], copper for its cost-effectiveness [114], and zinc oxide for its favorable safety profile [115]. These NPs also vary in shape, surface chemistry, and particle size, all of which influence their interaction with biological and chemical environments.

MNPs can be synthesized via chemical, physical, or biological (green) methods, each of which offers different advantages and limitations. Chemical methods, such as chemical reduction and sol-gel synthesis, are effective for controlling NP size and shape but often require toxic reagents and generate hazardous by-products [116]. Physical methods, like laser ablation or thermal evaporation, create MNPs through the breakdown of bulk metal, but these processes tend to be energy-intensive and less scalable [116]. A promising alternative is green synthesis, an eco-friendly approach that utilizes natural reducing agents—derived from plant extracts, bacteria, fungi, or algae—to reduce metal ions into NPs [117]. Green synthesis avoids toxic chemicals, operates under milder conditions, and produces biocompatible MNPs, making it highly suitable for applications in medicine and environmental technologies.

As previously discussed, MNPs are widely used as antimicrobial agents due to their broad-spectrum efficacy against a range of pathogens, including bacteria and viruses. When incorporated into polymeric platforms, such as NFs, MNPs extend their applications to diverse fields like food preservation [118], cosmetics [119], antibacterial textiles [120], surface coatings [121], and medical devices [122]. The integration of MNPs into polymeric matrices enables controlled release, enhanced stability, and direct application to specific sites, making them highly effective in applications that require sustained antimicrobial activity.

The antimicrobial mechanisms of MNPs against bacteria, though not yet fully elucidated, appear to be multifaceted, allowing them to target bacterial cells through various pathways and reducing the likelihood of resistance development, as shown in Figure 5. A primary mechanism involves the generation of reactive oxygen species (ROS), such as hydroxyl radicals and superoxide ions. ROS induce oxidative stress within bacterial cells, damaging critical cellular components, including lipids, proteins, and DNA, ultimately leading to cell death. In addition to cellular component damage, ROS can compromise the bacterial cell wall, disrupt membrane permeability, and reduce the proton motive force, which can facilitate the internalization of MNPs and their released ions [123]. Another central mechanism is the release of metal ions (e.g., Ag^{+}, Cu^{2+}, Zn^{2+}), which can penetrate bacterial cells, interfere with essential biochemical pathways, and further disrupt cell membrane integrity [124]. Additionally, MNPs bind to bacterial cells through electrostatic interactions, increasing membrane permeability and causing structural destabilization. This interaction results in the leakage of intracellular contents, loss of cellular integrity, and, ultimately, bacterial cell death [125].

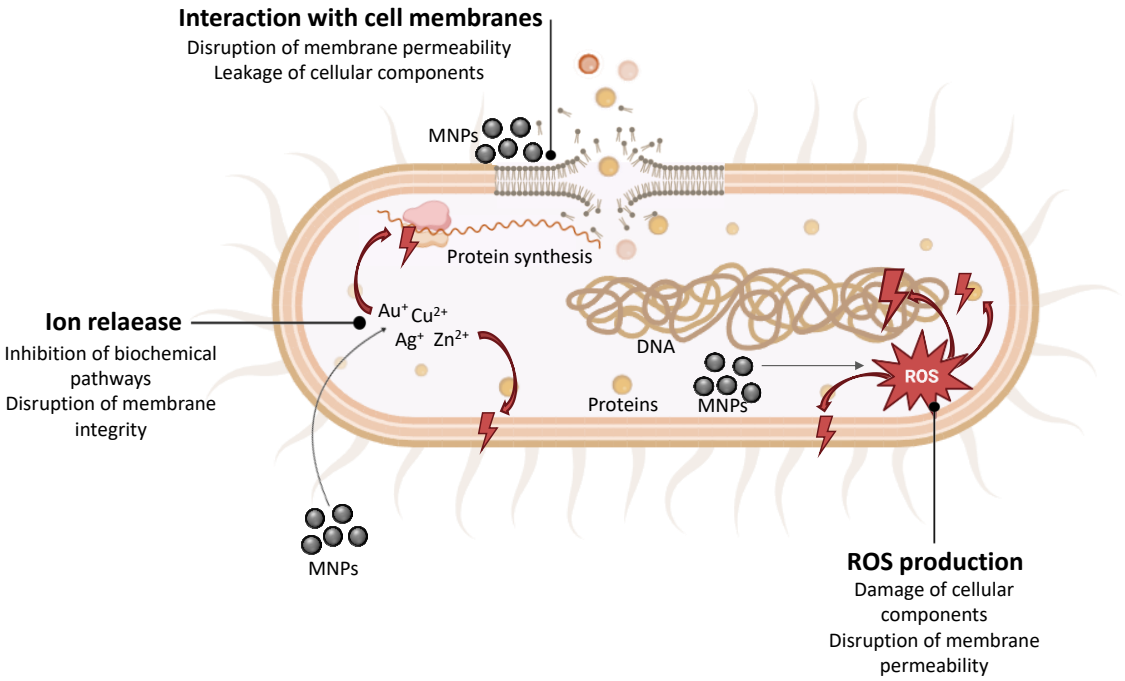

Figure 5. Antibacterial mechanisms of metal nanoparticles (MNP). Red bolts in the image represent damage to cellular components or processes.

MNPs have also demonstrated effectiveness as antiviral agents. Viruses pose a significant public health and economic burden, as exemplified by the severe acute respiratory syndrome coronavirus 2 (SARS-CoV-2) pandemic [126]. Additionally, many viruses can be transmitted via surfaces in the environment [127], highlighting the potential utility of incorporating MNPs into polymeric platforms to create antiviral materials for surface applications aimed at reducing viral transmission. Regarding their mechanisms of action, MNPs can interfere with viral infection by disrupting the ability of virus to attach to host cells. This interference can occur through interactions with viral surface proteins, such as gp120 in human immunodeficiency virus (HIV) or hemagglutinin in influenza viruses [128], which can block virus-host binding or prevent viral penetration [129]. Other mechanisms include inactivating viral particles before they can enter host cells, binding directly to the viral genome, or interacting with viral particles to inhibit their replication [130]. Additionally, MNPs release metal ions that can interact with viral envelopes and generate ROS, which damage viral nucleic acids, proteins, and other essential biomolecules [126].

APPROACH

2. INTEGRATION AND CONTRIBUTION OF RESEARCH PAPERS TO THESIS THEMATIC FIELD

The development of advanced nanomaterials and innovative nanoformulations continues to hold great promise for therapeutic applications and the prevention of pathogen transmission. With their unique properties, nanomaterials stand out as valuable tools for tackling complex biomedical challenges. Despite the significant progress achieved so far, there is still considerable potential to improve their performance and expand their applications. Harnessing the unique capabilities of nanomaterials could significantly enhance their effectiveness in combating microbial threats. Ongoing efforts to refine their design, synthesis and formulation will be crucial in unlocking their full potential for these critical uses.

This Thesis focuses on the development of innovative polymeric nanocomposites incorporating antimicrobial agents for potential applications in combating microbial threats. The five chapters that comprise this Thesis explore distinct yet interconnected aspects of antimicrobial nanomaterial synthesis, characterization, and functionalization. Collectively, these studies advance the field by investigating both natural and synthetic antimicrobial agents, as well as optimizing their encapsulation within polymeric matrices to ensure controlled and sustained release. Through a combination of experimental and review-based approaches, this work aims to contribute practical solutions and foundational insights that may facilitate the next generation of effective antimicrobial nanomaterials. Figure 6 illustrates the interconnections between the various chapters of this Thesis, highlighting their overlap across distinct yet interrelated research fields.

Chapter 1. Fish skin mucus extracts: an underexplored source of antimicrobial agents

This initial review explores the potential of fish skin mucus as a source of bioactive compounds with antimicrobial properties. As a foundational study, it establishes a natural reservoir of antimicrobials that can later be utilized in nanomaterial synthesis, setting the stage for more targeted development of biomaterials that can harness these compounds.

Chapter 2. Bovine serum albumin and lysozyme nanofibers as versatile platforms for preserving loaded bioactive compounds

Building on the insights from Chapter 1, this study focuses on the development of NFs composed of proteins with varying molecular weights to encapsulate bioactive agents, including antimicrobial compounds derived from fish skin mucus. This chapter highlights the versatility of protein-based NFs as delivery vehicles derived from natural compounds, demonstrating their viability for the effective preservation and sustained release of antimicrobial agents. The work emphasizes the role of these protein matrices in protecting sensitive bioactives, thereby enhancing their stability and efficacy in antimicrobial applications.

Chapter 3. Viricidal activity of thermoplastic polyurethane materials with silver nanoparticles.

Transitioning to a more industrial focus, this study investigates a polymeric matrix embedded with commercial AgNPs for viricidal applications, employing protocols suitable for large-scale production. This chapter presents a robust approach to creating AgNP-based materials designed to limit viral spread on surfaces, broadening the application scope of antimicrobial nanomaterials beyond bacterial targets to include virus control.

Chapter 4. Phytochemical-based nanomaterials against antibiotic-resistant bacteria: an updated review.

Complementing the prior focus on synthetic approaches, this review explores green synthesis methods for antibacterial nanomaterials derived from phytochemicals, presenting a sustainable alternative to conventional production. By harnessing the bioactive properties of plant-based compounds, this study encourages a shift toward eco-friendly nanomaterial production, reducing reliance on synthetic agents without compromising antimicrobial efficacy.

Chapter 5. An innovative approach based on the green synthesis of silver nanoparticles using pomegranate extract for antibacterial purposes.

Building on insights from Chapters 3 and 4, this study employs pomegranate peel extract (PGE) to synthesize AgNPs, creating an antibacterial nanomaterial with a greener, more sustainable profile. The use of PGE not only provides a natural reducing and stabilizing agent but also enhances the eco-friendliness of the synthesis process. These AgNPs are then incorporated into the nanofibrous polymeric matrix produced in Chapter 2, enabling controlled, sustained release and enhancing the applicability of the material for antimicrobial delivery in various settings.

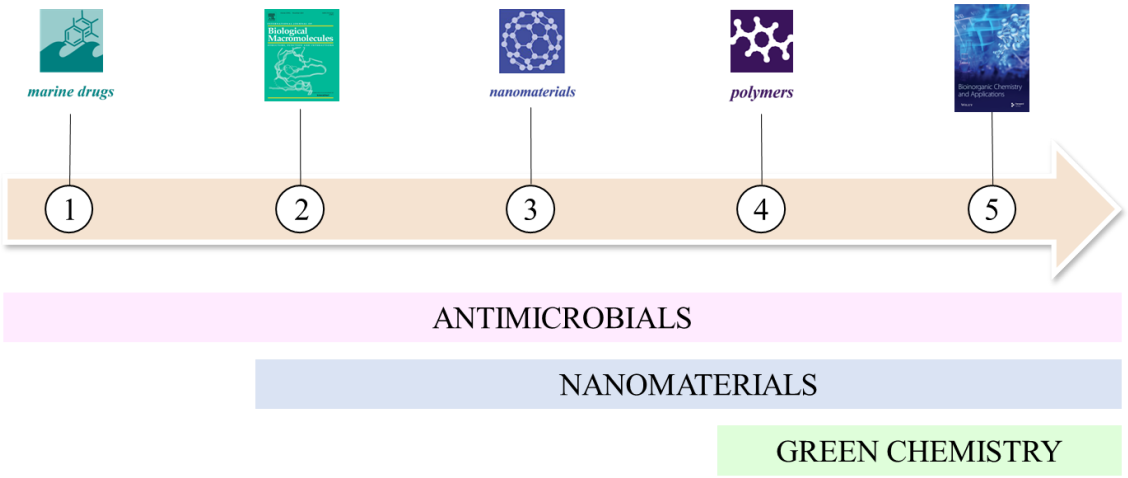

Figure 6. Thematic relationships across the five chapters comprising this Thesis.

OBJECTIVES

3. OBJECTIVES

With the growing global threat of infectious diseases caused by resistant bacteria and viruses, there is an urgent need for the development of advanced nanomaterials that can effectively prevent and control microbial proliferation. Accordingly, the **primary objective** of this Thesis, titled "*Development of new polymeric nanocomposite materials with antimicrobial activity*", is to **design, develop, and characterize novel, versatile polymeric nanomaterials embedded with potent antimicrobial agents aimed to reduce the spread of infections across various environments, offering valuable solutions to pressing public health challenges posed by drug-resistant pathogens and viral outbreaks.**

To achieve this primary objective, the work is divided into seven specific objectives (SO) which are interconnected as illustrated in Figure 7. Given that this Thesis is organized into five chapters, each one is linked to one or more SO as follows:

SO1. To conduct a literature review on new antimicrobial compounds from underexplored natural sources (Chapter 1).

SO2. To design and characterize polymeric nanostructured systems incorporating antimicrobial compounds, with evaluation of their antimicrobial and antiviral efficacy (Chapters 2, 3 and 5).

SO3. To develop, synthesize, and characterize novel protein-based NFs as natural polymeric materials, incorporating innovative bioactive compounds to combat bacterial infections (Chapter 2).

SO4. To characterize commercial polyurethane-based polymeric materials embedded with AgNPs and evaluate their antiviral capacity using standardized protocols of a technical nature and internationally validated (Chapter 3).

SO5. To perform a literature review on more sustainable synthesis methods for antibacterial nanostructures, with a focus on combating antibiotic-resistant bacteria (Chapter 4).

SO6. To design, synthesize, optimize, and characterize AgNPs created through green synthesis as antimicrobial agents (Chapter 5).

SO7. To integrate green-synthesized AgNPs into polymeric nanofibrous matrices for targeted antimicrobial applications (Chapter 5).

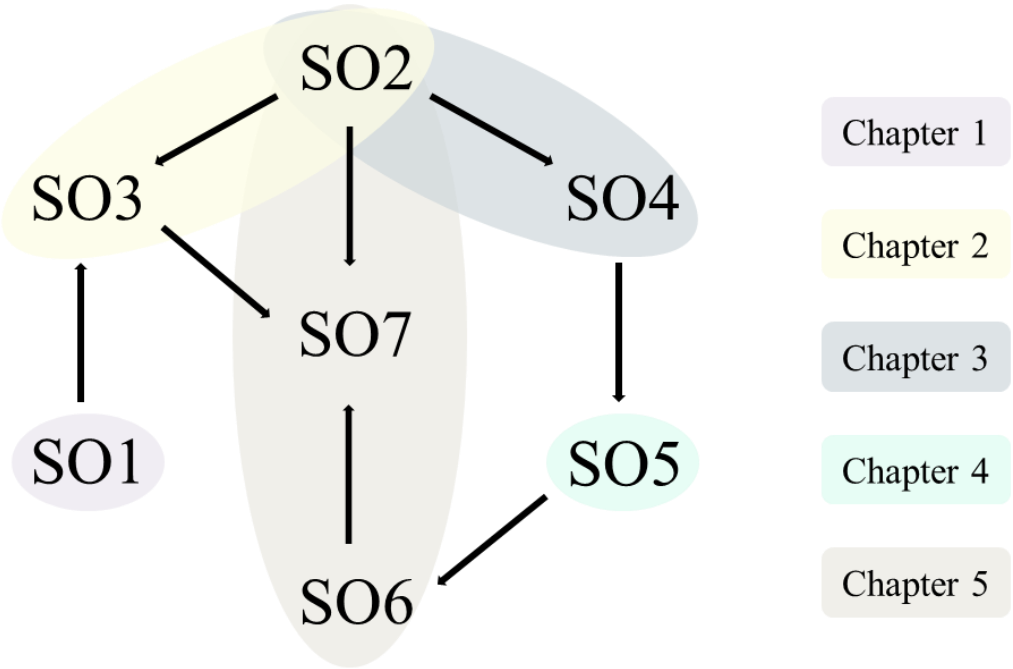

Figure 7. Relationship between the thesis-specific objectives and the specific objectives addressed in each chapter.

MATERIALS & METHODS

4. MATERIALS AND METHODS

4.1. Materials

4.1.1. Manufacturers

All reagents were procured from various suppliers, including Bio-Rad Laboratories GmbH (Munich, Germany), Condalab (Madrid, Spain), Genscript Biotech Corp (Piscataway, NJ, USA), Merck (Darmstadt, Germany), Panreac, ITW Reagents (Barcelona, Spain), and Sigma-Aldrich (St. Louis, MO, USA).

4.1.2. TPU materials with AgNPs

The samples used for the study of the antiviral activity of thermoplastic polyurethane (TPU)-based materials in Chapter 3 included a commercial additive, 746-3BV (Esenttia, Bogotá, Colombia), which contains AgNPs encapsulated in a ceramic polyethylene matrix (D98 < 40 μm) at a concentration of 16% w/w in molten polypropylene (0.91 g/cm³, Duraflon®). This additive was homogeneously mixed at a 1:16 ratio with molten TPU (1.22 g/cm³, Ultimaker BV) at 220 °C to produce the AgNP–TPU composite material. The control TPU material was fabricated following the same process, excluding the commercial AgNP additive.

4.1.3. Preparation of solutions

The preparation of solutions for NF fabrication in Chapters 2 and 5 required one or more of the following compounds: bovine serum albumin (BSA), horseradish peroxidase (HRP)-conjugated goat anti-mouse IgG (HRP-IgG, A5278), lysozyme (LYZ, chicken egg white, A3711,0050; Activity 20,780 U/mg), piscidin-1 (PIS, from European sea bass, accession #MT066191, C-terminal amidation and purity >90 %), and polyethylene oxide (PEO, Mw = 600–1000 kg/mol).

4.1.4. Extract characterization

The PGE used as a reducing agent in Chapter 5 was prepared in the laboratory from organic pomegranate peel of the "Mollar de Elche" variety collected in Elche (Alicante, Spain), which holds Protected Designation of Origin status. Its synthesis is detailed in the Methods section. It was characterized using various analytical techniques. These techniques required different reagents, including 2,2'-azinobis(3-ethylbenzothiazoline)-6-sulfonic acid (ABTS), 3,5-dinitrosalicylic acid (DNS), 6-hydroxy-2,5,7,8-tetramethylchroman-2-carboxylic acid (Trolox), aluminum chloride ($AlCl_3$), BSA, Coomassie Brilliant Blue G-250, Folin–Ciocalteu phenol reagent, gallic acid, glucose, phenol, potassium acetate (CH_3CO_2K), potassium persulfate ($K_2S_2O_8$), punicalagin molecular standard, sodium carbonate (Na_2CO_3), sodium metabisulfite ($Na_2S_2O_5$), and sodium potassium tartrate ($KNaC_4H_4O_6$).

4.1.5. AgNPs synthesis

For the green synthesis of AgNPs in Chapter 5, only two reagents were required: commercial $AgNO_3$ and PGE.

4.1.6. Antimicrobial assays

The bacterial strains used in the antimicrobial assays in Chapters 2 and 5 included *Aeromonas salmonicida* (CECT 894), *Bacillus circulans* (CECT 10), *Bacillus subtilis* (CECT 35), *E. coli* (CECT 45), *Micrococcus luteus* (CECT 243), and *S. epidermidis* (CECT 231), obtained from the Spanish Type Culture Collection (CECT, Valencia, Spain), as well as *S. aureus* and MRSA, sourced from clinical samples of patients at the General University Hospital of Alicante. The

reagents used in antimicrobial assays and for subsequent bacterial processing included glutaraldehyde, p-iodonitrotetrazolium chloride (INT), Mueller-Hinton (MH) agar and broth, osmium tetroxide (OsO_4), and phosphate-buffered saline (PBS).

4.1.7. Cellular assays

The cell lines used for cytotoxicity assays in Chapter 3 included epithelioma papulosum cyprinid (EPC) cells (American Type Culture Collection ref.: CRL-2872) and Vero E6/TMPRSS2 cells. Reagents used for cell maintenance included Dulbecco's Modified Eagle Medium (DMEM), Dutch modified Roswell Park Memorial Institute (RPMI) 1640 medium, fetal bovine serum (FBS), gentamicin, glutamine, non-essential amino acids, penicillin, sodium pyruvate, and streptomycin. The reagent 3-(4,5-dimethylthiazol-2-yl)-2,5-diphenyltetrazolium bromide (MTT) was used to determine cytotoxicity.

4.1.8. Viricidal assays

The viricidal activity of the materials in Chapter 3 was evaluated against the fish pathogen spring viremia of carp virus (SVCV, isolate 56/70) using EPC cells and against SARS-CoV-2 using Vero E6/TMPRSS2 cells.

4.2. Methods

4.2.1. Bibliographic search

For Chapters 1 and 4 involving literature searches, the databases Scopus and MedlinePlus were selected, using keywords tailored to each study. The inclusion criteria for selecting articles relevant to each chapter were: (i) publication in English, (ii) appearance in peer-reviewed journals, and (iii) alignment with the specific focus of each chapter. Preference was given to articles published within the last five years at the time each Thesis chapter was written.

4.2.2. Preparation of samples

4.2.2.1. AgNP-TPU samples

The AgNP-TPU materials used in Chapter 3 were processed to comply with the guidelines outlined in ISO 21702:2019: "Measurement of antiviral activity on plastics and other non-porous surfaces." To this end, the materials to be tested and their respective controls were molded to the dimensions specified in the procedure (5 × 5 × 0.5 cm plates). The AgNP-TPU and control TPU plates were then placed in sterile Petri dishes, onto which 400 µL of test inoculum was added to the surface of the materials. Subsequently, 4 × 4 cm polypropylene cover films were applied, ensuring they covered the inoculum and spread it toward the edges of the film without allowing it to leak out. Incubations were conducted in this arrangement inside humid chambers at a constant temperature. The specific temperature, duration of incubation, and type of test inoculum varied depending on the particular test being performed.

4.2.2.2. Electrospinning solutions and viscosity determination

The polymeric solutions used for electrospinning NFs in Chapters 2 and 5 were prepared as follows, with all concentrations expressed as weight/weight (w/w) percentages unless stated otherwise. PEO solutions containing protein (BSA or LYZ) were prepared by dissolving 5–20% protein and 3% PEO in Milli-Q water. All solutions were stirred for 12 hours to ensure complete dissolution and homogeneity.

After optimization, an electrospinnable solution containing 15% total protein and 3% PEO was selected as the base solution for the incorporation of additional antimicrobial and bioactive

compounds. In Chapter 2, PIS, a small 22-residue AMP, was added at 0.1% to both BSA (BSA/PIS) and LYZ (LYZ/PIS) solutions to compare the antibacterial activity of the resulting NFs. To assess the stability of larger, more complex proteins within the nanofibrous system, HRP-IgG, commonly used as a secondary antibody for immunolabeling assays, was added at 1% in BSA solutions (BSA/Ab). In Chapter 5, optimized AgNPs were incorporated at 0.2% into the base solution. All concentrations were chosen based on the minimum amount required to observe activity.

The kinematic viscosity (ν) of the solutions in Chapter 2 was measured using a series of calibrated Cannon-Fenske capillary viscometers (series 400–450, Vidra Foc, Barcelona, Spain) to determine their electrospinnability. The corresponding density (ρ) was measured with a calibrated volumetric flask, and shear viscosity ($\eta = \nu\rho$ [mPa·s]) was estimated. The average value of three measurements at 313 K was reported as the mean ± standard deviation (SD).

4.2.2.3. Pomegranate peel extract preparation

The PGE used as a reducing agent for synthesizing AgNPs in Chapter 5 was prepared in the laboratory following these steps. Initially, the peels were thoroughly washed and then dried at 60 °C in a ZHWY-100B incubator oven (Zhicheng Instruments, Shanghai, China). Figure 8 shows the obtained product after this step. The dried peels were ground using an MF10 basic mill (IKA, Staufen, Germany) to achieve uniform particle sizes of 1–2 mm.

Figure 8. Dried "Mollar de Elche" pomegranate peels used to obtain PGE extract in this Thesis.

Subsequently, an ultrasound-assisted extraction was conducted, providing an energy input of 100 J/mL to the extraction medium, which consisted of distilled water maintained at 60 °C, using a UP400St ultrasonicator (Hielscher, Teltow, Germany). After one hour of agitation, the extract was filtered through a Colombo plate filter equipped with V4 filters (Rover Pompe, Polverara, Italy). The filtered extract was then concentrated using a R-220 Pro rotary evaporator (Büchi, Flawil, Switzerland) and finally dried to a powdered form using a B-290 spray dryer (Büchi).

4.2.3. Synthesis techniques

4.2.3.1. Electrospinning

NFs synthesized in Chapters 2 and 5 were produced through electrospinning. The prepared polymer solutions were transferred into 2 mL syringes (Becton Dickinson, Franklin Lakes, NJ, USA) fitted with blunt-end stainless steel hypodermic needles (outer diameter: 1.27 mm, inner diameter: 0.84 mm; Sigma-Aldrich). The electrospinning process was conducted at a controlled

flow rate using a KDS 100 infusion pump (KD Scientific, Holliston, MA, USA) and a high-voltage power supply (Glassman High Voltage Inc., Whitehouse Station, NJ, USA).

The optimization of electrospinning conditions was a multi-step process that involved fine-tuning both the polymer solution and the electrospinning parameters. Key parameters adjusted during the process included the applied voltage, tip-to-collector distance, and flow rate. These parameters were systematically varied within the following ranges: voltage from 10 to 20 kV, tip-to-collector distance from 12 to 18 cm, and flow rate from 0.2 to 0.5 mL/h. The selected ranges were based on previous studies conducted by our research group.

Through this systematic variation, the optimal electrospinning conditions were identified as an applied voltage of 18 kV, a tip-to-collector distance of 17 cm, and a flow rate of 0.25 mL/h, all maintained at 20–40% relative humidity and 25 °C. Under these conditions, NFs were produced with the most desirable morphology and size, effectively minimizing electrospray, small droplets, and defects such as beads or ribbon-like structures. The resulting NFs were subsequently deposited onto aluminum foil-coated glass slides for further analysis.

4.2.3.2. Green synthesis of AgNPs and optimization

In Chapter 5, a green synthesis approach was used to produce AgNPs by preparing a 0.1 M $AgNO_3$ stock solution and a 50 mg/mL PGE stock solution in Milli-Q water. For the synthesis, varying volumes of PGE (0.16, 0.32, or 0.48 mL) were combined with 5, 10, or 15 mM $AgNO_3$ solutions, derived from the $AgNO_3$ stock. The total volume of each reaction mixture was maintained at 50 mL. Each mixture was stirred using a magnetic stirrer, with the temperature held at 20, 50, or 80 °C for 24 hours, depending on the specific experiment. After this period, the AgNPs were isolated by centrifugation at 15,000 rpm for 30 minutes. The supernatant was discarded, and the precipitated AgNPs were resuspended in Milli-Q water and sonicated for 15 minutes, a process repeated twice to ensure purity. The resulting AgNPs were then freeze-dried to yield solid material suitable for further characterization.

To optimize AgNP synthesis, a three-factor, three-level Box-Behnken Design (BBD) was implemented using Python in a Jupyter Notebook on Colab, utilizing the DOEPY (Design of Experiment Generator in Python) library. This BBD comprised 15 trials, including three replicated central points, to assess the influence of independent variables: $AgNO_3$ concentration (X_1), PGE concentration (X_2), and reaction temperature (X_3), each varied at three levels (low, medium, high). Upper and lower bounds for each factor were informed by literature and preliminary trials. The responses measured were hydrodynamic diameter (HDD, Y_1), polydispersity index (PDI, Y_2), and zeta potential (ZP, Y_3), with the optimization goal to minimize each parameter for ideal AgNP characteristics.

4.2.4. Characterization techniques

4.2.4.1. Characterization of extract

4.2.4.1.1. Phenolic content determination

The total phenolic content (TPC) of the extracts was quantified using the Folin-Ciocalteu method in a 96-well plate format, an established assay for determining phenolic compounds, as shown in Figure 9. The Folin-Ciocalteu method is based on an oxidation-reduction reaction [131]. The Folin-Ciocalteu reagent contains phosphomolybdic and phosphotungstic acid complexes, which, in the presence of phenolic compounds, are reduced to a blue-colored complex. This color change is proportional to the phenolic content, allowing for a quantitative assessment when absorbance is measured spectrophotometrically. By comparing sample absorbance to a gallic acid standard curve, the total phenolic content can be accurately expressed in terms of gallic acid equivalents.

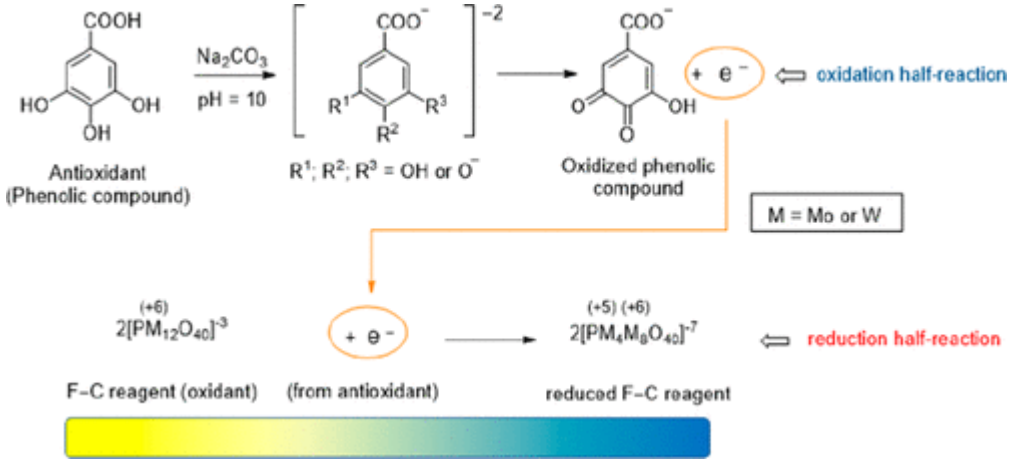

Figure 9. General redox reaction in the Folin–Ciocalteu assay. Source: Pérez et al. (2023) [132].

Briefly, 10 µL of each sample was added to a well, followed by 50 µL of Folin-Ciocalteu phenol reagent. After a 1-minute incubation, 100 µL of 20% (w/v) Na_2CO_3 solution and 840 µL of distilled water were added. The mixture was left in the dark for 30 minutes to allow full color development. Absorbance was then measured at 700 nm using a BioTek Synergy HTX Multi-Mode Microplate Reader (Agilent Technologies, Santa Clara, CA, USA). A standard curve of gallic acid was prepared for calibration, and results were expressed as gallic acid equivalents (g GAE/100 g of dry extract).

4.2.4.1.2. Total flavonoids quantification

Flavonoid quantification was carried out using the aluminum chloride ($AlCl_3$) colorimetric method [133], a widely applied technique that leverages the formation of a stable yellow-colored complex between hydroxyl and carbonyl functional groups of flavonoids and aluminum ions. This complex can be quantified through spectrophotometry due to its distinct absorbance properties. In this assay, 0.5 mL of PGE was mixed with 4.5 mL of a 0.2% methanolic $AlCl_3$ solution and 0.1 mL of 1 M potassium acetate. The mixture was then left to react for 30 minutes at room temperature to allow complex formation. The absorbance was measured at 415 nm using a BioTek Synergy HTX Multi-Mode Microplate Reader (Agilent Technologies). For quantification, a standard curve of quercetin was used, with results expressed as grams of quercetin equivalents per 100 grams of dry extract (g QE/100 g).

4.2.4.1.3. High-performance liquid chromatography (HPLC)

The molecular composition of the PGE in Chapter 5 was analyzed through high-performance liquid chromatography (HPLC) using an Agilent LC 1100 series system (Agilent Technologies), shown in Figure 10, as previously described [134]. The HPLC setup included a pump, autosampler, UV–vis diode array detector (DAD), and column oven, all managed by Chemstation software. The chromatographic separation was performed on an Agilent Poroshell 120 RP-C18 column (4.6 × 150 mm, 2.7 µm), optimized for efficient resolution of phenolic compounds.

For compound separation, a linear gradient of 1% formic acid in water (solvent A) and acetonitrile (solvent B) was employed. The gradient began at 5% B, increased to 25% B over 30 minutes, then to 45% B by 45 minutes, before returning to 5% B at 51 minutes, with an additional 5 minutes for column re-equilibration. A consistent flow rate of 0.5 mL/min was maintained. The DAD monitored absorbance at 280, 320, and 340 nm, wavelengths commonly associated with phenolic compounds.

Compound identification was achieved using HPLC-DAD and a custom phenolic compound library. Peak retention times and UV spectra were compared with authentic standards and

literature data. Punicalagin, a primary phenolic compound in PGE, was identified using a molecular standard as the main component. OpenChrom 1.4 software (Lablicate GmbH, Hamburg, Germany) facilitated spectral interpretation and peak identification, ensuring precise characterization of the phenolic profile of the extract.

Figure 10. Agilent LC 1100 chromatograph, located at Miguel Hernández University and used for the characterization of the extract employed in the green synthesis of AgNPs.

4.2.4.1.4. Antioxidant capacity determination

The antioxidant capacity of the PGE was evaluated using the Trolox Equivalent Antioxidant Capacity (TEAC) assay, a widely-used method to quantify the ability of a sample to neutralize free radicals [135]. This assay relies on the radical cation $ABTS^{\bullet+}$, which is generated by reacting ABTS (2,2'-azinobis-(3-ethylbenzothiazoline-6-sulfonic acid)) with potassium persulfate. After incubating the ABTS solution with potassium persulfate for 12–24 hours at room temperature, the $ABTS^{\bullet+}$ radical cation, characterized by its intense blue-green color, is formed.

For the assay, the $ABTS^{\bullet+}$ solution was diluted with water to achieve an absorbance of 0.70 (± 0.02) at 734 nm, corresponding to an approximate concentration of 45 µM. When the PGE samples were added, antioxidants within the extract reduced $ABTS^{\bullet+}$, leading to a decrease in color intensity proportional to the antioxidant content of the sample. This change in color was measured at 734 nm, allowing the quantification of the antioxidant capacity of the sample.

A standard curve was prepared using Trolox, a water-soluble analog of vitamin E, with concentrations up to 10 µM. The antioxidant capacity of PGE was calculated by comparing sample absorbance changes to the Trolox standard curve, and results were expressed as millimoles of Trolox equivalents per 100 grams of dry extract (mmol TE/100 g).

4.2.4.1.5. Protein determination

The protein content of the PGE was determined using the Bradford assay, originally developed by Bradford (1976) and commonly used for protein quantification due to its sensitivity and speed [136]. This method relies on the binding of Coomassie Brilliant Blue G-250 dye to proteins, which induces a spectral shift in the absorbance maximum from 465 nm (unbound) to 595 nm (protein-bound). This shift is visually identifiable by a color change from brown to blue, with the intensity of the blue color being directly proportional to the protein concentration in the sample.

To quantify protein content, a standard curve was generated using BSA as the reference protein. Known BSA concentrations were prepared and reacted with the Coomassie dye under identical conditions as the PGE samples, creating a calibration curve that enabled precise protein quantification. For each assay, 200 µL of Coomassie Brilliant Blue G-250 reagent was added to either BSA standards or PGE samples, bringing the total volume in each reaction tube to 1 mL.

After a short incubation period to allow for full color development, absorbance readings at 595 nm were taken using a BioTek Synergy HTX Multi-Mode Microplate Reader (Agilent Technologies). The absorbance of each sample was compared to the BSA standard curve to determine protein concentration, expressed in terms of mg protein per g of dry extract.

4.2.4.1.6. Total reducing sugars

Reducing sugars in the PGE were quantified using a modified version of the DNS method, originally described by Miller (1959) [137]. This colorimetric assay is commonly used for quantifying reducing sugars because it relies on the ability of free aldehyde or ketone groups in sugars to reduce DNS, resulting in the formation of 3-amino-5-nitrosalicylic acid, a compound with a characteristic reddish-brown color. The intensity of this color correlates with the concentration of reducing sugars in the sample and can be quantified by spectrophotometry.

To prepare the DNS reagent, 1.87 g of 3,5-dinitrosalicylic acid and 3.48 g of sodium hydroxide (NaOH) were dissolved in distilled water. Then, 53.9 g of sodium potassium tartrate (used to stabilize the color complex), 1.34 mL of phenol, and 1.46 g of sodium metabisulfite were added to the solution. This mixture was brought to a final volume of 250 mL with distilled water, creating the DNS reagent necessary for the assay.

A standard curve was generated using known concentrations of glucose, providing a reference to calculate the reducing sugar concentration in the PGE samples. For each assay, 1 mL of the glucose standard or PGE sample was mixed with 1 mL of DNS reagent. The reaction mixture was then incubated in a boiling water bath for 5 minutes to facilitate the reduction process. Following this, the samples were cooled to room temperature, and absorbance readings were taken at 540 nm using a BioTek Synergy HTX Multi-Mode Microplate Reader (Agilent Technologies).

4.2.4.2. Characterization of nanomaterials

4.2.4.2.1. FESEM

The morphological structure of the materials analyzed in this Thesis was studied using Field Emission Scanning Electron Microscopy (FESEM) with a Schottky cathode SIGMA 300 VP (Zeiss, Oberkochen, Germany), equipped with an energy-dispersive X-ray (EDX) system to assess the elemental composition of the samples (Figure 11). For the morphological examination of NFs in Chapters 2 and 5, samples were first sputter-coated with chromium to enhance imaging quality. In general, samples were imaged at 1 kV electron high tension (EHT) with a secondary electron detector (SE2) to capture detailed surface features. After capturing images, the average diameter of various NF types was measured using ImageJ software (National Institutes of Health), based on 100 measurements per NF type from multiple FESEM images. To assess size uniformity, the coefficient of variation (CV) was calculated by dividing the SD by the mean diameter.

Figure 11. FESEM equipment, model SIGMA 300 VP by ZEISS, with a Schottky hot cathode field emission source, located at Miguel Hernández University.

For AgNP morphology analysis in Chapter 5, a drop (approximately 10 µL) of each AgNP solution was placed onto a silicon wafer and allowed to dry. These samples were imaged under an electron high tension of 10-20 kV using a backscattered electron detector (AsB), which is suitable for visualizing MNPs.

The AgNP-TPU materials studied in Chapter 3 were imaged using both backscattered electron (BSE) and variable pressure secondary electron (VPSE) detectors, allowing for a comprehensive view of the surface and internal morphology of the material.

4.2.4.2.2. UV-vis

UV-vis spectrophotometry was employed in Chapter 5 to confirm the successful formation of AgNPs by detecting the characteristic absorption peak associated with localized surface plasmon resonance (LSPR). This LSPR band results from the collective oscillation of electron density at the metal-medium interface, induced by interactions between incident photons and MNPs. The LSPR peak arises when the frequency of incident photons matches the natural frequency of surface plasmons, leading to an absorption peak observable in the UV-vis spectrum [138].

The UV-vis spectrum of the synthesized AgNPs was obtained using a 1 cm path length quartz cell on a Shimadzu UV-1700 UV-vis spectrophotometer (Kyoto, Japan). The absorbance of the solutions was measured at room temperature across a wavelength range of 250–800 nm with a resolution of 1 nm.

4.2.4.2.3. FTIR

In Chapters 2 and 5, Fourier Transform Infrared (FTIR) spectroscopy was employed to identify the chemical bonds present in the evaluated samples through the generation of an infrared absorption spectrum. A Spectrum Two™ FTIR spectrometer (PerkinElmer, MA, USA) was used for this analysis. Samples were powdered and thoroughly mixed with KBr in a mortar before being pressed into pellets. Four spectral scans were averaged in transmission mode across the spectral range of 4000–450 cm^{-1} with a resolution of 4 cm^{-1} at room temperature.

4.2.4.2.4. Electrophoresis

Electrophoresis is a technique used to separate molecules based on their size and charge, and it was utilized in Chapter 2 to assess protein integrity in the NFs following electrospinning through SDS-PAGE analysis. For this purpose, NFs obtained from 5 to 15% protein solutions were redissolved in water to achieve protein concentrations of 10 μg/μL. These samples were then separated under denaturing conditions by SDS-PAGE using 4–20% TGX gels (Bio-Rad Laboratories Inc.) and visualized with Coomassie Brilliant Blue R-250 staining (Bio-Rad Laboratories Inc.). Molecular weight markers (Precision Plus Protein Standards Dual Color, Bio-Rad Laboratories Inc.) were loaded into the first well of the gel to serve as a reference for protein sizing.

4.2.4.2.5. DLS

Dynamic Light Scattering (DLS) and ZP analyses were employed in Chapters 3 and 5 to determine particle size distribution in suspension and surface charge of NPs, respectively. The average HDD, PDI and ZP of the AgNPs were measured using a Zetasizer Nano-ZS ZEN 3600 (Malvern Instruments Limited, Worcestershire, United Kingdom). For ZP analysis, AgNP samples were placed in U-shaped capillary cells. Measurements were conducted at 25 °C in triplicate. Before analysis, the AgNPs were suspended in Milli-Q water and sonicated for 10 minutes to ensure adequate dispersion.

4.2.4.2.6. ICP-MS

Inductively Coupled Plasma Mass Spectrometry (ICP-MS) is an elemental and isotopic inorganic analysis technique capable of identifying and quantifying elements with high sensitivity. In Chapter 3, ICP-MS was used to determine the ionic composition of moieties released from the TPU plates. Analyses were conducted using an ICPMS-2030 instrument (Shimadzu) calibrated with standards for ^{107}Ag, ^{27}Al, and ^{24}, ^{25}, and ^{26}Mg, achieving regression coefficients (R^2) equal to or greater than 0.9996 for all calibration curves.

The test samples consisted of Milli-Q water incubated with the TPU plates at 20 °C for 2, 8, and 24 hours, with the latter being the incubation period specified by ISO 21702:2019 for antiviral activity testing. Prior to analysis, these samples were diluted 1:30 (v/v) with 1% (v/v) nitric acid to reach a final volume of 3 mL.

4.2.4.2.7. XRD

X-ray diffraction (XRD) is an analytical technique that enables the determination of the three-dimensional geometry of crystalline materials. In Chapter 5, XRD was employed to confirm the formation of AgNPs by verifying their crystalline structure. XRD patterns were collected using a D8 Advance diffractometer (Bruker, Karlsruhe, Germany) equipped with a 1D LynxEye detector and Ni-filtered Cu Kα radiation. The powdered sample was placed in a low-background off-cut silicon crystal sample holder. Diffraction patterns were recorded at room temperature in Bragg-Brentano geometry, scanning the angle range $5° \leq 2\theta \leq 80°$, with a step size of 0.01° and a dwell time of 1 second per step.

4.2.5. Biological properties

4.2.5.1. Cytotoxicity assays

The potential cytotoxicity of moieties released from AgNP-TPU materials when incubated with aqueous inocula was assessed in EPC and Vero E6/TMPRSS2 cell lines in Chapter 3. Culture media appropriate for each cell type were used as test inocula, incubated at 20 °C (EPC medium) or 30 °C (Vero E6/TMPRSS2 medium) for 24 hours with both control and AgNP-TPU materials. Cell viability was determined by measuring the reduction of MTT, a compound reduced by

cellular mitochondrial enzymes to produce an insoluble purple formazan product, which correlates with the number of viable cells.

For this assay, confluent cell monolayers in 96-well plates were treated with the collected inocula at 1:10 and 1:100 dilutions in fresh media (100 µL per well). After 24 hours of incubation under specific growth conditions for each cell line, the treatment media were replaced with fresh medium containing 0.5 mg/mL MTT (from 10x stocks in PBS, Gibco, Thermo Fisher) at 100 µL per well. Cells were incubated with MTT for an additional 2 hours under the same conditions, after which the MTT solution was carefully removed. The resulting purple formazan product was dissolved in 100 µL of dimethyl sulfoxide (DMSO, Sigma), and absorbance was measured at 570 nm, with 620 nm as a reference wavelength, using a Cytation™ 3 cell imaging multi-mode microplate reader (BioTek Instruments, Inc., Winooski, VT, USA). Optical density values were expressed as percentages relative to the untreated control group, representing cell viability, calculated by the formula:

$$\text{Cell viability} = 100 * \frac{\text{Absorbance of treated cells}}{\text{Absorbance of untreated cells}}$$

4.2.5.2. Viral infections

In Chapter 3, the antiviral activity of AgNP-TPU materials was evaluated against two viruses. Initially, SVCV was used for general characterization of the viricidal properties. SVCV inocula at 10^5 focus-forming units (ffu) per mL in 2% FBS culture medium (SVCV infection medium) were incubated with the TPU plates under different temperature conditions (5, 10, and 20 ℃ for 24 hours) and time intervals (2, 8, and 24 hours at 20 °C). Subsequently, antiviral activity was tested against SARS-CoV-2, using inocula at 5×10^5 plaque-forming units (pfu) per mL incubated at 30 °C for 24 hours. For each condition, corresponding virus inocula were incubated with control TPU plates as a baseline comparison. Virus inactivation was assessed by calculating the percentage reduction in viral titers compared to control samples. SVCV and SARS-CoV-2 titers were determined using focus-forming and plaque assay methods, respectively. All experiments involving SARS-CoV-2 were conducted in biosafety level 3 (BSL-3) facilities at CNB-CSIC, following institutional guidelines.

4.2.5.3. Antibacterial activity

For the antibacterial assays in Chapters 2 and 5, bacteria were cultured in MH broth and incubated at 30 or 37 °C for 24 or 48 hours, depending on the optimal growth conditions for each species.

Antibacterial activity was assessed using the broth microdilution method to determine the minimum inhibitory concentration (MIC) and minimum bactericidal concentration (MBC). A volume of 50 µL of each sample was added to the wells of a 96-well plate at varying concentrations, based on the sample. A 20 µL bacterial suspension, prepared to a 0.5 McFarland standard, was added to each well. The final volume in each well was adjusted to 200 µL with MH broth. Plates were incubated at 30 or 37 °C for 24 or 48 hours, depending on the bacterial strain. After incubation, 50 µL of INT solution (1 mg/mL) was added to each well and incubated for an additional 30 minutes. The MIC was defined as the lowest concentration where no color change (red) was observed. To determine the MBC, 50 µL from the wells that showed no visible bacterial growth was plated on MH agar plates and incubated overnight. The lowest concentration at which no colonies were detected was considered the MBC.

To observe the morphology of bacteria treated with AgNPs in Chapter 5, cells treated with the MIC for 24 hours were fixed on borosilicate cover glass slides following the protocol outlined by Pulingam et al. (2019) [139]. Briefly, the cells were initially treated with 4 % glutaraldehyde for 30 minutes, washed with PBS, and then further fixed with 1 % osmium tetroxide for an additional

30 minutes. The samples were progressively dehydrated with ethanol at concentrations of 30%, 50%, 70%, 80%, 90%, and 100%, with each step lasting 15 minutes. Micrographs of the bacteria were obtained using FESEM, and EDX analysis was performed to identify the presence of AgNPs within the bacterial cells.

4.2.5.4. Peroxidase activity

In Chapter 2, the peroxidase activity of HRP-IgG was determined to verify that its activity remained intact after incorporation into NFs via electrospinning. For this, stored samples of HRP-IgG-containing NFs were dissolved in Tris-buffered saline (TBS) to achieve a final 1:500 dilution of the initial HRP-IgG stock, or an equivalent dilution for control NFs without HRP-IgG. Two-fold serial dilutions were then prepared from these samples up to a 1:16,000 dilution. Fresh HRP-IgG was also diluted in parallel to serve as a positive control and to establish a calibration curve. Subsequently, 5 µL of each sample was added in triplicate to MaxiSorp™ 96-well plates (NUNC, Rochester, NY, USA) and incubated with an additional 95 µL of tetramethylbenzidine (TMB) substrate commercial solution for 30 minutes at 37 °C in the dark. The reaction was then stopped by adding 50 µL of 1 N H_2SO_4, and the absorbance was measured at 450 nm using an UltraEvolution automatic plate reader (Tecan, Männedorf, Switzerland).

4.2.5.5. Antigen-recognition activity

For the same purpose as the peroxidase assay, Chapter 2 describes the assessment of the viability of encapsulated HRP-IgGs using an adapted direct ELISA procedure. MaxiSorp™ 96-well plates were coated with 50 µL of a 1:4 dilution of an in-house hybridoma supernatant in TBS containing 0.4 mg/mL of protein, as determined using a Nanodrop 2000c (Thermo Scientific, Wilmington, DE, USA), and incubated overnight at 4 °C. After three washes of 5 minutes each with 200 µL of TBS supplemented with 0.05% (v/v) Tween-20 (TTBS) and one wash with TBS, the plates were blocked with 100 µL of 1% (w/v) BSA in TBS for 1 hour at 37 °C. Following the washing steps, 50 µL of each dilution of the dissolved NFs and corresponding control samples were added to the wells. The plates were incubated at 37 °C for 1 hour and washed again. Finally, the reaction was developed with TMB substrate (100 µL/well) and absorbance was measured as described above.

CHAPTER 1

5. RESULTS

CHAPTER 1: FISH SKIN MUCUS EXTRACTS: AN UNDEREXPLORED SOURCE OF ANTIMICROBIAL AGENTS

SUMMARY OF RESULTS

This review paper investigates the antimicrobial potential of fish skin mucus, a rich but underutilized source of bioactive molecules capable of combating pathogenic microbes. With the rapid emergence of antibiotic-resistant bacteria (ARB) and the slow pace of novel antibiotic discovery, researchers are increasingly exploring natural sources of antimicrobial agents. Fish skin mucus, which protects fish in microbe-rich marine environments, harbors a variety of molecules with antimicrobial properties, making it a promising candidate for new therapeutic options. This study provides a thorough overview of the bioactive compounds found in fish skin mucus, particularly AMPs, proteins, and various secondary metabolites, all of which contribute to its defense mechanism against bacteria, fungi, and viruses.

AMPs, such as piscidins, defensins, and histone-derived peptides, are highlighted for their ability to inhibit microbial growth by disrupting cell membranes, rendering it difficult for pathogens to develop resistance. These peptides exhibit broad-spectrum antimicrobial activity, targeting bacteria, fungi, protozoa, and even some viruses. Additionally, the mucus contains antimicrobial proteins like LYZ, which break down bacterial cell walls, and lectins, which prevent pathogen colonization by binding to microbial sugars. Other components include proteases that degrade pathogenic proteins, cytoskeletal proteins like keratin with pore-forming abilities, and lipid molecules that contribute to pathogen membrane destabilization. Together, these elements provide a multi-layered antimicrobial defense that supports fish survival in hostile environments.

Extraction techniques play a significant role in isolating these bioactive components. The study compares several extraction methods—aqueous, organic, and acidic—each of which can affect the activity and stability of the molecules. Aqueous extractions are the most commonly used but may lack the efficacy of organic or acidic extractions, which are better suited for isolating hydrophobic or cationic molecules, respectively. Organic solvents like ethanol and dichloromethane help extract hydrophobic compounds known for disrupting microbial membranes, while acidic solvents, such as acetic acid, are effective for isolating cationic peptides and low-molecular-weight proteins. Through these methods, the study cataloged the antimicrobial efficacy of mucus extracts across over 47 fish species, finding that the more intensive organic and acidic methods tend to yield extracts with higher antimicrobial potency against both Gram-positive and Gram-negative bacteria.

Further, the paper discusses the application of omics technologies—genomics, transcriptomics, proteomics, metabolomics, and multiomics—as essential tools for identifying and characterizing new antimicrobial agents within fish mucus. These technologies can expedite the discovery of novel bioactive compounds by providing comprehensive insights into the molecular composition of mucus, its functional properties, and how it varies across fish species and environmental conditions. This in-depth analysis could potentially reveal previously unidentified antimicrobial molecules that may be developed into drugs or therapeutic agents. Finally, it is emphasized the promising potential of fish skin mucus as an alternative source of antimicrobials for biomedical and veterinary applications and call for continued research to fully harness its antimicrobial capabilities. In a world facing rising AMR, this natural defense system in fish may offer valuable solutions for combating infections in humans and animals.

Fish Skin Mucus Extracts: An Underexplored Source of Antimicrobial Agents

Rocío Díaz-Puertas, Mikolaj Adamek, Ricardo Mallavia and Alberto Falco

Abstract

The slow discovery of new antibiotics combined with the alarming emergence of antibiotic-resistant bacteria underscores the need for alternative treatments. In this regard, fish skin mucus has been demonstrated to contain a diverse array of bioactive molecules with antimicrobial properties, including peptides, proteins, and other metabolites. This review aims to provide an overview of the antimicrobial molecules found in fish skin mucus and its reported in vitro antimicrobial capacity against bacteria, fungi, and viruses. Additionally, the different methods of mucus extraction, which can be grouped as aqueous, organic, and acidic extractions, are presented. Finally, omic techniques (genomics, transcriptomics, proteomics, metabolomics, and multiomics) are described as key tools for the identification and isolation of new antimicrobial compounds. Overall, this study provides valuable insight into the potential of fish skin mucus as a promising source for the discovery of new antimicrobial agents.

Keywords: marine organisms; fish; skin mucus; extract; antimicrobial; antibacterial; antifungal; antiviral; omics.

1. Introduction

The windfall for human and animal health in terms of effectively fighting infectious diseases is being threatened by the resurgence and appearance of dangerous pathogens, which largely outpace the discovery and implementation of new antimicrobials. Growing resistance to current antibiotics [140], antifungals [141], and antivirals [142] is one of the greatest reasons for this. This situation is substantially worsened by the long-lasting drought (with a few recent exceptions [143]) in the discovery of new classes of antibiotics since 1962 [140,144] and the continued scarcity and specificity of antifungals [145] and antivirals [146]. On top of that, factors including population growth, intensive farming, globalization, pollution, and climate change are also contributing notably to this issue by negatively unbalancing the pathogen–host–environment interplay [147].

Thus, in order to address the public health menace posed by both new and "renewed" infectious diseases that are quite often unfortunately associated with considerable morbidity and mortality, it is crucial to expand the arsenal of antimicrobials. This is because, even in an unfavourable scenario of rapid generation of antimicrobial resistance, their availability would at least help to buy time for the development of other countermeasures, such as effective vaccines. In this regard, different antimicrobial search and development strategies with high expectations are being adopted [148-150]. However, this is not an easy task.

To paraphrase Spellberg et al., (2007) [140], in this war against microorganisms, humanity has definitely underestimated the power of an enemy army that outnumbers, outweighs, and out-experiences us by several orders of magnitude in all its main divisions (viruses, bacteria, and fungi) (Table 4) [151-153]. Furthermore, as mentioned above, society is currently running out of effective ammunition, i.e., antimicrobials, because they have become obsolete in the face of today's new needs. In this sense, and particularly referring to antibiotics, it should not be disregarded that most of the known antibiotics, as well as their resistance determinants, already existed in nature since ancient times, and humans only discovered them [154]. Indeed, most of them are secondary metabolites or their synthetic derivatives (i.e., natural or semisynthetic antibiotics) that originated primarily from microorganisms, among which the actinobacteria of the genus *Streptomyces* stands out as having provided about two-thirds of the natural antibiotics

currently used clinically [155]. This should not discourage rational design efforts to expand the repertoire of synthetic antibiotics that, while still small (e.g., azoles, sulfones, ethambutol, nitrofurans, phenazines, quinolones, and thioamides), have already shown promise in terms of activity and safety [156,157]. However, there is no doubt that the search for natural antimicrobials in biological allies with far more combat experience against these enemies should continue, and that screening capabilities should be improved by exploiting existing and new technologies [150].

Table 4. Estimates of number, mass, and time of origin on Earth for taxa relevant to this study.

Variable[1]	Virus	Bacteria	Fungi	Human	Livestock	Fish
Number [158]	10^{31}	10^{30}	10^{27}	10^{10}	10^{10}	10^{15}
Mass, Gt C [158]	0.2	70	12	0.06	0.1	0.7
Time, years	3.8×10^9 [159][2]	3.8×10^9 [160]	1.5×10^9 [161]	3×10^5 [162]	84×10^6 [163]	5×10^8 [164]

[1] This table is intended to give a general idea of the enormous differences in magnitude in terms of number, mass, and time since emergence of the various taxa relevant to this study, in order to understand the great challenge addressed in this study. Of course, not all microorganisms pose a pathogenic threat. In fact, most of the antibiotics used come from bacteria and fungi [155], most of the viruses are bacteriophages that modulate the density of bacterial communities in the oceans [151,165], and, as a whole, microorganisms are critical elements in the regulation of ecosystems [151,160,165,166]. [2] Like other studies, the estimated time of the origin of viruses on Earth is proposed here to be the same as that of the origin of life.

2. Fish Skin Mucus as a Promising Source of Antimicrobials

In this context, marine ecosystems still remain an option with great potential for the discovery of new compounds, as they are relatively unexplored in this regard. Furthermore, they are the most extensive and ecologically diverse ecosystems, and, therefore, harbor the largest biological and hence biochemical diversity on the planet [167-170]. As expected, in this highly competitive environment [165,167], microorganisms are currently the fastest growing group of marine producers from which new compounds and antimicrobials are being discovered [171,172].

However, the contribution of higher counterparts, such as algae, plants, and animals, has been, and still is, particularly important [171,173], even considering that many compounds initially attributed to them may actually belong to associated or symbiotic microorganisms [171,174]. Among the animals, the majority of suppliers are invertebrates, mainly (in order of contribution) sponges as the overall top producer of marine natural compounds so far, molluscs, tunicates, coelenterates, echinoderms, and bryozoans [171,173]. In this ranking, the contribution of marine vertebrates, almost entirely represented by fish, is still rather modest (just right after coelenterates) [171,172], but certain factors, which will be commented on next, encourage further research into the potential antimicrobials that they may offer, especially from their skin mucus [175-177].

Fish are the oldest living vertebrates, with ancestors dating back to the mid-Cambrian period more than 500 million years ago. Among them, the ray-finned fishes (subclass *Actinopterygii*) are numerically dominant, with about 30,500 species, representing 95% of all fishes (about 32,000 species) and 50% of all vertebrates (about 60,000 species) (Table 4). They diverged about 385 My ago in the mid-Devonian period. The success of this divergence is represented by their enormous diversity as a consequence of having adapted to nearly any aquatic habitat since then [164,178]. This was made possible by a highly advantageous biological innovation (vertebrate evolution) and great genetic flexibility (gene duplication [179], teleost-specific whole-genome duplication events [180], and deletion of genome parts [181]) in a vast environment with extremely diverse conditions and high biological competition. However, this is also applicable to microorganisms.

Marine ecosystems are regulated by complex interactive fluxes that are primarily controlled by microorganisms due to the predominance of their biomass [182]. With a focus on viruses, bacteria, and fungi, some quantitative studies have estimated the abundance of each of the first two groups in the millions per milliliter of seawater [165,183,184]. The virus is the predominant microorganism in the ocean, accounting for about 1030 particles, about 15 times more than estimated bacteria (and archaea) [165]. There is little information on the quantitative abundance of fungi in aquatic environments, although it is assumed to be relatively high based on data on their enzymatic activity in certain environments compared to bacteria [185]. However, of note is not only their quantity, but also the extremely high diversity observed in all these groups, which also comprise pathogenic microorganisms [165,167,183,185].

As a result, fish have co-evolved under this selective pressure by also developing a complex network of defense mechanisms, such as the adaptive immune system [186-188]. However, although they have one of the earliest forms of adaptive immunity, their innate immunity still plays a central role in protecting them from and responding to infection [186,189], especially through a complex system of mucosal barriers responsible for fending off pathogens on first contact [186,189,190]. In fact, leukocyte distribution in fish is more organized in the mucosal tissues of the gut, gills, and skin than in the liver or gonads, for example [186,190]. Besides the cellular immune component, the humoral aspect of these tissues is of special relevance because of its antimicrobial function [191]. Among these major mucosa-associated lymphoid tissues (MALT), i.e., gut (GALT), gills (GIALT), and skin (SALT), mucosal glands are much more numerous in the skin [189,192], which is reasonable considering its continuous and intimate exposure to large amounts of microorganisms [165,183-185]. Together with the fact that the skin is the largest tissue of any organism and its mucus can be obtained non-invasively, the use of such fish fluid for biomedical purposes is very promising given its content of antimicrobial factors [193-195]. This is particularly true considering the large fish farming industry already established, which can valorize these previously overlooked natural by-products.

To explore the potential of fish mucus as a valuable source of antimicrobials, this review study conducted a search of the scientific databases PubMed, Scopus, and Web of Science. Keywords, such as "fish skin mucus," in combination with "antimicrobial activity" or "composition," were used in the search. The search period included studies published from the earliest available records to the present to ensure a thorough investigation. Inclusion criteria for the articles were: (i) published in English; (ii) in peer-reviewed journals; (iii) focused on the in vitro antimicrobial activity of fish skin mucus; and (iv) sufficiently described the mucus extraction method. Studies were selected based on their relevance to the topic and their adherence to predefined criteria.

3. Composition of Fish Skin Mucus in Innate Immunity Antimicrobial Molecules

The mucosal layer is a biochemical matrix that serves as a protective interface between the fish and the external environment [196]. Its multiple functions, which can be summarized as mechanical, physiological, and immunological, are dependent on its molecular components [177,196]. These are secreted by specific cell types (i.e., goblet, club, and sacciform cells) and the overall composition is influenced by developmental, hormonal, environmental, and nutritional factors [177,196,197]. The high-molecular-weight glycoproteins, called "mucins," are the most representative component of the mucus and provide it with the characteristic gel structure that allows for the correct performance of all the above-mentioned functions [177,189,196-198]. The immunologic importance of this mucosal layer and its epithelial scaffold is demonstrated by the fact that its disruption increases the incidence and severity of infections [199,200]. In a recent example study, it was shown that such a disruption caused by the cyprinid herpesvirus 3 (CyHV-3) facilitates the occurrence of secondary infections that are ultimately responsible for

exacerbated health complications and even death [200]. Besides the mucins themselves, which have been reported to have direct antimicrobial activity, fish skin mucus also contains a broad repertoire of antimicrobial factors apart from antibodies [175,189,190,197,201]. Mucus has often been recognized as a source of new antimicrobials [176,202,203]. Known compounds are summarized in this section.

3.1. Antimicrobial Peptides (AMPs)

AMPs, also known as Host Defense Peptides (HDPs), are gene-encoded peptides of up to approximately 80 amino acid residues, mostly characterized by a cationic, amphipathic chemical nature and antimicrobial properties. They are ancient innate immune molecules present in all groups of organisms. Their mature forms in eukaryotic cells are often cysteine-rich molecules with multiple intramolecular disulfide bridges. Through conservation or reduction of these bonds, some families of AMPs can modulate their type and/or level of activity [204-207]. For instance, in defensins (one of the most studied families of AMPs), some reports on a particular group of human beta-defensins indicate that the reduction of such bonds affects their function by disabling their chemotactic activities and triggering their direct antimicrobial ones [206]. Indeed, AMPs are generally known for their microbicidal activity exerted directly on the target microorganism, but they can also be endowed with potent immunomodulatory and receptor-mediated chemotactic activities, which together explain their broad antimicrobial activity against bacteria, protozoa, fungi, and both enveloped and non-enveloped viruses, as well as the difficulty of selecting resistant mutants against them [204,205]. In general, the mechanism of action for their direct antimicrobial activity is based on the affinity and fixation of the peptide to the generally anionic surface membrane of the pathogen and its subsequent destabilization through pore formation or, simply, bilayer disruption [204].

The large number of AMPs discovered (the Antimicrobial Peptide Database (APD) of the University of Nebraska Medical Centers currently counts 3569 and growing [accessed 5 May 2023]) can be classified into different families based on (i) their primary sequence; (ii) the presence and organization of various functional regions, such as the propeptide, which inhibits and protects the region corresponding to the mature peptide until its cleavage and is located at either the C- or N-terminal; (iii) their molecular structure, for which the simplest distinction is between linear and disulfide-stabilized peptides, and, in the latter case, the number, location, and association pattern of their cysteine residues; and (iv) the origin of the mature peptide, which may be produced directly after typical post-translational modifications and minor cleavages of accessory regions as it occurs in most cases, but may also be derived from the cleavage of a larger protein, often with a very different primary function, e.g., peptides derived from histone and ribosomal proteins [95,204,208,209].

Given the importance of these molecules in the innate immune system, they are extremely diverse in fish and include not only families of AMPs found in other animal groups, such as cathelicidins, defensins, hepcidins, and histone-derived peptides, but also exclusive fish AMP families, such as piscidins and pleurocidins [208,209]. Probably also for this reason, the skin mucus is the major source of AMPs in fish, with approximately 70% of all AMPs expressed in the skin compared to 52% and 29% expressed in the gills and the gut, respectively [189,192]. Besides expression, several AMPs were isolated from skin mucus, and their antimicrobial activities were tested. Representatives of several families of AMPs isolated from skin mucus are listed in Table 5.

Table 5. Examples of AMPs isolated from skin mucus.

Family	AMP	Species	Ref.
Histone 2A*	N-acetylated Histone 2A	*Oncorhynchus mykiss*	[210]
	Hipposin	*Hippoglossus hippoglossus*	[211]
	Parasin I	*Parasilurus asotus*	[212,213]
Histone 2B*	Histone H2B	*Gadus morhua*	[214]
Histone H1*	Oncorhyncin II	*O. mykiss*	[215]
	SAMP H1	*Salmo salar*	[216]
Myxinidin	Myxinidin	*Myxine glutinosa*	[217]
Non-histone chromosomal protein H6 *	Oncorhyncin III	*O. mykiss*	[218]
Pelteobagrin	Pelteobagrin	*Pelteobagrus fulvidraco*	[219]
Pardaxin	Pardaxin I, II	*Pardachirus marmoratus*	[220]
Piscidin	Piscidin 1, 2, 2β	*G. morhua*	[221]
Pleurocidin	Pleurocidin	*Pleuronectes americanus*	[222]
Ribosomal proteins*	40S Ribosomal protein S30	*O. mykiss*	[223]
	60S Ribosomal protein L35, L36A, L40	*G. morhua*	[214]

* peptides derived from these proteins.

Histone-derived AMPs were first described in fish [224] just a few years after their discovery in the Asian toad *Bufo bufo gargarizans* [225]. Robinette et al., (1998) [224] isolated two histone-like proteins (HLP-1 and HLP-2) in the epidermis of channel catfish that were found to be inhibitory to bacterial and fungal pathogens. Shortly thereafter, several histone-derived peptides were isolated from fish skin mucus [210-213]. In general, this family of AMPs is thought to be released from cells during infection-induced apoptosis [226]. Oncorhyncin III is a 66-residue N-terminal fragment of the non-histone chromosomal protein H6 from *Oncorhynchus mykiss* skin mucus and was shown to be active against Gram-negative and Gram-positive bacteria [218]. Other AMPs derived from larger proteins isolated from skin mucus are the peptidic fragments from the 40S and 60S ribosomal subunits. The AMP 40S ribosomal protein S30 was found in rainbow trout and showed antibacterial activity against Gram-positive bacteria [223]. The 60S ribosomal proteins L40, L36A, and L35 were isolated from Atlantic cod (*G. morhua*) mucus extracts [214].

Other peptides found in fish skin mucus include myxinidin, pardaxin, pelteobagrin, and piscidin, all of which are unique to this group of animals and have been reported to have broad-spectrum antimicrobial activity. Myxinidin is a cationic 12-amino acid peptide isolated from the skin mucus of hagfish (*M. glutinosa*) [217]. Pardaxin was first isolated from the Red Sea Moses sole (*P. marmoratus*) and described as a single, helical, monomeric, acidic toxin [220]. Its antibacterial activity against Gram-negative and Gram-positive bacteria was subsequently demonstrated [227]. Pelteobagrin is a 20-amino acid amphipathic α-helical peptide and was identified in the skin mucus of yellow catfish (*P. fulvidraco*) [219]. The piscidin family also comprises α-helical peptides, with low molecular weight and cationic charge at physiological pH [228] .

3.2. Proteins

Animal mucosa, in a broad sense, is characterized by the presence of mucins, which are glycosylated proteins responsible for providing viscoelastic and rheological properties, as well as trapping pathogens and contributing to cell surface signaling [175]. Additionally, they possess a diverse range of other proteins, including many with antimicrobial/immune-related and structural functions [189,190,196,197]. In this sense, a large number of defense proteins against pathogens have been described in fish mucosa, especially in the skin, besides the immunoglobulins IgG and the teleost-specific IgT [189,190,197].

Other types of glycoproteins have been found in fish skin mucus. For example, Ebran et al., (2000) [229] isolated and characterized glycoproteins from rainbow trout (*O. mykiss*), European eel (*Anguilla anguilla*), and tench (*Tinca tinca*) skin mucus. These proteins possess both α-helix and random coil structures and show antibacterial activity correlated with pore-forming properties. Transferrin glycoprotein has also been isolated from Atlantic cod [230] and Atlantic salmon (*Salmo salar*) [231] skin mucus. Transferrin is responsible for iron transporting in absorption, storage, and disposal sites in vertebrates. As all organisms require iron for their growth, transferrin plays an important role in the innate defense mechanisms of fish by binding to iron and reducing its availability to pathogens by chelating it [232].

Lectins are a diverse class of highly specific carbohydrate-binding proteins [233]. They have been found in the skin mucus of fish, where they provide an external defense mechanism via the agglutination process to stop pathogen penetration and colonization [234]. There are several types of different lectins depending on their structure; for example, C-type lectins, whose binding is dependent on Ca^{2+}, F-type lectins or fucolectins, which are distinguished by their α-l-fucose recognition domain, galectin family or S-type, which require thiol, and pentraxins or pentameric lectins, or P-type lectins, which target glycoproteins containing mannose 6-phosphate [233]. The isolation of C-type lectins has been described in cichlid (*Symphysodon aequifasciata*) skin mucus [235]. Another example includes fucose-binding lectin (FBL, F-type lectin), which was identified in European sea bass (*Dicentrarchus labrax*) skin mucus [236] and is responsible for the agglutination, immobilization, and opsonization of microorganisms and phagocyte activation. Mannose-binding lectin (MBL, P-type lectin) and galectin were also found in Atlantic cod skin mucus [237]. MBL plays a significant role in opsonization and the initiation of the lectin pathway of complement activation, and galectin binds to pathogens and orchestrates several immune processes. Another type of MBL, named "pufflectin," was reported in pufferfish (*Takifugu rubripes*) [238]. Pentraxins play an important role in inflammatory responses and pathogen recognition and have been identified in common skate (*Dipturus batis*) [239] and lumpsucker (*Cyclopterus lumpus*) [240] skin mucus. C-reactive protein (CRP) belongs to the pentraxin family, and it is part of the innate immune defense system because it has the ability to activate the classical complement pathway [241]. CRP was reported in tilapia (*Tilapia mossambica*) skin mucus, and its levels were found to increase in response to inflammation and necrosis [242].

Lysozyme (N-acetylmuramide glucanohydrolase or muramidase) is a bacteriolytic enzyme and an important component of the immune system. It has been reported in the skin mucus of several fish species, including mrigal carp (*Cirrhinus mrigala*), catla (*Catla catla*), spotted snakehead (*Channa punctata*), Japanese eel (*Anguilla japonica*), and Nile tilapia (*Oreochromis niloticus*) [243-245]. Given its ability to hydrolyze the bond between N-acetylmuramic acid and 3-acetyl amino-2-deoxy-D-glucose residues of the mucopolysaccharide found in bacterial cell walls [246], it acts directly on Gram-positive bacteria. In Gram-negative bacteria, lysozyme can also attack the inner peptidoglycan layer after the disruption of the outer wall by complement and other enzymes [244].

Proteases are enzymes of great importance in the mechanisms of the immune system. Their role is to hydrolyze the peptide bonds of proteins. Proteases can be classified into serine, cysteine, aspartic, and metalloproteases based on their catalytic mechanisms [197]. They are associated with resistance to infection because of their ability to degrade the proteins of pathogens. Proteases, including trypsin (serine protease), cathepsin B and L (cysteine proteases), cathepsin D (aspartic protease), aminopeptidases, and metalloproteases, have been reported in the skin mucus of several species, such as rainbow trout [247], Japanese eel [248], European eel [249], catfish (*Parasilurus asotus*) [213], and Atlantic salmon [250].

Cytoskeletal proteins with potential antimicrobial activity have also been reported in fish skin mucus. For example, keratin has been identified in skin mucus from lumpsucker [240], Atlantic

cod [237], European sea bass [236], and gilthead sea bream (*Sparus aurata*) [251]. Although keratin is a structural protein, pore-forming properties have also been described in keratin from the skin mucus of rainbow trout [252] and may therefore contribute to host defense against water-borne pathogens. Likewise, actin is a structural protein involved in several roles associated with cellular membranes, such as cell migration, phagocytosis, pinocytosis, cytokinesis, and cytoplasmic streaming [253]. Beta actin has been reported in lumpsucker [240], European sea bass [236], Atlantic cod [237], and gilthead sea bream [251,254]. Increased actin fragmentation by proteases has been linked to stress situations, and actin fragments generated could trigger an immune response [255].

3.3. Other Components

The lipid composition of fish skin mucus has not been studied as thoroughly as other mucous secretions, such as gut mucus. However, some studies show that skin mucus may also be a significant source of lipids. Mono-unsaturated fatty acids (MUFA), such as oleic acid, poly-unsaturated fatty acids (PUFA), such as linoleic, alpha-linoleic, docosahexaenoic, arachidonic, eicosapentaenoic, and moroctic acid, and saturated fatty acids (SFA), such as palmitic and stearic acid, have been reported in gilthead sea bream and flathead grey mullet (*Mugil cephalus*) [256,257]. Lipids are thought to be involved in maintaining the internal structure of the mucus through interactions with glycoproteins [258]. Figure 12 shows the chemical structures of the compounds mentioned in this paragraph.

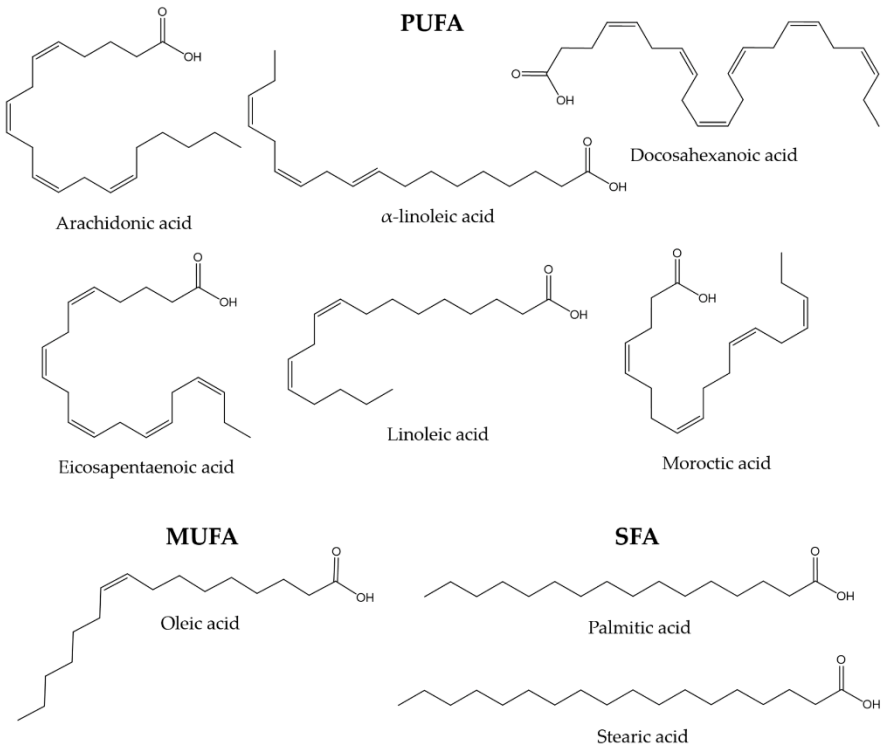

Figure 12. Chemical structures of some MUFA, PUFA, and SFA molecules found in the skin mucus of gilthead sea bream and flathead grey mullet [118,119].

Regarding other types of molecules, Ekman et al. (2015) [259] described the metabolite profile of fathead minnow (*Pimephales promelas*) skin mucus with the aim of providing a tool for environmental monitoring and surveillance. Some of the metabolites found are associated with antibacterial properties. For instance, azelaic acid has been shown to inhibit bacterial growth by interfering with protein synthesis [260], and hydroxyisocaproic acid has been found to be effective against both bacteria and fungi [261]. In another study conducted by Patel et al. (2020) [262], the metabolic profile of the skin mucus of the pool barb (*Puntius sophore*) was characterized. In this

research, compounds found with proven antimicrobial activity included amino sugars, such as glucosamine and neuraminic acid, cysteamine (organic disulfide), dihydrosphingosine (amino alcohol), and phytosphingosine (sphingolipid), among others. Figure 13 shows the chemical structures of the compounds mentioned in this paragraph.

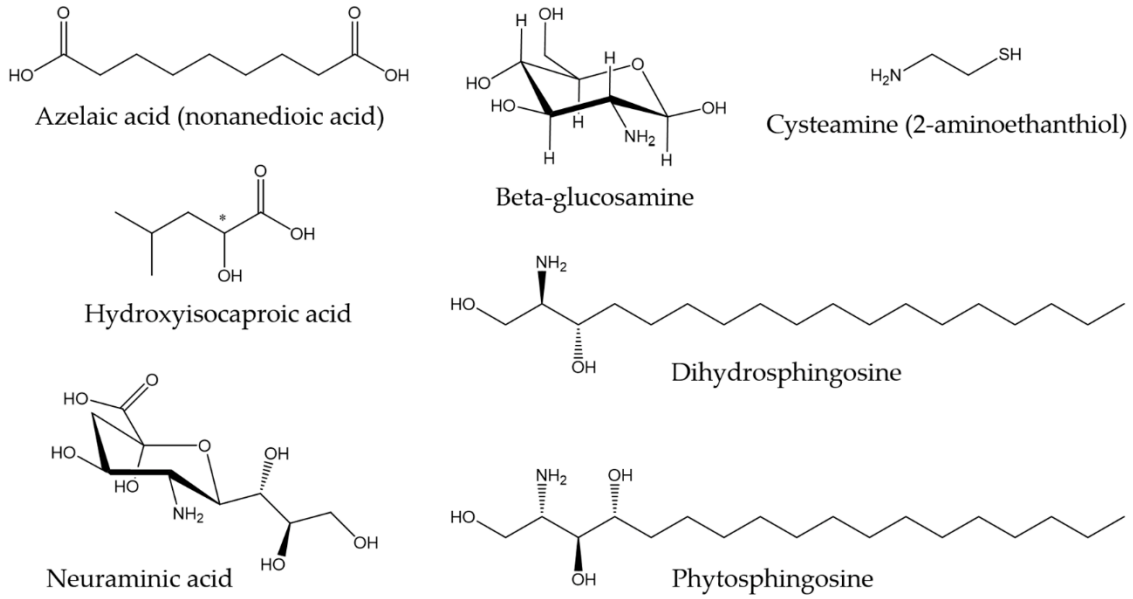

Figure 13. Chemical structures of other metabolites found in skin mucus of fathead minnow and pool barb [259,262].

4. Antimicrobial Activity of Fish Skin Mucus

The humoral component of fish skin mucus has been extensively studied for its high content in molecules endowed with antimicrobial properties and, thus, its potential for implementation in biomedical and veterinary applications [176,189,190,197]. Such a variety of compounds has also necessitated the use of different molecular extraction approaches in mucus samples (Figure 14) [202,263]. However, it appears that the amount of functional data is relatively small compared to the overall progress made in researching and developing new methods. This section summarizes the activity demonstrated against different groups of microorganisms by different types of fish skin mucus extracts, mentioning the techniques used to determine this activity when specified in the studies.

4.1. Antibacterial Activity of Fish Skin Mucus Extracts

Fish skin mucus has proven to be effective against bacteria that affect not only fish, but humans as well. Table 6 summarizes the results of an extended list of studies on antibacterial activity of fish skin mucus extracts. In total, there are 47 fish species represented, most of which are teleosts (exceptions include *Myxine glutinosa* (Myxini) and *Dasyatis pastinaca* (Elasmobranch)). The different extraction methods can be divided almost entirely into aqueous, organic, and acidic extractions. Some authors also used crude mucus with only minor processing steps.

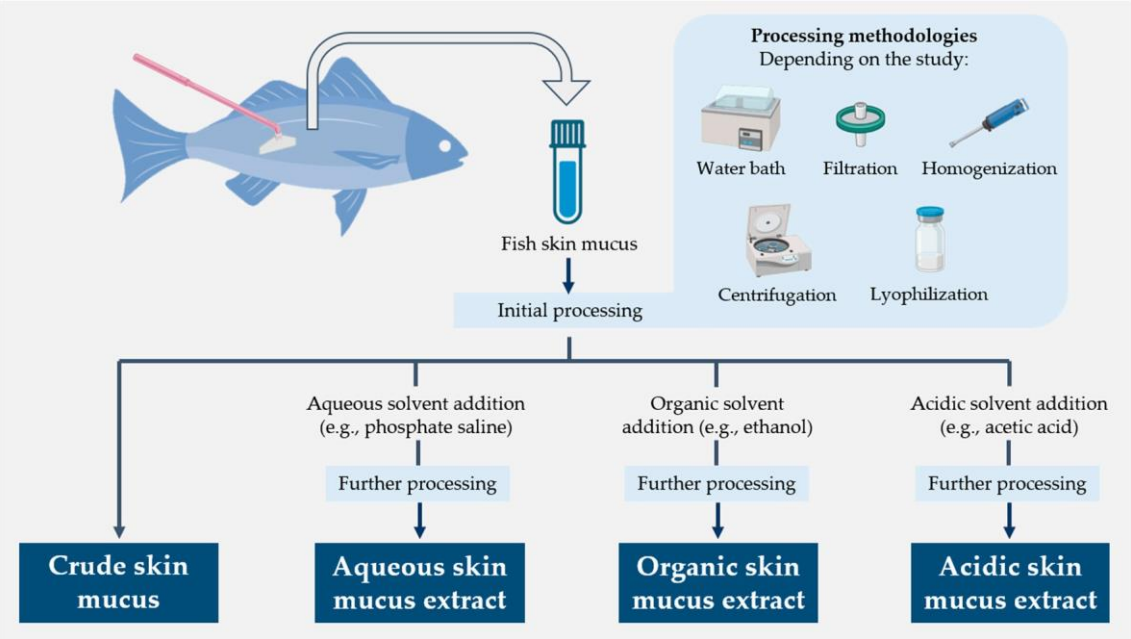

Figure 14. Schematic diagram summarizing the different molecular extraction approaches used for fish skin mucus samples [202,263].

Table 6. Antibacterial effect observed in extractions of mucus of different fish species.

Extraction	Aqueous								Organic				Acidic				Crude		Ref
Solvent	W		AB		PS		TBS		E		DCM		AA		TFA				
Gram	+	-	+	-	+	-	+	-	+	-	+	-	+	-	+	-	+	-	
Perciformes order																			
Amphiprion clarkii																			[264]
Anabas testudineus																			[265]
Argyrosomus regius																			[266]
Channa argus																			[267]
Channa marulius																			[268]
Channa micropeltes																			[268]
Channa striata																			[268-271]
Dentex dentex																			[272]
Dicentrarchus labrax																			[266, 272-274]
Epinephelus marginatus																			[272]
Epinephelus tauvina																			[275]
Labrus bergylta																			[276, 277]
Morone saxatilis																			[278]
Oreochromis niloticus																			[279-281]
O. mossambicus																			[282]
Pagellus bogaraveo																			[273]
P. schlosseri																			[283]
Sparus aurata																			[266, 272, 274]
Umbrina cirrosa																			[272]
Anguilliformes order																			
Anguilla anguilla																			[273, 284]

Table 6. Antibacterial effect observed in extractions of mucus of different fish species.

Extraction	Aqueous								Organic				Acidic				Crude		Ref
Solvent	W		AB		PS		TBS		E		DCM		AA		TFA				
Gram	+	-	+	-	+	-	+	-	+	-	+	-	+	-	+	-	+	-	
Siluriformes order																			
Arius maculatus																			[285]
Clarias batrachus																			[280, 282, 286, 287]
Heteropneustes fossilis																			[271]
Rita rita																			[288]
Cypriniformes order																			
B. schwanenfeldii																			[289]
Catla catla																			[284, 290, 291]
Cirrhinus mrigala																			[284, 292, 293]
Ctenopharyngodon idella																			[290, 291, 294]
Cyprinus carpio																			[278, 294]
H. nobilis																			[290, 291, 294, 295]
Labeo rohita																			[290, 291]
Puntius sophore																			[262]
Anabantiformes order																			
Channa gachua																			[268]
Channa punctatus																			[268, 288, 293]
Myliobatiformes order																			
Dasyatis pastinaca																			[296]
Gadiformes order																			
Gadus morhua																			[214, 276]
M. aeglefinus																			[278]
Pollachius virens																			[276]
Myxiniformes order																			
Myxine glutinosa																			[278]
Salmoniformes order																			
Oncorhynchus mykiss																			[297]
Salvelinus alpinus																			[278]
Salvelinus fontinalis																			[278]
Pleuronectiformes order																			
Platichthys flesus																			[276]
Scophthalmus rhombus																			[276]
Scophthalmus maximus																			[274]
Solea senegalensis																			[298]
Solea solea																			[276]

Antibacterial effect: no effect; low or variable inhibition; strong inhibition. W: water; AB: ammonium bicarbonate; PS: phosphate saline; TBS: Tris-buffered saline; ET: ethanol; DCM: dichloromethane; AA: acetic acid; TFA: trifluoroacetic acid. Fish family and species full names: *Anabantidae*: *Anabas testudineus* Bloch; *Anguillidae*: *Anguilla anguilla* L.; *Ariidae*: *Arius maculatus* Thunberg; *Bagridae*: *Rita rita* Hamilton; *Channidae*: *Channa argus* Cantor, *Channa* gachua Hamilton, *Channa marulius* Hamilton, *Channa micropeltes* G. Cuvier, *Channa punctatus* Bloch, *Channa striata* Bloch; Cichlidae: *Oreochromis mossambicus* W. K. H. Peters, *Oreochromis niloticus* L., *Clarias batrachus* L.; *Cyprinidae*: *Barbonymus schwanenfeldii* Bleeker, *Catla catla* Hamilton, *Cirrhinus mrigala* Hamilton, *Ctenopharyngodon idella* Valenciennes, *Cyprinus carpio* L., *Hypophthalmichthys nobilis* Richardson, *Labeo rohita* Hamilton, *Puntius sophore* Hamilton; *Dasyatidae*: *Dasyatis pastinaca* L.; *Gadidae*: *Gadus morhua* L., *Melanogrammus aeglefinus* L., *Pollachius virens* L.; *Heteropneustidae*: *Heteropneustes fossilis* Bloch; *Labridae*: *Labrus bergylta* Ascanius; *Moronidae*: *Dicentrarchus labrax* L., *Morone saxatilis* Walbaum; *Myxinidae*: *Myxine*

glutinosa L.; *Oxudercidae*: *Periophthalmodon schlosseri* Pallas; *Pleuronectidae*: *Platichthys flesus* L.; *Pomacentridae*: *Amphiprion clarkii* Bennet; *Salmonidae*: *Oncorhynchus mykiss* Walbaum, *Salvelinus alpinus* L., *Salvelinus fontinalis* Mitchill; *Sciaenidae*: *Argyrosomus regius* Asso, *Umbrina cirrosa* L.; *Scophthalmidae*: *Scophthalmus maximus* L., *Scophthalmus rhombus* L.; *Serranidae*: *Epinephelus marginatus* Lowe, *Epinephelus tauvina* Forsskål; *Soleidae*: *Solea senegalensis* Kaup, *Solea solea* L.; *Sparidae*: *Dentex dentex* L., *Pagellus bogaraveo* Brünnich, *Sparus aurata* L.

4.1.1. Aqueous Extractions

Of all the experiments presented in Table 6, the most frequently used extraction method was the aqueous one. The most commonly employed solvents in these studies, listed in order of frequency of use, were physiological saline, water, ammonium bicarbonate, and Tris-buffered saline. Further information about these studies can be found in Table S-1.

Although aqueous extraction was the most popular extraction method, it also showed the least antibacterial activity. This was particularly evident in those experiments where different extraction methods were compared. In some experiments, aqueous extracts did not show any antibacterial activity [265,275-279,289]. For example, Subramanian et al., (2008) [278] found antimicrobial agents, such as lysozyme, cathepsin B, and trypsin-like proteases, in the aqueous skin mucus extracts of several fish species, but they did not exert any antimicrobial activity. Al-Rashed et al., (2018) [265] used aqueous and acidic extracts of the skin mucus of the climbing perch (*Anabas testudineus*), but only found antibacterial activity in the latter. Similarly, Hellio et al., (2002) [276] performed aqueous and organic extractions of the skin mucus of the ballan wrasse (*L. bergylta*), but only observed antibacterial activity with the organic extracts. Subhashini et al., (2013) [289] did not find antimicrobial activity in the aqueous extract of the skin mucus of tinfoil barb fish (*Barbonymus Schwanenfeldii*), even if the amount of protein was higher than in the organic extracts obtained in parallel.

The lack of activity of these extracts has been attributed by different authors to several causes: (i) inactivation of enzymes, such as lysozyme, trypsin, or proteases, by the high incubation temperatures and/or low pH conditions used in the procedure [278]; (ii) low concentration of antimicrobial compounds in the media, probably because some of these enzymes regulate their production [213]; and (iii) inter- and intraspecies variability of mucus composition, influenced by both internal (e.g., sex and developmental stage) and external factors (e.g., stress, hyperosmolarity, pH, and infection) [201]. This last point is particularly noticeable in the species studied in several studies performing aqueous extractions. The aqueous skin mucus extract of the common snakehead (*Channa striata*) has been shown in some studies to be active against Gram-negative and Gram-positive bacteria [268,270,271]. However, Wei et al., (2010) [299] also tested the antibacterial activity of this extract and found inhibition only against *Aeromonas hydrophila* but not against other bacteria previously tested (i.e., *Bacillus subtilis*, *Klebsiella pneumoniae*, *Proteus vulgaris*, and *Pseudomonas aeruginosa*).

In other studies, the aqueous skin mucus extract did inhibit both Gram-negative and Gram-positive bacteria [268,270-273,287,290,291,293-295]. Guardiola et al., (2014) [272] demonstrated that an aqueous extract of the skin mucus of grouper (*Epinephelus marginatus*) inhibited Gram-positive and Gram-negative bacteria. They also found high levels of lysozyme, alkaline phosphatase, esterase, protease, and antiprotease activities, which are associated with defense against bacterial infections. In a study by Kumari et al., (2019), [294] the aqueous skin mucus extract of several carp species exhibited high antibacterial activity against both Gram-negative and Gram-positive bacteria.

4.1.2. Organic Extractions

For the organic extractions, the most used solvents have been ethanol and dichloromethane. Some authors performed alcoholic extractions and then partitioned distilled water with dichloromethane to obtain aqueous and organic phases [276,289]. High antibacterial activity has been reported for

organic fish skin mucus extracts (see Tables 3 and S-2 for further details). Indeed, in some studies, all bacteria tested were inhibited, both Gram-positive and Gram-negative [214,276,283,289]. The main reasons explaining such activity are that (i) the presence of hydrophobic groups is often a common feature of antimicrobial molecules because of their affinity for membranes and their ability to disrupt them [300]; and (ii) these extracts are enriched in hydrophobic molecules because organic solvents favor their isolation by reducing the interactions between hydrophobic groups, which hinders their aggregation [301]. In fact, Mahadevan et al., (2019) [283] obtained greater inhibitory activity against Gram-negative and Gram-positive bacteria using organic mucus extracts compared to aqueous ones. Hellio et al., (2002) [276] correlated high antimicrobial activity with low polarity of the solvents used; they also showed that extracts from the dichloromethane phase were more active than those from the aqueous phase. In a study by Bergsson et al., (2005) [214], an organic (acetonitrile (ACN) + 1% trifluoroacetic acid (TFA)) extract of cod skin mucus exhibited high antimicrobial activity against Gram-positive and Gram-negative bacteria. In these extracts, they also identified four peptides with known antimicrobial activity, i.e., those derived from the histone H2B and the 60S ribosomal proteins L40, L36A, and L35.

In some studies, the same species were used to obtain the organic extracts of skin mucus. García-Marciano et al., (2019) [279] and Wibowo and Maftuch (2015) [281] tested the organic skin mucus of tilapia against *V. harveyi*, and in both studies, bacterial growth was inhibited. Katra et al., (2016) [277] and Hellio et al., (2002) [276] employed the same methodology to obtain organic skin mucus extracts from ballan wrasse (*L. bergylta*) and these two studies, no activity against Gram-positive bacteria was found. However, Hellio et al., (2002) [276] found antimicrobial activity against Gram-negatives, while Katra et al., (2016) [277] did not. These contradictory results were attributed to the possible development of antimicrobial resistance in the strains used, or to seasonal, housing, or dietary differences between the two studies that may have affected the experimental animals.

4.1.3. Acidic Extractions

For acidic extractions, the most common solvent was acetic acid (AA) followed by TFA. In general, acidic extracts showed greater antibacterial activity than other extracts (see Tables 3 and S-3 for further information) [262,265,275,278-280,288,289,299]. In most studies using acidic extractions to determine antibacterial capacity, all bacteria tested were inhibited [262,275,278,280,292,299]. This may be due to the presence of cationic peptides and defensive low-molecular-weight proteins. This type of molecule has been shown to be more soluble in mildly acidic solutions [302].

Subramanian et al., (2008) [278] tested the antimicrobial activity of brook trout (*Salvelinus fontinalis*), haddock (*Melanogrammus aeglefinus*), and hagfish acidic (AA) skin mucus extracts against Gram-negative (*A. salmonicida*, *E. coli*, *Listonella anguillarum*, *Salmonella enterica*, *P. aeruginosa*, *Yersinia ruckeri*) and Gram-positive (*Staphylococcus epidermidis*) bacteria, and all species studied were inhibited. Hagfish mucus was the most active one, and its protein profile showed mainly low-molecular-weight proteins below 20 kDa. This was related to the fact that hagfish are evolutionarily the most primitive of the species studied and they lack essential components of adaptive defense, as well as their presence in muddy ocean bottoms, which requires a greater amount of antimicrobial components for their survival [278].

Nigam et al., (2017) [292] identified the antimicrobial protein histone H2B in acidic (AA and TFA) mrigal carp skin mucus extracts. However, the TFA extract only inhibited two (*Salmonella paratyphi*, *Vibrio cholerae*) of the five bacteria tested. Patel et al., (2020) [262] detected some metabolites in the acidic (AA) pool of barb mucus extract that were associated with antimicrobial activity, such as 10-nitro-9Z,12Z-octadecadienoic acid, 3alpha,6beta,7alpha-trihydroxy-

5betacholan-24-oic acid, 1-octanoyl-rac-glycerol, di-hydrosphingosine, phytosphingosine, 5beta-chol-2-en-24-oic acid, neuraminic acid, glucosamine, and cysteamine. It has been described that antimicrobial lipids probably act by inducing cell wall and membrane destabilization of bacteria [303].

4.1.4. Crude Mucus

Finally, some studies have evaluated the activity of fish skin mucus in its almost raw form, without any type of solvent extraction. Tables 3 and S-4 provide additional information about these studies. Sanahuja et al., (2019) [266] compared the crude skin mucus of gilthead sea bream, European sea bass, and meagre (*Argyrosomus regius*). In particular, meagre mucus showed biocidal activity against all bacterial species tested, i.e., *E. coli*, *V. anguillarum*, and *P. anguilliseptica* (all Gram-negative), which was associated with higher levels of non-specific defenses, such as protease and carboxylesterase activities. Fuochi et al., (2017) [296] studied the antibacterial activity of common stingray (*D. pastinaca*) crude skin mucus and found that it inhibits the bacterial growth of Gram-negative, but not Gram-positive, bacteria. This observation was attributed to a strong interaction between the outer membrane (present in Gram-negatives only) and the biomolecules present in the mucus. They also demonstrated the presence of chitinase 1, an enzyme involved in the degradation of chitin [296].

Other authors have compared the antibacterial activity between the crude mucus and some of its solvent extracts. Kumari et al., (2019) [294] found that the crude mucus of several carp species shows higher antibacterial activity than its aqueous extract. Wei et al., (2010) [299] compared crude, aqueous, and acidic mucus from common snakehead. Although the crude mucus was found to contain a higher amount of protein than the other extracts, it inhibited only the fish pathogen *A. hydrophila*. In this work, the crude mucus did not exert any effect against the human bacteria pathogens tested, unlike the other extracts.

4.2. Antifungal Activity of Fish Skin Mucus Extracts

Fish skin mucus has also shown antimicrobial activity against fungal pathogens. However, the number of studies evaluating antifungal activity is much lower than the number of studies evaluating antibacterial activity. Of the 39 selected studies that evaluated antibacterial and antifungal activity, 28 evaluated only antibacterial activity, two evaluated antifungal activity exclusively, and nine evaluated both. The antifungal studies conducted using fish skin mucus are shown in Table 7.

Table 7. List of antifungal studies using skin mucus from different fish species.

Fish Species (Family)	Extraction[1]	Sensitive Fungi	Non-Sensitive Fungi	Antimicrobial Assay[2]	Ref.
Anguilla anguilla L. (*Anguillidae*)	-	*Aspergillus awamori*, *Colletotrichum falcatum*, *Fusarium oxysporum*		DD	[284]
Catla catla Hamilton (*Cyprinidae*)	PS	*Aspergillus flavus*, *Aspergillus niger*, *Candida albicans*, *Mucor globosus*, *Rhizopus arrhizus*		DD	[291]
	C	*A. awamori*, *C. falcatum*, *F. oxysporum*		DD	[284]
Cirrhinus mrigala Hamilton (*Cyprinidae*)	C	*A. awamori*, *C. falcatum*, *F. oxysporum*		DD	[284]
Clarias batrachus L. (*Clariidae*)	-	*A. niger*, *Aspergillus nidulans*, *Fusarium moniliforme*, *C. albicans*, *Trichoderma koningi*		DD	[287]

Table 7. List of antifungal studies using skin mucus from different fish species.

Fish Species (Family)	Extraction[1]	Sensitive Fungi	Non-Sensitive Fungi	Antimicrobial Assay[2]	Ref.
Ctenopharyngodon idella Valenciennes (*Cyprinidae*)	PS	*A. flavus, C. albicans, M. globosus, R. arrhizus*	*A. niger*	DD	[291]
Cyprinus carpio L. (*Cyprinidae*)	PS, AA, DCM	*C. albicans*		BD	[278]
Dasyatis pastinaca L. (*Dasyatidae*)	C	*C. albicans, Candida glabrata, C. tropicalis*		BD	[296]
Gadus morhua L. (*Gadidae*)	ACN + 1% TFA	*C. albicans*		AWD, BD	[214]
	W, DCM	*C. albicans, Candida brusei, C. tropicalis, Issatchenkia orientalis, Saccharomyces cerevisiae*		AWD, BD	[276]
Hypophthalmichthys Molitrix Valenciennes (*Cyprinidae*)	PS	*A. flavus, A. niger, M. globosus*	*C. albicans, R. arrhizus*	DD	[291]
Labeo rohita Hamilton (*Cyprinidae*)	NaOH, NaOH + TH	*C. albicans*		AWD	[304]
	PS	*A. flavus, A. niger, C. albicans, M. globosus, R. arrhizus*		DD	[291]
Melanogrammus aeglefinus L. (*Gadidae*)	AB, AA, ET, DCM	*C. albicans*		BD	[278]
Monopterus albus Zuiew (Synbranchidae)	C, W, PS	*C. albicans, Candida krusei, Cryptococcus neoformans, Fusarium* sp.		DD	[305]
Morone saxatilis Walbaum (Moronidae)	AB, AA, ET, DCM	*C. albicans*		BD	[278]
Myxine glutinosa L. (Myxinidae)	AB, AA, ET, DCM	*C. albicans*			[278]
Oncorhynchus mykiss Walbaum (*Salmonidae*)	C		*C. albicans, Candida parapsilosis*		[297]
Periophthalmodon schlosseri Pallas (*Gobiidae*)	PS, ET	*C. albicans, A. flavus, Mucor sp., Trichoderma longibriachtin*		DD, BD	[283]
Salvelinus alpinus L. (*Salmonidae*)	AB, AA, ET, DCM	*C. albicans*		BD	[278]
Salvelinus fontinalis Mitchill (*Salmonidae*)	AB, AA, ET, DCM	*C. albicans*		BD	[278]
Scophtalamus rhombus L. (*Scophthalmidae*)	W, ET, DCM	*C. tropicalis, S. cerevisiae*	*C. brusei, C. albicans, I. orientalis*	AWD, BD	[276]

[1] C: crude; PS: physiological saline; AA: acetic acid; DCM: dichloromethane; ACN: acetonitrile; TFA: trifluoroacetic acid; W: water; AB: ammonium bicarbonate; ET: ethanol; TH: tris hydrochloride; [2] DD: disc diffusion; BD: broth dilution; AWD: agar-well diffusion.

Several studies have produced mixed results using crude fish skin mucus. On the one hand, the antifungal activity of crude skin mucus of catla, mrigal carp, and European eel inhibited the growth of *Aspergillus awamori*, *Colletotrichum falcatum*, and *Fusarium oxysporum* in the study by Pethkar et al., (2017) [284]. Fuochi et al., (2017) [296] also found that the crude skin mucus of the common stingray was active against *Candida albicans*, *Candida glabrata*, and *Candida tropicalis*. On the other hand, Hisar et al., (2014) [297] tested the crude skin mucus of rainbow trout against *C. albicans* and *Candida parapsilosis*, but no antifungal activity was observed. Ikram

et al., (2013) [305] screened the antifungal activity of crude and aqueous (i.e., PBS and water) skin mucus of Asian swamp eel (*Monopterus albus*) against *C. albicans*, *Candida krusei*, *Cryptococcus neoformans*, and *Fusarium* spp., but only the water extract revealed an inhibitory effect, with activity against all the fungi tested and mostly against *Fusarium* spp.

A few studies only investigated aqueous mucus extractions. For example, walking catfish (*Clarias batrachus*) aqueous skin mucus inhibited *Aspergillus niger*, *Aspergillus nidulans*, *Fusarium moniliforme*, *C. albicans*, and *Trichoderma koningi* in the study by Loganathan et al., (2011) [287]. Balasubramanian et al., (2011) [291] tested the antifungal activity of catla, silver carp (*Hypophthalmichthys molitrix*), rohu (*Labeo rohita*), and grass carp (*Ctenopharyngodon idella*) aqueous skin mucus against *Aspergillus flavus*, *A. niger*, *C. albicans*, *Mucor globosus*, and *Rhizopus arrhizus*. The catla and rohu extracts inhibited all the species tested, the silver carp extract inhibited *M. globosus*, *A. flavus*, and *A. niger*, and the grass carp extract inhibited all species except *A. niger*.

Other studies carried out aqueous and organic or acidic extractions in parallel and compared their activity. Hellio et al., (2002) [276] screened the antifungal activity of the aqueous and organic skin mucus extracts of pollock (*Pollachius virens*), ballan wrasse, European flounder (*Platichthys flesus*), common sole (*Solea solea*), and brill (*Scophthalmus rhombus*) against *Candida brusei*, *C. albicans*, *C. tropicalis*, *Saccharomyces cerevisiae*, and *Issatchenkia orientalis*. Antifungal activity was found only in the aqueous and organic fractions of the organic extraction of brill mucus against *C. tropicalis*, *I. orientalis*, and *S. cerevisiae*. In the study by Subramanian et al., (2008) [278], the aqueous, acidic, and organic skin mucus extracts of arctic char (*Salvelinus alpinus*), brook trout (*Salvelinus fontinalis*), Eurasian carp (*Cyprinus carpio* sub sp. Koi), striped bass (*Morone saxatilis*), haddock (*Melanogrammus aeglefinus*), and hagfish were tested against *C. albicans*. The results showed that the acidic skin mucus of arctic char, brook trout, and hagfish exerted fungicidal activity, and the acidic skin mucus extracts of European carp and striped bass were fungistatic. Mahadevan et al., (2019) [283] showed that the aqueous and organic skin mucus extracts of the giant mudskipper (*Periophthalmodon schlosseri*) inhibited *C. albicans*, *A. flavus*, *Mucor* sp., and *Trichoderma longibriachtin*.

Bergsson et al. (2005) [214] extracted the skin mucus of Atlantic cod using 60% ACN containing 1% TFA. They evaluated its activity against *C. albicans*, which was fully eliminated when Medium E (salt solution) was added to the medium. Without Medium E, only mild inhibition was observed. In another study, al-Arifa et al., (2011) [304] demonstrated that the use of alkali treatments to induce the production of skin mucus in rohu before its collection inactivated its antifungal properties, and they were not restored after the neutralization of its pH. Instead, it favored the growth of *C. albicans*.

The antifungal activity of mucus components, such as lysozyme [306,307] or chitinases [308], have been demonstrated. Some studies suggest that the lysozyme may disrupt cell wall integrity by hydrolyzing the glycosidic linkages between cell wall proteins and polysaccharides [306]. Other hypotheses include that lysozyme is likely to induce apoptosis in this fungus accompanied by activation of membrane potassium channels [307]. Regarding chitinases, they catalyze the hydrolysis of chitin, a main component of the cell wall in fungi [308].

4.3. Antiviral Activity of Fish Skin Mucus

Information on the antiviral activity of fish skin mucus extracts is scarce to date. Raj et al., (2011) [309] investigated the role of carp epidermal mucus as an innate immune barrier against CyHV-3 entry. They found that skin mucus inhibits CyHV-3 binding on epidermal cells and leads to a significant reduction in the number of viral plaques. This reduction only occurred when cells were pre-incubated with mucus, but not when mucus was added after the incubation period. Most of

the studies, however, report antiviral activity of compounds that had been previously isolated from skin mucus. For instance, Valero et al., (2020) [310] reported the presence of NK-lysin in Atlantic salmon skin mucus, and Falco et al., (2019) [311] demonstrated its antiviral activity against SVCV by inhibiting not only the binding of viral particles to host cells, but also the fusion of virus and cell membranes. Beta-defensins, an important factor in the antimicrobial barrier function of the skin [312], have also been shown to have antiviral activity against another rhabdovirus, the viral haemorrhagic septicaemia virus (VHSV) [313]. Furthermore, lysozyme [314] and piscidin (PIS) [315] have antiviral activity. However, the scarcity of systemic and functional data shows that more research on the antiviral role of fish mucus is required to draw clear conclusions and to develop new strategies to treat viral infections.

5. Omics Techniques as a Promising Tool in Fish Skin Mucus Research

The field of fish skin mucus research has generally been limited by the complexity of its composition, as well as the interactions between its components. Omic techniques have recently emerged to provide a holistic approach to cellular components and their interactions, providing an effective tool towards a deeper understanding of marine systems [316]. The progress of these techniques has allowed the field of studies of fish skin mucus to grow quickly in recent years [175]. These techniques have been applied to fish skin mucus research in different topics, such as welfare, health, and nutrition. However, the discovery of antimicrobial agents through these methods is an underexplored opportunity. Genomics have provided insights into molecular and genetic mechanisms in fish.

Ao et al., (2015) [317] sequenced and assembled the genome of *Larimichthys crocea* using a bacterial artificial chromosome and a whole-genome shotgun hierarchical strategy. They identified 159 genes related to mucin biosynthesis and mucus production based on previous studies in mammals, thus suggesting that the mucin synthetic pathway is conserved between fish and mammals. Carda-Diéguez et al., (2017) [318] searched for genomic and metagenomic evidence in wild eel to discover if fish mucus could constitute an adequate niche for the evolution of mucosal aquatic pathogens in natural environments. The results obtained suggest that skin mucus concentrates in bacteria present in water with abilities to attach, resist innate immunity, and compete with other bacteria, and that it favors the exchange of genes encoding these functions.

Transcriptomics provides information on the RNA transcripts produced by the genome, from protein coding (mRNA) to noncoding RNA. A recent study examined the efficacy of whole-transcriptomic profiling of mahi-mahi epidermal mucus as a method for oil exposure detection using RNASeq [319]. Transcripts involved in immune response, cardiotoxicity, and calcium homeostasis showed differential expression after oil exposure, which indicates that mucus is a promising source for noninvasive monitoring techniques. Parida et al., (2018) [320] examined the transcriptome of immune-relevant genes in the mucus of infected rohu to characterize mucosal immune responses. The results show, in general, the upregulation of immune-related transcripts, such as interleukins, toll-like receptor 22, and lysozyme G, which broadens our knowledge of mucosa-associated molecular events that occur during infections and reinforces the role of mucus as the first line of defense against pathogens.

Proteomics is the characterization of proteins expressed in an organism. It is the most studied omic technique in fish mucus research. Proteomics provides information about the entire effect of the gene expression process and encompasses post-transcriptional and post-translational protein expression regulation [321]. Proteomic profiles of the skin mucus of gilthead seabream [251], Atlantic cod [237], Atlantic salmon [322], mudskipper [323], discus fish (*Symphysodon* spp.) [324], European sea bass [236], and lumpsucker [240] have been published, allowing for the possibility of comparative studies to better understand the dynamics of fish mucus. Moreover, the

proteomic profile of fish mucus subjected to different types of stress has been studied, such as chronic wounds [254], bacterial infection [237,325], parasitic infection [326], artificial stressors [327], and sample collection [328]. These types of studies expand our knowledge of proteomic changes associated with immune processes, and they can be a starting point to develop a powerful tool to identify bioindicators of fish welfare and physiological status via non-invasive methods.

Metabolomics can be defined as the quantitative complement of all low-molecular-weight molecules present in cells in a particular physiological or developmental state [329]. Metabolomics is situated downstream of proteomics, transcriptomics, and genomics, thus making metabolomics extremely useful for understanding organism responses and for biomarker discovery [37]. Analytical methods in metabolomics commonly include mass spectrometry (MS), often in conjunction with gas chromatography (GC) and liquid chromatography (LC), and nuclear magnetic resonance (NMR). Studies on fish metabolomics cover a wide range of fields of knowledge, including fish physiology and development, pollutants' effects on fish, fish condition and disease, and fish as foodstuff [330]. Ekman et al., (2015) [259] characterized fathead minnow skin mucus metabolites using LC-MS in order to report a minimally invasive sampling method. Results indicate that the metabolome varies between sexes and that it is very sensitive to chemical exposure, suggesting that metabolomics is useful for environmental monitoring and surveillance. Wen et al., (2020) [331] analyzed discus fish skin mucus metabolites using LC-MS/MS-based metabolomics and found changes in metabolite profiles as they entered the stage of parental care; those variations were sex-specific in parental fish. Ivanova et al., (2018) [332] employed LC-MS metabolomics to detect small metabolites using different sample collection techniques. The results suggest that the scraping method to collect mucus is more invasive than other methods due to changes in metabolic profiles.

A combination of different omic techniques pursues the integration of different biological entities to understand their interrelation and the functioning of larger systems, and serves to identify new biomarkers in specific tissues. For instance, multiomic analysis of gilthead sea bream skin mucosa was carried out by measuring the entirety of biomolecules differentially expressed by means of skin transcriptomic analyses and the modification in mucus layer exudation by the analysis of the mucus proteome [333]. Information on fish mucus at genomic, transcriptional, protein, and metabolic levels has significantly moved fish mucus research forward. Applications associated with fish health and welfare, monitoring, food safety, and aquaculture production can be achieved using omic techniques. Important insights can be found not only within those techniques but also through understanding the interactions between them.

6. Conclusions

Besides being a key component in several physiological functions, fish skin mucus provides an effective chemical and physical barrier against pathogens. The performance of this activity is highly dependent on mucus composition. Therefore, the choice of a suitable molecular extraction method is crucial for its antimicrobial use in other applications. Indeed, notable differences in antimicrobial activity have been shown for the different types of extracts reviewed here, which is particularly relevant in those studies comparing different extraction methods on the same samples. In general, acidic extracts, followed by organic ones, showed the highest antimicrobial activity. This may be because these procedures favor the isolation of cationic and/or amphipathic antimicrobial compounds, such as AMPs, their enrichment in the final extracts and, apparently, the minimization of molecular inactivation events.

The general analysis of the studies reviewed here shows that 76% of the authors tested antibacterial activity against both Gram-negative and Gram-positive bacteria, while the remaining 24% used Gram-negative bacteria only. In this sense, *E. coli* and *S. aureus* were the most commonly used Gram-negative and Gram-positive bacteria, respectively. With regard to the

origin (or host target) of the pathogens tested, most studies used both human and fish pathogens (57%), while 35% and 8% used only human and fish pathogens, respectively. In some experiments, the (mostly acidic and organic) extracts inhibited the replication of Gram-negative, but not Gram-positive, bacteria. One of the reasons for this may be the higher affinity of the cationic antimicrobial molecules in the extracts for the negatively charged outer membrane of gram-negative bacteria, which is not present in gram-positive bacteria.

Focusing now on the procedures to quantify antimicrobial activity, and, mostly, antibacterial and antifungal activity, the most common methods employed are, in order, disc diffusion (46%), agar-well diffusion (26%), broth dilution (12%), optical density measurement (7%), and broth dilution recorded by optical measurement (5%). The disc diffusion and agar-well diffusion assays are simple, inexpensive, and intuitive to interpret; however, their low sensitivity makes them unsuitable for comparative studies and for determining precise inhibitory factors, such as the minimum and half-maximal inhibitory concentration (MIC and IC50, respectively). Therefore, and as a preview of the next section, it would be recommended that the methods used to evaluate the antimicrobial activity of compounds in this particular area of research be standardized to allow for appropriate comparisons.

7. Recommendations and Future Perspectives

This review emphasizes the importance of mucus composition for its antimicrobial activity. However, this composition may differ notably depending on several factors, such as species, sex, age, and environment. Therefore, more information on these factors should be included in such studies to improve reproducibility. A practical option could be to focus these studies on animals at harvesting stages in order to normalize the results at the most appropriate time for industrial exploitation. In this sense, it would also be of great interest to develop efficient technologies for the collection of fish skin mucus at harvesting sites.

However, the momentum needed to accelerate progress in these lines of research and their translation into practice requires a substantial increase in the need for these products. The urgency for new antimicrobials noted in the introduction to this review is one such need. However, new ideas that define the targets against which these compounds could already make a difference would greatly accelerate their development. Examples include the use of marine antimicrobials in high ionic strength environments, such as the mucosal tissues of cystic fibrosis patients [334] or food preservation [335]. In this line of research, it would also be interesting to study formats to increase their stability and to improve their delivery; for example, by encapsulating them in micro- or even nanomaterials.

Finally, it is important to reiterate that the study and understanding of the fish skin mucus interactome using omic techniques provides new, unprecedented opportunities for antimicrobial drug discovery. Multiomics may also allow for the discovery of clinically important metabolites, interactions between components, and the mechanisms by which components exert their antimicrobial activity.

Supplementary material

Fish Skin Mucus Extracts: An Underexplored Source of Antimicrobial Agents

Rocío Díaz-Puertas, Mikolaj Adamek, Ricardo Mallavia and Alberto Falco

Table S-1. List of antibacterial studies using aqueous skin mucus extracts from different fish species.

Fish species	Extraction[1]	Bacteria[2]		Antimicrobial assay[3]	Ref.
		Sensitive	Resistant		
Amphiprion clarkii	W	G-: *Aeromonas hydrophila, Pseudomonas fluorescens, Vibrio alginolyticus, Vibrio harveyi, Vibrio parahaemolyticus*	G+: *Micrococcus lysodeikticus, Staphylococcus aureus*	BD	[264]
Anabas testudineus	AB		G+*: Bacillus subtilis, S. aureus* G-*: A. hydrophila, Escherichia coli, Pseudomonas aeruginosa, Salmonella spp., Salmonella choleraesuis, Serratia marcescens*	AWD	[336]
Anguilla anguilla	PS	G+: *S. aureus*, G-: *V. alginolyticus, Vibrio fluvialis, V. parahaemolyticus*	G+: *Enterococcus faecium, Staphylococcus epidermidis* G-: *A. hydrophila, E. coli, Klebsiella pneumoniae, Photobacterium damselae* subsp. *piscicida, P. aeruginosa, Salmonella typhi, Vibrio anguillarum*	DD	[337]
Arius maculatus	PS	G-: *E. coli, P. aeruginosa, Salmonella spp., Shigella spp., Vibrio cholerae*		DD	[285]
Barbonymus schwanenfeldii	W		G+: *Bacillus cereus, S. aureus* G-: *Shigella boydii, E. coli*	DD	[289]
Catla catla	PS	G-: *A. hydrophila, Aeromonas sobria, P. fluorescens, V. anguillarum.*		DD	[290]
	PS	G-: *E. coli, K. pneumoniae, P. aeruginosa, S. typhi, V. cholerae*		DD	[291]
Channa gachua	PS	G-: *A. hydrophila, E. coli, P. aeruginosa, V. anguillarum, Vibrio fischeri*		DD	[268]

Table S-1. List of antibacterial studies using aqueous skin mucus extracts from different fish species.

Fish species	Extraction[1]	Bacteria[2]		Antimicrobial assay[3]	Ref.
		Sensitive	Resistant		
Channa marulius	PS	G-: *A. hydrophila, E. coli, P. aeruginosa, V. anguillarum, V. fischeri*		DD	[268]
Channa micropeltes	PS	G-: *A. hydrophila, E. coli, P. aeruginosa, V. anguillarum, V. fischeri*		DD	[268]
Channa punctatus	PS	G+: *Lactobacillus bulgaricus, S. aureus* G-: *E. coli, Klebsiella oxytoca, K. pneumoniae, P. aeruginosa, Proteus mirabilis, S. paratyphi, S. typhi, V. cholerae*		DD	[293]
	PS	G-: *A. hydrophila, E. coli, P. aeruginosa, V. anguillarum, V. fischeri*		DD	[268]
	W	G+: *S. aureus, Micrococcus luteus*	G -: *E. coli, P. aeruginosa, S. typhi*	DD	[338]
Channa striatus	W	G-: *A. hydrophila*	G+: *B. subtilis* *G-: K. pneumoniae, P. aeruginosa, Proteus vulgaris, Salmonella enteritidis*	DD, BD	[299]
	W	G+: *L. bulgaricus, S. aureus* G-: *E. coli, K. oxytoca, P. aeruginosa, K. pneumoniae, S. paratyphi, S. typhi, P. mirabilis, V. cholerae*		AWD	[270]
	PS	G+: *B. subtilis, M. luteus, S. aureus, Steptococcus pyogenes* G-: *E. coli, P. vulgaris, P. aeruginosa, Salmonella typhimurium, V. cholera, Mycobacterium smegmatis*		AWD	[271]
	PS	G-: *A. hydrophila, E. coli, P. aeruginosa, V. anguillarum, V. fischeri*		DD	[268]
Cirrhinus mrigala	PS	G+: *L. bulgaricus S. aureus* G-: *E. coli, K. oxytoca, K. pneumoniae, P. aeruginosa, P. mirabilis, S. paratyphi, S. typhi, V. cholerae*		DD	[293]

Table S-1. List of antibacterial studies using aqueous skin mucus extracts from different fish species.

Fish species	Extraction[1]	Bacteria[2]		Antimicrobial assay[3]	Ref.
		Sensitive	Resistant		
	W	G-: *P. aeruginosa, S. paratyphi, S. typhi, V. cholerae*	G+*: S. aureus,*	DD	[292]
Clarias batrachus	AB	G+: *S. aureus* G-: *A. hydrophila, E. coli, K. pneumonia, P. aeruginosa, P. vulgaris*	G+: *Bacillus coagulans*	DD	[339]
	PS	G-: *A. hydrophila, E. coli, P. aeruginosa, V. anguillarum, V. fischeri*		DD	[287]
Ctenopharyngodon idella	PS	G+: *B. cereus, S. aureus, S. epidermidis* G-: *A. hydrophila, E. coli, K. pneumoniae, P. aeruginosa*		AWD	[294]
	PS	G-: *A. hydrophila, A. sobria, P. fluorescens, V. anguillarum.*		DD	[290]
	PS	G-: *E. coli, K. pneumoniae, P. aeruginosa, S. typhi, V. cholerae*		DD	[291]
Cyprinus carpio	AB		G+: *S. epidermis* G-: *Aeromonas salmonicida, E. coli, Listonella anguillarum, P. aeruginosa, Salmonella enterica, Yersinia ruckeri*	BD	[278]
	PS	G+: *S. epidermis* G-: *A. salmonicida, E. coli, L. anguillarum, P. aeruginosa, S. enterica, Y. ruckeri*		AWD	[294]
Dentex dentex	TBS	G+: *B. subtilis* G-: *E. coli, P. damselae, Shewanella putrefaciens, V. harveyi, V. angillarum*		OD	[272]
Dicentrarchus labrax	PS	G+: *S. aureus*	G-: *P. damselae* subsp. *piscicida, Tenacibaculum maritimum, V. anguillarum, V. damsela*	DD	[340]
	PS	G+: *S. aureus* G-: *V. alginolyticus, V. fluvialis, V. parahaemolyticus*	G+: *E. faecium, S. epidermidis* G-: *A. hydrophila, E. coli, K. pneumoniae, P. damselae* subsp. *piscicida, P. aeruginosa, S. typhi, V. anguillarum,*	DD	[337]
	TBS	G+: *B. subtilis* G-: *E. coli, P. damselae, S. putrefaciens, V. harveyi, V. angillarum*		OD	[272]
Epinephelus marginatus	TBS	G+: *B. subtilis* G-: *E. coli, P. damselae, S.*		OD	[272]

Table S-1. List of antibacterial studies using aqueous skin mucus extracts from different fish species.

Fish species	Extraction[1]	Bacteria[2]		Antimicrobial assay[3]	Ref.
		Sensitive	Resistant		
		putrefaciens, V. harveyi, V. angillarum			
Epinephelus tauvina	AB		G-: *A. hydrophila, E. coli, S. typhi, K. pneumonia, P. mirabilis, P. fluorescens, V. alginolyticus, V. harveyi, V. parahemolyticus*	AWD	[341]
Heteropneustes fossilis	PS	G+: *B. subtilis, M. luteus, S. aureus, S. pyogenes* G-: *E. coli, P. vulgaris, P. aeruginosa, S. typhimurium, V. cholera, M. smegmatis*		AWD	[271]
Hypophthalmichthys nobilis	PS	G+: *B. cereus, S. aureus, S. epidermidis* G-: *A. hydrophila, E. coli, K. pneumoniae, P. aeruginosa*		AWD	[294]
	PS	G-: *A. hydrophila, A. sobria, P. fluorescens, V. anguillarum.*		DD	[290]
	PS	G-: *E. coli, K. pneumoniae, P. aeruginosa, S. typhi, V. cholerae*		DD	[291]
	PS	G+: *B. cereus, S. aureus, S. epidermidis* G-: *A. hydrophilla, E. coli, K. pneumonia, P. aeruginosa,*		AWD, APD	[295]
Labeo rohita	PS	G-: *A. hydrophila, A. sobria, P. fluorescens, V. anguillarum.*		DD	[290]
	PS	G-: *E. coli, K. pneumoniae, P. aeruginosa, S. typhi, V. cholerae*		DD	[291]
Labrus bergylta	W		G+: *B. cereus, B. subtilis, Bacillus megaterium, S. aureus, Streptococcus sp.* G-: *E. coli, K. pneumoniae, P. vulgaris, P. aeruginosa, S. marcescens*	AWD, BD	[276]
	W		G+: *B. subtilis, Lactobacillus plantarum* G-: *A. sobria, Citrobacter sp., Edwardsiella tarda, E. coli, Enterobacter sp., L. anguillarum, Shewanella baltica, Y. ruckeri*	DD	[342]
Melanogrammus aeglefinus	AB		G+: *S. epidermis* G-: *A. salmonicida, E. coli, L. anguillarum, P.*	BD	[278]

Table S-1. List of antibacterial studies using aqueous skin mucus extracts from different fish species.

Fish species	Extraction[1]	Bacteria[2]		Antimicrobial assay[3]	Ref.
		Sensitive	Resistant		
			aeruginosa, S. enterica, Y. ruckeri		
Morone saxatilis	AB		G+: *S. epidermis* G-: *A. salmonicida, E. coli, L. anguillarum, P. aeruginosa, S. enterica, Y. ruckeri*	BD	[278]
Myxine glutinosa	AB		G-: *S. enterica*	BD	[278]
Oreochromis niloticus	W		G-: *V. harveyi, V. parahaemolyticus*	BD, OD	[343]
Oreochromis mossambicus	AB	G+: *S. aureus* G-: *A. hydrophila, E. coli, K. pneumonia, P. aeruginosa, P. vulgaris*	G+: *B. coagulans*	DD	[339]
Pagellus bogaraveo	PS	G-: *V. parahaemolyticus*	G+: *E. faecium, S. aureus, S. epidermidis* G-: *A. hydrophila, E. coli, K. pneumoniae, P. damselae* subsp. *iscicida, P. aeruginosa, S. typhi, V. alginolyticus, V. anguillarum, V. fluvialis*	DD	[337]
Periophthalmodon schlosseri	PS	G+: *Bacillus anthracis, S. aureus* G-: *E. coli, P. mirabilis, P. aeruginosa, S. typhi, V. cholerae, K. pneumoniae*		DD, BD	[283]
Platichthys flesus	W	G+: *B. cereus, B. subtilis, B. megaterium, S. aureus, Streptococcus sp.* G-: *E. coli, K. pneumoniae, P. vulgaris, P. aeruginosa, S. marcescens*		AWD, BD	[276]
Pollachius virens	W	G+: *B. cereus, B. subtilis, B. megaterium, S. aureus, Streptococcus sp.* G-: *E. coli, K. pneumoniae, P. vulgaris, P. aeruginosa, S. marcescens*		AWD, BD	[276]
Rita rita	W	G+: *S. aureus, M. luteus* G -: *S. typhi*	G -: *E. coli, P. aeruginosa*	DD	[338]
Salvelinus alpinus	AB		G+: *S. epidermis* G-: *A. salmonicida, E. coli, L. anguillarum, P. aeruginosa, S. enterica, Y. ruckeri*	BD	[278]
Salvelinus fontinalis	AB		G+: *S. epidermis* G-: *A. salmonicida, E. coli, L. anguillarum, P.*	BD	[278]

Table S-1. List of antibacterial studies using aqueous skin mucus extracts from different fish species.

Fish species	Extraction[1]	Bacteria[2]		Antimicrobial assay[3]	Ref.
		Sensitive	Resistant		
			aeruginosa, S. enterica, Y. ruckeri		
Scaphtalamus rhombus	W	G+: *B. cereus, B. subtilis, B. megaterium, S. aureus, Streptococcus sp.* G-: *E. coli, K. pneumoniae, P. vulgaris, P. aeruginosa, S. marcescens*		AWD, BD	[276]
Scophthalamus maximus	PS	G+*: S. aureus* G-: *P. damselae* subsp. *piscicida, V. anguillarum*	G-: *T. maritimum, V. damsela*	DD	[340]
Solea senegalensis	TBS	G+: *B. subtilis* G-: *E. coli, P. damselae subsp. piscicida, S. putrefaciens, V. anguillarum, V. harveyi*		OD	[298]
Solea solea	W	G+: *B. cereus, B. subtilis, B. megaterium, S. aureus, Streptococcus sp.* G-: *E. coli, K. pneumoniae, P. vulgaris, P. aeruginosa, S. marcescens*		AWD, BD	[276]
Sparus aurata	PS	G+: *S. aureus*	G-: *P. damselae* subsp. *piscicida, T. maritimum, V. anguillarum, V. damsela*	DD	[340]
	TBS	G+: *B. subtilis* G-: *E. coli, P. damselae, S. putrefaciens, V. harveyi, V. angillarum*		OD	[272]
Umbrina cirrosa	TBS	G+: *B. subtilis* G-: *E. coli, P. damselae, S. putrefaciens, V. harveyi, V. angillarum*		OD	[272]

[1]: AB: ammonium bicarbonate; PS: physiological saline; W: water; TBS: tris buffered saline
[2]: G+: Gram-positive; G-: Gram-negative
[3]: APD: agar plate dilution; AWD: agar well diffusion; BD: broth dilution; DD: disc diffusion; OD: optical density

Table S-2. List of antibacterial studies using organic skin mucus extracts from different fish species.

Fish species	Extraction[1]	Bacteria[2]		Antimicrobial assay[3]	Ref.
		Sensitive	Resistant		
Barbonymus Schwanenfeldii	ET, DCM	G+: *Bacillus cereus, Staphylococcus aureus* G-: *Shigella boydii, Escherichia coli*		DD	[289]
Cyprinus carpio	DCM	G-: *Salmonella enterica*		BD	[278]
Epinephelus tauvina	ET		G-: *Aeromonas hydrophila, E. coli, Salmonella typhi, Klebsiella pneumonia, Proteus mirabilis, Pseudomonas fluorescens, Vibrio alginolyticus, Vibrio harveyi, Vibrio parahemolyticus*	AWD	[341]
Gadus morhua	ACN + 1% TFA	G+: *Bacillus megaterium* G-: *E. coli*		AWD, BD	[344]
Labrus bergylta	DCM	G-: *E. coli, K. pneumoniae, Proteus vulgaris, Pseudomonas aeruginosa, Serratia marcescens*	G+: *B. cereus, Bacillus subtilis, B. megaterium, S. aureus, Streptococcus sp.*	AWD, BD	[276]
	DCM		G+: *B. subtilis, Lactobacillus plantarum* G-: *Aeromonas sobria, Citrobacter sp., Edwardsiella tarda, E. coli, Enterobacter sp., Listonella anguillarum, Shewanella baltica, Yersinia ruckeri*	DD	[342]
Melanogrammus aeglefinus	DCM		G-: *S. enterica*	BD	[278]
Morone saxatilis	DCM	G-: *S. enterica*		BD	[278]
Myxine glutinosa	DCM		G-: *S. enterica*	BD	[278]
Oreochromis niloticus	DCM	G-: *V. harveyi*	G-: *V. parahaemolyticus*	BD, OD	[343]
	ET	G-: *V. harveyi*		DD, BD	[281]
Periophthalmodon schlosseri	ET	G+: *Bacillus anthracis, S. aureus* G-: *E. coli, P. mirabilis, P. aeruginosa, S. typhi, Vibrio cholerae, K. pneumoniae*		DD, BD	[283]
Platichthys flesus	DCM	G+: *B. cereus, B. subtilis, B. megaterium, S. aureus, Streptococcus sp.* G-: *E. coli, K. pneumoniae, P. vulgaris, P. aeruginosa, S. marcescens*		AWD, BD	[276]
Pollachius virens	DCM	G+: *B. cereus, B. subtilis, B.*		AWD, BD	[276]

Table S-2. List of antibacterial studies using organic skin mucus extracts from different fish species.

Fish species	Extraction[1]	Bacteria[2]		Antimicrobial assay[3]	Ref.
		Sensitive	Resistant		
		megaterium, S. aureus, Streptococcus sp. G-: *E. coli, K. pneumoniae, P. vulgaris, P. aeruginosa, S. marcescens*			
Salvelinus alpinus	DCM		G-: *S. enterica*	BD	[278]
Salvelinus fontinalis	DCM	G-: *S. enterica*		BD	[278]
Scaphtalamus rhombus	DCM	G+: *B. cereus, B. subtilis, B. megaterium, S. aureus, Streptococcus sp.* G-: *E. coli, K. pneumoniae, P. vulgaris, P. aeruginosa, S. marcescens*		AWD, BD	[276]
Solea solea	DCM	G+: *B. cereus, B. subtilis, B. megaterium, S. aureus, Streptococcus sp.* G-: *E. coli, K. pneumoniae, P. vulgaris, P. aeruginosa, S. marcescens*		AWD, BD	[276]

[1]: ACN: acetonitrile; DCM: dichloromethane; ET: ethanol; TFA: trifluoroacetic acid.
[2]: G+: Gram-positive; G-: Gram-negative
[3]: AWD: agar well diffusion; BD: broth dilution; DD: disc diffusion; OD: optical density

Table S-3. List of antibacterial studies using acidic skin mucus extracts from different fish species.

Fish species	Extraction[1]	Bacteria[2]		Antimicrobial assay[3]	Ref.
		Sensitive	Resistant		
Anabas testudineus	AA	G+*: Bacillus subtilis, Staphylococcus aureus* G-*: Aeromonas hydrophila, Escherichia coli, Pseudomonas aeruginosa, Salmonella spp., Salmonella choleraesuis, Serratia marcescens*		AWD	[336]
Channa punctatus	AA, TFA	G+: *S. aureus, Micrococcus luteus*	G -: *E. coli, P. aeruginosa, Salmonella typhi*	DD	[338]
Channa striatus	AA	G+: *B. subtilis* G-: *A. hydrophila, Klebsiella pneumoniae, P. aeruginosa, Proteus vulgaris, Salmonella enteritidis*		DD, BD	[299]
	AA	G+: *Enterococcus faecalis, M. luteus, S. aureus,* G-: *A. hydrophila, E. coli, K. pneumoniae, P. aeruginosa*		AWD	[345]
Cirrhinus mrigala	AA	G+*: S. aureus,* G-: *P. aeruginosa, S. paratyphi, S. typhi, V. cholerae*		DD	[292]
	TFA	G-: *S. paratyphi, V. cholerae*	G+*: S. aureus,* G-: *P. aeruginosa, S. typhi*	DD	[292]
Clarias batrachus	AA	G+: *E. faecalis, M. luteus, S. aureus* G-: *A. hydrophila, E. coli, K. pneumoniae, P. aeruginosa*		AWD	[345]
Cyprinus carpio	AA		G+: *Staphylococcus epidermis* G-: *Aeromonas salmonicida, E. coli, Listonella anguillarum, P. aeruginosa, Salmonella enterica, Yersinia ruckeri*	BD	[278]
Epinephelus tauvina	AA	G-: *A. hydrophila, E. coli, S. typhi, K. pneumonia, Proteus mirabilis, Pseudomonas fluorescens, Vibrio alginolyticus, Vibrio harveyi, Vibrio parahemolyticus*		AWD	[341]
Melanogrammus aeglefinus	AA	G+: *S. epidermis* G-: *A. salmonicida, E. coli, L. anguillarum, P. aeruginosa, S. enterica, Y. ruckeri*		BD	[278]
Morone saxatilis	AA		G-: *S. enterica*	BD	[278]
Myxine glutinosa	AA	G+: *S. epidermis* G-: *A. salmonicida, E. coli, L. anguillarum, P. aeruginosa, S. enterica, Y. ruckeri*		BD	[278]

Table S-3. List of antibacterial studies using acidic skin mucus extracts from different fish species.

Fish species	Extraction[1]	Bacteria[2]		Antimicrobial assay[3]	Ref.
		Sensitive	Resistant		
Oreochromis niloticus	AA	G-: *V. harveyi*	G-: *V. parahaemolyticus*	BD, OD	[343]
	AA	G+: *E. faecalis, M. luteus, S. aureus,* G-: *A. hydrophila, E. coli, K. pneumoniae, P. aeruginosa*		AWD	[345]
Puntius sophore	AA	G+: *B. subtilis, S. aureus* G-: *E. coli, P. aeruginosa*		AWD	[346]
Rita rita	AA, TFA	G+: *S. aureus and M. luteus* G -: *S. typhi*	G -: *E. coli, P. aeruginosa*	DD	[338]
Salvelinus alpinus	AA		G-: *S. enterica*	BD	[278]
Salvelinus fontinalis	AA	G+: *S. epidermis* G-: *A. salmonicida, E. coli, L. anguillarum, P. aeruginosa, Salmonella enterica, Y. ruckeri*		BD	[278]

[1]: AA: acetic acid TFA: trifluoroacetic acid.
[2]: G+: Gram-positive; G-: Gram-negative
[3]: AWD: agar well diffusion; BD: broth dilution; DD: disc diffusion; OD: optical density

Table S-4. List of antibacterial studies using crude skin mucus from different fish species.

Fish species	Bacteria[1]		Antimicrobial assay[2]	Ref.
	Sensitive	Resistant		
Argyrosomus regius	G-: *Escherichia coli, Pseudomonas anguilliseptica, Vibrio anguillarum*		OD	[266]
Channa argus	G-: *E. coli*		OD	
Channa striatus	G-: *A. hydrophila*	G+: *Bacillus subtilis* G-: *Klebsiella pneumoniae, Pseudomonas aeruginosa, Proteus vulgaris, Salmonella enteritidis*	DD, BD	[299]
Clarias batrachus	G+: *B. subtilis, Staphylococcus aureus* G-: *K. pneumoniae, P. vulgaris, P. aeruginosa, S. paratyphi*		DD	[286]
Ctenopharyngodon idella	G+: *Bacillus cereus, S. aureus, Staphylococcus epidermidis* G-: *A. hydrophila, E. coli, K. pneumoniae, P. aeruginosa*		AWD	[294]
Cyprinus carpio	G+: *B. cereus, S. aureus, S. epidermidis* G-: *A. hydrophila, E. coli, K. pneumoniae, P. aeruginosa*		AWD	[294]
Dasyatis pastinaca	G-: *E. coli, K. pneumoniae, P. aeruginosa*	G+: *E. faecalis, S. aureus, Streptococcus agalactiae*	CC	[296]
Dicentrarchus labrax	G-: *E. coli, V. anguillarum*	G-: *Pseudomonas anguilliseptica*	OD	[266]
Oncorhynchus mykiss		G+: *B. cereus, S. aureus, S. pneumoniae* G-: *Citrobacter freundii, Enterobacter aerogenes, E. coli, Klebsiella oxyttoca, K. pneumoniae, Neisseria lactamica, Proteus mirabilis, Pseudomonas fluorescens, P. vulgaris, P. aeruginosa*	DD	[297]
Sparus aurata	G-: *E. coli, Pseudomonas anguilliseptica, V. anguillarum,*		OD	[266]

[1]: G+: Gram-positive; G-: Gram-negative

2: AWD: agar well diffusion; BD: broth dilution; CC: cell counting; DD: disc diffusion; OD: optical density

CHAPTER 2

CHAPTER 2: BOVINE SERUM ALBUMIN AND LYSOZYME NANOFIBERS AS VERSATILE PLATFORMS FOR PRESERVING LOADED BIOACTIVE COMPOUNDS

SUMMARY OF RESULTS

This study presents an innovative approach to encapsulating therapeutic proteins within electrospun NFs, using PEO in combination with proteins such as BSA and LYZ. Electrospinning was optimized to produce NFs with diameters between 300 and 750 nm, with higher protein concentrations yielding more uniform fibers. Protein integrity and structure were confirmed post-electrospinning using SDS-PAGE and FTIR analysis, showing that the process preserved the active forms of BSA and LYZ, which is critical for applications requiring intact protein functionality.

To evaluate the feasibility of the platform for delivering functional bioactives, the study incorporated the AMP PIS and antibody HRP-IgG into the BSA and LYZ NFs. These additions allowed the team to explore the NFs' ability to maintain bioactivity post-encapsulation. Antibacterial assays revealed that PIS retained its activity within the NFs, effectively inhibiting a broad range of bacterial species, including resistant strains such as MRSA. Interestingly, LYZ/PIS NFs often demonstrated higher antibacterial efficacy than BSA/PIS NFs, suggesting a potential synergistic effect between LYZ and PIS. This synergy could represent a promising avenue for developing antimicrobial materials with enhanced potency, especially in medical applications where resistance is a concern.

In addition to antimicrobial efficacy, the study assessed the stability and functionality of the antibody encapsulated within NFs. HRP-IgG-loaded NFs maintained notable peroxidase activity, particularly in the BSA-based formulations, which appeared to offer a protective effect on the antibody, reducing activity loss during storage and processing. This outcome aligns with known stabilizing properties of BSA, which help shield proteins from denaturation and enzymatic degradation. The study demonstrated that BSA/HRP-IgG NFs retained around 32% of the antibody activity, with preserved epitope recognition, a critical feature for therapeutic and diagnostic uses. These findings highlight the potential for using protein-enriched NFs as encapsulation platforms for complex proteins, enhancing their stability while maintaining their biological activity.

The implications of the study extend to a range of promising applications where controlled release and stability are essential. The electrospun PEO-based NFs developed here represent a versatile approach, leveraging the biocompatibility and tunable properties of PEO alongside the functional diversity of proteins. By adjusting the polymer-protein ratios and electrospinning conditions, the research opens doors to custom-designed NFs capable of encapsulating and delivering various bioactives, from antimicrobial agents to antibodies and enzymes. Future work may involve refining these nanofibrous systems with additional polymer modifications to optimize release profiles, enhance bioactivity preservation, and explore new synergistic interactions between encapsulated compounds.

Bovine serum albumin and lysozyme nanofibers as versatile platforms for preserving loaded bioactive compounds

Rocío Díaz-Puertas, Enrique Rodríguez-Cañas, María Jesús Lozoya-Agulló, Pedro Valentín Badía-Hernández, Francisco Javier Álvarez-Martínez, Alberto Falcó, Ricardo Mallavia

Abstract

In this study, the electrospinning procedure was optimized to create polyethylene oxide (PEO) NFs highly enriched in proteins with non-structural functions while preserving their activity. For this purpose, several immune-related proteins of low, medium and high molecular weights were used as molecular models. Initially, the electrospinning parameters were adjusted using 3 % w/w PEO and bovine serum albumin (BSA, 5–20 % w/ w). As determined by FESEM, their average diameters ranged from 301 to 752 nm, and those with higher protein content (15–20 %) yielded more uniform NFs in both size and morphology terms. Protein integrity remained stable as determined by SDS-PAGE and FTIR. Similar results were observed for the polypeptide lysozyme (LYZ) when incorporated in NFs under these settings. To further explore the potential of these materials, the antimicrobial peptide piscidin (PIS) and an antibody (Ab, HRP-IgG) were used to produce BSA/PIS, LYZ/PIS and BSA/ Ab NFs and evaluate the preservation of their activity. The antibacterial assays showed that, in most bacterial species, the activity of PIS remained consistent after being incorporated into the NFs. Furthermore, the activity of HRP-IgG was maintained within the NFs, with enhanced preservation observed in BSA/Ab NFs. These findings expand the possibilities of protein utilization across various applications through nanomaterials.

Keywords: electrospinning; nanofibers; proteins; antimicrobial peptides; antibody.

1. Introduction

Natural bioresources offer a vast array of protein structures, collectively representing a rich source of important, specific, and often unique bioactivities with potential for exploitation in various applications. Through dedicated research and development, there is a significant opportunity to harness these functionalities for the prevention, mitigation, and treatment of numerous medical conditions. In fact, the successful application of certain proteins in treating severe diseases has recently transformed the pharmaceutical and biotechnological industries, sparking growing interest in further advancements. As a consequence, there has been a significant increase in the number of protein-based drugs approved by the US Food and Drug Administration (FDA) in the last decades, reaching about 894 therapeutic proteins in 2024 as it is collected in the THPdb2 database of all FDA-approved therapeutic proteins [347], what implies nearly 4 times more than in its previous version, THPdb (239), released 7 years before [348].

Despite the promising potential of proteins as therapeutics and the growing advances in the field of biotechnology, several limitations reducing their therapeutic activity impede the progress of many candidates through industrial pipelines. Regardless of their route of administration, therapeutic proteins encounter common challenges that compromise their safety and efficacy, such as immunogenicity, low solubility, poor stability and short half-life. Additionally, their practical use and affordability are limited by factors like short shelf life and high costs. Therapeutic proteins intended for topical applications also face additional constraints such as inadequate skin absorption and lack of suitable delivery formats [349]. Innovative strategies such as chemical modifications of the active ingredients have contributed to notably meliorate some particular limitations, but attention is now focused on excipient development due to the recent multiple benefits provided by new forms and compositions of the overall delivery system formulation. For topical applications, besides the film-forming and ionic liquid systems [350], the

implementation of nanocarriers or nano-delivery systems (i.e., transporters which nanometric size confers them with new unique properties) has improved therapeutic performances of several drugs.

Among the different types of nanocarriers, polymeric NFs offer several interesting therapeutic advantages for topical applications extensively discussed in the literature [351]. One common method for synthesizing polymeric NFs is electrospinning, a technique that produces fibers with controlled diameters and high surface area. As for any other nanomaterial, the high surface-to-volume ratio of NFs increases their loading capacity not only for the specific drug, but also for additional adjuvants. In the specific case of polymeric NFs, the molecular rearrangements inherent to the electrospinning process, together with the wide availability of different biocompatible polymers (and therefore physicochemical conditions), allow the encapsulation of poorly soluble compounds, as well as multiple design options to tune the release kinetics as desired. This versatility can also be used to enhance the protection and molecular stability of the content, thereby extending the shelf life of the formulation and increasing its commercial interest. Other advantages of this particular format include the ability of creating favorable physiological microenvironments functionally mimicking the natural extracellular matrix to enhance cell migration, attachment and proliferation and thus processes such as wound healing and hemostasis [352]. Finally, it is also remarkable that these nanoformulations allow more precise dosage control and ease of administration at the site of disease, which promotes therapeutic efficacy and patient compliance, as well as safe shelf management.

Despite these advantages, research on encapsulating therapeutic proteins in polymeric NFs remains both limited and often biased. A likely explanation for this is that the intricate structural complexity of many therapeutic proteins may be compromised during NF fabrication, either due to physicochemical conditions and/or direct interactions with the polymer or solvent. This, in turn, could impair their activity, as outlined by Anfinsen's dogma. Indeed, most studies in this field tend to focus on filamentous proteins, such as collagen [353] elastin [354], gelatin [355], keratin [356], and silk fibroin [78], whose structural roles are less dependent on their conformation. By contrast, for proteins with a more critical dependence on molecular structure-activity relationships, such as enzymes (e.g., lysozyme [357,358], lipase [359], and peroxidase [360]), or antibodies [361], their incorporation to NFs is typically achieved through covalent immobilization to the polymer used. Fewer studies have explored the free incorporation of these proteins into NFs, specially by electrospinning, and then assessed their activity. Among them, BSA stands out as one of the most extensively studied globular proteins, valued for its wide availability, low cost, and crucial role as a transporter and stabilizing agent. For instance, dressings of 11 % (w/w) polycaprolactone (PCL) NFs loaded with 1–3 % (w/w) BSA stimulated wound healing processes [362]. In another study, PEO (5 %, w/w) NFs with BSA (0.5 %, w/w) were produced by needleless electrospinning without altering the protein structure [363]. LYZ, an important protein of the innate immune system with potent antimicrobial activity and which structure-activity relationship has been widely described [364], was also encapsulated (0.2 %, w/w relative to polymer mass) into NFs of PCL/PEO blends via emulsion electrospinning [365]. Remarkably, in this study it was demonstrated that the release of LYZ was facilitated by the hydrophilic nature of PEO, which enhanced the diffusion of water into the electrospun NFs [365].

PEO, also known as polyethylene glycol (PEG) for molecular weights below 20 kDa, is a commercially available polyether that comes in a wide range of molecular weights at relatively low cost. Its exceptional resistance to protein adsorption, along with poor cell adhesion and minimal toxicity and immunogenicity, has led to its approval by the FDA for various biomedical applications. Additionally, it offers high chemical stability and, importantly, high solubility in water [366], the ideal solvent (aqueous solutions) for therapeutic proteins. These properties make this polymer highly promising for the nanoencapsulation of therapeutic proteins; specifically, in

the case of NFs, the higher molecular weight of PEO enhances polymer entanglement [367,368] and impermeability [369], thereby improving the stability of the resulting nanomaterial.

In this study, we aim to further explore this approach by testing the suitability of electrospun PEO NFs as a delivery vehicle for therapeutic proteins for potential biomedical applications. To this end, we begin by using BSA (approximately 66 kDa) to optimize the electrospinning parameters, allowing us to refine the fabrication of NFs with three proteins of quantifiable activity, spanning a wide range of molecular sizes and structural complexities: the AMP PIS from European seabass (PIS, 2.6 kDa), chicken LYZ (14.3 kDa), and HRP-IgG (nearly 200 kDa). Finally, after analyzing the integrity of the encapsulated proteins, we assess their activity in order to determine the retainment of activity after the full process.

2. Materials and methods

2.1. Materials

PEO (Mw 600–1000 kg/mol), Standard Fetal Bovine Serum, DMEM and Dulbecco's PBS were acquired from Thermo Fisher Scientific (Waltham, MA, USA). LYZ (chicken egg white, A3711,0050; Activity 20,780 U/mg) was procured by Panreac, ITW Reagents (Barcelona, Spain). BSA (heat shock fraction, pH 7, purity >98 %; A7906-50G), INT, MH agar and HRP-IgG, A5278) were obtained from Sigma-Aldrich (St. Louis, MO, USA). MH broth was provided by Condalab (Madrid, Spain). PIS (from European sea bass, accession # MT066191, C-terminal amidation and purity >90 %) was purchased from Genscript Biotech Corp (Piscataway, NJ, USA). TMB was acquired from Bio-Rad Laboratories GmbH, Munich, Germany.

2.2. Preparation of solutions for electrospinning

2.2.1. Starting solutions and viscosity determination

Hereafter all concentrations expressed as percentages will be based on weight/weight (w/w), unless stated otherwise. PEO solutions with protein (BSA or LYZ) were obtained by dissolving 5 to 20 % protein and 3 % PEO in Milli-Q water (solvent compatible with both types of molecules, especially proteinic ones). All the solutions were kept stirring for 12 h until their complete dissolution and homogenization. The kinematic viscosity (ν) of all blend solutions was performed by using a series of calibrated Cannon-Fenske capillary viscometers series 400–450 (Vidra Foc, Barcelona, Spain) to elucidate their electrospinnability. Corresponding density (ρ) was measured with calibrated volumetric flask, in order to estimate their shear viscosity (η νρ [mPa·s]). The average value of three measurements at 313 K was represented as mean and SD.

2.2.2. Peptide and antibody solutions

After optimization, an electrospinnable solution containing 15 % of total protein and 3 % of PEO was selected to add the peptide and anti- body. The concentrations were chosen based on the minimum concentration added at which activity was observed. The chosen peptide was PIS, a small 22-residue AMP. PIS was added at 0.1 % in both BSA (BSA/PIS) and LYZ (LYZ/PIS) solutions to compare the anti- bacterial activity of both types of NFs. To assess the stability of larger and more complex proteins within the NF system studied here there were produced NFs loaded with peroXidase-conjugated antibody, in particular an HRP-IgG commonly used as secondary antibody for immunolabelling assays. HRP-IgG was added at 1 % in BSA solutions (BSA/Ab).

2.3. Electrospinning

The solutions were transferred to 2 mL syringes (Becton Dickinson, Franklin Lakes, NJ, USA) attached to a blunt-end stainless steel hypo- dermic needle (5 cm in length, outer diameter of 1.27

cm and inner diameter of 0.84 cm) (Sigma-Aldrich). Solutions were electrospun at a sustained flow controlled by a KDS 100 infusion pump (KD Scientific, Holliston, MA, USA) and using a high voltage source (Glassman High Voltage Inc., Whitehouse Station, NJ, USA) as previously described [370]. The optimization of the electrospinning conditions was a multi-step process involving the fine-tuning of both the polymer solution (i.e., by testing the concentration gradient described above) and the electro- spinning parameters. The key parameters that were modified included the applied voltage, the tip-to-collector distance, and the flow rate. These parameters were systematically varied within the following ranges: voltage from 10 to 20 kV, tip-to-collector distance from 12 to 18 cm, and flow rate from 0.2 to 0.5 mL/h. These ranges were chosen based on our previous studies, some of which used water as a solvent [370,371]. Through this systematic variation, the optimal electrospinning conditions were determined to be an applied voltage of 18 kV, at a tip-to-collector distance of 17 cm, with a flow rate of 0.25 mL/h, always at 20–40 % relative humidity and 25 ◦C. These conditions were found to produce NFs with the most desirable morphology and size, including minimization of electrospray, small droplets and NF defects such as beads or ribbon-like structures. The obtained NFs were deposited in aluminum foil-coated glass slides. After the electrospinning process, which involved solvent evaporation, the protein and polymer content varied, as reflected in Table 8. The NFs were not further processed for subsequent analyses unless otherwise stated in the corresponding section.

Table 8. Polymer (PEO) and protein content in the starting polymeric solutions and obtained NFs.

Polymeric solutions (w/w %)		Electrospun NFs (w/w %)	
PEO	Protein	PEO	Protein
3	5	37	63
	10	23	77
	15	17	83
	20	13	87

2.4. Microscopy

NFs were initially screened using a Microsystems DMI3000B inverted fluorescence optical microscope (Leica, Bensheim, Germany) with a Leica EL6000 compact light source and a Leica DFC 3000G digital camera. The images were processed using the program Leica Application Suite AF 6000 Module Systems. The morphology and size of NFs were later analyzed by FESEM with a Schottky cathode model SIGMA 300 VP (Zeiss, Oberkochen, Germany) apparatus after chrome metallization. The average diameter of different types of NFs was determined using Image J (National Institutes of Health) image processing and analysis software from 100 measurements for each type of NFs using different FESEM images. The CV was calculated by dividing the SD by the mean.

2.5. Electrophoresis

The protein integrity after electrospinning was assessed by SDS-PAGE. NFs from 5 to 15 % protein solutions were dissolved back in water to reach 10 µg/µL protein concentrations, separated by SDS-PAGE (Bio-Rad Laboratories Inc., CA, USA) under denaturing conditions in 4–20 % TGX gels (Bio-Rad Laboratories Inc.), and visualized with Brilliant Blue R-250 (Bio-Rad Laboratories Inc.). Molecular weight markers (Precision Plus Protein Standards Dual Colour, Bio-Rad Laboratories Inc.) were loaded in the first well of the gel.

2.6. Infrared spectroscopy

FTIR spectroscopy was performed to define the functional groups of all samples using a Spectrum Two™ FTIR spectrometer (PerkinElmer, MA, USA). PEO, BSA and LYZ powder samples were mixed with KBr and pressed into pellets. Nanofibrous mats were directly measured. Four spectral

scans in transmission mode were averaged throughout the spectral range of 4000–450 cm^{-1} with the resolution of 4 cm^{-1} at room temperature.

2.7. Antibacterial evaluation

Aeromonas salmonicida (CECT 894), *Bacillus circulans* (CECT 10), *Bacillus subtilis* (CECT 35), *Escherichia coli* (CECT 45), *Micrococcus luteus* (CECT 243) and *Staphylococcus epidermidis* (CECT 231) bacterial species were obtained from the Spanish Type Culture Collection (CECT, Valencia, Spain). *S. aureus* and MRSA were obtained from clinical samples of patients at the General University Hospital of Alicante. Bacteria were cultured in MH broth and incubated at 30 or 37 ◦C for 24 or 48 h, depending on the species optimal growth conditions.

Antibacterial activity of commercial LYZ and PIS, and LYZ/PIS and BSA/PIS NFs was determined by broth microdilution method by MIC and MBC calculation. The pure compounds or the NF mats were first dissolved in Milli-Q water and filtered using sterile CA syringe filters with pore size of 0.22 μm. 50 μL were added in 96-well plates at different concentrations depending on the sample. A bacterial suspension of 20 μL at 0.5 McFarland were added to each well. The volume of each well was brought to 200 μL by adding MH broth. The plates were incubated at 30 or 37 ◦C for 24 or 48 h depending on the strain. A volume of 50 μL of INT solution at 1 mg/mL was added to each well and allowed to incubate for 30 min. The MIC was defined as the minimum concentration where no red colour was observed. To determine the MBC, 50 μL of the wells that did not show any signs of bacterial growth were plated and incubated overnight on MH agar plates. The lowest concentration at which no colonies were detected was defined as the MBC.

2.8. Peroxidase activity of encapsulated HRP

Stored samples of HRP-IgG-containing NFs were dissolved back in TBS to reach a final 1:500 dilution of the initial HRP-IgG stock or equivalently in the case of control NFs without HRP-IgG. Two-folded serial dilutions were subsequently prepared from these samples up to 1:16000 dilution. Equivalent dilutions of the fresh HRP-IgG were also prepared to serve as positive control and calibration curve. Then, 5 μL of each were inoculated into MaxiSorp™ 96-well plates (NUNC, Rochester, NY, USA) in triplicate and incubated with additional 95 μL of TMB substrate commercial solution for 30 min at 37 ºC in the dark.

Finally, the reaction was stopped with 50 μL of 1 N H2SO4, and the absorbance measured at 450 nm using an UltraEvolution automatic plate reader (Tecan, Männedorf, Switzerland).

2.9. Antigen-recognition activity of encapsulated IgG

The assessment of the viability of the encapsulated HRP-IgGs was carried by adapting a direct ELISA procedure. Thus, MaxiSorp™ 96-well plates were coated with 50 μL of a 1:4 dilution of an in-house hybridoma supernatant in TBS containing 0.4 mg/ml of protein as determined using a Nanodrop 2000c (Thermo Scientific, Wilmington, DE, USA), and incubated overnight at 4 ºC. After three washes of 5 min with 200 μL TBS supplemented with 0.05 % (v/v) Tween-20 (TTBS) and one with TBS, plates were blocked with 100 μL of 1 % (w/v) BSA in TBS for 1 h at 37 ºC. Subsequently, the washing steps were repeated and 50 μL of each dilution of the dissolved NFs and corresponding control samples described above were added. Plates were incubated at 37 ºC for 1 h and washed again. Finally, the reaction with TMB substrate (100 μL/well) and the absorbance measurement were carried out as described above.

2.10. Data analysis

All experimental data are expressed as mean values ± SD. Data manipulation, analysis and graph creation were carried out using Prism v8 software (GraphPad software, La Jolla, CA, USA), depending on each particular experimental design.

3. Results

3.1. Solution viscosity and electrospinning

Firstly, the viscosity of different PEO solutions at concentrations ranging from 2 to 5 % was evaluated to determine the optimal concentration for NFs formation and their molecular weight. The viscosity of PEO solutions increased with concentration and ranged from 189 ± 3 mPa·s at 2 % to 8060 ± 113 mPa·s at 5 % (Figure 15A). In basis on these viscosity results, the nominal molecular weight of PEO was estimated around 580–620 kg/mol.

Only PEO solutions with a concentration of 4 % or higher (viscosity of 3515 ± 25 mPa·s) were able to form continuous NFs without beads. Although the 3 % PEO solution (viscosity of 749 ± 37 mPa·s) was not able to form fibers on its own, when the protein was added at concentrations of 5 to 20 %, it was able to be electrospun. Therefore, a 3 % concentration of the building polymer was chosen to synthesize the protein NFs. Figure 15B shows the viscosities of the BSA and LYZ solutions, which increased with protein concentration.

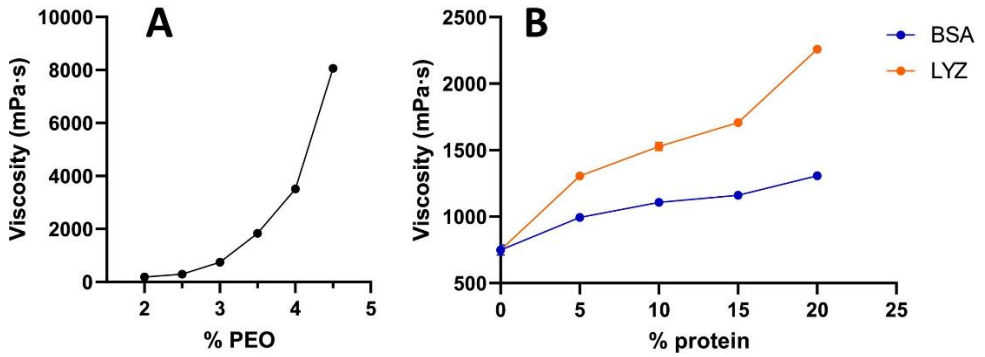

Figure 15. Viscosity of polymeric solutions containing different concentrations of PEO (A) and containing 3 % PEO and different concentrations of BSA and LYZ (B). Relative error < 5 % for n = 3

3.2. Morphology of nanofibers

The morphology of the electrospun NFs was analyzed using FESEM. Figure 16 displays both the detailed FESEM images and the frequency histograms of the diameter distribution of the NFs of BSA and LYZ at different concentrations. The general images of the NFs at lower magnification can be observed in Figure S-1.

As can be observed in Figure 16, the diameter of the NFs increased with increasing protein concentration and CVs were within the range of 11–24 % in both cases. The appearance of the NFs from 15 and 20 % of protein solutions (BSA and LYZ) was smooth and uniform, without any visible deformities or irregularities. However, the NFs produced from 5 % solutions, especially 5 % BSA NFs, displayed certain irregularities such as small droplets, fused fibers or beads. Based on these results, the 15 % protein solutions were selected to further functionalize this NFs, as it was the lowest concentration at which no fused NFs, deformations, or excessive electrospray were observed.

3.3. Protein integrity

SDS-PAGE was conducted to verify that the proteins have not undergone alterations affecting their size, such as degradative processes or covalently stabilized aggregations, as these could have implications for their activity. To do so, the amount of protein present in the NFs was estimated and normalized to the same amount of protein. Figure 17 shows the bands revealed in the gels with BSA and LYZ NFs. It was found that the electrophoretic mobility of the electrospun BSA and LYZ NFs was equivalent to that of the commercially available BSA and LYZ. The gel analysis of BSA NFs revealed a consistent molecular weight of approximately 65 kDa in all lanes, which corresponds to the expected molecular weight of BSA (lane 1). The band density observed in lanes 2–5 was around 100 % compared to the control protein (lane 1). On the other hand, for LYZ gel, the molecular weights of all lanes were approximately 12 kDa, consistent with the expected molecular weight of LYZ (lane 1), and the band densities in lanes 2–4 were also close to 100 % compared to lane 1 or LYZ control.

The FTIR spectra of the electrospun NFs were obtained to investigate their chemical composition and are shown in Figure 18, together with their starting components prepared in pellets. Hence, they exhibit characteristic bands of the base polymer (PEO) corresponding to the frequencies 1103 cm^{-1} (C-O-C stretching) and 956 and 840 cm^{-1} (asymmetric CH_2 rocking motion). These spectral features were also discernible in the spectra of the NFs containing proteins, as depicted in the inset of the spectral figures. Furthermore, there is no discernible alteration in the amide bands of the native proteins under investigation (BSA and LYZ). In both cases, the predominant presence of these proteins in the NFs closely resembles that observed in the unprocessed source material. Consequently, the stability and constancy of amide I at 1657 cm^{-1}, as well as amide A, amide II, and amide III (at 3303 cm^{-1}, 1540 cm^{-1}, and 1240 cm^{-1}, respectively) is noteworthy.

Finally, the integrity of the LYZ NFs was also evaluated in terms of maintaining their antibacterial activity. Initially, a screening of commercial LYZ against all bacteria used in this study was conducted, and it was observed that it was only capable of inhibiting *B. circulans*. Subsequently, the antibacterial capacity of the LYZ NFs (5–20 %) was evaluated, and it was observed that the antibacterial activity was maintained at the same level as the free LYZ (Table S-5).

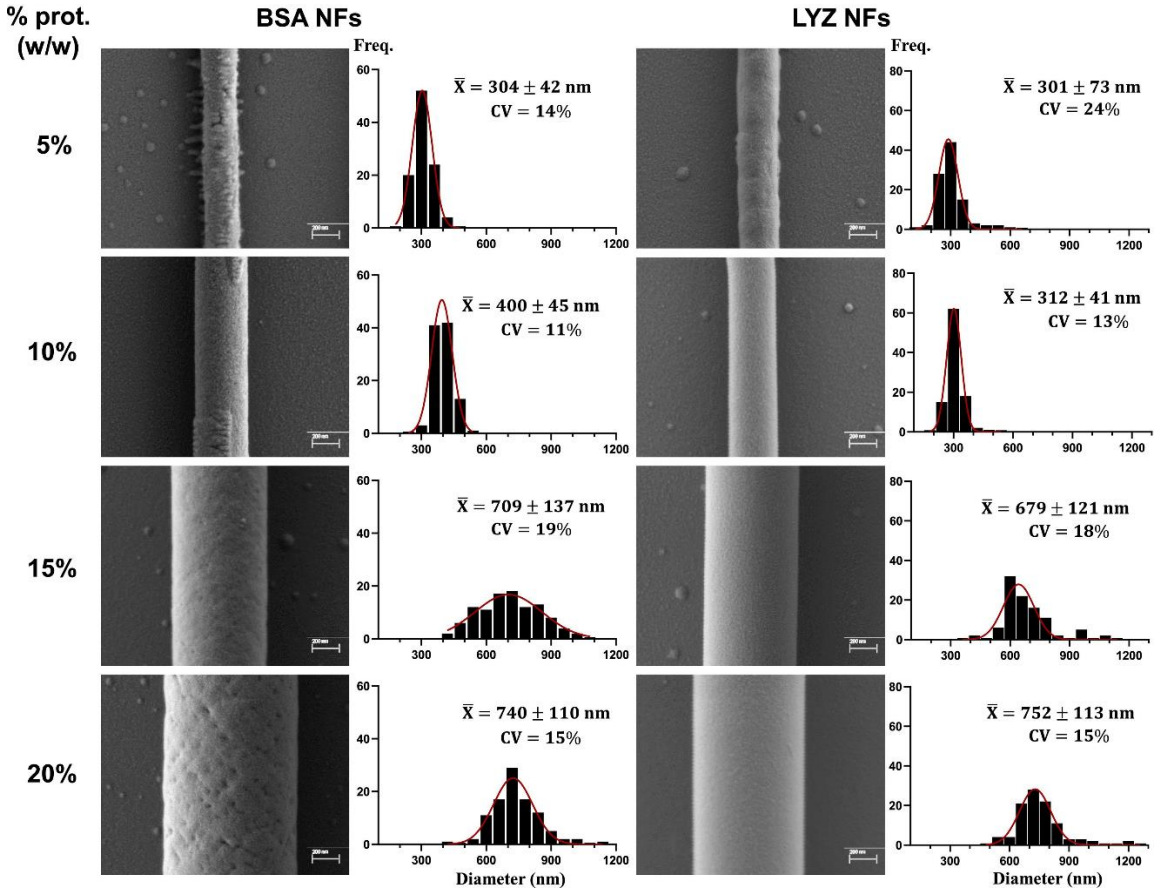

Figure 16. FESEM images and diameter frequency histograms of electrospun NFs containing PEO and different concentrations of BSA and LYZ. Representative FESEM micrographs and corresponding diameter frequency histograms for BSA (5–20 %) and LYZ (5–20 %) are shown. Prot. refers to the BSA and LYZ proteins, as appropriate. Histogram data were obtained from multiple micrographs (100 individual measurements). Best-fit adjustments to a Gaussian distribution are indicated in red. Average diameter (X) ± SD, as well as coefficient of variation (CV, %) are also stated. Scale bar: 200 nm.

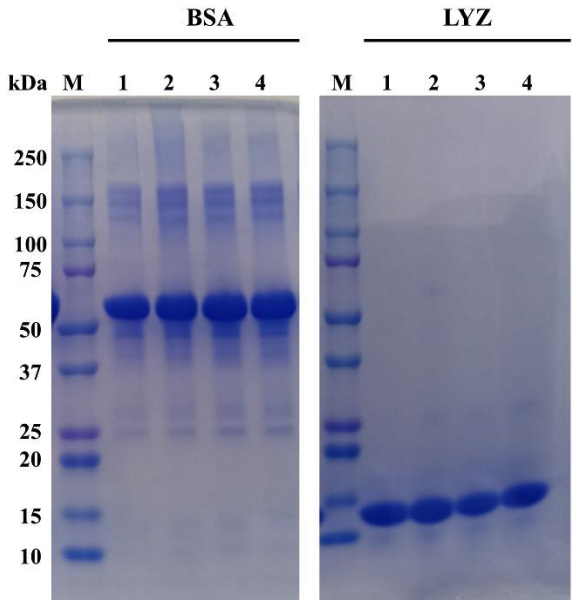

Figure 17. SDS-PAGE results of BSA (left) and LYZ (right) NFs. In each lane, NFs corresponding to 10 µg of protein were loaded. M: marker; Lane 1: protein (BSA or LYZ) control; lane 2: 5 % protein NFs; lane 3: 10 % protein NFs; lane 4: 15 % protein NFs; M: marker.

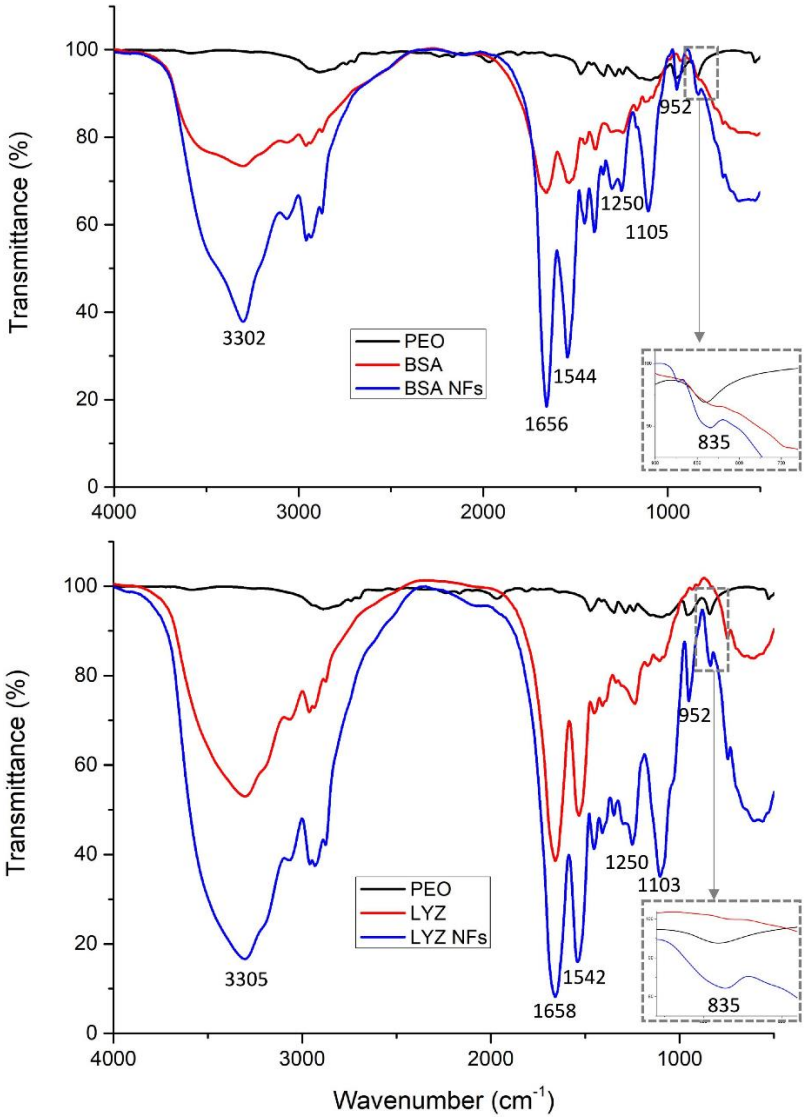

Figure 18. FTIR spectra of BSA, PEO and BSA/PEO NFs (top) and LYZ, PEO and LYZ/PEO NFs (bottom). The PEO and unprocessed protein samples were prepared into KBr pellets. The NFs were prepared from 15 % protein and 3 % PEO solutions, and the mats were measured in their unprocessed state. Inset: enlarged detail of 840 cm^{-1} band corresponding to the PEO asymmetric CH_2 rocking motion.

3.4. Preparation of PIS NFs and determination of antibacterial activity

First, a screening of the antibacterial activity of PIS against Gram-negative bacteria *A. salmonicida* and *E. coli*, and Gram-positive bacteria *B. circulans*, *B. subtilis*, *M. luteus*, *S. aureus* (including MRSA) and *S. epidermidis* was conducted, and it was able to inhibit all tested bacteria. Therefore, PIS was incorporated into both BSA and LYZ NFs. The synthesized NFs can be observed in Figure 19. In both cases, the NFs were uniform, and the diameters were 625 ± 58 nm for the BSA/PIS NFs and 618 ± 73 nm for the LYZ/PIS NFs. FESEM images of the NFs at lower magnification can be found in Figure S-2.

Subsequently, the antibacterial potential of BSA/PIS and LYZ/PIS NFs against all bacterial species was assessed. Table 9 shows the results of the 96-well microdilution assays of the free PIS and the proportional part to the PIS of the BSA/PIS and LYZ/PIS NFs.

In this study, free PIS was capable to inhibit all bacteria tested with MIC values ranging 3.9–15.6 μg/mL and MBC from 7.8 to 62.5 μg/mL. Regarding the BSA/PIS and LYZ/PIS NFs, all of them

also showed antibacterial activity against all tested bacteria. In bacterial species *M. luteus*, *S. aureus*, MRSA and *S. epidermidis*, the MIC remained unchanged. However, in *A. salmonicida*, *B. circulans*, *B. subtilis* and *E. coli*, both the MIC and the MBC were increased, especially in the BSA/PIS NFs. Additionally, in most cases, the activity of the LYZ/PIS NFs was greater than that of the BSA/PIS NFs, even surpassing that of the free PIS in some species, as highlighted in bold in Table 9.

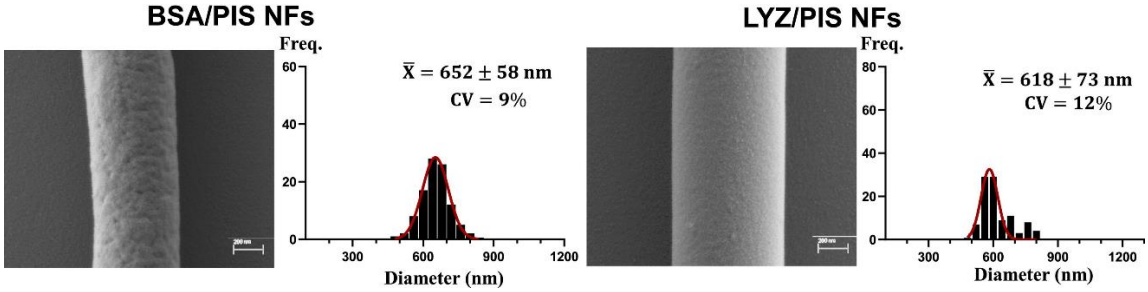

Figure 19. FESEM images and diameter frequency histograms of BSA/PIS (left) and LYZ/PIS (right) electrospun NFs. Histogram data were obtained from multiple micrographs (100 individual measurements). Best-fit adjustments to a Gaussian distribution are indicated in red. Average diameter (X) ± SD, as well as coefficient of variation (CV, %) are also stated. Scale bar: 200 nm.

Table 9. Minimum inhibitory concentration (MIC) and minimum bactericidal concentration (MBC) of commercial PIS and the proportion of PIS contained in the BSA/ PIS and LYZ/PIS NFs against *A. salmonicida*, *B. circulans*, *B. subtilis*, *E. coli*, *M. luteus*, *S. aureus*, MRSA and *S. epidermidis*.

Microorganism	MIC (µg/mL)			MBC (µg/mL)		
	PIS	BSA/PIS	LYZ/PIS	PIS	BSA/PIS	LYZ/PIS
A. salmonicida	7.8	31.3	7.8	15.6	249.6	15.6
B. circulans	15.6	62.6	**5.0**	15.6	249.6	**7.8**
B. subtilis	15.6	31.3	**7.8**	31.3	62.6	31.3
E. coli	31.3	62.6	31.3	62.6	124.8	124.8
M. luteus	15.6	15.6	**7.8**	31.3	124.8	62.6
S. aureus	31.3	31.3	31.3	62.6	62.6	62.6
MRSA	15.6	15.6	**7.8**	31.3	31.3	31.3
S. epidermidis	3.9	3.9	**2.0**	7.8	7.8	**2.0**

3.5. Preparation of Ab NFs and activity analysis of peroxidase-conjugated antibody

To test the feasibility of the system with larger and more complex proteins with non-structural functions, the repertoire of proteins to be encapsulated was extended. A commercial combination of peroxidase and antibody, i.e., HRP-IgG, was incorporated into the BSA NFs. Figure 20 displays an image of the synthesized BSA/Ab NFs as well as the frequency histogram of diameters. The synthesized NFs were homogeneous, with an average diameter of 513 ± 70 nm. Figure S-3 shows general images of these NFs at lower magnification.

PEO and PEO/BSA NFs with HRP-IgG and without HRP-IgG (control) were used to test the retained activity of HRP-IgG. After 1 month of storage at 20 ºC, NFs were dissolved in TBS to a final dilution of 1:500 of the initial HRP-IgG stock, or an equivalent volume for control NFs, and 2-fold serially diluted up to 5 times. The retained peroxidase activity in these samples was then determined together with corresponding dilutions of the HRP-IgG fresh stock, which was found to adjust to a linear correlation ($Y = 1963\ X - 0.02739$; $R^2 = 0.9979$) (Figure 21A). Thus, it is

observed that, in comparison to HRP-IgG controls, the peroxidase activity of the HRP was reduced up to 7.4 ± 0.5 folds in NFs without BSA, but just only about 4 folds (precisely, 3.9 ± 0.26) in BSA NFs, meaning a residual activity of 13.5 ± 0.9 % and 25.7 ± 1.7 %, respectively.

Considering this result, in a follow-up ELISA assay targeting mouse IgG detection using these samples (Figure 21B), obtaining lower signals relative to the peroxidase activity would indicate a reduced epitope recognition activity of the antibody. However, this was not the case for NFs with BSA and encapsulated HRP-IgG. At least three dilutions from these samples showed signals above the assay's detection limit (0.0147 ± 0.003 a.u. of A_{450}). On average, these NFs retained 31.9 ± 0.9 % of their activity compared to controls (which adjusted to a quadratic correlation: $Y = 71854\,X^2 + 199.3\,X - 0.0247$; $R^2 = 0{,}9989$). For the NFs without BSA, only the lowest dilution (1:500) gave a signal within the detection limit of the assay (0.0111 ± 0.0042 a.u. of A_{450}). The average activity retention of HRP-IgG from these NFs was 8.5 ± 0.9 % compared to the control.

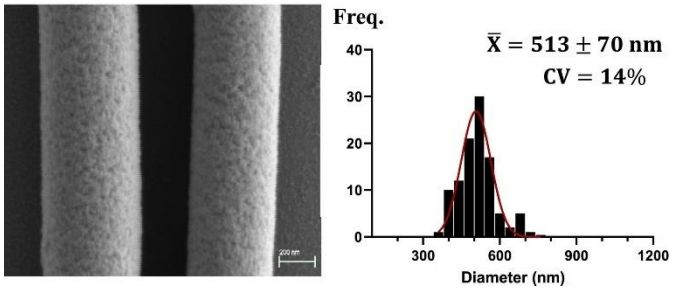

Figure 20. FESEM image and diameter frequency histogram of BSA/Ab electrospun NFs. Histogram data were obtained from multiple micrographs (100 individual measurements). Best-fit adjustments to a Gaussian distribution are indicated in red. Average diameter (X) ± SD, as well as coefficient of variation (CV, %) are also stated. Scale bar: 200 nm.

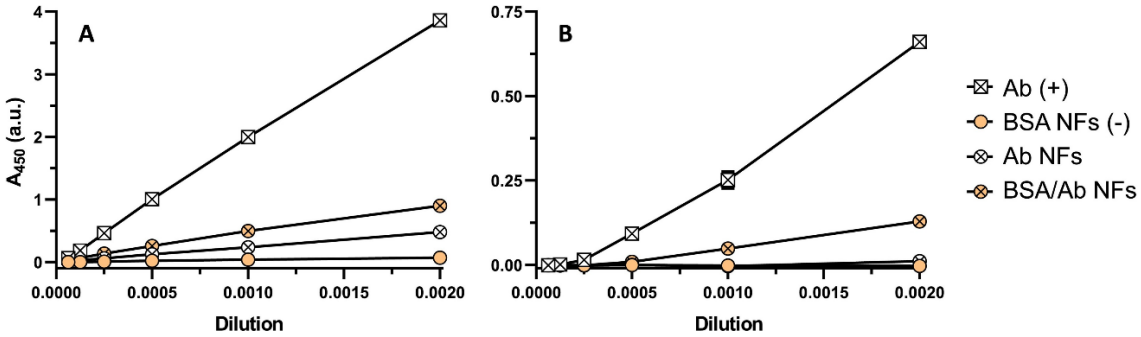

Figure 21. Peroxidase and antigen-recognition activity of NF-encapsulated HRP-IgG. Two-fold serial dilutions starting in 1:500 (i.e., 0.002 dilution) of experimental and control samples were tested for enzymatic peroxidase (A) and antigen-recognition (B) activity. Represented sample groups include HRP-IgG as positive control (Ab (+)), and BSA/PEO (negative control, BSA NF (—)), HRP-IgG-loaded PEO (Ab NF), and HRP-IgG-loaded BSA/PEO (BSA-Ab NF) NFs. Data is presented as means ± SD of absorbance values at 450 nm in arbitrary units (A_{450}, a.u.) from representative experiments, each performed in triplicate.

4. Discussion

This study represents the first report on the production and characterization of NFs with high content of two non-structural proteins, i.e., BSA and LYZ. To date, BSA and LYZ have been incorporated into NFs in combination with PEO in certain studies [362,372,373]. Nevertheless, in most of these studies, they have been utilized in limited amounts as model proteins to examine drug release, rather than serving as the primary constituent of the NFs. PEO was selected as the copolymer based on previous studies that identified PEO (nominal 600 kg/mol PEO) as an

interesting polymer for electrospinning due to its optimal biocompatibility and biodegradability properties [363].

The present study has identified viscosity of the solutions as a crucial factor in the formation of NFs. Previous reports have also highlighted the notable impact of viscosity on morphology and size during the electrospinning process [374]. Some studies indicate that viscosity ranges of 300 to 2000 mPa·s in polymeric PEO solutions are considered appropriate for electrospinning [374-376]. However, the optimal viscosity range may differ based on the specific conditions and electrospinning setup being utilized. As shown in Figure 15, viscosity increased with protein concentration and LYZ solutions showed higher viscosity than BSA solutions, which could be attributed to the repulsion that PEO induces between LYZ molecules [377], leading in turn to an increase in resistance to flow [378]. Another notable aspect is that the viscosities of all electrospinnable protein solutions are below 2300 mPa·s. However, PEO solutions with such viscosities were not able to be electrospun. This suggests that the addition of proteins can significantly improve the electrospinnability of the PEO solutions, acting as stabilizing agents. The addition of proteins in electrospinning solutions has been shown to increase conductivity [379], which in turn can enhance the uniformity of the electrospun fibers [380].

The NFs from solutions with lower protein concentration displayed certain defects, such as small droplets, which could be attributed to a combination of electrospraying and electrospinning, possibly resulting from the low viscoelasticity of the solution [381]. Overall, all NFs showed uniformity in diameter, as confirmed by CVs. A low CV suggests that there is less variation and greater consistency in a measured characteristic. Normally, a CV above 30 % indicates a high variability and therefore issues in the experiment [382]. In this case, all calculated CVs were within the range of 11–24 %, indicating high similarity in diameters within each sample.

The structure of the proteins within the NFs remained intact, as confirmed by SDS-PAGE and FTIR spectroscopy studies. Specifically, the electrophoretic mobility of the samples indicates that the proteins did not undergo any significant molecular conformation alterations during the electrospinning and solution preparation processes, as there were no significant indications of aggregation or hydrolysis [383]. On the other hand, the FTIR spectroscopy results showed distinct peaks for PEO, BSA, and LYZ, which agreed with previous findings [362,384]. BSA and LYZ NFs also exhibited these characteristic peaks, confirming the correct incorporation of protein in the NFs and indicating that the protein was not significantly altered during the electrospinning process. Finally, the structure of LYZ also demonstrated its preservation within the NFs, as the antibacterial activity was maintained at comparable levels to those of the free protein.

Once the integrity and stability of the synthesized NFs were demonstrated, the potential of these platforms as encapsulation and preservation systems for bioactive compounds was explored. To this end, proteins from the immune system with specific functions whose activities were easily evaluable were selected.

PIS was chosen for its loading into NFs due to its potent antimicrobial activity and because its incorporation into NFs had not been previously described. Its inclusion was carried out in both BSA and LYZ NFs to determine if there were differences in the antibacterial activity when evaluating it alongside a protein with and without activity. The NFs synthesized with PIS, i.e., BSA/PIS and LYZ/PIS, showed homogeneity and diameters of 625 ± 58 nm and 618 ± 73 nm, respectively. Their antibacterial activity was determined against pathogenic bacteria and an ARB (MRSA). The results obtained with free PIS are consistent with studies conducted by Pan et al., where MICs ranging from 3 to 50 μg/mL were obtained against Gram-negative bacteria [385]. Regarding the activity of the BSA/PIS and LYZ/PIS NFs, the MICs were calculated taking into account the proportion of PIS present in the NFs. It was observed that all NFs showed antibacterial activity, to a greater or lesser extent. In some species, the activity decreased compared to the free

PIS, especially in the BSA/PIS NFs, with a higher MIC or MBC being observed. The lower activity observed in BSA/PIS NFs may be related to the use of BSA as a protective agent in NFs, aiding in the controlled and sustained release of drugs and thus preventing their initial burst releases [386,387]. In some other bacterial species, it was observed that the MIC or MBC of LYZ/PIS NFs was lower than that of BSA/PIS or even free PIS, even though these bacteria were not susceptible to LYZ. This suggests a potential synergy between LYZ and PIS, which could be a promising avenue for future research.

So far, the potentially therapeutic proteins incorporated into the NF system developed here have been of low/medium molecular weight, and therefore with relatively simple and renaturable higher structures (i.e., secondary and tertiary). Consequently, it was decided to incorporate more complex proteins, such as antibodies, specifically the HRP-IgG antibody. This strategy also allowed the evaluation of both the enzymatic and antigen recognition activity of a protein complex that is larger (almost 200 kDa) than its components (about 44 kDa for HRP and 150 kDa for IgG).

Based on the results obtained, NFs without BSA exhibited a significant decrease in both peroxidase activity and epitope recognition, possibly attributed to antibody denaturation occurring during electrospinning or storage [388,389]. Conversely, the inclusion of BSA in NFs appears to suggest a potential protective effect on the peroxidase activity of HRP-IgG. Despite the reduced peroxidase activity, the epitope recognition of the antibody in NFs with BSA remained relatively intact. This observation aligns with the well-documented stabilizing properties of BSA, which can act to prevent enzyme inactivation and protect proteins from unfolding or degradation [390,391]. The inclusion of BSA within the NFs likely creates a more favorable microenvironment for HRP-IgG, mitigating the potential stresses of encapsulation and storage. Future studies will focus on this direction, as well as on tuning the polymer composition to optimize the release kinetics, with special attention to the potential synergistic effects of blends of PEO and other polymers. Such modifications could pave the way for improved control over the release profiles, which is critical for applications in drug delivery.

5. Conclusions

The study successfully synthesized BSA and LYZ NFs as stable encapsulation platforms based on high protein amounts. Besides facilitating electrospinning, this platform serves as a stabilization system for the incorporation of other bioactive compounds. The uniform appearance of proteins in the NFs, as well as their structural integrity, which remained intact even at higher concentrations, indicate the potential of the synthesized NFs for effective biomedical applications. The antibacterial activity of PIS was generally maintained compared to free PIS, with LYZ/PIS NFs being more active than BSA/PIS NFs. The Ab activity was preserved in the NFs incorporating HRP-IgG, with preservation being notably higher in the NFs containing BSA. These findings support the viability of NFs as platforms for bioactive drug administration, highlighting their ability to maintain biological activity while enhancing stability.

Supplementary material

Bovine serum albumin and lysozyme nanofibers as versatile platforms for preserving loaded bioactive compounds

Rocío Díaz-Puertas, Enrique Rodríguez-Cañas, María Jesús Lozoya-Agulló, Pedro Valentín Badía-Hernández, Francisco Javier Álvarez-Martínez, Alberto Falcó, Ricardo Mallavia

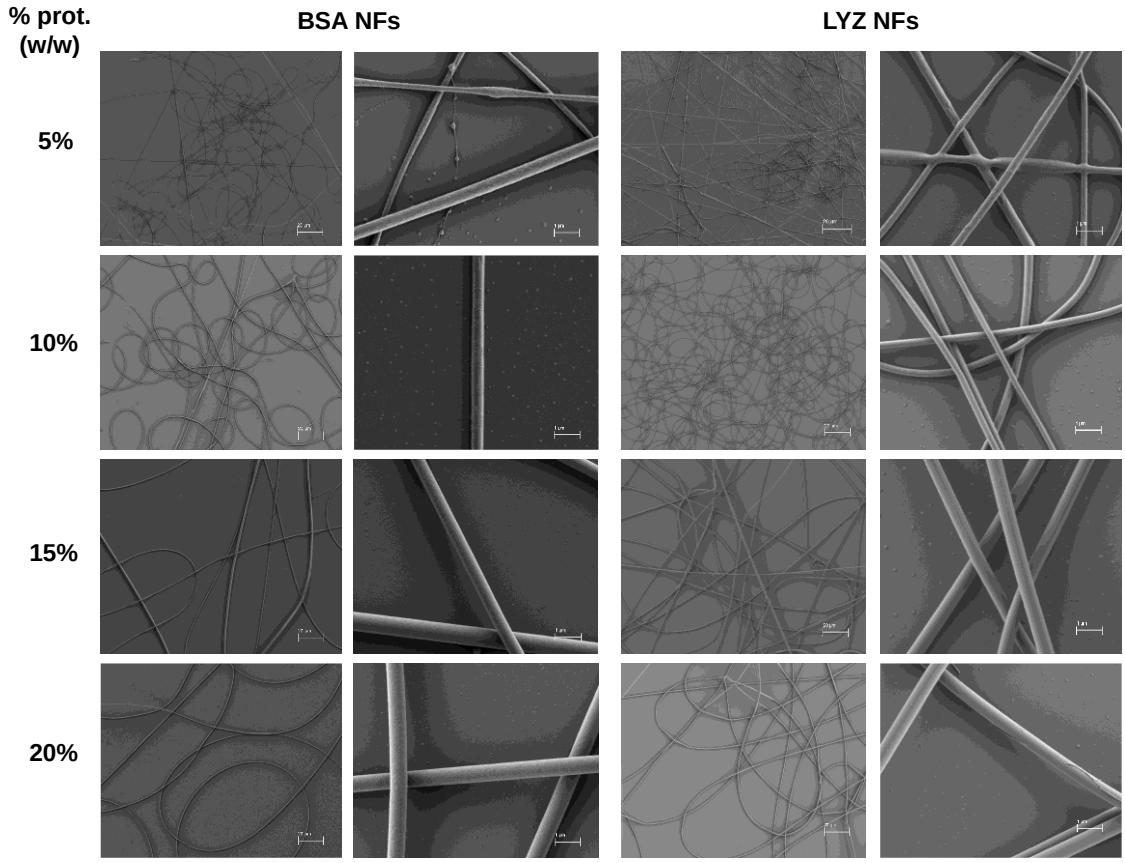

Figure S-1. FESEM images of electrospun NFs containing PEO and different concentrations of BSA and LYZ (5-20%). Scale bar: 20 µm (images on the left) and 1 µm (images on the right).

Table S-5. Minimum inhibitory concentration (MIC) and minimum bactericidal concentration (MBC) of commercial LYZ and LYZ NFs from solutions containing 5-20% w/w of LYZ against *B. circulans*.

	MIC (µg/mL)	MBC (µg/mL)
LYZ	7.5	12.5
5% NFs	10	17.5
10% NFs	7.5	15.0
15% NFs	5	12.5
20% NFs	5	12.5

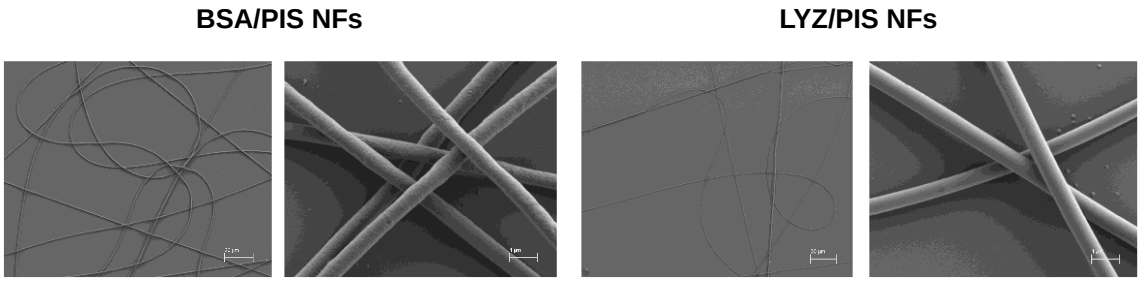

Figure S-2. FESEM images of electrospun BSA/PIS and LYZ/PIS NFs. Scale bar: 20 µm (images on the left) and 1 µm (images on the right).

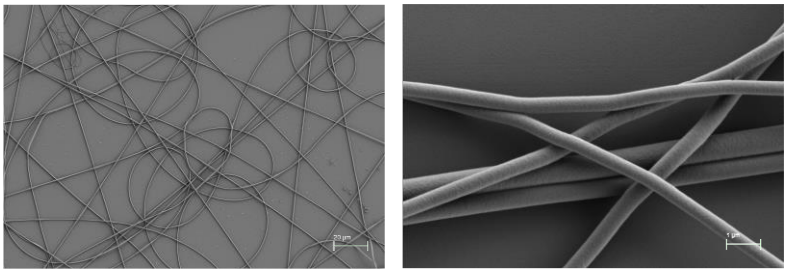

Figure S-3. FESEM images of electrospun BSA/Ab NFs. Scale bar: 20 µm (left) and 1 µm (right).

CHAPTER 3

CHAPTER 3: VIRICIDAL ACTIVITY OF THERMOPLASTIC POLYURETHANE MATERIALS WITH SILVER NANOPARTICLES

SUMMARY OF RESULTS

This research paper explores the antiviral activity of TPU materials embedded with ceramic-coated AgNPs, aiming to limit virus transmission via surface contact. This study leverages favorable properties of TPU—durability, flexibility, and biocompatibility—enhancing them with AgNPs for added antiviral functionality.

The development process involved characterizing the structure of the composite and ion-release profile. FESEM and EDX analysis confirmed the successful integration of AgNPs within the TPU, identifying silver particles averaging 54 nm in size. These particles were found within a ceramic matrix containing phosphorus, magnesium, and aluminum, a composition designed to stabilize the AgNPs and modulate their ion release. ICP-MS measured ion-release rates, finding that silver and aluminum ions were released at approximately 4 ppm/h, while magnesium was released at seven times higher rate, indicating a steady availability of bioactive ions in aqueous environments that could effectively interact with viral particles.

The biological assays revealed significant antiviral effects. Against SVCV, the AgNP-TPU composite reduced viral infectivity by approximately 75 % after a 24-hour incubation. This viricidal activity was found to increase with higher temperatures and longer exposure times. For example, SVCV infectivity reduction was 45 % at 5 °C, 52.4 % at 10 °C, and 74.1 % at 20 °C, indicating that the antiviral effect strengthens as ion release accelerates with temperature. SARS-CoV-2 showed a similar reduction in infectivity, with AgNP-TPU materials reducing viral titers by approximately 80.7%. The study suggests that silver ions likely disrupt viral integrity or interfere with viral attachment, as reported in previous research on antiviral mechanisms of silver, which include binding to viral proteins and RNA, ultimately inhibiting replication.

In addition to viricidal activity, the study examined the safety profile of the AgNP-TPU materials. Cytotoxicity tests in EPC and Vero E6/TMPRSS2 cell lines showed no significant decrease in cell viability when exposed to the AgNP-TPU eluate, supporting its effectivity for safe application in environments requiring antiviral protection. The cytotoxicity findings align with prior studies suggesting that AgNP concentrations up to 100 ppm are generally non-toxic to certain cell types. This confirms that while the AgNP-TPU composite releases sufficient ions to exhibit antiviral activity, it does not release them at levels harmful to surrounding biological tissues.

These findings underscore the potential of AgNP-TPU composites in creating safer, antiviral surfaces that can reduce the transmission of pathogens in healthcare and public environments. The stability of TPU combined with the sustained release of viricidal silver ions from embedded AgNPs makes this material a viable candidate for use in any area where high-contact surfaces are at risk for viral contamination.

Viricidal Activity of Thermoplastic Polyurethane Materials with Silver Nanoparticles

Rocío Díaz-Puertas, Enrique Rodríguez-Cañas, Melissa Bello-Pérez, Marta Fernández-Oliver, Ricardo Mallavia, and Alberto Falcó

Abstract

The use of diverse Ag-based nanoparticulated forms has shown promising results in controlling viral propagation. In this study, a commercial nanomaterial consisting of ceramic-coated silver nanoparticles (AgNPs) was incorporated into thermoplastic polyurethane (TPU) plates using an industrial protocol, and the surface composition, ion-release dynamics and viricidal properties were studied. The surface characterization by FESEM-EDX revealed that the molar composition of the ceramic material was 5.5 P:3.3 Mg:Al and facilitated the identification of the embedded AgNPs (54.4 ± 24.9 nm). As determined by ICP-MS, the release rates from the AgNP–TPU into aqueous solvents were 4 ppm/h for Ag and Al, and 28.4 ppm/h for Mg ions. Regarding the biological assays, the AgNP–TPU material did not induce significant cytotoxicity in the cell lines employed. Its viricidal activity was characterized, based on ISO 21702:2019, using the Spring viraemia of carp virus (SVCV), and then tested against the severe acute respiratory syndrome coronavirus 2 (SARS-CoV-2). The results demonstrated that AgNP–TPU materials exhibited significant (75%) and direct antiviral activity against SVCV virions in a time- and temperature-dependent manner. Similar inhibition levels were found against SARS-CoV-2. These findings show the potential of AgNP–TPU-based materials as a supporting strategy to control viral spread.

Keywords: 3D nanomaterials; thermoplastic polyurethane; ceramic; Ag nanoparticles; viricidal activity.

1. Introduction

Infectious diseases are a major global health concern and can have a significant negative socio-economic impact, particularly in developing countries. According to the World Health Organization (WHO), infectious diseases are a leading cause of morbidity and mortality, responsible for approximately 25 % of all fatalities worldwide [392]. In particular, viruses can infect a wide range of hosts, including animals, plants and microorganisms. In humans, they can cause multiple diseases with a wide ranging severity of prognoses from the common cold to more critical conditions such as acquired immune deficiency syndrome (AIDS) [393], Ebola virus disease (EVD) [394], Middle East respiratory syndrome (MERS) [395] or severe acute respiratory syndrome (SARS) [396]. In this sense, it is worth mentioning the recent global COVID-19 pandemic caused by SARS-CoV-2 and initiated in December 2019, which officially resulted in more than 250 million infected people and 5 million deaths within less than two years [397].

Viruses can be transmitted through various routes including direct or physical contact, oral (ingestion), sexual, vertical, vector-borne, aerosol (airborne) and fomites (contaminated inanimate objects) [398]. In the latter case, especially through frequently used objects in crowded and healthcare settings [399], fomites can be an important contributor to the spread of viruses such as human adenoviruses (HAdV) [400], rotavirus [401], human rhinovirus (hRV) [402], norovirus [403], influenza A virus (IFV-A) [404], SARS coronavirus [405], MERS-CoV [406] or SARS-CoV-2 [407].

The viability of the viral particles on fomites depends on the stability of their components and structural arrangements, which can be affected by environmental factors occurring over time such as humidity, temperature and irradiation [399]. For this reason, DNA and non-enveloped viruses

are usually more resistant to adverse environments [408,409]. Associated with this, the chemical nature of the fomites also plays an important, sometimes crucial, role. For instance, SARS-CoV-2 shows less stability on porous materials (e.g., cotton) in comparison to non-porous surfaces (glass, plastic, metal, etc.), where infective virions were detected for 4 to 21 days [410].

In addition to new disinfection systems such as more sophisticated germicidal light irradiation treatments [411], new strategies to limit fomite-mediated virus transmission are focused on the development and implementation of new materials with upgraded viricidal properties [412]. Advances in the field of nanotechnology, such as nanomaterial coating strategies or NP-based antiviral agents, offer new approaches to prevent the spread of viruses [413]. NPs have emerged as antimicrobial materials due to their high surface-to-volume ratio and the specific chemical and physical properties with which they can be designed [414]. The use of metallic NPs as viricidal agents has grown rapidly due to their ability to target different molecular sites in viruses and, therefore, minimize resistance development events [128]. Two main mechanisms have been proposed to explain how metallic NPs, usually AgNPs, interfere with viral replication: (i) via sulfur-bearing residues on cell and virus surface glycoproteins, preventing the attachment and entry of the virus into the host cell, and (ii) via cell membrane penetration and effectively blocking internal cellular factors necessary for the proper assembly of viral progeny [415]. Recently, the ability of AgNPs to inhibit SARS-CoV-2 has been investigated [416,417]. AgNPs (diameter: 2–15 nm) were capable of inhibiting extracellular SARS-CoV-2 virions and preventing their entry to host cells by disturbing viral integrity [416].

AgNP preparations in liquid environments limit their use for antiviral applications; however, great progress is being made in the use of AgNPs in solid and semi-solid preparations [418]. Recently, the incorporation of AgNPs into electrospun nanofibrous membranes of TPU and polyvinyl alcohol (PVA) for the manufacture of personal protection equipment was studied, and their antiviral activity against Human immunodeficiency virus-1 (HIV-1) and SARS-CoV-2 was evaluated. Briefly, AgNP-loaded TPU (AgNP–TPU) NFs were found to be more effective in inhibiting HIV-1 and SARS-CoV-2 than those made of PVA [419]. In this sense, TPU's interesting properties such as ease of processability, high durability, flexibility, excellent biocompatibility and great abrasion resistance make it suitable for a wide range of applications [420]. However, to the best of our knowledge, the use of TPU as a matrix scaffold for AgNPs for antimicrobial and, especially, antiviral applications has only been reported in the form of NFs.

The development of 2D and 3D AgNP–TPU nanomaterials as antimicrobial coatings for implementation in strategic areas to support public health could help slow the spread of some viral diseases. In this work, the viricidal ability of AgNP–TPU materials produced by an industrial protocol was assessed according to the general methodology described in the ISO 21702:2019 international standard, compliance with which is obligatory to certify this quality for plastics and other non-porous surfaces, but rarely addressed in scientific reports. Additionally, the surface and inner morphology of the materials were characterized, as well as their composition, including the release dynamics of metal ions in contacting aqueous solutions. Taken together, this study also aims to provide useful descriptions of methodological approaches to evaluate the potential implementation of experimental materials in virus protection applications.

2. Materials and Methods

2.1. Materials

Commercial additive 746-3BV (Esenttia, Bogotá, Colombia) consisting of AgNPs encapsulated in a polyethylene ceramic material (D98 < 40 μm) at 16 % w/w in molten polypropylene (0.91 g/cm3, Duraflon®) was homogeneously mixed in a 1:16 ratio with molten thermoplastic polyurethane (TPU) (1.22 g/cm^3, Ultimaker BV) at 220 °C to produce the AgNP–TPU material.

Control TPU material was fabricated in the same way without adding the commercial AgNP additive. All products were supplied and assembled by Soorim 3D Solutions S.L. (Alicante, Spain), which is also the holder of the patent for the use of these materials for antimicrobial applications (patent number: U202031871).

2.2. Experimental Design

The experimental design of the analytical and biological trials was carried out by following the general guidelines described in ISO 21702:2019: "Measurement of antiviral activity on plastics and other non-porous surfaces". Thus, the materials to be tested and their respective controls were molded to meet the dimensions required by this procedure (5 × 5 × 0.5 cm plates). Figure 22 shows schematic and visual representations of the disposition of the materials. Briefly, the AgNP–TPU and control TPU plates were placed in sterile Petri dishes and 400 µL of test inoculum was added onto the surface of the materials. Then, 4 × 4 cm polypropylene cover films were placed, covering and spreading the test inoculum towards the film edges without letting it leak beyond. The incubations were performed in such an arrangement inside humid chambers and at constant temperature. The temperature and duration of the incubations, as well as the type of test inoculum, varied depending on each particular test. All experiments were performed in triplicate.

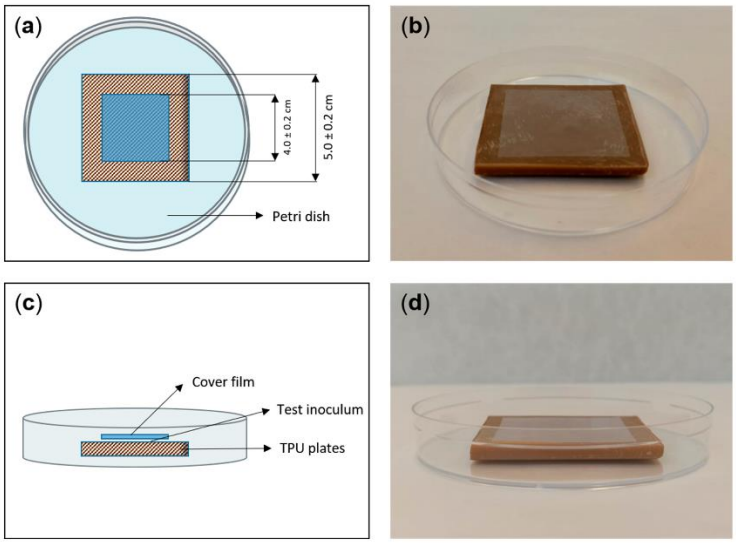

Figure 22. Schematic representations of the top (a) and side (c) views of the material and cover film layout, and corresponding example pictures ((b) and (d), respectively).

2.3. Characterization of the Material Surface, the Released AgNPs and the Ion-Release Dynamics

The TPU plates were visualized using a Schottky-type Sigma 300 VP FESEM with a coupled energy dispersive X-ray system (EDX) to determine their element composition (Carl Zeiss Microscopy GmbH, Oberkochen, Germany). Images were generated using both backscattered electron (BSE) and variable pressure secondary electron (VPSE) detectors.

The average HDD and the PDI of the AgNPs potentially released from the experimental materials into Milli-Q water inocula (co-incubated for 24 h at 20 °C) were determined by DLS using a 90 Plus Nanoparticle Size Analyzer (Brookhaven Instruments Corporation, Holtsville, NY, USA) [371]. All measurements were performed three times at 25 °C.

The ionic composition of the moieties released from the TPU plates was determined by ICP-MS (ICPMS-2030, Shimadzu Company, Kyoto, Japan) calibrated with 107 Ag, 27 Al and 24, 25 and 26 Mg standards, being regression coefficient values (R^2) equal or higher than 0.9996 for all

calibration curves. The test inoculum used for this assay consisted of Milli-Q water samples incubated with the corresponding TPU plates at 20 °C for 2 and 8 h, as well as 24 h, which is the incubation time indicated by ISO 21702:2019 for testing the antiviral activity. Prior to analysis, these samples were diluted 1:30 (v/v) with nitric acid 1 % (v/v), reaching a final volume of 3 mL. The non-diluted and non-treated water inocula, dried over silicon wafers, were also analyzed by FESEM-EDX (Carl Zeiss Microscopy GmbH) for this purpose.

2.4. Cells and Virus

The potential viricidal activity of the experimental TPU materials was tested with the fish pathogen SVCV (isolate 56/70) in EPC cells (American Type Culture Collection ref.: CRL-2872) [421] and SARS-CoV-2 in Vero E6/TMPRSS2 cells [411].

EPC cell monolayers were grown at 28 °C in a 5 % CO_2 atmosphere in a Dutch modified RPMI 1640 medium (Sigma, St. Louis, MO, USA) containing 10 % FBS (BioWhittaker, Inc., Walkersville, MD, USA), 1 mM sodium pyruvate (Sigma), 2 mM glutamine (Sigma), and 50 µg/mL gentamicin (Thermo Fisher, Waltham, MA, USA).

Vero E6/TMPRSS2 cell monolayers were grown at 37 °C in a 5 % CO_2 atmosphere in DMEM (Sigma), supplemented with 10 % FBS (BioWhittaker), 2 mM l-glutamine (Sigma), 1 % non-essential amino acids (Sigma), and 100 units/mL penicillin and 100 µg/mL streptomycin (Thermo Fisher).

2.5. Cytotoxicity Assays

In compliance with ISO 21702:2019, prior to assessing the viricidal activity of the TPU materials, the potential citotoxicity of the moieties released from them when incubated with aqueous inocula was tested on EPC and Vero E6/TMPRSS2 cells. Thus, their corresponding culture media were used as test inocula and incubated at 20 °C (EPC medium) or 30 °C (Vero E6/TMPRSS2 medium) for 24 h, with both control and AgNP–TPU materials. Cell viability changes were determined by the reduction of MTT (Panreac AppliChem, Barcelona, Spain) assay. Briefly, confluent cell monolayers in 96-well plates were treated with the collected inocula at 1:10 and 1:100 dilutions in corresponding fresh media (100 µL/well). After 24 h of incubation at each cell-type growing conditions, treatments were replaced by a cell medium containing 0.5 mg/mL MTT (from ten-fold concentrated stocks in PBS (Gibco, Thermo Fisher)); in fresh media (100 µL/well) was used to replace treatments. MTT solutions were incubated with cells under the same conditions for 2 h and then carefully removed. The colored formazan product was dissolved in 100 µL of DMSO (Sigma) and the absorbance at 570 nm (and 620 nm as reference) was measured by means of a Cytation™ 3 cell imaging multi-mode microplate reader (BioTek Instruments, Inc., Winooski, VT, USA). Optical density is expressed in percentages relative to the control group consisting of untreated cells. Therefore, cell viability was calculated by the formula: 100× treated cell absorbance/untreated cell absorbance.

2.6. In Vitro Viral Infections

SVCV was used for the general characterization of the viricidal properties of the experimental TPU materials. Thus, SVCV inocula at 105 focus-forming units (ffu) per mL in 2 % FBS culture medium (SVCV infection medium) were incubated with the TPU plates, as described above, testing different temperatures (5, 10, and 20 °C for 24 h) and time periods (2, 8, and 24 h at 20 °C). Regarding SARS-CoV-2, inocula at 5 × 105 plaque-forming units (pfu) per mL were tested at 30 °C for 24 h. For each condition, corresponding virus inocula were incubated with control TPU plates. Virus inactivation was determined as the viral titer reduction in percentage relative to control samples. SVCV and SARS-CoV-2 titers were determined by the focus-forming [311,421] and plaque assay [411] methods, respectively. All the experiments involving SARS-

CoV-2 were performed in biosafety level 3 (BSL-3) facilities at CNB-CSIC according to the guidelines of the institution.

2.7. Statistical Analysis and Graphics

Data are shown as mean and SD (n = 3, unless stated otherwise). Prism v7 (GraphPad software, La Jolla, CA, USA) and Microsoft Excel from the Microsoft Office Professional Plus 2019 package (Microsoft Corporation, Redmond, WA, USA) were used for creating the graphs. Prism v7 was used for performing the statistical analysis depending on each particular experimental design. Significant differences are indicated as: * ($p < 0.05$), ** ($p < 0.01$), and *** ($p < 0.001$).

3. Results and Discussion

3.1. Physicochemical Characterization of the Experimental TPU Materials

3.1.1. Morphology and Composition

According to the FESEM images (Figure 23a–e) and the EDX analysis (Figure 23f) from the surface of the experimental materials, most of the elements are carbon and oxygen and correspond to the TPU moiety of both control TPU and AgNP–TPU materials, which is their matrix component and is visualized as dark background in the BSE images (Figure 23b,d,e). In these images, irregular light-grey granulation is also observed in the surface of the AgNP– TPU plates (Figure 23b,d), which belongs to the ceramic additive since it is associated to the presence of magnesium, aluminum and phosphorus, as determined by EDX spectroscopy (Figure 23f). Within such granule-like forms of 9.9 ± 6.4 µm (average value for 25 granules from different FESEM images), bright dots corresponding to AgNPs of 54.4 ± 24.9 nm (average value for 25 NPs from different granules) were also detected (Figure 23e,f).

It is worth mentioning that such a pattern is also shown along the entire cross section of the AgNP–TPU plates, as can be observed in the FESEM image from Figure 24. Several general EDX analyses across the surface of the section (Figure 24) confirm the composition described above, as well as the presence of traces of other elements, due to the much higher area analyzed (around 140 μm^2) for each spectrum in comparison to the spectra shown in Figure 24 (punctual measurements).

The chemical composition of the components released from the AgNP–TPU material into contacting solutions was also studied by EDX spectroscopy. For this purpose, Milli-Q-water samples were incubated over the experimental materials, as described in the Material and Methods section herein and the ISO 21702:2019. Incubations were carried out at 20 ºC for different time periods (2, 8 and 24 h). Thus, no differential major elements were found in the composition of the inocula incubated with control TPU plates in comparison to that of the original solution. In contrast, the ceramic components (P, Mg and Al) and Ag were detected in the inoculum samples from AgNP–TPU materials. It is worth highlighting the noteworthy non-release into the inocula (i.e., the absence) of those trace elements found in the general composition of the solid materials described in Figure 24: mainly S and Ba ions corresponding to barium sulphate molecules that are usually employed as filler additive in TPU materials.

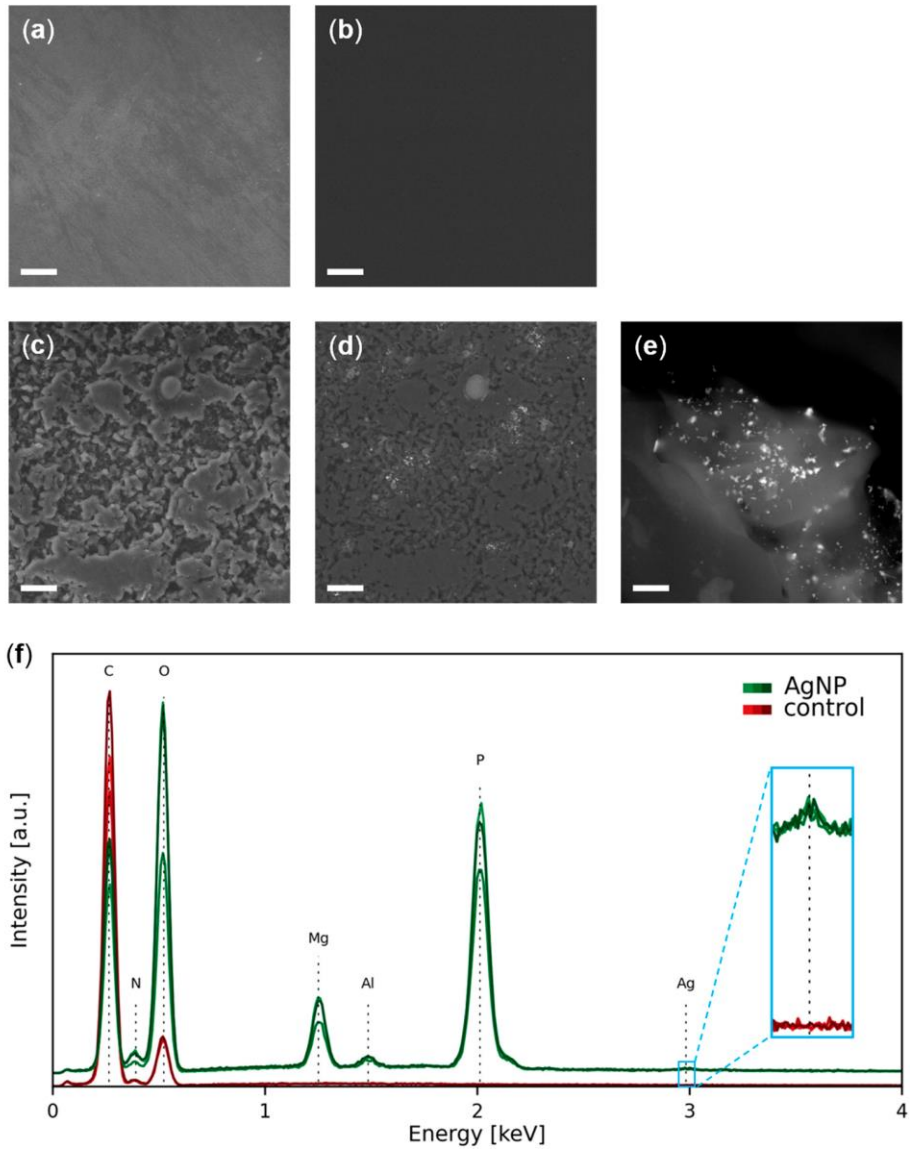

Figure 23. Representative FESEM images of the surface of the TPU (a,b) and AgNP–TPU (c–e) materials using VPSE (a,c) and BSE (b,d,e) detectors. The dark background in BSE images corresponds to the TPU moiety, the grey granules to the ceramic additive and the bright dots to the AgNPs. Scale bar of 20 µm for images (a–d) and 500 nm for image (e). (f) EDX analysis of the surface of the experimental materials. Three representative spectra for each type of material are shown. The analysis sites for the control material were randomly chosen, for the AgNP–TPU materials were restricted to the granulated regions. a.u., arbitrary units.

Figure 25 shows a ternary diagram displaying the relative amounts of P, Mg and Al ions detected in the surface of AgNP–TPU plates and the inocula at each time point. The ratio between the indicated components was found to be 5.5 P: 3.3 Mg: Al (table inset in Figure 25) or, in atomic composition, 4.8 P: 3.7 Mg: Al for the AgNP–TPU solid material. Similar percentages were found for the inocula, although with a notable increase in P, probably as a consequence of its higher partial solubility in aqueous solutions.

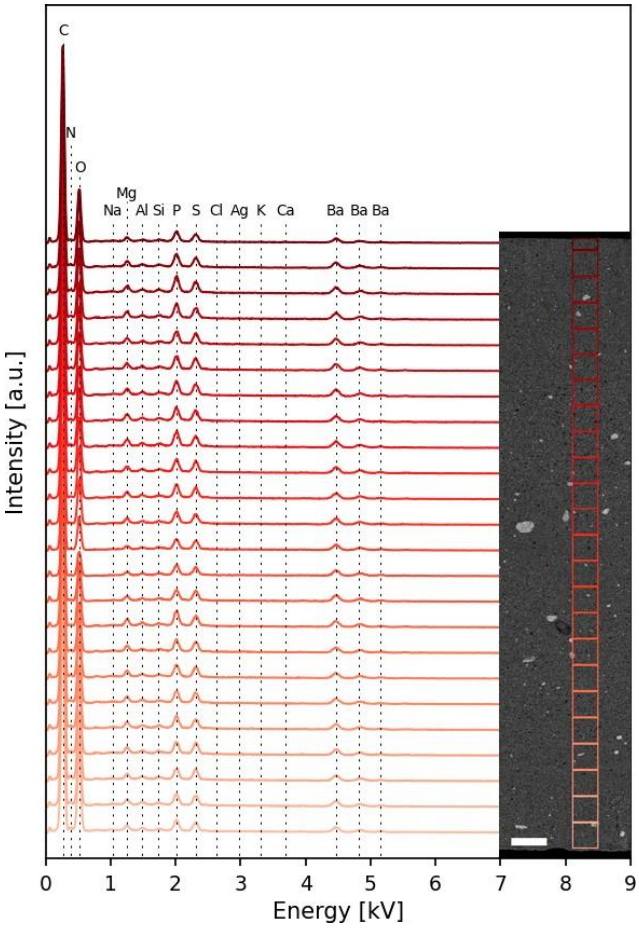

Figure 24. EDX analysis of the surface composition of the cross section of the AgNP–TPU material. a.u., arbitrary units. Scale bar: 200 µm.

DLS analysis confirmed the absence of NPs in the inocula recovered from control TPU materials. On the contrary, they were detected in the inocula incubated with AgNP–TPU plates. Their mean HDD and PDI values were 1032 ± 148 and 0.382 ± 0.152 nm, respectively (Figure S-4). Regarding PDI values, they range from 0 to 1 and indicate the breadth of the particle size distribution. PDI values below 0.3 typically indicate a uniform distribution of particle sizes [422]. The values obtained are slightly higher than this threshold, which can be attributed to mild aggregation events that are common in MNPs and depend on several chemical parameters of their immediate environment [423,424]. This may explain why particle size measurements obtained by this technique are much larger than expected.

3.1.2. Ceramic Component Degradation Dynamics and Ion Release Rate

The same water inocula incubated with the materials and previously characterized by EDX were also analyzed by ICP-MS for a more precise quantitation of relevant components released from the NPs (Ag) and the ceramic matrix (Al and Mg) of the AgNP–TPU materials. According to these data (Figure 26), there is a significant increment of ions in the co-incubated inocula along time ($F = 7.234$; $p < 0.01$), as well as a significant difference of cumulated ions between the elements studied ($F = 10.45$; $p < 0.001$). In these regards, there are several conditioning factors such as, mainly, the ability of each element to be released from the source material and their solubility in water. In comparison to other studies, similar delivery trends associated with the degradation of ceramic components have already been described [425,426]. In quantitative terms for each particular element, the release rate of Ag and Al ions was approximately 4 ppm/h for each one, while that of Mg was about six times higher (28.4 ± 5.7 ppm/h).

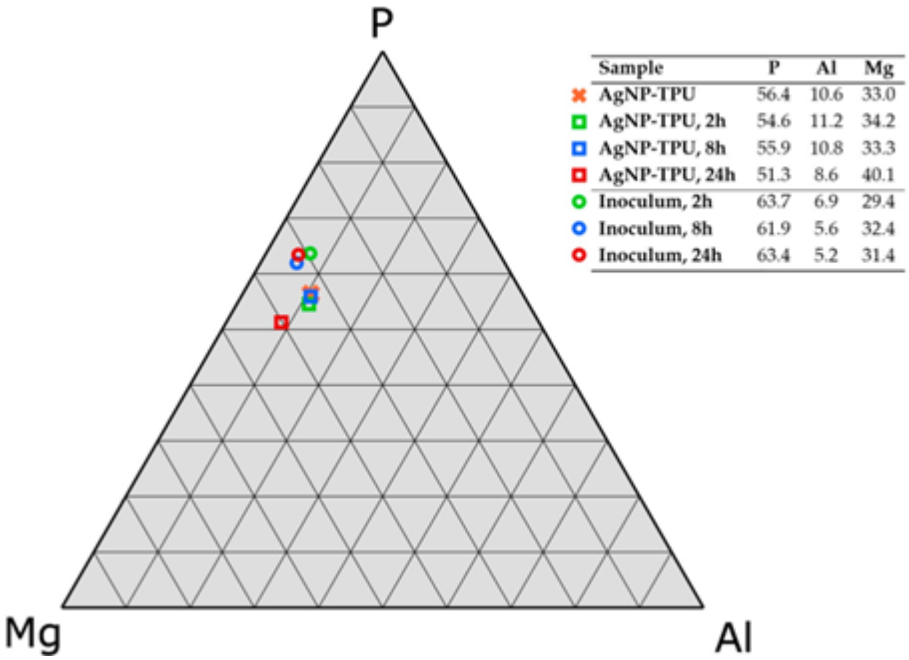

Figure 25. Ternary diagram of the relative populations of the ceramic components (P, Mg and Al) from the commercial additive in the experimental materials (square symbols) and the corresponding inocula (circular symbols) after incubation for 2, 8 and 24 h at 20 ◦C. Data obtained by EDX spectroscopy. Results shown as the mean value from three independent measures, relative error lower than 0.5%.

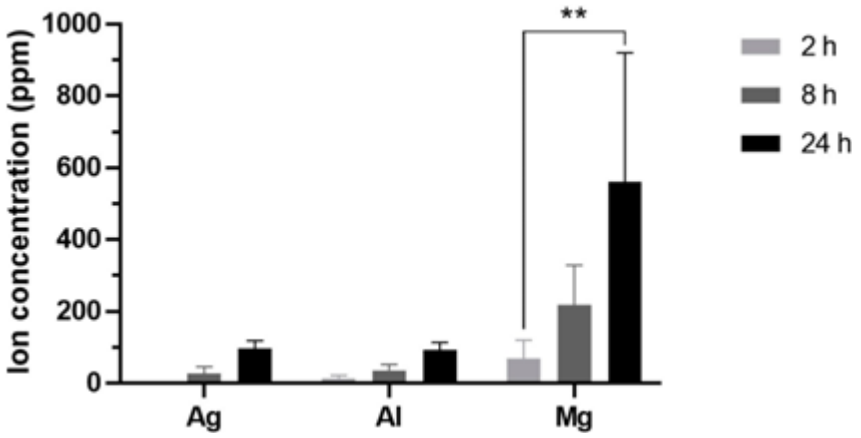

Figure 26. Time evolution of the concentration of Ag, Al and Mg (ppm) cumulated in the aqueous inocula released from AgNP–TPU materials after their incubation for 2, 8 and 24 h at 20 ◦C. Analysis performed by ICP-MS. The results are represented as means ± SD (n = 3). Statistically significant differences between groups (two-way ANOVA with Tukey's multiple comparisons correction) are shown on binding braces. **, $p < 0.01$.

3.2. Biological Properties

3.2.1. Cytotoxicity Assays

The potential cytotoxicity of the moieties released from the experimental materials was assessed before determining their viricidal activity. For this purpose, EPC and Vero E6/TMPRSS2 media were incubated with the TPU plates at 20 ºC and 30 ºC, respectively, for 24 h. Then, they were used at different dilutions to treat the corresponding cells for 24 h before performing the MTT assay. Thus, as shown in Figure 27, no significant viability changes were observed in any of the cases ($F = 0.873$ and $p = 0.4929$ for EPC; and $F = 0.9511$ and $p = 0.4576$ for Vero E6/TMPRSS2).

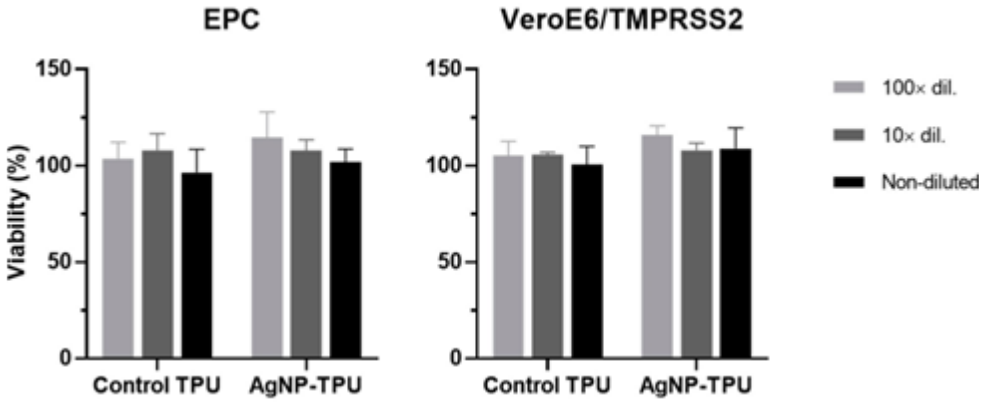

Figure 27. Cytotoxicity in EPC and VeroE6/TMPRSS2 cells of culture media previously incubated with the experimental materials. The inocula were tested undiluted, 1:10 and 1:100 diluted in cells. The results correspond to four independent experiments and are represented as means with SD in viability percentages in comparison to the viability obtained from the treatment of cells with culture medium incubated independently with no contact of any of the materials. Statistically significant differences between groups were calculated by using two-way ANOVA with Tukey's multiple comparisons correction; however, no statistically significant differences were found.

Although this aspect has been extensively studied for AgNPs in different cell lines, there is no consensus on their particular cytotoxic concentration since this is affected by several factors such as particle size, medium type, temperature, surface functionalization and particle crystallinity [427]. Based on our ICP-MS analysis, the Ag concentration in the non-diluted inocula was about 100 ppm (i.e., 100 µg/mL) after 24 h of incubation with the experimental materials. Therefore, these cytotoxicity results are consistent with previous studies showing that AgNPs at a concentration of up to 100 µg/mL do not decrease the viability of progenitor human adipose-derived stem cells [428]. Neither did Carrola et al. (2016) observe cytotoxicity in HaCaT keratinocytes after 48 h of treatment with Ag nanoprisms and spherical AgNPs at a concentration of 100 ppm [429], or Rogers et al. (2008) with 100 ppm of 10-nm AgNPs in Vero cells [430]. Nevertheless, other authors did observe cytotoxicity at equal or lower concentrations in HEK293 [431], HT22 [432], Calu-3 and Vero E6/TMPRSS2 [416] cells.

It is important to note here that the mechanisms underlying the toxicity of AgNPs, which are also largely related to their antimicrobial activity, operate at different molecular and cellular levels and are still under investigation. Therefore, although these nanomaterials are already present in a wide range of consumer products; due to their potential impact on the environment and public health; further studies are needed in this regard to ensure their safety, in particular for environmental, health, food and textile applications [433].

3.2.2. Viricidal Activity

Once it was verified that the inocula previously incubated with the experimental materials did not exert relevant cytotoxic effects on the host cells, we proceeded to determine whether they were endowed with viricidal properties and, if so, the specific source of such activity within the material (Figure 28). Thus, SVCV inocula showed an about 75% titter reduction when directly incubated with the AgNP–TPU plates in comparison to the titters determined for the incubations with the control material. We then revealed that such antiviral activity comes from the moieties of the material that are released into the inoculum during the incubations; since when they consist of just medium and are used to treat SVCV,virus infectivity is inhibited to the same extent as in SVCV-material direct incubations. Finally, it was also demonstrated that this effect is not due to a reduction in the sensitivity of cells to viral infections, since the treatment of host cells with culture medium that had been previously incubated with the materials did not confer antiviral protection on them. We note that all incubations and treatments were performed at 20 ◦C for 24 h

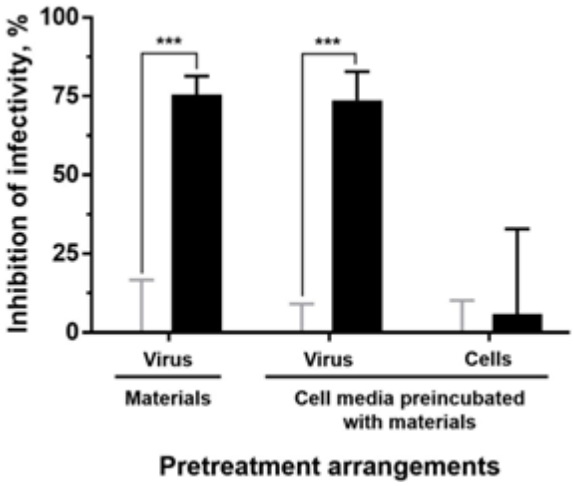

Figure 28. Potency and origin of the antiviral activity against SVCV of the experimental materials. To assess the type of antiviral activity exerted by the materials, three different pretreatment arrangements were performed (in order): direct incubation of the virus inoculum with the material; and the treatment (prior to infection) of either virus stocks or host cells with 2% FBS culture medium that had been previously incubated with the materials. The results correspond to three independent experiments and are represented as means ± SD of the infectivity inhibition associated with AgNP–TPU materials (black bars) in percentages relative to corresponding control groups (i.e., viricidal activity of control TPU materials, grey bars). Statistically significant differences between corresponding control and AgNP–TPU groups (two-way ANOVA with Tukey's multiple comparisons correction) are shown: ***, $p < 0.001$.

To further characterize the viricidal activity of the materials, different incubation periods (24 h as stated in the ISO 21702:2019, but also 2 and 8 h) at 20 ºC were tested. The results obtained (Figure 29a) indicate that the incubation time has an effect in this regard by reducing the virus infectivity along time (one-way ANOVA, $F = 12.87$, $p < 0.01$). The inhibition of the infectivity was significant in virus inocula incubated for 8 (44.4 ± 19.3 %) and 24 h (74.1 ± 12.8 %) with the AgNP–TPU plates, in comparison to control groups (Student's t-test, $p < 0.05$). In addition, such time-dependent inhibition of virus infectivity coincides with the Ag release trend shown before for the AgNP–TPU materials (Figure 26).

Several studies have reported the antiviral activity of AgNPs against a range of viruses such as herpes simplex virus (HSV) [434], HIV [435], IFV-A [436], monkeypox virus (MPV) [430], Newcastle disease virus (NDV) [437], respiratory syncytial virus (RSV) [415] or SARS-CoV- 2 [424]. Particularly, in the study of Rogers et al. (2008), a concentration of 100 ppm of 10 nm AgNPs decreased the plaque formation of the MPV by 79 % in Vero cells [430]. In a recent study, inhibitions of 64 to 79 % in the replication of NDV using AgNPs at concentrations of 80 to 320 ppm [437] were also shown. Altogether, these results are consistent with the data obtained in this study since the exposure of the inocula to the AgNP–TPU material for 24 h delivered Ag ions up to a concentration of around 100 ppm into them, thus conferring in them the ability to inhibit SVCV infectivity by up to about 74%.

Similarly, the viricidal activity of the AgNP–TPU materials was also found to depend on the temperature of incubation (Figure 29b, one-way ANOVA, $F = 11.16$, $p < 0.01$). For these assays, incubation temperatures of 5 and 10 ºC were tested, in addition to 20 ºC. The exposure time was set at 24 h, as specified by ISO 21702:2019. Ultimately, incubation with the AgNP–TPU material reduced SVCV infectivity by 45 ± 8.7 % at 5 ◦C, 52.4 ± 8.2 % at 10 ºC, and 74.1 ± 6.4% at 20 ºC. These results are in line with previous studies describing that the dissolution of AgNPs in an aqueous solution increases with temperature [438,439]. The temperature also affects the release profile of several metallic ions from NPs in the same way, due to the temperature dependence of the ionic diffusion coefficient. Indeed, Zhang et al. (2011) developed a kinetic model using the

Arrhenius equation (Equation S-1) to explain the release of Ag ions based on the hard sphere theory [440]. According to this equation, the higher the temperature, the higher the release rate of Ag ions.

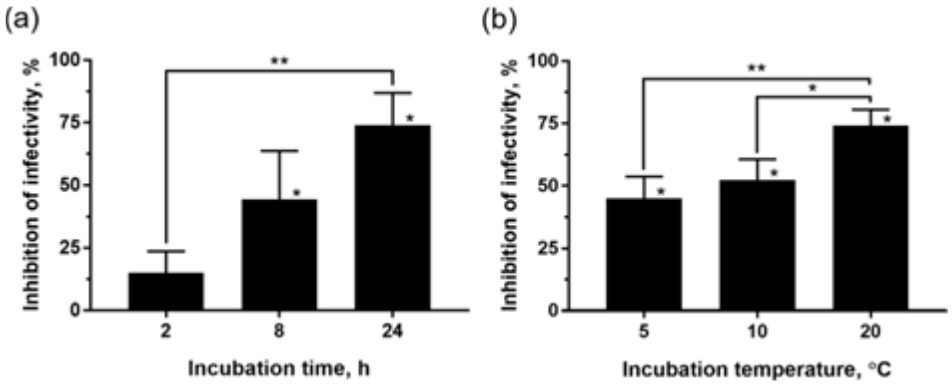

Figure 29. Effect of (a) the incubation time (2, 8 and 24 h) at 20 ºC and (b) the incubation temperature (5, 10 and 20 ºC) for 24 h, in the viricidal activity against SVCV of the AgNP–TPU materials. The results correspond to three independent experiments and are represented as means ± SD of the infectivity inhibition in percentages relative to corresponding control groups. Statistically significant differences between groups (one-way ANOVA with Tukey's multiple comparisons correction) are shown on binding braces. Statistically significant differences compared to their respective control groups (two-tailed unpaired Student's t-test with Welch's correction) are shown above each column. *, $p < 0.05$; **, $p < 0.01$.

Finally, the viricidal activity of the experimental materials was also tested against a clinically relevant virus, SARS-CoV-2. For these assays, the virus inocula were incubated with the TPU materials at 30 ºC for 24 h prior to their titration. According to the data, the AgNP–TPU plates reduced the SARS-CoV-2 infectivity in 80.77 ± 14.73% in comparison to the TPU control (two-tailed Mann-Whitney U test, $n = 4$, $p = 0.0286$), and, therefore, this was similar to the inhibition ranges determined against SVCV.

4. Conclusions

This study aimed to evaluate the viricidal ability (by following the general guidelines of ISO 21702:2019) against SVCV (virus model) and SARS-CoV-2 of a composite material consisting of a TPU matrix with embedded AgNPs. Thus, this material exerts a viricidal activity of about 75 % directly through the AgNPs released into the inoculum with which it is incubated. In addition, such activity is shown to be time- and temperature-dependent, probably due to the release trend over time of Ag ions from the AgNP-materials shown here. The compounds released by the AgNP–TPU materials do not present significant levels of cytotoxicity in EPC and Vero E6/TMPRSS2 cells under the tested conditions. These findings postulate TPU–AgNP as promising candidate materials for viricidal applications to decrease the spread of viruses such as SARS-CoV-2.

Supplementary material

Viricidal Activity of Thermoplastic Polyurethane Materials with Silver Nanoparticles

Rocío Díaz-Puertas, Enrique Rodríguez-Cañas, Melissa Bello-Pérez, Marta Fernández-Oliver, Ricardo Mallavia, and Alberto Falcó

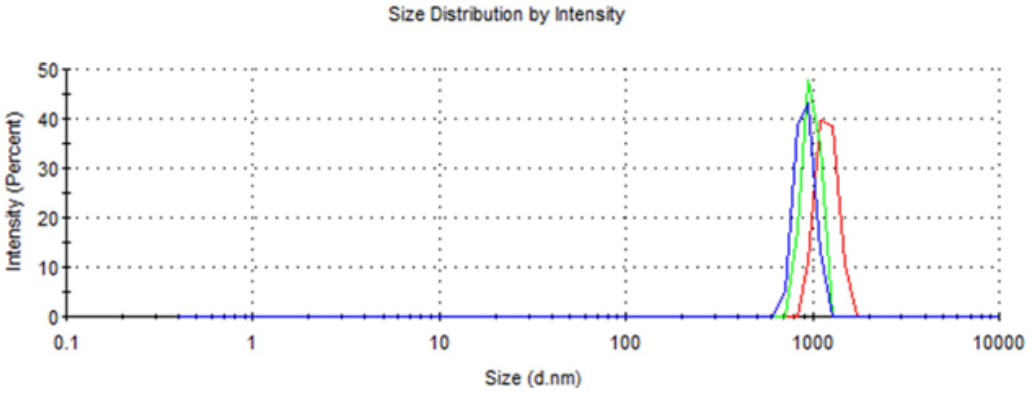

Figure S-4. Hydrodynamic diameter (HDD) determined by dynamic light scattering (DLS) of NPs released into Milli-Q water inocula incubated with AgNP-TPU materials for 24 h at 20 °C. Results from three independent experiments, each shown in a different color.

$$\Upsilon_{Ag^+} = \frac{3}{4}\left(\frac{8\pi k_b T}{m_B}\right) p^{-1} \exp\left(\frac{-E_a}{k_b T}\right) [Ag]_r^{-1} [O_2]^{0.5} [H^+]^2 \qquad \text{(S1)}$$

Equation S-1: Kinetic model based on the hard sphere theory using the Arrhenius equation. γ_{Ag+}: Ag^+ release rate; k_b: Boltzmann constant (1.38×10^{-23} J/K); T: temperature (298 K); m_B: molecular weight of oxygen or protons; E_a: activation energy (J); $[Ag]_r$: released Ag^+ concentration. Developed by Zhang et al. (2011) [440].

CHAPTER 4

CHAPTER 4: PHYTOCHEMICAL-BASED NANOMATERIALS AGAINST ANTIBIOTIC-RESISTANT BACTERIA: AN UPDATED REVIEW

SUMMARY OF RESULTS

This review paper titled explores innovative solutions for combating ARB through the integration of phytochemicals with nanotechnology. This review highlights the potential of phytochemicals—bioactive compounds derived from plants—as antimicrobial agents, especially when incorporated into nanomaterials like polymeric NFs and NPs, which enhance their effectiveness against ARB by improving properties such as bioavailability, stability, and controlled release.

The motivation behind this study is the urgent need to address AMR, a significant global health threat that causes millions of fatalities annually due to infections that are increasingly difficult to treat with standard antibiotics. The slow pace of new antibiotic development and overuse of existing antibiotics have led to the emergence of ARB strains, making alternative solutions critical. Phytochemicals such as polyphenols, alkaloids, and terpenoids, known for their antimicrobial properties, serve as effective agents against ARB. However, limitations like low potency and poor pharmacokinetics restrict their clinical application. Nanotechnology provides a solution by enabling the creation of nanomaterials, including polymeric NFs and NPs, which improve the phytochemicals' bioavailability, mechanical stability, and release properties.

NFs are fine, one-dimensional fibers with diameters in the nanometer range. Due to their high surface area-to-volume ratio, NFs provide a unique structure that can enhance the delivery and controlled release of antimicrobial agents, including phytochemicals, when applied in biomedical contexts. The primary method of synthesizing NFs is electrospinning, which involves loading a polymer solution and extruding it through a charged needle. Variants of electrospinning, such as blend, coaxial, and emulsion electrospinning, are used to encapsulate phytochemicals in NF matrices, either by dispersing them uniformly within the NF or by embedding them within a core-shell structure. Key polymers used in NFs include gelatin, PVA and PCL. Phytochemicals like curcumin have shown broad-spectrum antibacterial activity through mechanisms such as disrupting bacterial membranes, inducing oxidative stress, and inhibiting biofilm formation. In NFs, efficacy of curcumin is further enhanced by its sustained release, improving its interaction with bacterial cells and thereby enhancing its antimicrobial effects.

NPs, including polymeric and MNPs, are advantageous in delivering phytochemicals due to their small size, large surface area, and modifiable surface properties. Phytochemical-loaded polymeric NPs are effective in precisely targeting bacteria and sustaining release, which is critical in fighting persistent infections caused by ARB. Polymeric NPs can be produced from synthetic polymers like PLA and PVA or from natural polymers like chitosan, which has intrinsic antibacterial properties. The most common synthesis methods include dispersion of preformed polymers, polymerization of monomers, and ionic gelation. On the other hand, MNPs are extensively researched for their antimicrobial properties. The green synthesis approach uses plant extracts as reducing and stabilizing agents, creating eco-friendly NPs. MNPs often employ a multifaceted approach against bacteria, including ion release, ROS generation, and physical disruption of cell walls.

The review concludes that while phytochemical-based NFs and NPs present a promising solution against ARB, challenges remain in standardizing synthesis methods, ensuring consistent antibacterial efficacy, and minimizing toxicity for clinical use. Moving forward, research should focus on optimizing NP and NF properties for maximum therapeutic efficiency, standardizing antibacterial testing, and conducting *in vivo* studies to validate their clinical plausibility.

Phytochemical-Based Nanomaterials against Antibiotic-Resistant Bacteria: An Updated Review

Rocío Díaz-Puertas, Francisco Javier Álvarez-Martínez, Alberto Falcó, Enrique Barrajón-Catalán and Ricardo Mallavia

Abstract

Antibiotic-resistant bacteria (ARB) is a growing global health threat, leading to the search for alternative strategies to combat bacterial infections. Phytochemicals, which are naturally occurring compounds found in plants, have shown potential as antimicrobial agents; however, therapy with these agents has certain limitations. The use of nanotechnology combined with antibacterial phytochemicals could help achieve greater antibacterial capacity against ARB by providing improved mechanical, physicochemical, biopharmaceutical, bioavailability, morphological or release properties. This review aims to provide an updated overview of the current state of research on the use of phytochemical-based nanomaterials for the treatment against ARB, with a special focus on polymeric nanofibers (NFs) and nanoparticles (NPs). The review discusses the various types of phytochemicals that have been incorporated into different nanomaterials, the methods used to synthesize these materials, and the results of studies evaluating their antimicrobial activity. The challenges and limitations of using phytochemical-based nanomaterials, as well as future directions for research in this field, are also considered here. Overall, this review highlights the potential of phytochemical-based nanomaterials as a promising strategy for the treatment against ARB, but also stresses the need for further studies to fully understand their mechanisms of action and optimize their use in clinical settings.

Keywords: nanotechnology; nanofibers; nanoparticles; green synthesis; electrospinning; plants; antimicrobial

1. Introduction

Bacterial infections pose a major threat to human health worldwide, especially when resistant to conventional antibiotics. In 2019, over 4.95 million fatalities worldwide were associated with AMR illnesses, among which 1.27 million were directly linked by them, i.e., fatalities that could have been prevented if the infections had been susceptible to antibiotics, thereby becoming a leading cause of death worldwide in low-resource environments [87]. Due to the alarming appearance of ARB on multiple antibiotics, their rapid spread, and the slow discovery of new antibiotics, conventional therapies are gradually losing effectiveness [441]. There are several factors contributing to the development of ARB, including: (i) the overuse and the misuse of antibiotics[442], often as a consequence of a lack of new ones [443], (ii) poor infection control measures [444], (iii) genetic factors, and (iv) environmental factors [445].

Alternative and complementary treatments to antibiotics have been steadily pursued in the last few decades to address this issue [96]. In this sense, it is predicted that natural sources still harbor a huge number of bioactive molecules that are yet to be discovered, particularly within plants (kingdom *Plantae*) [446]. Plant extracts can contain a wide variety of phytochemicals such as polyphenols, alkaloids, and terpenoids with proven antibacterial capacity, even against ARB [134,447]. Phytochemicals are usually less potent than traditional antibiotics, although often endowed with therapeutically interesting properties such as molecular promiscuity or AMR-modifying capacities. Not in vain, plant extracts have been used by human communities since ancient times, when scientific knowledge was practically nil and only reduced to trial-and-error screenings [448]. Nowadays, the development of modern technology can help to optimize the use

of these phytochemicals and to enhance their benefits for human health, as is the case for nanotechnology.

In recent years, the use of nanotechnology in biomedical applications has been increasing rapidly, observing a pronounced upward trend in the number of scientific articles published in this regard. Nanomaterials such as NFs and NPs can tackle limitations related to traditional approaches [449] and provide beneficial morphologies and surface features to fight bacteria [450]. In addition, the characteristics of these nanomaterials, i.e., size, shape, constituents, and surface, can adjust their mechanical, biological, and physicochemical properties to match the required needs [451]. The polymeric matrices of nanomaterials can result in desirable characteristics, such as small size and high surface-to-volume ratio. These properties can enhance the permeability and solubility of drugs encapsulated within them, making them ideal for drug delivery. Phytochemicals could potentially utilize these features to exert their antimicrobial effects [452]. These features can also improve the biopharmaceutical properties of the final products, with a special interest on low bioavailable compounds [453].

The present study reviews the recent advancements in the development of polymeric NFs and NPs loaded or synthesized with phytochemicals as promising tools to fight against ARB.

2. Study Design

The Scopus and MedlinePlus databases were used to perform a bibliographic search using the following keywords: “nanomaterials” OR “nanoparticles” OR “nanofibers” AND “antibacterial” AND “resistance” AND “plant extract” OR “essential oil” OR “phytochemical”. Among the 378 results retrieved, about 77% (224) corresponded to publications from the last 5 years. A selection was made among the publications from 2014 onwards. The inclusion criteria for articles were: (i) published in English; (ii) in peer-reviewed journals; and (iii) focused on the use of phytochemical-based nanomaterials for the treatment of ARB. A total of 170 articles were included in the final review. From those, 34 publications were experimental studies focused on phytochemical-based nanomaterials against ARB, from which 18 belonged to the last two years. The remaining 136 publications were included in the body of the article, i.e., Introduction and other sections not directly related to experimental studies.

3. Antimicrobial Capacity of Phytochemicals

As briefly mentioned above, poultices and infusions have been prepared from local plants for medicinal purposes since ancient times, including curing bacterial infections [448]. Since the discovery and implementation of antibiotics in the middle of the 20th century, the use of plants as antimicrobials has been drastically reduced. However, the rise of ARB has pushed researchers to search for new antimicrobial compounds from various sources, thus revisiting the plant world as it represents a large reservoir of bioactive molecules with therapeutic potential yet to be explored in depth [454].

One of the main advantages of the use of phytochemicals for antimicrobial purposes is their multifactorial capacity or molecular promiscuity. While traditional antibiotics usually act on a specific bacterial molecular target with great efficacy, phytochemicals can bind to several, but generally with less affinity than that of antibiotics. Such promiscuity or multitarget affinity potentially hinders the generation of possible resistance mechanisms in the bacteria [455]. As it is schematized in Figure 30, the different bacterial molecules targeted by phytochemicals include cell wall [456] and the cell membrane components [457] as well as proteins with diverse locations and functions [458], and thus with the ability of even interfering in the nutrient metabolism and motility [459]. In addition to these pharmacological direct activities, it has been shown that there are phytochemicals, such as certain polyphenols, that are capable of sensitizing ARB by reversing their resistance mechanisms and making them more susceptible to traditional drugs [460,461].

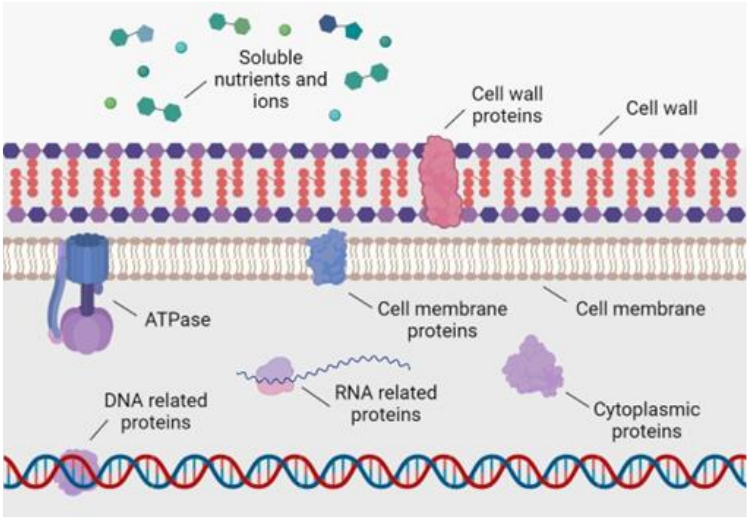

Figure 30. Main bacterial molecular targets of phytochemicals with antibacterial activity.

Phytochemicals may also act in synergy with antibiotics, such as antibiotic adjuvants [462], enhancing their antimicrobial activity and potentially reducing the amount of antibiotic needed to treat an infection [463]. This combination may help to slow the development of AMR, as well as to minimize their adverse effects and environmental impact [464]. Additionally, phytochemicals may help to boost the immune system and improve the overall health of an individual, conferring protection to infection [465].

To date, the literature on AMR to phytochemicals is limited. One example is a study linking genetic changes in *Lysteria monocytogenes* (deletion of the sigB gene) with increased resistance to carvacrol, thereby showing that it is feasible for bacteria to develop resistance to specific polyphenols with unique or few molecular targets [466]. Another example of AMR to botanicals is the presence of "tannin-resistant" Gram-positive bacteria (*Streptococcus* sp.) at sites of high exposure to these polyphenols, such as goat, sheep, and deer rumens [467]. This type of bacteria is thought to protect ruminants from possible tannin anti-nutritional dietary influences [468]. Mechanisms by which bacteria overcome the inhibitory effects of tannins on growth include substrate modification, dissociation of tannin-substrate complexes, formation of extracellular polysaccharides, cell membrane modification, and metal ion chelation [469]. Importantly, bacteria prevalent in ruminant gastrointestinal tannin media may not themselves be resistant. This resistance may be more related to improve the nutrient accessibility of bacteria in the special microenvironment of the ruminant stomach [470]. However, drug resistance seems unlikely to develop when complex mixtures of polyphenols affecting multiple molecular targets on bacterial cells are used [471,472], and so it occurs for plant extracts that contain an amalgam of phytochemicals [473].

One of the main limitations for the use of phytochemicals as antibacterial agents is the low availability and poor pharmacokinetic properties. Widely studied phytochemicals such as quercetin [474] and curcumin [475] present these limitations. The use of drug delivery systems, such as nanomaterials, could help to overcome these limitations [476]. In the following sections, the combinations of phytochemicals and different types of nanomaterials will be described.

4. Nanofibers

NFs are one-dimensional nanomaterials whose properties make them suitable for a wide range of applications, including drug delivery [477,478], tissue engineering [479], water/air filtration [480], energy storage [481], protective clothing [482], sensors or photocatalytics [483], among others [484,485]. One of the key features of NFs is their large surface area to volume ratio, which allows

them to interact with their surroundings in ways that are not possible with larger fibers [486]. This can make them more effective at adsorbing or filtering small molecules or particles [487].

NFs can be prepared from natural or synthetic polymers, metals, ceramics, semiconducting, composite, and carbon-based materials [488]. Synthetic and natural polymers are particularly used in the synthesis of NFs for biomedical applications due to their biocompatibility, biodegradability, and processability [370,450]. Synthetic polymers include PEG, a water-soluble biocompatible polymer with good drug-carrying capacity [489]; PVA, a water-soluble biocompatible polymer [490]; polyvinylpyrrolidone (PVP), a water-soluble polymer with high biocompatibility [491]; PCL, a biocompatible and biodegradable polymer [492]; poly(lactic acid) (PLA), a biocompatible, biodegradable polymer that is often used in drug delivery applications [493]; or polyethyleneimine (PEI), a cationic polymer with good drug-carrying capacity and ability to evade the immune system [494]. The most widely used natural polymers for the synthesis of NFs in drug delivery applications are chitosan (CS), a biocompatible, biodegradable polymer derived from chitin [495]; gelatin, a protein derived from collagen, which is a natural polymer found in connective tissue [496]; alginate, a natural polymer derived from brown seaweed, brown algae (*Ochrophyta*, *Phaeophyceae*) and bacteria (*Azotobacter vinelandii* and *Pseudomonas species*) [497]; hyaluronic acid, a natural polymer found in connective tissue [498]; or dextran, a natural polymer derived from glucose [499]. Natural polymers are biocompatible and have good drug-carrying capacity, making them useful in drug delivery and tissue engineering applications [500]. Overall, the choice of polymer for NF synthesis for drug delivery applications depends on the specific requirements of the application, including the desired drug-carrying capacity, biocompatibility, and other factors. As for other nanomaterials, it is also important to consider the intended route of administration and the stability of the drug in the polymer matrix [501].

4.1. Synthesis of Polymeric NFs

Polymeric NFs can be synthesized using different technologies, such as electrospinning, self-assembly, template-based synthesis, polymerization or sonochemical synthesis [488]. Among the different methods that exist to produce them, electrospinning is the most used because it is simple, cheap, versatile, reproducible, and scalable [502]. Recently, the term "green electrospinning" has emerged as a method for synthesizing NFs using environmentally-friendly and sustainable materials and processes. It involves the use of biodegradable, biocompatible, and renewable materials, as well as energy-efficient and low-waste production methods. It is based on the use of natural or biosynthetic biodegradable polymers and the use of non-toxic solvents [503].

Electrospinning allows NFs to be created by loading and expelling a polymer solution through a needle subjected to a high-voltage electric field. The solution with the desired polymer is drawn into a syringe attached to a needle and pumped at low speeds until a drop forms at the tip of the needle. Subsequently, the solution is subjected to a high electrical charge produced by a high voltage source. As the voltage increases, the drop at the tip of the needle begins to deform until it begins to exert a magnitude of force, such as the surface tension of the solution itself. At this time, a cone shape with convex sides and a rounded tip, known as Taylor cone, begins to form [504]. When a certain voltage threshold is reached, a jet of liquid begins to be emitted. During the movement of the jet between the needle and the collector, the solvent evaporates and a solid polymer fiber is collected. The collector is also connected to the high voltage source and is usually made of conductive metal [505].

Drug encapsulation in NFs can be performed by electrospinning using methods such as blend electrospinning, coaxial electrospinning, and emulsion electrospinning (Figure 31). In blend electrospinning, the drug is mixed with the polymeric solution before the electrospinning process. Therefore, the drug is expected to be dispersed in the polymeric matrix and uniformly distributed in the NFs [91]. Coaxial electrospinning is based on the co-spinning of two solutions using two

needles located coaxially, one with the polymeric solution and the other with the therapeutic solution. Core-shell fibers are obtained, where normally the polymeric matrix is found in the outer core and the therapeutic agent is incorporated in the inner core [450]. Emulsion electrospinning solutions are based on two or more immiscible liquid phases that will be electrospun together using the same set up as blend electrospinning [91]. The distribution of the compounds in the NFs depends on their molecular weight. It has been observed that high molecular weight compounds tend to form core-shell structures, while low molecular weight compounds are distributed throughout the NFs [506].

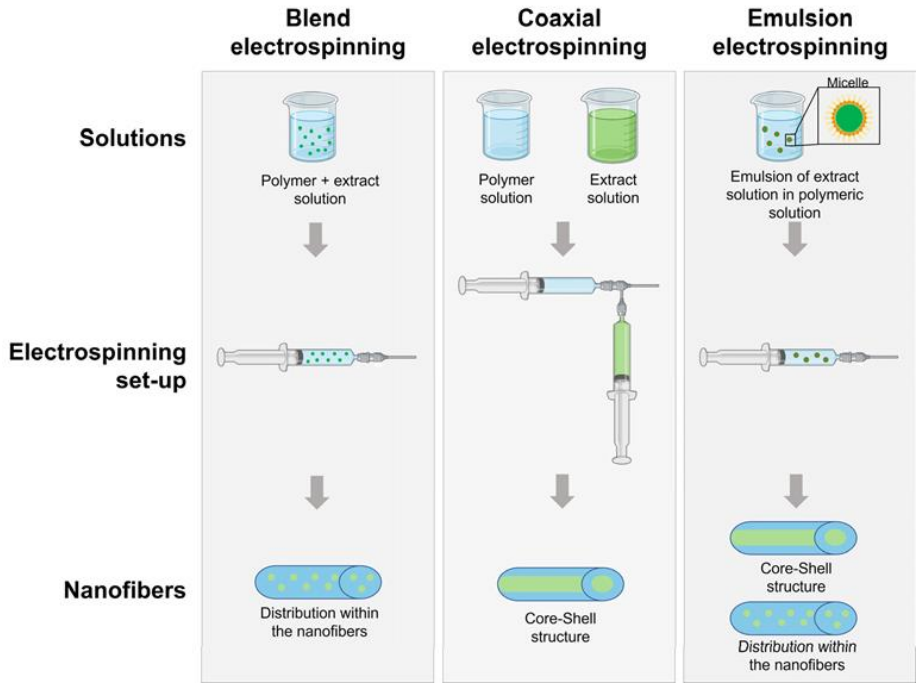

Figure 31. Diagram of electrospinning process for the manufacturing of NFs loaded with plant extracts.

4.2. Antibacterial Properties of Polymeric NFs

NFs can exert their antibacterial activity per se through a variety of mechanisms depending on the specific properties of the NFs, polymers used, and the type of bacteria being targeted. NFs with a small pore size or high surface area can physically entrap bacteria, preventing them from growing or spreading [507]. The surface chemistry of NFs can also affect their ability to interact with bacteria. For example, NFs with a positive charge may be able to attract and kill negatively charged bacteria, while those with a hydrophobic surface may be able to inhibit the growth of hydrophilic bacteria [450]. NFs can be designed to release antimicrobial agents, which can kill or inhibit the growth of bacteria [371]. NFs can also stimulate the immune system, helping to fight off bacterial infections [508]. In addition, by utilizing a polymer with antimicrobial capabilities, such as CS, NFs can exhibit their antibacterial activity. The antibacterial activity of CS can be attributed to its adsorptive characteristics to bacterial cells due to electrostatic interactions between the polycationic structure of CS and the anionic groups found on the bacterial cell surface [509]. This causes permeabilization of the cell membrane and the loss of essential constituents as enzymes, nucleotides, ions, and death of the bacterial cell.

4.3. Plant-Based NFs against ARB

The use of phytochemicals for the formulation of polymeric NFs is in continuous development and has attracted attention especially for their enhanced antimicrobial and wound healing activities [510]. Therefore, these formulations can be promising alternatives to treat ARB

infections. The combinations of polymers and phytochemicals for the synthesis of loaded NFs with antimicrobial application against ARB are summarized in Table 10.

Table 10. Electrospun polymer NFs loaded with phytochemicals against ARB.

Polymer	Extract/Phytochemical	Diameter (nm)*	Electrospinning Synthesis	Antibacterial activity*	Reference
Gelatin	*Phaeodactylum tricornutuen* extract	700	Blend	99.9 % inhibition (MRSA)	[511]
PCL/gelatin	*Gymnema sylvestre* LE	302-340	Coaxial	ZOI 17.1 mm (MRSA)	[512]
PCL/gelatin	*Melia dubia* extract	256	Blend	ZOI 23 mm (MRSA)	[513]
PCL/PVP	Curcumin	880-740	Coaxial	37 % inhibition (MRSA)	[514]
PVA	Myrrh extract	220	Blend	ZOI 13.33 mm (DR *S. aureus*)	[515]
	Thymus vulgaris extract	167		ZOI 10 mm (MRSA)	[516]
	Salvia officinalis folium extract	143		ZOI 10 mm (MRSA)	
	Hyperici herba extract	137		ZOI 10 mm (MRSA)	
PVA/CS	Curcumin	125	Blend/coaxial	92 % inhibition after 6 days (MRSA)	[517]
PVP	Emodin	692	Coaxial	Growing ZOI (MRSA)	[518]
P(HEMA)	Curcumin	20-110	Blend	ZOI 17 mm (MRSA), 18 mm (ESBL *Escherichia coli*)	[519]
Silk fibroin/PEO	Manuka honey	843-2229	Blend	ZOI 0.7-6.7 mm (MRSA)	[520]

DR: drug-resistant; ESBL: extended-spectrum beta-lactamases; LE: leaf extract; MRSA: methicillin-resistant *Staphylococcus aureus*. PCL: polycaprolactone; PEO: polyethilene oxide; PVA: polyvinyl alcohol; PVP: polyvinylpyrrolidone; P(HEMA): poly(2-hydroxyethyl methacrylate); ZOI: zone of inhibition. * Mean values or a range of values are indicated in studies employing various conditions or concentrations.

Thamer et al. (2022) recently fabricated PVA/tragacanth gum (TG) NF mats loaded with an aqueous extract of myrrh (myrrh@PVA/TG NFs) [515]. Results showed that 15%-myrrh@PVA/TG NFs had a mean diameter of 220 nm and displayed antibacterial activity against drug-resistant (DR) *S. aureus* with 13.33 mm of inhibition zone. In a study by Ramalingam et al. (2021), core-shell NFs were synthesized by coaxial electrospinning using PCL/gelatin as shell structure [512]. *G. sylvestre* leaf extracts were added to the core and the antibiotic minocycline hydrochloride was added to the shell. Results prior to the synthesis of NFs showed synergism between plant extracts and minocycline against Gram-positive bacteria. The incorporation of *G. sylvestre* extract to the PCL/gelatin solution resulted in a reduction in the diameter of the ensuing NFs from 443 to 302–340 nm. In addition, the NFs were able to inhibit MRSA in a disc diffusion assay with inhibition zones of 15.2–19.1 mm.

There are many different polymers used to manufacture NFs, with PVP and PCL being the only ones used in combination with more than one phytochemical among the selected studies. These polymers are widely used in biomedicine thanks to their particular properties. PVP is water-soluble, pH-stable, temperature-resistant, non-toxic, biodegradable, and biocompatible [521]. PCL, a polyester, has been employed extensively in the field of tissue engineering due to its accessibility, reasonable cost, and appropriateness for modification. It can be utilized under difficult mechanical, physical, and chemical conditions without suffering a major loss of its qualities because its chemical and biological properties, physicochemical state, degradability, and mechanical strength can all be altered [492].

In the selected studies, the most used technique for the fabrication of NFs loaded with phytochemicals against ARB was blend electrospinning, most likely because it is a simpler process compared to coaxial or emulsion electrospinning, which can be more complex and require specialized equipment [522].

There is a great variety in the phytochemicals used in the NFs, curcumin being the only one that appears in different studies. Numerous investigations revealed that curcumin had antibacterial effects on both Gram-positive and Gram-negative bacteria. Curcumin's antibacterial properties include bacterial membrane rupture, oxidative stress induction, suppression of bacterial virulence factor synthesis, and biofilm formation [523]. These qualities also help to explain why curcumin functions as a broad-spectrum antibacterial adjuvant, as demonstrated by the substance's pronounced additive or synergistic interactions with numerous conventional antibiotics and non-antibiotic substances [524].

In some studies, the addition of phytochemicals or their concentration increase resulted in a reduction in the diameter of the fibers [513,515,516,518]. This phenomenon is attributed to the higher charge density and conductivity. Previous studies indicate that a higher charge density in the Taylor cone makes its radius of curvature smaller, causing a concentration of electrical stress at the tip. This occasions the initial jet to emerge from a smaller area and mass deposition decreases [525]. Therefore, the addition of phytochemicals can be advantageous, since smaller diameters more similar to the size of the bacteria can enhance bacterial attachment and inhibition [526].

Several types of NFs containing phytochemicals have been shown to have antibacterial activity against ARB. MRSA is the most studied bacteria in antibacterial assays employing NFs containing phytochemicals. Its widespread prevalence and ability to cause a range of infections, as well as its AMR to antibiotics, make MRSA a useful model organism for studying antibacterial agents and mechanisms of action [527].

Most assays employed to determine antibacterial activity of NFs were Kirby–Bauer. This can lead to difficulties when comparing different studies, since although the diameter of the inhibition zone is provided, in many cases data on the mass of NFs used for the test are not disclosed. Thus, there is a lack of information on the amount of phytochemicals released into the medium. This fact makes it difficult to compare the results with other studies that provide specific MIC [528].

5. Nanoparticles

NPs represent a relatively new strategy to tackle ARB. Its unique characteristics are a result of its physical properties, which are often interrelated. Their very high specific surface area results in enhanced reactivity, increased solubility in certain solvents, improved drug-carrying capacity and enhanced catalytic activity [6]. In addition, they have high mobility in free state and in porous media, which can allow them to more easily reach their target site, interact with their surroundings, disperse in a particular medium and increase their sensitivity to certain factors, such as temperature or pH [529]. Finally, NPs of 10 nm or less exhibit quantum confinement effect due to the restriction of charge carrier motion to a small volume [6]. The quantum confinement of electrons in NPs can enhance optical and electronic properties and increase stability and reactivity [530].

NPs can be classified into carbon-based, metal, ceramics, semiconductor, polymeric and lipid-based NPs [531]. Among them, polymeric and MNPs are widely used for antimicrobial applications. Polymeric NPs offer advantageous properties for the encapsulation of antimicrobial drugs, such as controlled release of antimicrobial agents [532], target delivery [494], biocompatibility [533], improvement of bioavailability [534], possibility of reducing the administered dose [535], permanence in the circulatory system for longer periods [536] and

customizability [537]. On the other hand, MNPs have shown to possess bactericidal capacity by themselves using mechanisms that will be described in subsequent sections. During the last few years, a multitude of phytochemicals have been used for the green synthesis of MNPs [538].

5.1. Polymeric NPs

Polymeric NPs can be made of synthetic or natural polymers. Synthetic polymers employed for NPs synthesis include PVA, poly(N-isopropylacrylamide) (PNIPAM), poly(lactic-co-glycolic acid) (PLGA), PLA, PCL, or PEG [501]. Natural polymers include CS, alginate, albumin, hydroxyapatite, pectin, or hyaluronic acid [539]. Polymeric NPs can also be classified into nanospheres and nanocapsules, depending on their morphological structure. Nanospheres are formed by a solid polymeric framework with a spherical structure in which the drugs are embedded or attached to its surface. Nanocapsules are formed by a polymeric shell that surrounds an interior space where the drugs of interest are located [540]. In addition, nanocapsules are typically smaller and have a higher drug-carrying capacity and a slower release rate compared to nanospheres [541].

5.1.1. Synthesis of Polymeric NPs

Three main methods can be used to create polymeric NPs: the dispersion of preformed polymers, polymerization of monomers, and ionic gelation/coacervation of hydrophilic polymers. The different methods for the synthesis of polymeric NPs are described in Figure 32. The synthesis strategy will depend on the type of drug to be encapsulated, its administration, area of application, or size requirements, among other factors [452].

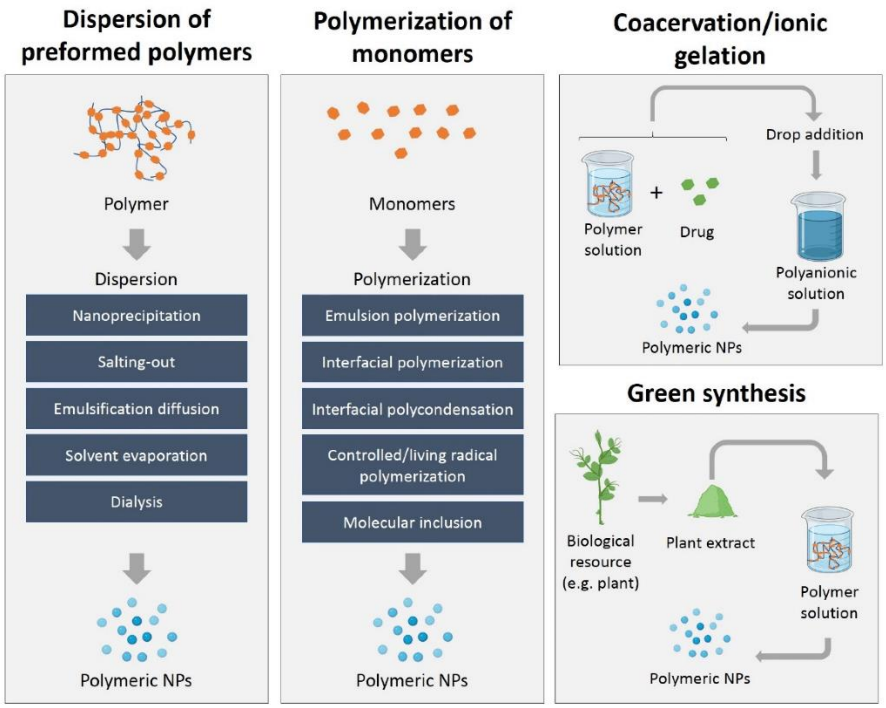

Figure 32. Schematic diagram of the different methods of synthesis (dispersion of preformed polymers, polymerization of monomers, coacervation/ionic gelation, green synthesis) of polymeric NPs.

In the synthesis by polymerization of monomers, the NPs are synthesized by techniques such as emulsion polymerization, interfacial polymerization, interfacial polycondensation, controlled/living radical polymerization, or molecular inclusion [452]. Polymeric NPs can also be synthesized by the dispersion of preformed polymers using techniques such as nanoprecipitation, salting-out, emulsification diffusion, emulsification evaporation, and double emulsion solvent evaporation [542].

The ionic gelation/coacervation method is based on the mixture of a polymer and a coacervating agent, which is usually a polyelectrolyte. As the coacervating agent is added, it begins to interact with the polymer, causing the polymer chains to coacervate and form NPs. The size and shape of the NPs can be controlled by adjusting the concentration of the polymer and coacervating agent, as well as the pH and temperature of the solution [543].

Recently, the synthesis of chitosan NPs

(CSNPs) using biological systems was described for the first time. This new methodology is based on the mixture of a chitosan solution at 1.08% with an extract solution of *Pelargonium graveolens* and its incubation for approximately 1 h at 50 °C. The plant *P. graveolens* was selected as a bioconverting agent due to its nonhazardous and environmentally friendly character [544].

5.1.2. Antibacterial Properties of Polymeric NPs

Polymeric NPs have suitable characteristics for use in drug delivery applications of antimicrobial agents, such as low toxicity, biocompatibility, biodegradability, or surface modification for specific targeting, among others [540]. These characteristics make it possible to improve the therapeutic index of drug loads in this type of system and to carry out a therapy focused on the infection site [545]. Some polymers, such as CS, have intrinsic antimicrobial activity, thus being able to kill bacteria or inhibit their growth by disrupting their cell membranes or inhibiting their metabolism [509]. Polymeric NPs can also coat surfaces and prevent bacteria from adhering to them. This can be useful for preventing the formation of biofilms, which are layers of bacteria that can be difficult to remove [546]. When exposed to light, polymeric NPs can produce ROS, which can damage bacterial cells and inhibit their growth, thus being beneficial for photodynamic therapy, a type of treatment that uses light and photosensitizers to kill bacteria [547]. Polymers can also be modified to incorporate cationic and hydrophobic moieties such as peptides, small molecules, carbohydrates, antibodies, proteins, nucleic acids or antimicrobial drugs. This facilitates entry into the bacterial membrane, since cell walls are normally negatively charged [548]. Another possible mode of action of polymeric NPs is through the release of antimicrobial agents. Polymeric NPs can be loaded with antimicrobial agents, which are then released in a controlled manner when the NP comes into contact with the bacterial cell [549]. This can enhance the efficacy of the antimicrobial agent by allowing it to accumulate at the site of infection for a longer period of time [550].

There are several parameters that affect the antimicrobial activity of polymeric NPs, for example, crosslinking, micellization, molecular weight, polymer type and concentration, size, surface area, surface chemistry, or surface charges. The effects of these parameters on the antimicrobial activity can be seen in Table 11.

Table 11. Parameters affecting antimicrobial activity of polymeric NPs.

Parameters	Effects	References
Crosslinking	Crosslinked NPs may be more resistant to degradation and may release the antimicrobial agent more slowly.	[551]
Micellization	High critical micelle concentration can lead to higher antimicrobial activity due to due to the greater activity of the polymeric chains as free molecules in solution	[552]
Molecular weight	High molecular weight polymers have shown greater antimicrobial activity against Gram-negative bacteria, due to the entrapment of the polymers by the peptidoglycan layer	[553]
Polymer type and concentration	Some polymers, such as CS or PEI, have intrinsic antimicrobial activities and higher concentration may lead to a greater antimicrobial effect.	[554]
Size	Smaller sizes can enhance antimicrobial activity due to internalization to bacterial cells	[555]

Table 11. Parameters affecting antimicrobial activity of polymeric NPs.

Parameters	Effects	References
Surface area	Larger surface-to-volume NPs provide more active sites for bacterial interaction	[556]
Surface chemistry	Type and density of functional groups in NPs surfaces can affect their antibacterial capacity by influencing their interactions with the bacterial cell surface.	[557]
Surface charges	Cationic charges increase antibacterial activity due to interaction with bacterial cell walls.	[558]

CS: chitosan; NPs: nanoparticles; PEI: polyethyleneimine.

5.1.3. Plant-Based Polymeric NPs against ARB

The use of polymeric NPs loaded with phytochemicals offers a promising strategy for the treatment against ARB, as it combines the antimicrobial activity of the phytochemicals with the controlled release and targeted delivery capabilities of the nanoparticles. Table 12 summarizes studies focused on polymeric NPs loaded with phytochemicals against ARB.

Table 12. Polymeric NPs loaded/synthesized with phytochemicals against ARB.

Polymer	Phytochemical or extract	Synthesis	Diameter (nm)*	Antibacterial activity	Reference
CS	Cardamom EO	Ionic gelation	50-100	Growth control for 2 days (MRSA, ESBL *E. coli*)	[559]
CS	*Eucalyptus globulus* LE	Green synthesis	7-10	ZOI of 12-30 (MDR *Acinetobacter baumannii*)	[560]
CS/HPMC	*Schinopsis brasiliensis* LE / Ceftriaxone	Polyelectrolytic complexation	150-500	MIC of 15 µg/ml (ESBL, KPC)	[561]
PLA/PVA	*Pistacia lentiscus* var. *chia* EO	Solvent evaporation	240-665	MIC higher than 3.4 mg/ml (DR *Bacillus subtilis* sub. *spizizenii*)	[562]

CS: chitosan; DR: drug-resistant; EO: essential oil; ESBL: extended-spectrum beta-lactamases; HPMC: hydroxypropyl methylcellulose; LE: leaf extract; MDR: multi-drug-resistant; MRSA: methicillin-resistant *S. aureus*; PLA: polylactic acid; PVA: polyvinyl alcohol; ZOI: zone of inhibition. * Mean values or a range of values are indicated in studies employing various conditions or concentrations.

Jamil et al. (2016) encapsulated cardamom essential oil (EO) in CSNPs using ionic gelation process. The size of the NPs was 50–100 nm and their antibacterial activity was tested against MRSA and ESBL *E. coli*. CSNPs loaded with cardamom EO could control bacterial growth for up to 7 days, while empty CSNPs could only maintain their antibacterial activity for 48 h [559].

Recently, CSNPs loaded with *E. globulus* leaf extract were synthesized via green synthesis method. The polymeric NPs were spherical with a diameter ranging 6.92–10.10 nm. Their antibacterial activity was tested against biofilm forming *A. baumanii*, and zones of inhibition of 12, 16, and 30 mm were recorded using concentrations of 12.5, 25, and 50 mg/mL, respectively. In addition, damage to the bacterial cell membrane, leaks of the cytoplasmic content into the extracellular medium, and the appearance of coagulations in the cytoplasm were observed [560].

CS is the most used polymer to make polymeric NPs loaded/synthesized with phytochemicals against ARB among studies included in Table 12. CS is a popular polymer for making NPs because of its biocompatibility and biodegradability [563]. This means that it is non-toxic to living cells and can be safely disintegrated by the body after it is no longer needed. CS can also form stable NPs with a range of different compounds, including both hydrophilic and hydrophobic molecules [564]. In addition, CS is a relatively inexpensive and widely available material, which makes it an attractive choice for use in NPs production [565]. Overall, the combination of these properties makes CS a popular choice for making polymeric NPs in a variety of applications.

The heterogeneity in the rest of the parameters included in Table 12, as well as the scarcity of existing studies that use phytochemical-loaded polymeric NPs against ARBs, hinder the direct comparison of the remaining information.

5.2. Metal NPs

MNPs are nanomaterials formed from pure metals (eg Au, Ag, Cu, Fe, Pt, Pd, Ti, or Zn) or their compounds (e.g., CuO, Fe_3O_4, TiO_2, ZnO) and have dimensions in the nanometer range (1–100 nanometers). MNPs have unique physical and chemical properties that are different from those of bulk metals, due to the influence of their small size and high surface area-to-volume ratio [95]. Currently, they are widely used in biomedical sciences and engineering due to their enhanced properties, such as high mechanical and thermal stability, high surface area, and high optical and magnetic properties [112].

5.2.1. Synthesis of MNPs

MNPs synthesis methods can be divided into two types: top-down and bottom-up approaches. Top-down approaches use destructive methods to break down a larger molecule into nanometer-sized particles in successive steps. This can be achieved through techniques such as grinding, attrition, sputtering, and laser ablation, among others [566]. Bottom-up approaches refer to methods in which MNPs are formed from simpler substances by self-assembly. Methods based on chemical reactions are widely used in this approach. Some examples are sol-gel, physical/chemical vapor deposition, spray/flame pyrolysis, chemical reduction, hydrothermal/solvothermal methods, or biological methods [6].

MNPs synthesis can also be classified according to the generation method. Thus, they can be generated by physical, chemical, and biological approaches. The physical methods of synthesis of MNPs mostly employ top-down strategies. Although physical and chemical can produce high purity MNPs, elevated energy consumption or the use of toxic chemical agents limit the applications of these methods [567]. Biological or "green" synthesis employs biological routes from bacteria, fungi, or plants for the synthesis of NPs [538]. Some of its advantages include the minimization of waste, the use of safer solvents as well as renewable feedstock, its simplicity, and its cost-effectiveness [568]. Plants are especially used for the synthesis of NPs, since they are non-pathogenic and have biomolecules, such as proteins, amino acids, polysaccharides, terpenes, alkaloids, phenolics, saponins, and vitamins [538], capable of reducing and stabilizing metal salts into NPs (Figure 33). The presence of MNPs within living plants after uptake of metal ions has been reported in species such as *Aloe vera*, *Medicago sativa*, or *P. graveolens*, among many others [569].

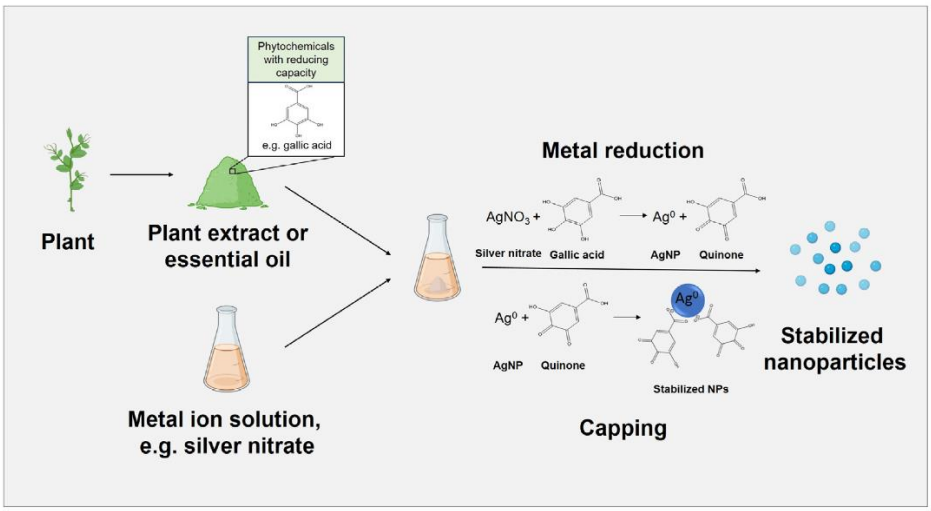

Figure 33. Schematic representation of the methodology used in the green synthesis of metallic nanoparticles using plant extracts.

5.2.2. Antibacterial Properties of MNPs

Although the exact mechanism of action of MNPs in bacterial cells remains unknown, some mechanisms have been proposed over the years. These include: the release of ions, which can disrupt the bacterial cell membrane and inhibit bacterial growth [570]; the production of ROS within microorganisms, damaging bacterial cells and inhibiting their growth [571]; the disruption of vital enzymes of the respiratory chain through microbial plasma membranes, damaging [572] or physically damaging bacterial cells due to their size and shape [573]. The mechanism of action of AuNPs against *E. coli* was studied by Cui et al. (2012). They demonstrated that AgNPs were capable of membrane collapse potential, inhibiting ATPase activities to decrease the ATP level, and inhibiting the subunit of ribosome from binding tRNA [574]. The ability of AgNPs to inhibit *S. aureus* bacterial growth was investigated by Li et al. (2011). They found that AgNPs were able to cross the cell wall and interfere with cell metabolism from the cell membrane. They were also able to cross the membrane and condense DNA to prevent it from replicating and cells from reproducing, producing the subsequent bacterial destruction [575].

5.2.3. Plant-Based MNPs against ARB

The use of plant parts, such as extracts or EOs from leaves, fruits, roots, stems, or seeds for the biosynthesis of NPs *in vitro* is being widely studied due to the biocompatibility, safety, and environmental harmlessness that this method presents [576]. The use of MNPs in combination with phytochemicals can be an effective strategy to combat ARB. Although there is evidence that bacteria can develop resistance strategies against MNPs, their nonspecific mode of action toward multiple cellular components suggests that development of resistance is less likely to occur compared to traditional antibiotics [146]. The use of phytochemicals to synthesize MNPs involves a more environmentally friendly approach for the fight against ARB. Table 13 shows NPs synthesized using phytochemicals for antimicrobial applications against ARB.

Table 13. Green-synthesized MNPs using phytochemicals against ARB.

NPs	Phytochemical or extract	Diameter (nm)*	MIC (µg/ml)*	Reference
AgNPs	*Aloe vera* extract	38.9	4.9-9.8 (KPC)	[577]
	Cinnamomum tamala LE	10-12	12.5 (MDR *E. coli*), 10 (MDR *K. pneumoniae*, 12.5 (MDR *S. aureus*)	[578]
	Cotyledon orbiculate LE	106-137	40 (MRSA)	[579]
	Flavopunctelia flaventior powder	69	0.156 (MRSA), 0.078 (VRE), 0.019 (MDR *Pseudomonas aeruginosa)*, 0.078 (MDR *E. coli*)	[580]
	Mespilus germanica LE	17.6	6.25-100 (MDR *K. pneumoniae*)	[581]
	Momordica charantia extract	9.6-16.4	4 (CR *A. baumannii)*, 4 (IR *A. baumannii*)	[582]
	Periploca hydaspidis extract	68.6- 114.2	10 (MDR *K. pneumoniae)*, 10-20 (MDR *S. aureus*),10 (MDR *E. coli)*, 5 (MRSA)	[583]
	Stenocereus queretaroensis PE	60-200	0.313 (MRSA)	[584]
	Syzygium cumini LE	10-15	8 (MRSA), 20 (VRSA)	[585]
	Vaccinium macrocarpon powder	1.4-8.6	18.3-39.5 (MRSA), 9.9-12.7 (MDR *P. aeruginosa*)	[586]
	Xanthoria parietina powder	145	0.078 (MRSA), 0.156 (VRE), 0.039 (MDR *P. aeruginosa)*, 0.156 (MDR *E. coli*)	[580]
AuNPs	*Anabaena spiroides*	80	25 (MDR *Klebsiella oxytoca*), 30 (MDR *Steptococcus pyogenes*), 20 (MRSA)	[587]
	Punica granatum extract	39.4	15.6 (MRSA)	[588]
CuNPs	*Syzygium cumini* LE	30-31	14 (MRSA), 16 (VRSA)	[585]
CuONPs	*Camellia sinensis* extract	61	125 (CREC), 125 (CRKP), 30 (MRSA)	[589]
	Prunus africana BE	68	125 (CREC), 125 (CRKP), 30 (MRSA)	
FeNPs	*Syzygium cumini* LE	40-46	11 (MRSA), 13 (VRSA)	[585]
PdNPs	*Padina boryana* extract	8.7	125 (MDR *S. aureus*), 62.5 (MDR E. *fergusonii)*, 62.5 (MDR *A. pittii*), 62.5 (MDR *P. aeruginosa)*, 62.5 (MDR *A. enteropelogenes*), 125 (MDR *P. mirabilis*)	[590]
TeNPs	*Aloe vera* extract	20-60	11.61 (MRSA), 3.53 (MDR *E. coli*)	[591]
ZnONPs	*Acacia nilótica* extract	94	0.45 (KPC)	[592]
	Bougainvillea FE	10-50	128 (MRSA), 128 (MREC)	[593]

BE: bark extract; CR: colistin-resistant; CREC: carbapenem-resistant *E. coli*; CRKP: carbapenem-resistant *K. pneumoniae*; FE: flower extract; IR: imipenem-resistant; KPC: *K. pneumoniae* carbapenemase; LE: leaf extract; MDR: multi-drug-resistant; MREC: methicillin-resistant *E. coli*; MRSA: methicillin-resistant *S. aureus*; NPs: nanoparticles; PE: peel extract; VRE: vancomycin-resistant *Enterococci*; VRSA: vancomycin-resistant *S. aureus*. * Mean values or a range of values are indicated in studies employing various conditions or concentrations.

Among the MNPs used in in vitro antibacterial activity assays against ARB, AgNPs are the most studied. Tyavambiza et al. (2021) used *C. orbiculate* leaf extract, a succulent plant indigenous to Southern Africa, to synthesize AgNPs. The AgNPs were formed using three different concentrations, 6, 3, and 1.5 mg/mL, whose mean diameters were 106, 110, and 137 nm, respectively [579]. Therefore, the average size of the AgNPs decreased as the concentration of the *C. orbiculate* extract increased, which was attributed to the presence of more reducing agents and a faster $AgNO_3$ reduction to form AgNPs. MIC and minimum bactericidal concentration (MBC) against MRSA were 40 µg/mL and 80 µg/mL, respectively. Lichen extracts were used as bioreducing agents to form AgNPs of 1–40 nm sizes in a study by Alqahtani et al. (2020) [580]. AgNPs inhibited the growth of both tested Gram-negative and Gram-positive multi-drug-resistant (MDR) strains with MIC and MBC values ranging between 0.019–0.156 and 0.039–0.625

mg/mL, respectively. Moorthy et al. (2021) produced AgNPs using aqueous and ethanolic bitter gourd (*M. charantia*) extracts (A-BG-AgNPs and E-BG-AgNPs, respectively) [582]. They found that E-BG-AgNPs were much smaller in size and showed greater agglomeration than the aqueous ones. A-BG-AgNPs showed better antibacterial performance than E-BG-AgNPs and both types of NPs produced morphological changes in *E. coli*, *S. aureus*, and *A. baumanii* cells.

Some studies used plant extracts for the biosynthesis of MNPs other than silver. Asghar et al. (2020) synthesized iron, copper, and silver NPs using *S. cumini* leaves extract [585]. The average diameters of Fe-, Cu-, and Ag-NPs were 58, 45, and 32 nm, respectively. Moreover, the antibacterial properties were found to be Ag- > Cu- > Fe-NPs, which showed that the size of NPs is an important factor in the effect of antibacterial activity, as stated in Table 11. Ssekatawa et al. (2022) used *C. sinensis* extract (CSE) and *P. africana* bark extract (PAE) to synthesize CuONPs [589]. The mean diameter for CSE and PAE NPs was 6 and 8 nm, respectively. Their antibacterial activity was significantly more extensive in MRSA, with lower MIC and MBC (30 µg/mL and 125 µg/mL, respectively) compared to MDR *E. coli* and *K. pneumoniae*. Palladium NPs with a diameter of 8.7 nm were synthesized using brown seaweed *P. boryana* extract in a study by Sonbol et al. (2021). They found that phytochemical compounds, such as tricosanoic acid, 2-methoxymethyl ester, 2-palmitoylglycerol, oleic acid chloride, oleic acid glycidyl ester, glycol stearate, monoolein, 9,12-octadecadienoyl chloride and oleic acid, 3-hydroxypropyl ester, were involved in the surface capping and stabilization of PdNPs. PdNPs were capable to inhibit Gram-positive and Gram-negative species and cause damage to the bacterial cell membrane permeability [590].

AgNPs stand out as the most used NPs, bringing together more than half of the total reports in Table 13. AgNPs have attracted a lot of attention in recent years, as evidenced by the significant demand for and investment in associated research [594]. AgNPs have seen steady market growth over the past 15 years, with an estimated 500 tons of NPs produced annually to meet demands across various industries. The research of their biological activity and safety, as well as the clarification of their precise mechanisms of action, have become matters of concern due to the rise of the NPs market globally [595].

The majority of the selected studies focus on DR strains of *S. aureus*, probably due to its use as a model bacteria in scientific research, as previously stated. It is followed by DR *K. pneumoniae* and DR *E. coli* strains, which are both common types of bacteria that can cause a range of infections, including urinary tract infections, pneumonia, and sepsis [485]. Some of the studies observed that Gram-negative bacteria showed greater sensitivity to NPs than Gram-positive ones [580,586,590,591], while other studies found the opposite case [578,589]. DR *P. aeruginosa* was used in various studies and its inhibition was especially remarkable compared to other ARB. The lower susceptibility of Gram-negative bacteria to the action of MNPs could be explained by cellular differences. Gram-positive bacteria have a thicker cell wall and more peptidoglycan, so they can become more resistant to the action of metal ions. Furthermore, the presence of negatively charged lipopolysaccharides in the cell wall of Gram-negative bacteria can promote the adhesion of MNPs [596].

Antibacterial activity was also shown to be dose-, size-, and shape-dependent [580]. Smaller MNPs are associated with an easier anchoring and penetration into bacterial cells. Furthermore, rod shape MNPs are related to a greater antibacterial capacity since they provide greater surface area [585]. The Z-potential is also a key parameter when determining antimicrobial activity. It has been observed that MNPs bind more efficiently to bacteria with a more negative Z-potential, which would also explain the greater susceptibility of Gram-negative bacteria [597].

In contrast to NFs, all studies of MNPs found used microdilution techniques to determine the MIC of the nanomaterials against ARB. These methods facilitate the comparison between different studies and their reproducibility.

6. Other Plant-Based Nanomaterials

Some studies used phytochemicals for synthesis or incorporation into nanomaterials other than NPs and NFs, which are summarized in Table 14. Qamar et al. (2020) synthesized CuO nanorods (NRs) via green synthesis using aqueous extracts of *Momordica charantia*. The synthesized NRs had a mean diameter of 61.48 nm in diameter and a length of 400–500 nm. In addition, CuO NRs were able to significantly inhibit MDR *B. cereus*, *Corynebacterium xerosis*, *E. coli*, *K. pneumoniae*, *Proteus vulgaris*, *P. aeruginosa*, *S. aureus*, *Staphylococcus epidermidis*, *Streptococcus mutans*, *S. pyogenes*, and *Streptococcus viridans* with the highest efficacy being observed against MDR *B. cereus* [598]. ZnO–CuO nanocomposites were biosynthesized using *Calotropis gigantea* extract in a study by Govindasamy et al. (2021). The rod-shaped binary NPs had a diameter of 7.5 nm and a length of 8.1 nm. In addition, they were able to inhibit ARB *K. pneumoniae* and *P. aeruginosa* and MRSA with MIC values of 0.625, 0.156, and 0.156 mg/mL, respectively [599]. Azizi et al. (2017) fabricated hydrogel beads based on κ-Carrageenan loading biosynthesized Ag-NPs using *Citrullus colocynthis* seed extract [600]. The mean diameter of the synthesized NPs was 23 nm, while dried bio-nanocomposite hydrogel beads were spherical with a diameter of about 1 mm. The bio-nanocomposite hydrogel showed an inhibition zone of 11 mm against MRSA.

Table 14. Nanomaterials other than NPs or NFs manufactured using phytochemicals with antimicrobial activity against ARB.

Nanomaterial	Phytochemical	Mean Size (nm)	Synthesis	Antibacterial activity	Reference
CuO NRs	*Momordica charantia* PE	61.5 x 450	Green synthesis	ZOI of 28. 66 (MDR *S. aureus, S. mutans, C. xerosis)*, 25.66 (MDR *E. coli, P. aeruginosa, S. pyogenes), 27.33 (*MDR *S. viridans)*, 23 (MDR *S. epidermidis), 31.66 (*MDR *B. cereus), 24.66 (*MDR *K. pneumoniae) and 26.33* (MDR *P. vulgaris) mm*	[598]
κ-Carrageenan/AgNPs hydrogel beads	*Citrullus colocynthis* SE	25	Green synthesis/Blending	ZOI of 11 mm (MRSA)	[600]
ZnO–CuO nanocomposites	*Calotropis gigantea* extract	8.1 x 7.5	Green synthesis	MIC of 0.16 (MDR *P. aeruginosa* and MRSA) and 0.63 (MDR *K. pneumoniae*) mg/ml	[599]

FE: flower extract; MDR: multi-drug-resistant; MIC: minimum inhibitory concentration; MRSA: methicillin- resistant *S. aureus*; NRs: nanorods; SE: seed extract; ZOI: zone of inhibition.

7. Future Perspectives and Conclusions

The need to find new antibacterial agents that are effective against ARB is imperative. In this review, plant extracts and phytochemicals have been shown to play an important role in this matter in combination with nanotechnology. Polymeric NFs and NPs are valuable tools to encapsulate these compounds, ensuring their stability and controlled release, protecting them from degradation. On the other hand, the synthesis of MNPs with these compounds through the

so-called "green synthesis" represents a more environmentally friendly approach that allows these tools to be used to fight ARB while limiting the use of toxic solvents and consumption of energy.

Many types of nanomaterials loaded or synthesized with a wide variety of natural compounds have shown activity against ARB. Among the polymers most used for the synthesis of NPs is CS, which shows intrinsic antibacterial properties and whose green synthesis has been recently described. In the case of NFs, the most used polymers are PCL and PVP, two biocompatible polymers. Silver NPs have been shown to be the most widely used MNPs for their study against ARB. It has been seen that the modulation of the properties of these nanocomposites (size, surface area, chemistry, porosity, etc.) can affect their antimicrobial activity.

Curcumin appears to be the most promising phytochemical for use in future developments, as it has been identified in three distinct studies in combination with electrospun NFs. The utilization of *A. vera* extract in two separate studies for the green synthesis of MNPs is also noteworthy. However, the effects of plant extracts are highly variable and dependent on several factors, such as their composition, which in turn can vary based on the extraction/purification method and the original raw materials used. These variables contribute to the multitude of antibacterial mechanisms that they possess, thereby rendering it challenging to identify any single extract as more significant than the others. Further research is needed in this direction to fully understand the mechanisms of action and potential limitations of this approach, evaluate the safety and toxicity of these combined phytochemical-nanomaterials, move on to the next phase of in vivo studies to discover the real therapeutic potential of these new biomedical tools, and be able to apply them onto practical biomedical applications. The fact that most of the studies found on this matter date from the last 5 years indicates the novelty and promising future of this technology, which can be decisive when developing tools to fight ARB. The innovativeness of this method explains the limited amount of information regarding the scale-up of green-synthesized nanomaterials. The next research steps should focus on optimizing various synthesis parameters to achieve the maximum yield possible while maintaining their desirable properties in the upscale process.

CHAPTER 5

CHAPTER 5: AN INNOVATIVE APPROACH BASED ON THE GREEN SYNTHESIS OF SILVER NANOPARTICLES USING POMEGRANATE EXTRACT FOR ANTIBACTERIAL PURPOSES.

SUMMARY OF RESULTS

This research chapter presents a study on the green synthesis of AgNPs using PGE from the "Mollar de Elche" variety as a sustainable reducing agent. The research aimed to develop a method that combines the natural properties of pomegranate with the high antibacterial effectiveness of AgNPs. The synthesis process was optimized using a BBD to streamline experiments and determine the ideal synthesis conditions based on three key variables: silver nitrate concentration, PGE concentration, and temperature. This method minimized the number of experimental trials while allowing for a systematic study of variable interactions.

The study demonstrated that PGE, rich in punicalagin and other polyphenolic compounds, serves as an effective bioreductant in AgNPs synthesis. Characterization of the optimized AgNPs showed that they were successfully created, as verified through techniques like UV-vis spectrophotometry, FTIR, and XRD. FESEM further confirmed that the AgNPs displayed anisotropic shapes and sizes.

The BBD analysis highlighted specific conditions under which the NPs exhibited ideal properties—such as optimal HDD, low PDI, and most negative ZP—ensuring the stability and uniform distribution of the AgNPs in solution. These parameters significantly enhance the ability of AgNPs to penetrate and disrupt bacterial cell walls, a critical feature in antibacterial efficacy.

Testing revealed that the optimized AgNPs displayed substantial antibacterial activity against *E. coli* and *S. aureus*, representing Gram-negative and Gram-positive bacterial models, respectively. The AgNPs disrupted bacterial cells effectively, with MIC observed to be between 2.5 and 10 µg/mL. For *E. coli*, exposure to the AgNPs caused cellular membrane damage, which was visible through wrinkling and structural deformation in treated cells. In contrast, *S. aureus* cells developed surface vesicles and exhibited internal penetration, suggesting that AgNPs disrupted cell viability by interfering with intracellular processes.

As a proof of concept for future biomedical applications, the AgNPs were incorporated into nanofibrous scaffolds using an electrospinning method, creating AgNPs-loaded NFs. Although the incorporation slightly reduced antibacterial effectiveness due to lower NP concentration in the fibers, the scaffolds maintained partial antibacterial activity. These NFs represent a promising application in wound dressings or other medical materials requiring sustained antimicrobial properties.

This research emphasizes the viability of PGE as a green, cost-effective reducing agent in NP synthesis, aligning with sustainability goals. The application of BBD facilitated efficient optimization, reducing resource and time consumption and establishing a reproducible protocol for the green synthesis of nanomaterials. Future research may focus on enhancing the uniform distribution of AgNPs in NFs and adjusting other critical parameters to enhance their effectiveness in antimicrobial applications.

An innovative approach based on the green synthesis of silver nanoparticles using pomegranate extract for antibacterial purposes.

Rocío Díaz-Puertas, Francisco Javier Álvarez-Martínez, Enrique Rodríguez-Cañas, Fernando Borrás, Artur JM Valente, José A Paixao, Alberto Falcó, Ricardo Mallavia

Abstract

This study describes a green synthesis method for silver nanoparticles (AgNPs) using autochthonous "Mollar de Elche" pomegranate peel extract and optimized through a Python programmed Box-Behnken Design (BBD) created specifically for the work. The bioactive compounds in pomegranate, particularly punicalagin, serve as effective reducing and stabilizing agents. BBD was used to analyze the effects of dependent variables like silver nitrate concentration, pomegranate extract concentration and temperature on responses such as hydrodynamic diameter, polydispersity index and zeta potential, minimizing experimental trials and highlighting variable interactions. Optimal conditions were experimentally validated and agreed well with the predicted values. The optimized AgNPs were characterized via ultraviolet-visible spectrophotometry, Fourier transform infrared spectroscopy, X-ray diffraction, and field emission scanning electron microscopy. These AgNPs demonstrated substantial antibacterial activity against *Escherichia coli* and *Staphylococcus aureus*. Furthermore, the AgNPs were incorporated into nanofibrous scaffolds as a proof of concept for potential biomedical applications, where their antibacterial activity was partially retained post-incorporation. This study highlights the potential of pomegranate extract as a sustainable medium for AgNP synthesis with promising antibacterial applications, and the ability of the BBD as a useful tool for efficient optimization of multivariable processes, including the synthesis of nanomaterials.

Keywords: Box-Behnken, green synthesis, *Punica granatum*, response surface methodology, silver nanoparticles, antibacterial activity.

1. Introduction

MNPs play an essential role in the area of nanotechnology and materials science due to their excellent physicochemical properties, such as remarkable mechanical and thermal stability, high surface area, and notable optical and magnetic properties [6]. These distinctive properties make MNPs highly valuable in diverse applications across various fields, including catalysis, medicine, electronics and environmental remediation [601]. In particular, AgNPs have garnered considerable scientific interest, primarily due to their unique chemical, physical, and biological characteristics. In particular, AgNPs have demonstrated substantial potential in biocidal and antimicrobial applications, exhibiting efficacy against both Gram-negative and Gram-positive bacterial strains [602].

AgNPs can be synthesized through physical, chemical, and biological approaches. While physical and chemical methods yield high-purity AgNPs, their drawbacks, such as high energy consumption and the use of toxic agents, restrict their applicability [603]. The pursuit of innovative AgNP synthesis now focuses on improving quality and properties while prioritizing environmental responsibility. In this context, "green" or biological synthesis has emerged as a promising sustainable alternative to traditional methods [604]. This environmentally friendly route uses microbial, plant, fungi or algae derived products as reducing and capping agents [605] and offers several advantages, including waste reduction, the utilization of safer solvents and renewable feedstock, simplicity, and cost-effectiveness [606].

The use of plant extracts/molecules in the green synthesis of AgNPs offers additional advantages to produce NPs with precise dimensions, morphology, and composition, including less hazardous procedures and a vast repertoire of biomolecules [607]. These extracts contain a diverse array of bioactive compounds, including proteins, amino acids, polysaccharides, terpenes, alkaloids, phenolics, saponins and vitamins [538]. This diverse set of biomolecules acts as highly effective reducing and capping agents, playing a central role in the transformation of Ag ions to assemble AgNPs [116]. Such compounds may enable the synthesis of AgNPs with unique properties, diverse shapes, sizes and functionality, which can be precisely tailored by adjusting the plant source, extraction conditions and synthesis process parameters [608,609]. Moreover, green synthesis using plant-based materials is associated with reduced cytotoxicity and improved biocompatibility of the resulting AgNPs, as demonstrated by different authors, making them ideal candidates for antimicrobial applications [610,611].

Pomegranate (*Punica granatum*), a fruit extensively cultivated in the Mediterranean region, has long been employed for its therapeutic properties, including its antioxidant, antibacterial and antitumor potential [134,612]. These activities are primarily attributed to the presence of bioactive tannins. Notably, the ellagitannin punicalagin and its derivative ellagic acid, prevalent in pomegranate peel, are key antioxidant constituents, boasting remarkable free radical-scavenging capabilities [613]. These compounds, in conjunction with several other polyphenols, proteins or sugars found in pomegranate peels, offer an exceptional blend of reducing and stabilizing agents, ideal for the green synthesis of various MNPs, including AgNPs [614-616], AuNPs [615] or ZnNPs [617] and metal oxide NPs such as ZnONPs [618,619].

Optimization of MNP synthesis is a critical step in achieving desired features. However, it is both resource-intensive and time-consuming, requiring a substantial number of trials and the detailed overlooking of potential interactions between the process factors [620]. These limitations can be more effectively addressed by employing a multi-level statistical design, such as the response surface methodology (RSM). RSM not only reduces the overall number of experiments but also facilitates the creation of appropriate models for process optimization, resulting in a more comprehensive understanding of the interactions between the variables [621]. Furthermore, RSM quantifies the relationship between the controllable input parameters and the resulting response surfaces [622]. One notable type of RSM is the BBD, which is renowned for its effectiveness in establishing correlations between response outcomes and the relevant factors through a carefully structured sequence of experiments, ultimately leading to the identification of the most favorable responses [623].

The present study focuses on the optimization of the green synthesis of AgNPs using PGE as the reducing and stabilizing agent. A BBD analysis for three factors is performed using a Jupyter Notebook hosted by Colab programmed in Python language created specifically for the work. It employs BBD to systematically investigate and fine-tune the process variables, including temperature, $AgNO_3$ concentration and PGE concentration, to enhance the quality and reproducibility of AgNPs production. The optimized AgNPs were thoroughly characterized, and their antimicrobial activity was evaluated. Finally, as a proof of concept, the AgNPs were incorporated into NFs, demonstrating their potential as a platform for targeted delivery.

2. Experimental section

2.1. Reagents and materials

Silver nitrate ($AgNO_3$), aluminum chloride ($AlCl_3$), Folin–Ciocalteu's phenol reagent, ABTS, gallic acid, glucose, 6-hydroxy-2,5,7,8-tetramethylchroman-2-carboxylic acid (Trolox), potassium bromide (KBr), potassium persulfate ($K_2S_2O_8$), Coomassie Brilliant Blue G-250, DNS, sodium potassium tartrate, phenol, sodium metabisulfite and INT were purchased from Sigma-

Aldrich (St. Louis, MO, USA). Punicalagin molecular standard was supplied by Merck (Darmstadt, Germany). Müller-Hinton (MH) broth was provided by Condalab (Madrid, Spain). Bacterial species Escherichia coli and Staphylocuccus aureus were obtained from Spanish Type Culture Collection (CECT, Valencia, Spain).

2.2. Extract preparation and characterization

2.2.1. Preparation of Punica granatum extract

The PGE employed in this study was prepared in the laboratory from organic pomegranate peel of the "Mollar de Elche" variety collected in Elche (Alicante, Spain), which holds Protected Designation of Origin (PDO) status. First, the peels were washed, dried at 60 °C in an ZHWY-100B incubator oven (Zhicheng Instruments, Shanghai, China) and grounded using a MF10 basic mill (IKA, Staufen, Germany) to obtain uniform particle sizes of 1-2 mm. Afterwards, an ultrasound-assisted extraction was performed by providing an energy of 100 J/mL to the extraction medium, which consisted of distilled water at 60°C, using a UP400St ultrasonicator (Hielscher, Teltow, Germany). After one hour of agitation, the extract was filtered using a Colombo plate filter with V4 filters (Rover Pompe, Polverara, Italy), taken to a R-220 Pro rotary evaporator (Büchi, Flawil, Switzerland) to concentrate, and finally dried to powder form using a B-290 spray-dryer (Büchi).

2.2.2. Phenolic content determination

The total phenolic content of the extracts was measured by using the Folin-Ciocalteu method in 96-well plates as previously described [624]. Briefly, 10 µL of each sample was mixed with 50 µL of Folin–Ciocalteu's phenol reagent. After 1 min, 100 µL of Na2CO3 solution (20 %, w/v) and 840 µL of distilled water were added to the mix. The reaction was kept in dark for 30 min. Plate absorbance was measured at 700 nm using a BioTek Synergy HTX Multi-Mode Microplate Reader (Agilent Technologies, Santa Clara, CA, USA). A standard curve of gallic acid was used for calibration, and results were expressed as gallic acid equivalents (g GAE/100 g of dry extract).

2.2.3. Total flavonoids quantification

The quantification of flavonoids was performed using the aluminum chloride ($AlCl_3$) colorimetric method [625], which involves the formation of a flavonoid-aluminum complex producing a yellow color measurable by spectrophotometry.. Briefly, 0.5 mL of PGE was mixed with 4.5 mL of 0.2 % $AlCl_3$ methanolic solution containing 0.1 mL of potassium acetate 1M and allowed to react for 30 minutes at room temperature. The absorbance of the resulting solution was measured at 415 nm using a BioTek Synergy HTX Multi-Mode Microplate Reader. A standard curve was generated using quercetin as a reference, and the flavonoid content in the samples was expressed as g of quercetin equivalents per 100 g of dry extract.

2.2.4. High-performance liquid chromatography (HPLC)

The molecular composition of the PGE was analyzed by HPLC using an Agilent LC 1100 series (Agilent Technologies). Briefly, HPLC instrument was equipped with a pump, autosampler, UV–vis diode array detector (DAD), and column oven. The HPLC instrument was controlled by Chemstation software. The chromatographic column used was an Agilent Poroshell 120 RP - C18 column (4.6 × 150 mm, 2.7 µm). The method used for PGE components separation consisted of a linear gradient of 1 % formic acid (A) and acetonitrile (B). Gradient started at 5 % of B, increasing to 25 % of B at 30 minutes, to 45 % of B at 45 minutes, then 5 % of B at 51 minutes and for an additional 5 minutes for column re-equilibration purposes. The flow rate was constant at 0.5 mL/min. The diode-array detector was set at 280, 320 and 340 nm.

Identification of the main compounds was performed by HPLC-DAD analysis using a home-made library of phenolic compounds and comparing the retention times and UV spectra data of the peaks in the samples with those of authentic standards or data reported in the literature. Punicalagin molecular standard was used to identify the main component of PGE. The interpretation of the spectra and identification of the main compounds was carried out using OpenChrom 1.4 software (Lablicate GmbH, Hamburg, Germany).

2.2.5. Antioxidant determination

The antioxidant capacity of the PGE was determined by the TEAC (Trolox Equivalent Antioxidant Capacity) assay. In this method, the radical precursor ABTS, pre-treated with potassium persulfate, produced the radical cation ($ABTS^{\bullet+}$) after 12−24 h of incubation at room temperature. For the study of extract, the $ABTS^{\bullet+}$ solution was diluted with water to an absorbance of 0.70 (± 0.02) at 734 nm (approximately 45 μM). $ABTS^{\bullet+}$ underwent a reduction process proportional to the antioxidant capacity of each extract sample. This reaction involves a loss of color intensity that was quantified at a wavelength of 734 nm. A calibration curve was prepared with different concentrations of Trolox up to 10 μM. Results are presented in mmol of Trolox equivalents per 100 g of dry extract [624].

2.2.6. Protein quantification

The protein content of PGE was quantified using the method described by Bradford (1976) [136] with some modifications. The method is based on the binding of Coomassie Brilliant Blue G-250 dye to proteins, which results in a shift of the dye's absorbance maximum from 465 nm to 595 nm. A standard curve was generated using known concentrations of BSA to determine the protein concentration in the samples. A volume of 200 μL of Coomassie Brilliant Blue G-250 was added to each standard curve or sample tube to achieve a total volume of 1 mL. Absorbance readings at 595 nm were measured using a BioTek Synergy HTX Multi-Mode Microplate Reader.

2.2.7. Total reducing sugars quantification

The quantification of reducing sugars was carried out using the DNS method described by Miller (1959) [137] with some modifications. This colorimetric assay relies on the reduction of DNS by free aldehyde or ketone groups present in reducing sugars, resulting in the formation of 3-amino-5-nitrosalicylic acid, which exhibits a reddish-brown color. DNS reagent was prepared by dissolving 1.87 g of 3,5-dinitrosalicylic acid and 3.48 g of NaOH in distilled water. To this solution, 53.9 g of sodium potassium tartrate, 1.34 mL of phenol, and 1.46 g of sodium metabisulfite were added. The final volume was adjusted to 250 mL with distilled water. A standard curve was established using known concentrations of glucose as a reference. In the assay, 1 mL of the standard or PGE samples was mixed with 1 mL of DNS reagent and incubated in a boiling water bath for 5 minutes to allow the reaction to proceed. After cooling to room temperature, the absorbance of the resulting solution was measured at 540 nm using a BioTek Synergy HTX Multi-Mode Microplate Reader.

2.3. AgNPs synthesis

A 0.1 M $AgNO_3$ stock solution and a 50 mg/mL pomegranate extract stock solution were initially prepared in Milli-Q water. To synthesize the AgNPs, different volumes of the PGE (ranging from 0.16 to 0.48 mL, equivalent to 0.16 to 0.48 mg/mL in the final reaction) were added into solutions of 5 to 15 mM $AgNO_3$, which were derived from the initial stock solution. The total volume of the reaction mixtures consistently remained at 50 mL. The solution was stirred with the help of a magnetic stirrer, with temperatures maintained within the range of 20 to 80 °C, depending on the experiment, for 24 hours. Following this, the AgNPs were subjected to centrifugation at 15,000 rpm for 30 min. The supernatant was discarded and precipitated AgNPs were redissolved in Milli-

Q water and sonicated for 15 min. This process was repeated twice. The resulting AgNPs were subjected to freeze-drying to facilitate subsequent characterization requiring solid material.

2.4. Response Surface Methodology

A three-factor, three-level BBD was employed to optimize AgNPs using a Jupyter Notebook hosted by Colab programmed in Python language created specifically for the work. The program uses Python DOEPY (Design of Experiment Generator in Python) library. The BBD comprised 15 experimental trials, incorporating three replicated central points. The independent variables consisted of $AgNO_3$ concentration (X_1), PG extract concentration (X_2), and reaction temperature (X_3). These three variables were manipulated at three different levels: low, medium and high. The upper and lower limits for the experimental factors were determined based on existing literature and preliminary experiments. The responses or dependent variables under investigation encompassed HDD (Y_1), PDI (Y_2), and ZP (Y_3). The optimization of AgNPs synthesis was based on achieving the minimum possible values for each of the responses. The variations in the process parameters are summarized in Supplementary Table S-6.

2.5. Nanoparticle characterization

2.5.1. Microscopy

A single drop (approximately 10 µL) of the different AgNPs solutions was dispensed onto a silicon wafer and allowed to dry. The morphological structure of the optimal synthesized AgNPs were analyzed by FESEM with a Schottky hot cathode field emission model Sigma 300 VP apparatus (Carl Zeiss Microscopy GmbH, Oberkochen, Germany) with a coupled energy dispersive X-ray system (EDX) to determine their element composition. Samples were imaged under 1 or 20 kV EHT and using a secondary electron detector (SE2) or a backscattered electron detector (AsB), depending on the sample.

2.5.2. UV-vis spectrophotometry

The UV-vis spectrum of the synthesized aqueous AgNPs was acquired using a 1 cm path length quartz cell on a Shimadzu UV-1700 (Kyoto, Japan) UV-vis spectrophotometer. The absorbance of the solutions was measured at room temperature in the 250–800 nm range with a resolution of 1 nm.

2.5.3. Dynamic light scattering (DLS)

Particle size and surface charge analyzer Zetasizer Nano-ZS ZEN 3600 (Malvern Instruments Limited, Worcestershire, United Kingdom) was used to determine the HDD and PDI through DLS. AgNPs samples were placed into U-shaped capillary cells for ZP analysis. The analysis was done at 25 ºC in triplicate. Prior to the analysis, the AgNPs were suspended in Milli-Q water and sonicated for 10 min.

2.5.4. Fourier transform infrared (FTIR) spectroscopy

The chemical composition of the samples was assessed through FTIR spectroscopy using a Spectrum Two™ FTIR spectrometer (PerkinElmer, Waltham, MA, USA). Two milligrams of the dried samples were pulverized with KBr salt at 25 ºC and compressed into a mold to create a pellet. The spectra were captured within a wavelength range of 450–4000 cm^{-1} at a resolution of 4 cm^{-1}.

2.5.5. X-Ray diffraction analysis (XRD)

The XRD pattern was collected on a D8 Advance diffractometer (Bruker, Karlsruhe, Germany) equipped with a 1D LynxEye detector, using Ni-filtered Cu Kα radiation. The powder sample

was mounted in a low background off-cut silicon crystal sample holder. The X-ray diffraction pattern was collected using Bragg–Brentano geometry, at room temperature, by scanning in the angle range $5^\circ \leq 2\theta \leq 80^\circ$ with a step of 0.01 º and a dwell of 1 s per step.

2.6. Antibacterial Assays

The antibacterial efficacy of AgNPs and AgNP-loaded NFs was assessed through the broth microdilution technique to determine the MIC. To determine the MIC, dried AgNPs were initially dissolved in Milli-Q water. Subsequently, 50 µL of this solution was added to the wells of a 96-well plate, with concentrations starting from 80 µg/mL and serially diluted by half. Additionally, 20 µL of a bacterial suspension at 0.5 McFarland was added to each well. MH broth was added to reach a total volume of 200 µL in each well. The plates were then incubated at 37 ºC for 24 hours. Following incubation, 50 µL of a 1 mg/mL INT solution was introduced into each well and allowed to incubate for 30 minutes. The MIC was defined as the lowest concentration at which no red color was observed.

2.7. Observation of bacterial cell morphology after AgNPs exposure

Bacterial cells, both untreated and treated with the MIC for 24 hours, were fixed on borosilicate cover glass slides according to the protocol described by Pulingam et al. (2019). Briefly, the cells were treated with 4 % glutaraldehyde (GLA) for 30 minutes, washed with PBS, and further fixed with 1 % osmium tetroxide for an additional 30 minutes. Samples were progressively dehydrated using ethanol (30, 50, 70, 80, 90, and 100 % for 15 minutes each). Micrographs of the bacteria were captured using a Sigma 300 VP FESEM (Carl Zeiss, Germany) at 1 kV without coating. EDX was employed to determine the presence of AgNPs inside the bacterial cells.

2.8. Nanoparticle incorporation into nanofibers

The optimized AgNPs (AgNPs-OPT) were selected to be incorporated into NFs as proof of concept, to evaluate their potential as scaffolds for biocidal applications. AgNPs (0.2 % w/w) were added to a PEO (3 % w/w) and BSA (15 % w/w) solution in distilled water, as previously described [626]. The solutions were left stirring overnight. Finally, the NFs were synthesized via electrospinning. For that purpose, the solutions were loaded into 2 mL syringes (Becton Dickinson, Franklin Lakes, NJ, USA) connected to a blunt-end stainless steel needle (5 cm long, outer diameter of 1.27 mm and inner diameter of 0.84 mm, Sigma-Aldrich). Electrospinning was conducted with a controlled flow rate of 0.25 mL/h using a KDS 100 infusion pump (KD Scientific, Holliston, MA, USA), a voltage of 18 kV using high voltage source (Glassman High Voltage Inc., Whitehouse Station, NJ, USA) and a tip-to-collector distance of 17 cm, under conditions of 20-40 % relative humidity and 25 °C. The obtained NFs were deposited in glass slides and characterized through FESEM after chrome coating (Q150T S plus, Quorum Tech., UK). The average diameter of the NFs was determined using Image J (National Institutes of Health, Bethesda, MD, USA) image processing and analysis software from 100 measurements using different images.

2.9. Data analysis

All experimental data from BBD were collected in triplicate and expressed as mean values ± SD. Graphs were carried out using Prism v8 software (GraphPad software, La Jolla, CA, USA), unless stated otherwise.

3. Results and discussion

3.1. PGE characterization

The total polyphenolic content of PGE, as determined by the Folin-Ciocalteu method, showed a value of 29.94 ± 0.36 g of GAE per 100 g of dry extract. This significant concentration indicates a robust presence of phenolic compounds, which are known for their antioxidant properties. Comparatively, green coffee extract typically exhibits polyphenolic content around 25 to 31 g GAE/100 g dry weight [627], and olive oil shows approximately 31 to 39 g GAE/100 g dry weight [628]. These values underscore the substantial polyphenolic concentration found in pomegranate peel when compared with other known polyphenolic-rich matrices.

To accurately determine the polyphenolic profile of PGE, different HPLC analysis were performed. The chromatograms of PGE at concentrations of 1 mg/mL and 3 mg/mL can be observed in Figure 34A and 34B, respectively.

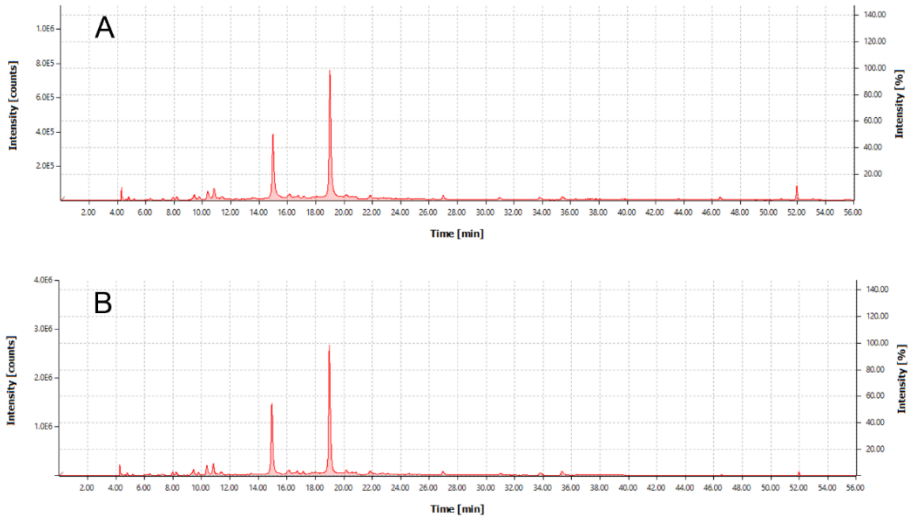

Figure 34. PGE chromatogram obtained by HPLC. PGE samples were analyzed at a concentration of (A) 1 mg/mL and (B) 3 mg/mL.

To identify and quantify the main components of the PGE chromatogram, a punicalagin molecular standard was used. This standard was chosen based on previous experience of the group and bibliography. The chromatograms of the punicalagin molecular standard analyzed at different concentrations, as well as the regression line (R^2 = 0.9961) calculated based on the areas of the peaks obtained, can be observed in Figures S-5 and S-6, respectively.

The analysis of the retention times and DAD of the molecular standard demonstrated that the main polyphenol present in the PGE is punicalagin, representing 29.45 ± 1.76 % of the total dry weight of the extract. This value means that punicalagin accounts for most of the total polyphenols measured by the Folin-Ciocalteu assay, which is consistent with the chromatograms obtained, in which the peaks corresponding to punicalagin are those that show greater intensity and area. These results agree with previous studies on pomegranate peel extracts, in which hydrolyzable tannins quantified as punicalagin equivalents by HPLC represented 30.46 % of the total dry weight of the extract [134]. The flavonoid content of PGE was determined, revealing a total of 5.15 ± 0.33 g of quercetin equivalents per 100 g of dry extract. This value is consistent with the chromatographic profile obtained from PGE, in which the major peaks belong to hydrolysable tannins such as punicalagin and the minor peaks could be related to flavonoids.

The PGE used in this work exhibits a remarkably high antioxidant capacity, quantified at 1379 ± 40 mmoles TROLOX equivalents per 100 g of dry extract. This value is notably higher when

compared to other plant extracts. For instance, the antioxidant capacity of green tea extract, a well-known antioxidant source, is around 460 mmoles TROLOX equivalents per 100 g, and other extracts of popular herbs such as the ones from Ilex paraguariensis (mate) or Salvia rosmarinus (rosemary) range from 128 to 154 mmoles TROLOX equivalents per 100 g [629]. The high antioxidant capacity of PGE can be attributed to the presence of highly active phenolic compounds such as punicalagins [630]. The analysis of total reducing sugars in PGE showed a concentration of 57.2 g glucose equivalents per 100 g of dry extract. This finding is consistent with the overall composition of pomegranate peel, which is known to be rich in various sugars [631]. The total protein concentration in PGE was 0.84 ± 0.07 g BSA equivalents per 100 g of dry extract, accounting for 0.84 ± 0.07 % of the PGE. This value is lower than other pomegranate peel extracts, which report values between 3.08 ± 0.02 % [632] and 4.98 ± 0.50 % [631]. These differences can be attributed to differences between pomegranate varieties and extraction methods.

3.2. Box-Behnken Design

3.2.1. Response surface plot

Response surface analysis was conducted employing 3D response surface plots and 2D contour plots to elucidate the contribution of independent variables to various response variables. Figure 35 illustrates the response surface analysis plots for HDD, PDI, and ZP.

Regarding HDD, it can be observed that at moderate temperatures (around 50 °C), the parameter is minimized in both temperature-PGE and temperature-$AgNO_3$ plots. The effect of PGE and $AgNO_3$ concentrations shows an increase in HDD with the rise in concentration in both cases.

For PDI, the relationship between temperature and PGE exhibits a curvilinear trend, showcasing minimal levels at lower temperatures alongside moderate to high PGE concentrations, followed by a decrease and subsequent increase at higher temperatures and moderate to low PGE concentrations. The relationship between temperature and $AgNO_3$ indicates that PDI is minimized at high temperatures and high concentrations of $AgNO_3$. Finally, the correlation between PGE and $AgNO_3$ unveils two separate minimum points: one occurring at moderate PGE concentrations and high $AgNO_3$ concentrations, and the other at high PGE concentrations and moderate $AgNO_3$ concentrations.

As for ZP, it appears to be the most minimized response in all cases. The relationship between temperature and PGE shows minimal ZP values under almost all conditions, although it is favored at medium to high temperature values and medium to low concentrations of PGE. The temperature-$AgNO_3$ relationship demonstrates that at intermediate temperature values (50-60 °C), ZP is minimized without influence from $AgNO_3$ concentration. Finally, the plot of PGE and $AgNO_3$ concentrations displays minimal ZP values at intermediate concentrations in both cases.

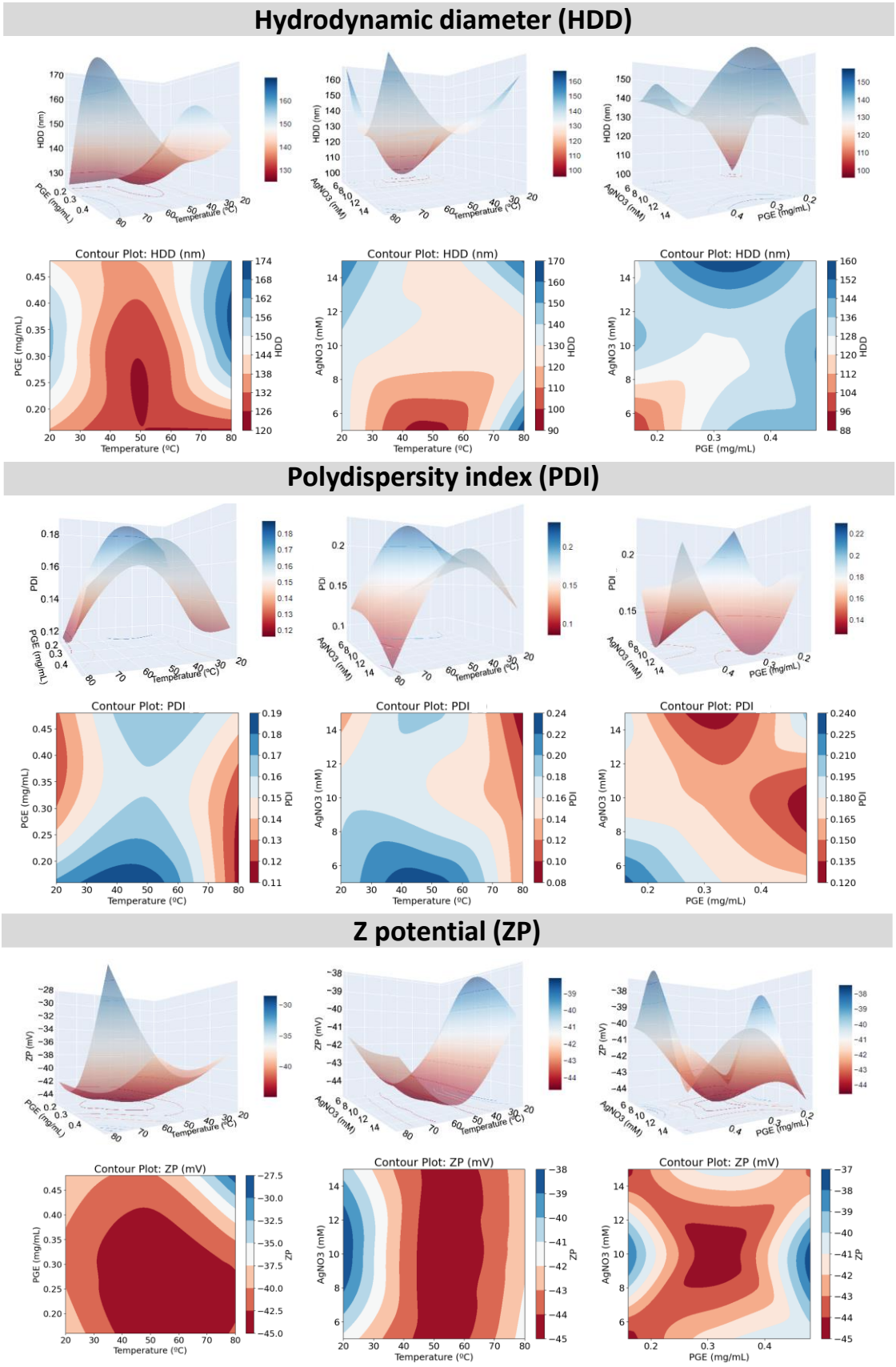

Figure 35. 3D response Surface plots and 2D contour plots of Box–Behnken statistical experimental design showing the interactions effects of temperature, PGE concentration and $AgNO_3$ concentration on HDD, PDI and ZP as response variables.

3.2.2. Polynomial model for each response

The obtained data were used to define polynomial models for each response (Y_1, HDD; Y_2, PDI; Y_3, ZP), which demonstrate interaction among all the analyzed variables and are described in Supplementary Table S-7.

Furthermore, a prediction-response comparison was performed, as shown in Figure 36. All parameters exhibited a Pearson correlation coefficient (r) greater than 0.9, with values of 0.971, 0.956, and 0.911 for HDD, PDI, and ZP, respectively. These values indicate a strong association among the variables, thus indicating a good fit of the data to the selected model [633].

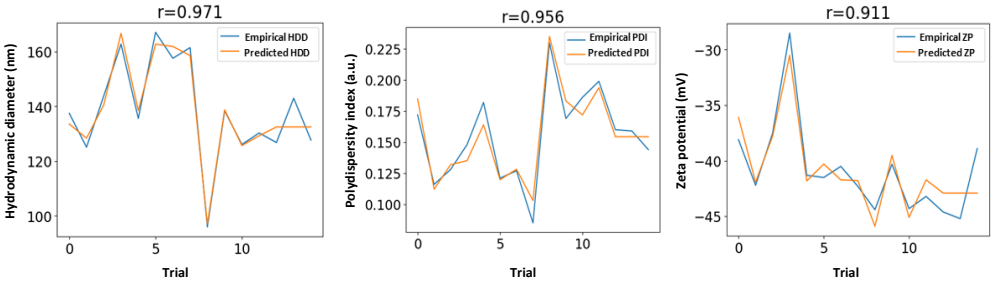

Figure 36. Comparison between the results predicted by the model (orange line) and the empirical results obtained in the 15 trials (blue line). r corresponds to Pearson correlation coefficient.

3.2.3. Optimal AgNPs production conditions

The study aimed to identify optimal conditions that would minimize all investigated responses simultaneously. A particular focus was placed on minimizing the HDD of the AgNPs. Smaller NPs possess a larger surface area to volume ratio, which facilitates increased interaction with bacteria [634], thereby enhancing their antibacterial properties. Additionally, minimization of PDI was also pursued since values below 0.2 generally indicate a monodisperse distribution, which is desirable for consistent material properties [635]. Finally, a ZP below -30.0 mV was sought as it signifies stable AgNP dispersions [636]. These optimized NPs were designated as AgNPs-OPT.

Additionally, conditions that optimized each parameter individually were also investigated. These include the smallest possible HDD (AgNPs-HDD), the lowest PDI (AgNPs-PDI), and the most negative ZP (AgNPs-ZP). Supplementary Table S-3 summarizes the conditions required to achieve optimal results in each case.

Subsequently, AgNPs were synthesized using the predicted conditions to validate the obtained results. The root-mean-square error (RMSE) was also calculated to allow evaluation of the predictive accuracy of the employed optimization model compared to other developed models in the future. These results are presented in Table 15. The graphical representations of the obtained experimental values can be found in Supplementary Figure S-7. As observed, the experimental values closely align with the model's predictions, demonstrating a strong fit of the selected design.

Table 15. Predicted and experimentally obtained values, as well as the RMSE for each of the responses related to the optimized conditions.

	Response	Predicted value	Experimental value	RMSE
AgNPs-OPT	HDD (nm)	131.3	130.3±12.0	9.9
	PDI	0.147	0.149±0.018	0.015
	ZP (mV)	-46.0	-48.3±0.6	2.3
AgNPs-HDD	HDD (nm)	96.7	96.4±0.5	0.5
AgNPs-PDI	PDI	0.092	0.115±0.006	0.024
AgNPs-ZP	ZP (mV)	-46.3	-44.6±1.8	2.2

3.3. Nanoparticle characterization

3.3.1. Microscopy

The morphology of the synthesized AgNPs was characterized using FESEM microscopy, as represented in Figure 37. The images confirmed that the synthesized NPs were within the nanoscale range and exhibited mixed anisotropic morphologies, including spherical, quasi-spherical, triangular, and hexagonal shapes. This observation aligns with the literature, as green-synthesized AgNPs are known to exhibit diverse shapes and sizes, with the most common forms being spherical, triangular, and hexagonal [637]. Furthermore, EDX analysis confirmed the presence of silver associated to each AgNP in all samples (Supplementary Figure S-8).

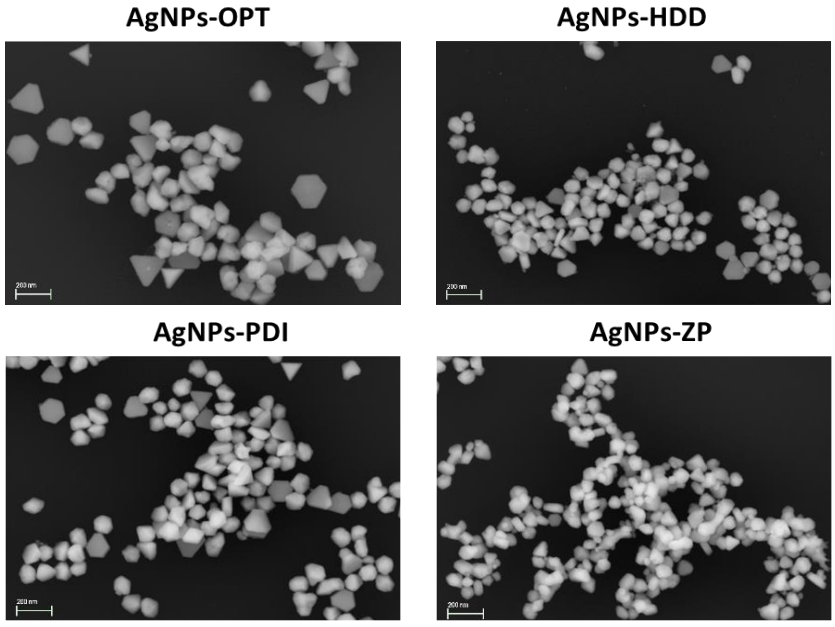

Figure 37. FESEM images (SE2 detector, EHT=1 kV) of the AgNPS-OPT, AgNPs-HDD, AgNPs-PDI and AgNPs-ZP. Scale bar: 200 nm.

3.3.2. UV-vis spectrophotometry

UV-vis spectrophotometry was employed to investigate the absorption spectrum of the optimized green synthesized AgNPs, as it provides information about the correct formation of the NPs. Spherical AgNPs typically exhibit a surface plasmon resonance (SPR) band extending in the range from 380 to 460 nm [138]. In the case of the AgNPs synthesized and optimized in this study (Figure 38), the maximum of the SPR band was observed in the range of 435-455 nm, closely

resembling the commercial AgNPs spectrum (AgNPs-control), which displays two distinct peaks at 415 and 462 nm. Their absorption spectrum is associated with the typical spectrum of NPs with a diameter close to 100 nm, as larger spheres tend to show increased scattering, leading to broadening and shifting of peaks towards longer wavelengths, a phenomenon known as red-shifting [638,639]. Furthermore, the AgNPs synthesized via green synthesis using PGE exhibit more than one SPR band, indicating their anisotropic nature [106].

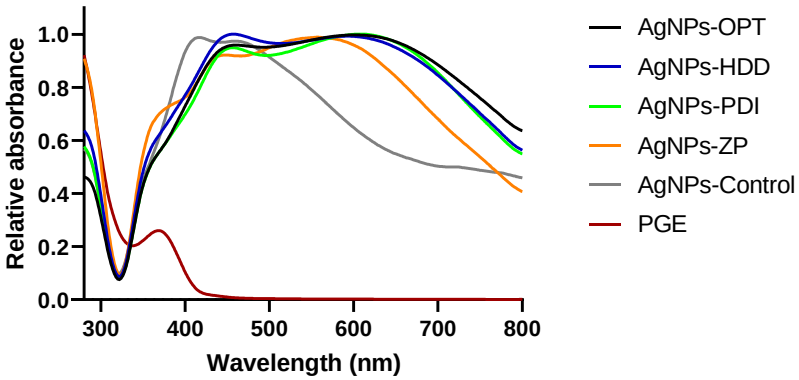

Figure 38. UV-vis spectrum of the four types of optimized green synthesized AgNPs and Punica granatum extract (PGE).

3.3.3. FTIR

The FTIR analyses were conducted to identify the functional groups of the potential biomolecules involved in the capping and stabilization of the AgNPs synthesized with PGE. The FTIR spectra of PGE and the optimized AgNPs were recorded in the wavenumber range of 4000-450 cm^{-1} and are shown in Figure 39A and 39B, respectively. The broad band observed in the FTIR spectrum of PGE (Figure 39A) at 3210 cm^{-1} is attributed to the characteristic O-H stretching vibration of phenolic groups [640]. Considering the high concentration of punicalagin in the utilized PGE, it is probable that the hydroxyl groups of this biomolecule predominantly account for the emergence of this spectral band. Other significant peaks were observed at 1728 cm^{-1} (C=O stretching) [641], 1615 cm^{-1} (C=C bending) [642], 1444 cm^{-1} (CH_2 bending) [643], 1347 cm^{-1}, 1174 cm^{-1} and 1042 cm^{-1} (C-O stretching) [644].

In the FTIR spectra of the optimized AgNPs, a prominent peak at 1385 cm^{-1} is consistently observed across all samples. This band is associated with commercial $AgNO_3$, indicating potential traces of unreacted starting material, as well as the C-O stretching from PGE. Additionally, the spectra of the optimized green synthesized AgNPs display peaks similar to those of PGE but with slight shifts or variations in intensity, indicating interactions between the AgNPs and functional groups of the capping agents [645]. Notably, the peak at 3210 cm^{-1} shifts to 3427 cm^{-1}, reflecting the bioreduction and stabilization of the AgNPs [646,647]. The reduced intensity of the peak at 3210 cm^{-1} further highlights the crucial role of O-H and N-H groups in the reduction and binding mechanisms [645].

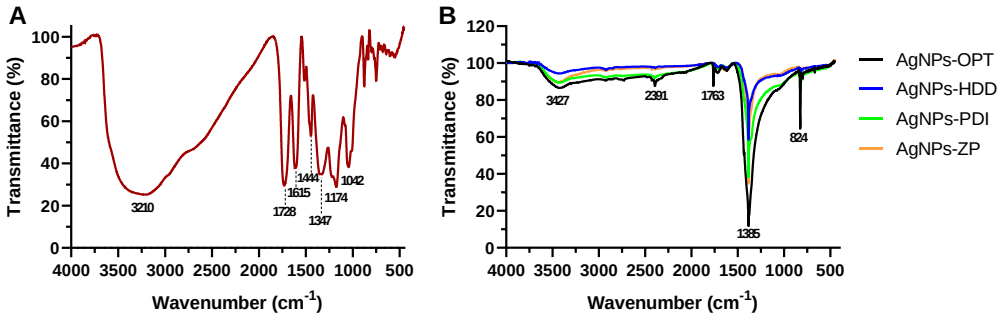

Figure 39. FTIR spectra of (A) *Punica granatum* extract (PGE), (B) four types of optimized green synthesized AgNPs.

3.3.4. XRD

XRD revealed the crystalline nature of the different optimized AgNPs, as depicted in Figure 40. Diffracted intensities were recorded from 10° to 100°. Four intense Bragg reflections were identified around 38°, 44°, 64.5°, and 77.4°. These are associated with the (1 1 1), (2 0 0), (2 2 0), and (3 1 1) crystal planes, respectively, and their indexing can be performed according to the faces present in the face-centered cubic crystal structure of silver [648]. The presence of additional smaller peaks is attributed to the presence of $AgNO_3$, the salt used in the synthesis of the NPs, which possibly remained as a residue in the optimized green synthesized AgNPs [649].

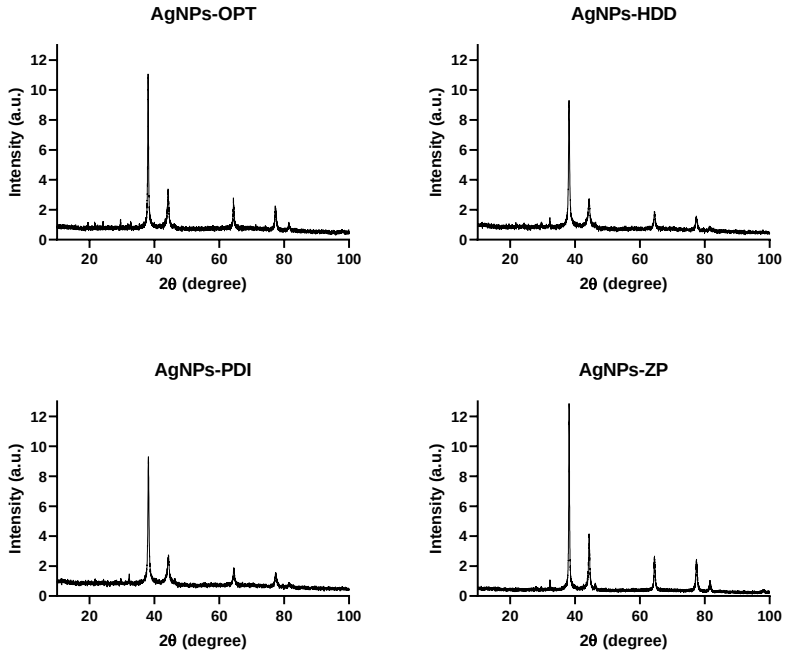

Figure 40. XRD pattern of the four types of optimized green synthesized AgNPs.

3.4. Antibacterial activity

AgNPs exhibit broad antimicrobial activity, and their potent activity is associated with their morphological and physicochemical characteristics such as size, shape, surface-to-volume ratio, surface charge or crystallinity, among others [650]. In this study, two bacteria models of biomedical interest were selected to evaluate antibacterial activity of AgNPs: *E. coli* (Gram-negative bacteria) and *S. aureus* (Gram-positive bacteria).

Firstly, the MIC of the four types of optimized green synthesized AgNPs was evaluated. The results obtained can be seen in Table 16. The MICs were similar among the different types of AgNPs and ranged from 2.5 to 10 µg/mL. These results stand out with respect to those described in the literature, where some authors have reported the MIC of AgNPs against *E. coli* in the range of 7.8-125 µg/mL [648,651,652] and that of *S. aureus* between 2-250 µg/mL [648,651,653,654]. The results obtained place the optimized AgNPs obtained here among those with greater antibacterial activity against *E. coli* and *S. aureus*.

Table 16. Antibacterial activity of four types of optimized green synthesized AgNPs, measured as minimum inhibitory concentration (µg/mL) against *E. coli* and *S. aureus*.

	AgNPs-OPT (µg/mL)	AgNPs-HDD (µg/mL)	AgNPs-PDI (µg/mL)	AgNPs-ZP (µg/mL)
E. coli	5.0	2.5	5.0	2.5
S. aureus	2.5	2.5	5.0	10

Subsequently, the effect of AgNPs-OPT on bacterial cell morphology was evaluated using FESEM microscopy. The results are presented in Figure 41, where Figures 41A and 41B show untreated and treated *E. coli*, respectively, and Figures 41D and 41E show untreated and treated *S. aureus*, respectively. The untreated bacteria were observed to have an intact cell membrane compared to bacterial cells treated with AgNPs. The bacteria treated with AgNPs exhibited irregularities in their morphology, depending on the type of bacteria tested. Gram-negative bacteria *E. coli* exhibited hollows and a more wrinkled surface compared to the control bacteria. Similar observations were reported by different authors, who found that cell membrane disruption occurred in *E. coli* following exposure to AgNPs [655-657], causing an increase in permeability and ultimately leading to bacterial cell death. In the present study, AgNPs appear to affect the cell membrane in *E. coli*, finally causing their death. However, no AgNPs were detected inside the Gram-negative bacterial cells after 24h of exposure (Figure 41C). On the other hand, the Gram-positive bacteria *S. aureus* also exhibited morphological alterations, though membrane damage was not as significant as in *E. coli*. Vesicles appeared on the surface, which may suggest a small leakage of cytoplasmic components. Additionally, invaginations were observed on the surface of *S. aureus*, likely due to the penetration of AgNPs into the bacterial cell (Figure 41F), as confirmed by EDX analysis in Supplementary Figure S-9. These findings are consistent with other studies that observed the presence of AgNPs within the cytoplasm of *S. aureus* [575] or other Gram-positive bacteria [658]. Once inside the cells, silver is known to deactivate respiratory enzymes, generate ROS, and disrupt the production of adenosine triphosphate (ATP) [659]. However, more research is needed to fully understand the intracellular mechanisms of AgNPs.

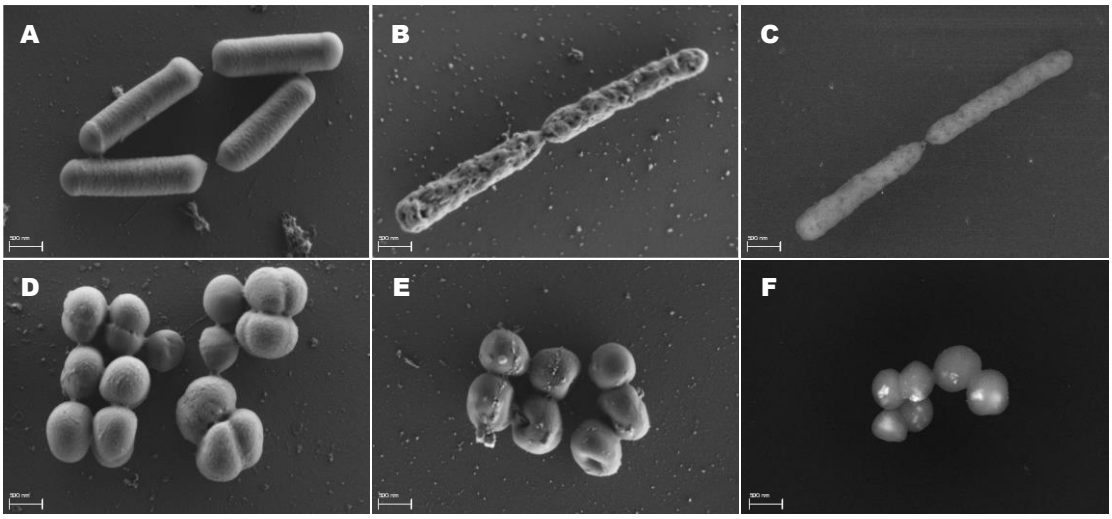

Figure 41. FESEM images showing (a) non-treated *E. coli* cells (SE2 detector, EHT=1 kV), (b) *E. coli* cells treated with AgNPs-OPT at MIC (SE2 detector, EHT=1 kV), (c) *E. coli* cells treated with AgNPs-OPT at MIC (AsB detector, EHT=20 kV), (d) non-treated *S. aureus* cells (SE2 detector, EHT=1 kV), (e) *S. aureus* cells treated with AgNPs-OPT at MIC (SE2 detector, EHT=1 kV), (f) *S. aureus* cells treated with AgNPs-OPT at MIC (AsB detector, EHT=20 kV).

3.5. AgNP incorporation into nanofibers

The incorporation of AgNPs into nanofibrous scaffolds presents a promising approach for their application in biomedical applications, particularly in combating bacterial infections [660]. In the present study, AgNPs-OPT were incorporated at 0.2 % into solutions containing 15 % BSA and 3 % PEO for the synthesis of NFs by electrospinning. BSA was used in polymer solution because certain studies suggest that this protein can provide spatial stability for AgNPs, and thus can be utilized as an effective protective agent to minimize their agglomeration [661].

The NFs obtained are depicted in Figure 42. The resulting NFs exhibited an average diameter of 576 ± 48 nm and demonstrated uniformity in both morphology and size, as illustrated in the diameter frequency histogram in Figure 42B. The appearance and morphology of the NF surface can be observed in Supplementary Figure S-10. The presence of AgNPs within the NFs is shown in Figure 42A, which were randomly distributed within the NFs. The silver composition of the AgNPs within the NFs was confirmed with EDX analysis (Supplementary Figure S-11). Additionally, some aggregation of AgNPs was observed in certain areas, which is common in one-step electrospinning processes of AgNPs with polymeric solutions [662].

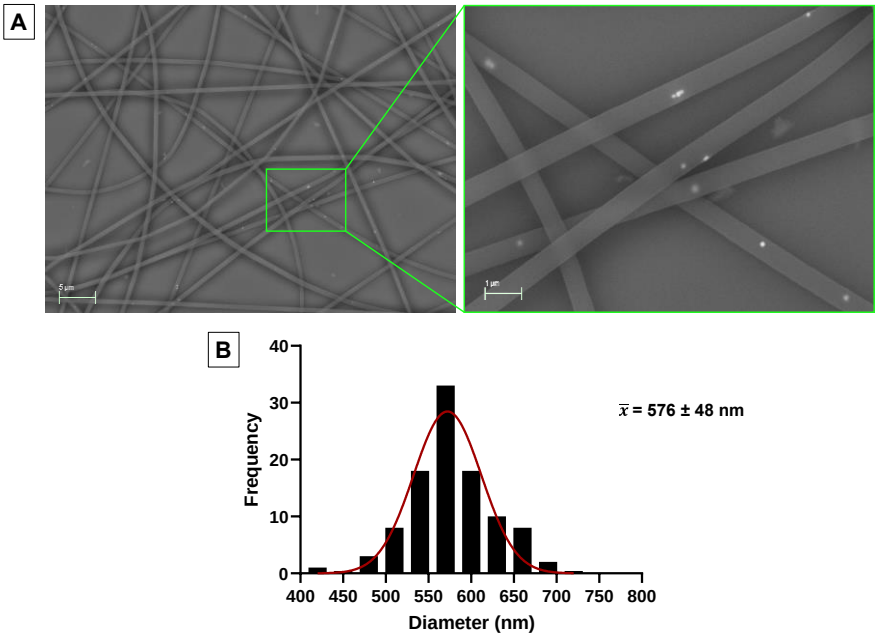

Figure 42. FESEM images (AsB detector, EHT=20 kV) of NFs synthesized from 3 % PEO/15 % BSA/0.2 % AgNPs-OPT. AgNPs appear as white bright dots. Scale bar: 5 µm. Close up scale bar: 1 µm. (B) Diameter frequency histograms of electrospun NFs. Best-fit adjustments to a Gaussian distribution are indicated in red.

Finally, the MIC of the NFs incorporating AgNPs-OPT was determined to be 10 µg/mL for both strains, based on the proportion of AgNPs within the NFs. Compared to the MIC of free AgNPs-OPT (Table 16), this represents an increase, suggesting that the antimicrobial activity was partially retained. This increase may be attributed to the low concentration of AgNPs within the NFs, leading to a non-homogeneous distribution, as observed in the FESEM images. Future work will focus on optimizing the concentration of AgNPs to achieve the most effective antimicrobial platform.

4. Conclusion

In this study, AgNPs were synthesized using a green synthesis approach and optimized using a BBD created specifically for the work. This optimization strategy resulted in the development of four distinct types of AgNPs, each tailored to optimize either HDD, PDI, ZP, or all three parameters simultaneously. The characterization of the AgNPs confirmed the correct synthesis and a good fit of the BBD. The AgNPs displayed effective and differential antibacterial activity against *E. coli*, primarily targeting the bacterial membrane, and *S. aureus*, where the AgNPs were observed to penetrate the bacterial cells. As a proof of concept for potential antibacterial applications, the optimized AgNPs were incorporated into NFs, partially retaining their antimicrobial activity after incorporation. These results underscore the potential of BBD to engineer AgNPs with specific, desired characteristics, facilitating the development of novel antibacterial materials. Future research will focus on investigating how AgNPs characteristics affect their mechanism of action, refining the concentration of AgNPs into synthesized NFs, and further adjusting other critical parameters to enhance their effectiveness in antimicrobial applications.

Supplementary material

An innovative approach based on the green synthesis of silver nanoparticles using pomegranate extract for antibacterial purposes.

Rocío Díaz-Puertas, Francisco Javier Álvarez-Martínez, Enrique Rodríguez-Cañas, Fernando Borrás, Artur JM Valente, José A Paixao, Alberto Falcó, Ricardo Mallavia

Table S-6. Experimental design layout of the Box-Behnken Design (BBD) for the green synthesis of AgNPs using pomegranate extract (PGE). The dependent variables are represented as mean ± S.D. of three measures. X_1: temperature (°C); X_2: PGE concentration (mg/mL); X_3: $AgNO_3$ concentration (mM); Y_1: hydrodynamic diameter (HDD, nm); Y_2: polydispersity index (PDI), Y_3: zeta potential (ZP, mV).

Trial	Independent variables			Dependent variables		
	X_1	X_2	X_3	Y_1	Y_2	Y_3
1	20	0.16	10	137.50±0.38	0.172±0.016	-38.10±0.67
2	80	0.16	10	125.10±1.94	0.116±0.016	-42.20±1.04
3	20	0.48	10	143.90±1.42	0.128±0.015	-37.50±0.70
4	80	0.48	10	162.80±1.67	0.148±0.012	-28.50±0.53
5	20	0.32	5	135.60±0.57	0.182±0.021	-41.30±0.69
6	80	0.32	5	167.10±0.23	0.121±0.018	-41.50±1.23
7	20	0.32	15	157.60±2.08	0.127±0.014	-40.50±1.60
8	80	0.32	15	161.50±1.16	0.085±0.019	-42.30±0.29
9	50	0.16	5	95.95±0.54	0.230±0.018	-44.40±0.15
10	50	0.48	5	138.40±0.56	0.169±0.019	-40.30±0.38
11	50	0.16	15	126.10±1.34	0.186±0.003	-44.30±0.44
12	50	0.48	15	130.30±1.31	0.199±0.026	-43.20±0.10
13	50	0.32	10	126.80±0.67	0.160±0.008	-44.60±0.44
14	50	0.32	10	143.00±2.30	0.159±0.013	-45.20±0.51
15	50	0.32	10	127.70±2.98	0.144±0.005	-38.90±0.78

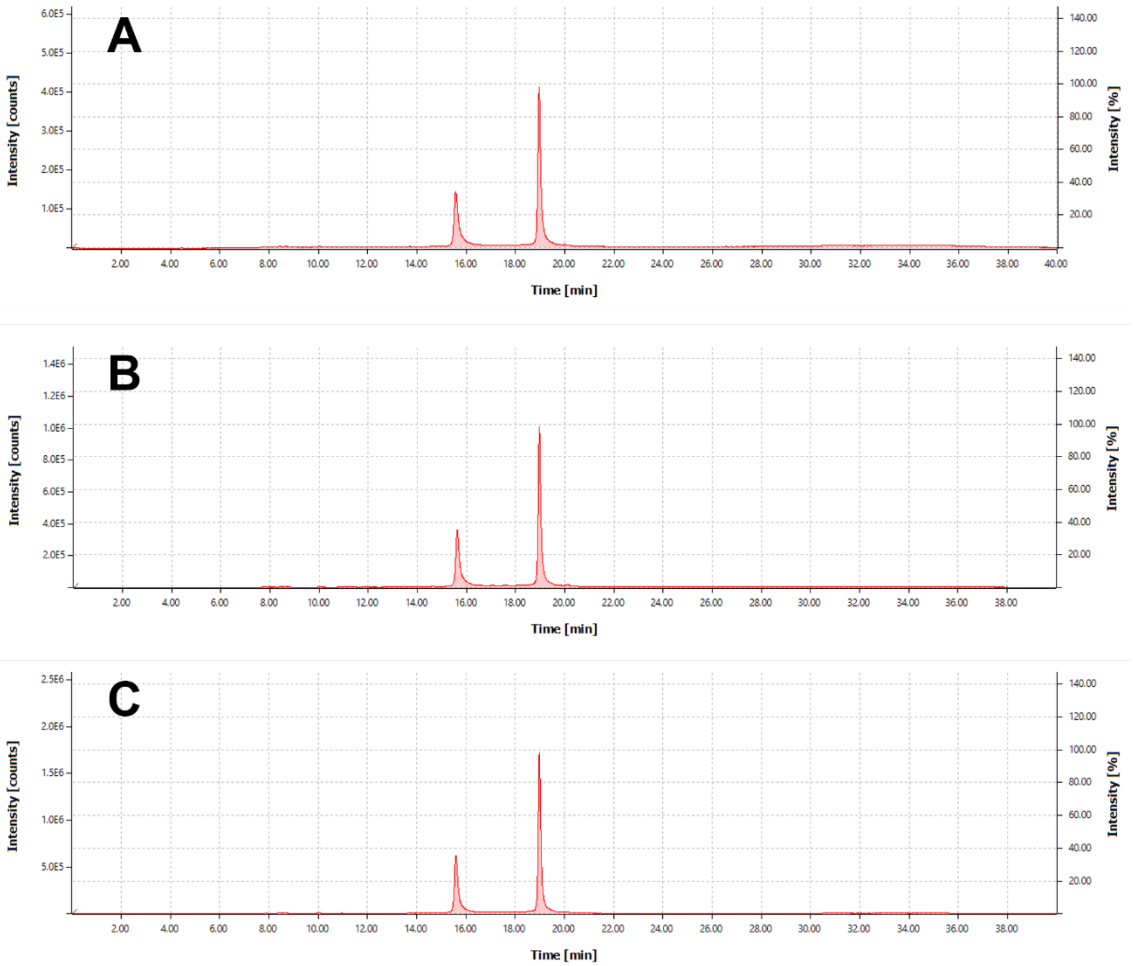

Figure S-5. (A) Chromatogram of the molecular standard of punicalagin at 0.1 mg/mL. Peak 1 area: 17413792.13, Peak 2 area: 34762477.23. (B) Chromatogram of the molecular standard of punicalagin at 0.3 mg/mL. Peak 1 area: 40499982.35, Peak 2 area: 81501109.39. Chromatogram of the molecular standard of punicalagin at 0.5 mg/mL (C). Peak 1 area: 71052585.02, Peak 2 area: 137654991.7.

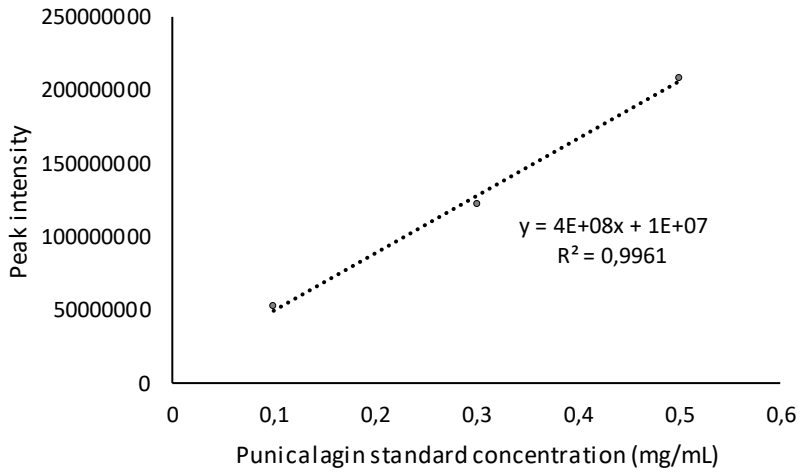

Figure S-6. Graphical representation of the standard line of punicalagin used for the quantification of PGE.

Table S-7. Polynomial models for the responses (Y_1: HDD; Y_2: PDI; Y_3: ZP) investigated in the Box Behnken Design. The first term of the equations corresponds to the intercept, while the rest of the terms are made up of a coefficient that multiplies one or two of the variables (X_1, temperature; X_2, PGE; X_3, $AgNO_3$).

Response	Polynomial model
HDD	$Y_1 = 76.204 + 5.761 \cdot X_1 + 395.638 \cdot X_2 - 2.253 \cdot X_3 - 11.953 \cdot X_1X_2 - 0.046 \cdot X_1X_3 + 1.630 \cdot X_2X_3 + 0.066 \cdot X_1^2 - 447.998 \cdot X_2^2 + 0.024 \cdot X_3^2$
PDI	$Y_2 = 0.433 - 0.0234 \cdot X_1 - 1.150 \cdot X_2 + 0.002 \cdot X_3 + 0.023 \cdot X_1X_2 + 3.416 \cdot 10^{-5} \cdot X_1X_3 + 0.004 \cdot X_2X_3 + 0.001 \cdot X_1^2 + 1.0531 \cdot X_2^2 - 4.477 \cdot 10^{-5} \cdot X_3^2$
ZP	$Y_3 = -30.619 + 2.353 \cdot X_1 - 67.943 \cdot X_2 - 0.623 \cdot X_3 - 0.938 \cdot X_1X_2 - 0.003 \cdot X_1X_3 + 0.682 \cdot X_2\ X_3 - 0.099 \cdot X_1^2 + 91.309 \cdot X_2^2 + 0.004 \cdot X_3^2$

Table S-8. Conditions required to achieve optimal results that simultaneously minimize the three investigated responses (HDD, PDI, and ZP) (AgNPs-OPT), as well as individually (AgNPs-HDD, AgNPs-PDI, AgNPs-ZP). Grey slots inidcate non-measured parameters.

	Temperature (ºC)	PGE concentration (mg/mL)	$AgNO_3$ concentration (mM)	Predicted value		
				HDD (nm)	PDI	ZP (mV)
AgNPs-OPT	61	0.200	15.0	131.3	0.147	-46.0
AgNPs-HDD	47	0.160	5.0	96.7		
AgNPs-PDI	80	0.257	12.7		0.092	
AgNPs-ZP	58	0.182	5.0			-46.3

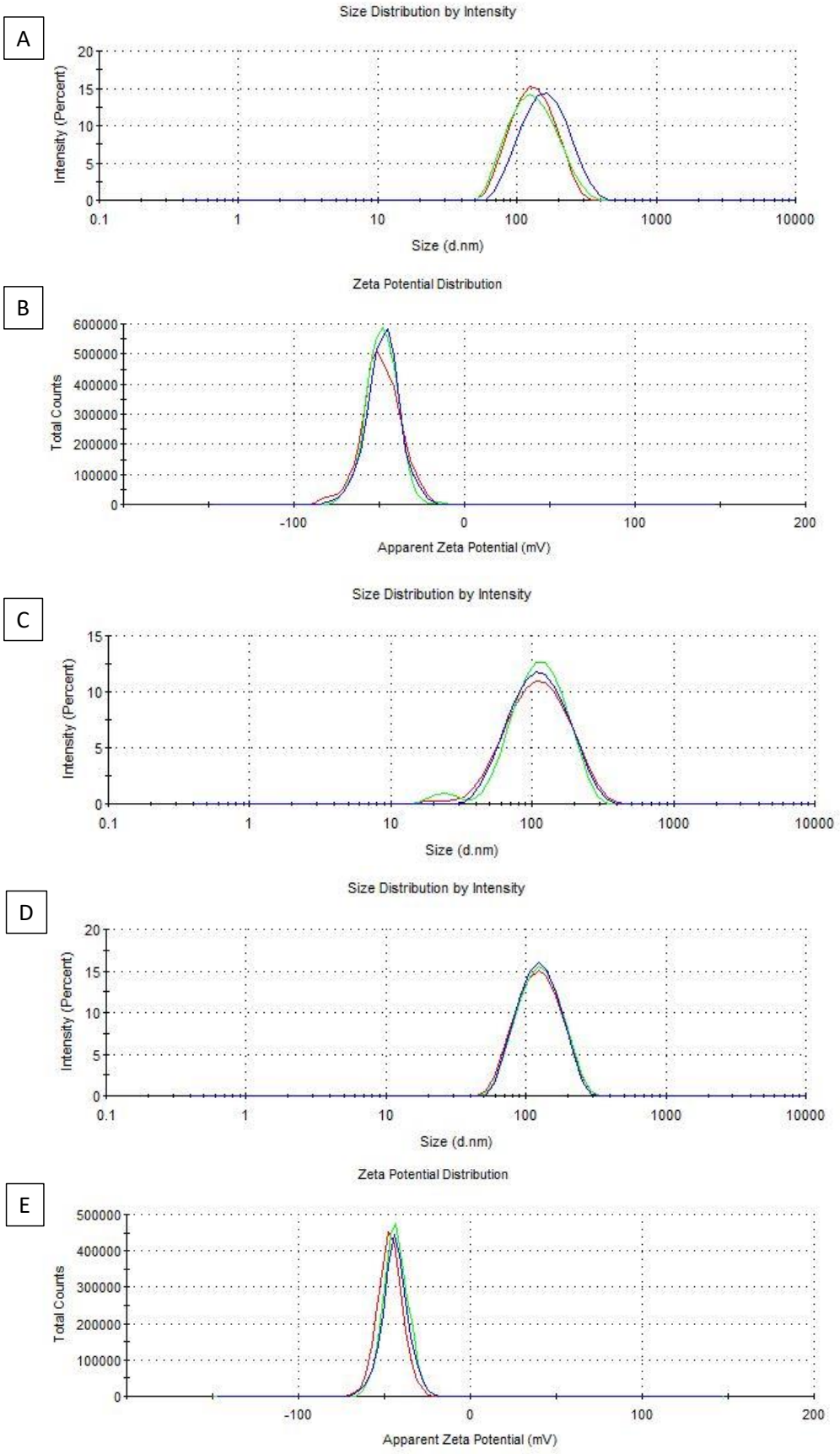

Figure S-7. (A) Size distribution of AgNPs-OPT. (B) Zeta potential analysis of AgNPs-OPT. (C) Size distribution of AgNPs-HDD (D) Size distribution of AgNPs-PDI (E) Zeta potential analysis of AgNPs-ZP.

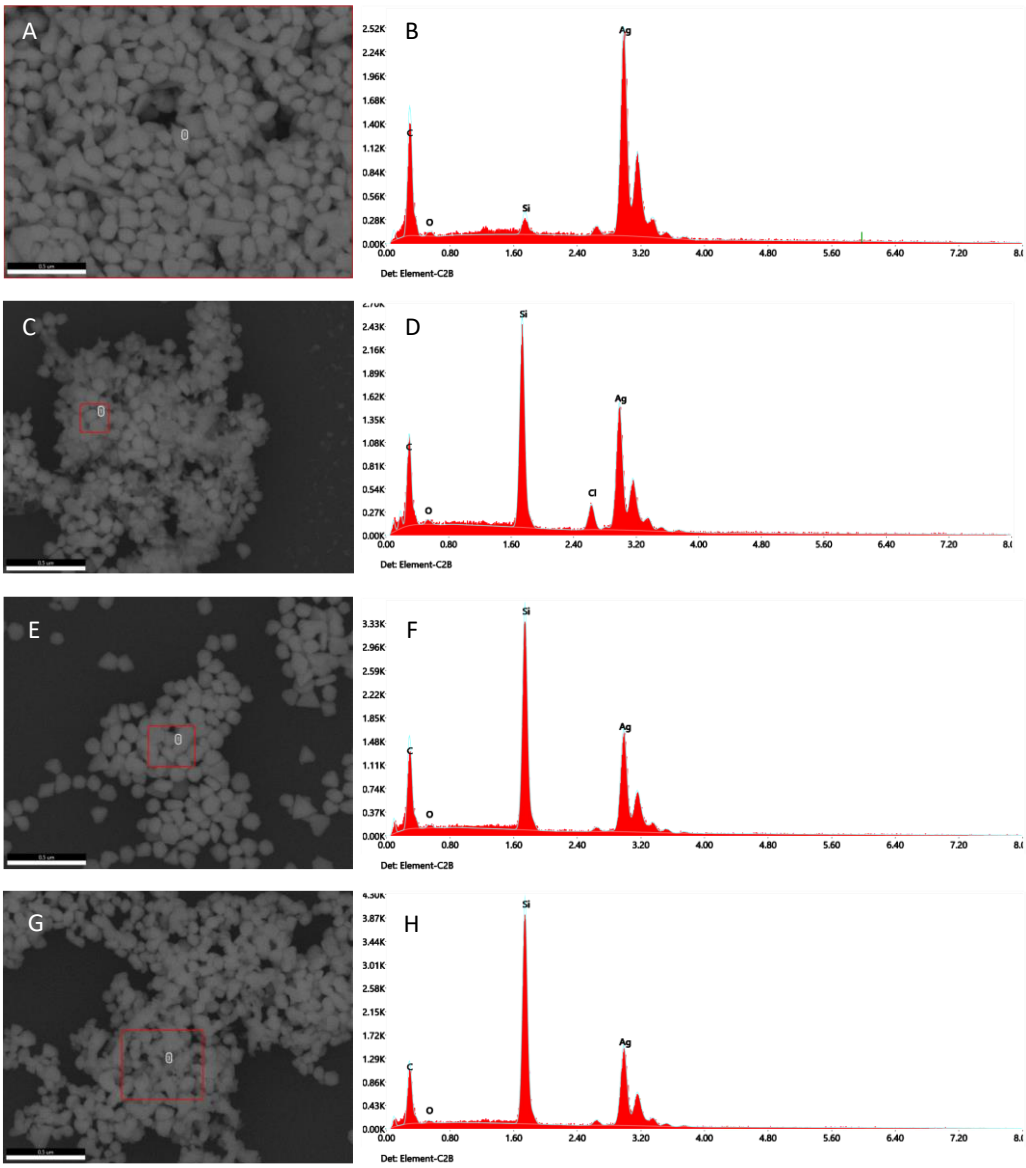

Figure S-8. (A) FESEM image of AgNPs-OPT used for elemental mapping (B) EDX analysis of AgNPs-OPT. (C) FESEM image of AgNPs-HDD used for elemental mapping (D) EDX analysis of AgNPs-HDD (E) FESEM image of AgNPs-PDI used for elemental mapping. (F) EDX analysis of AgNPs-PDI. (G) FESEM image of AgNPs-ZP used for elemental mapping. (H) (F) EDX analysis of AgNPs-ZP. Scale bar: 0.5 µm.

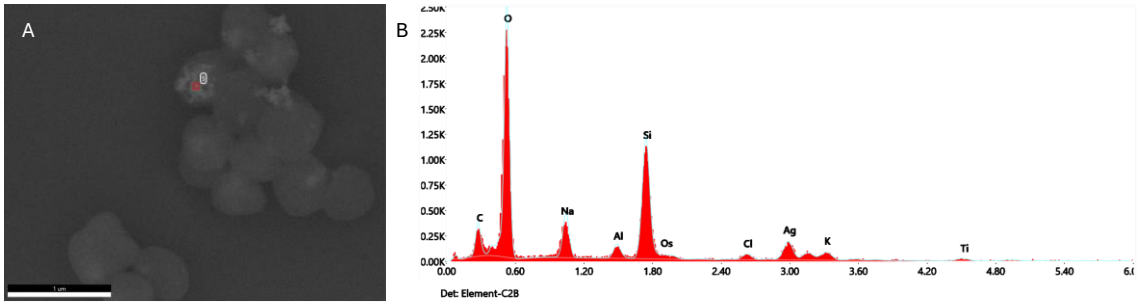

Figure S-9. (A) FESEM image of treated *S. aureus* used for elemental mapping. Scale bar: 1 µm. (B) EDX analysis of AgNPs found inside of *S. aureus*.

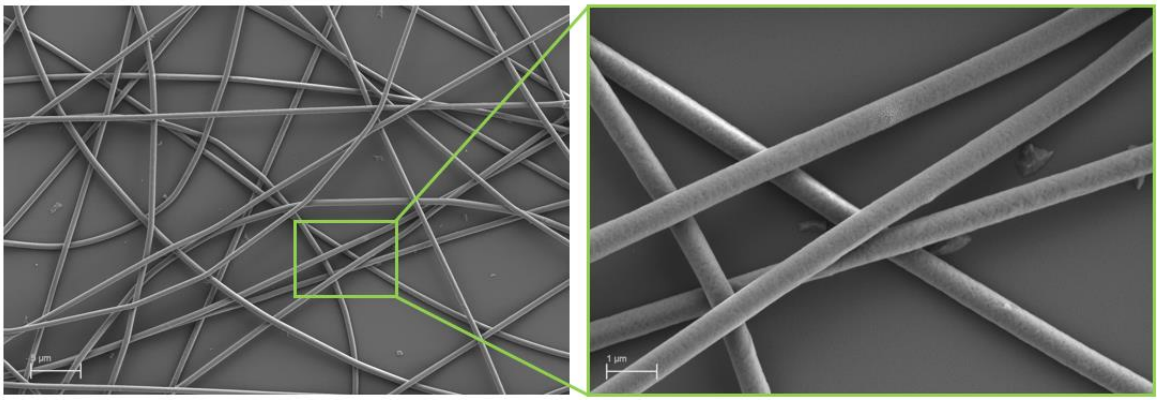

Figure S-10. FESEM image (SE2 detector, EHT=1 kV) of the surface of nanofibers synthesized from 3% PEO/15% BSA/0.2% AgNPs-OPT. Scale bar: 1 µm.

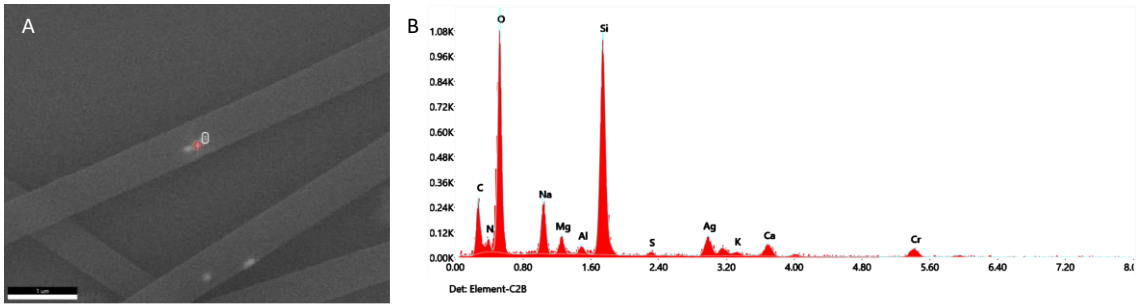

Figure S-11. (A) FESEM image of nanofibers synthesized from 3% PEO/15% BSA/0.2% AgNPs-OPT used for elemental mapping. (B) EDX analysis of AgNPs found inside of the nanofibers. Scale bar: 1 µm.

DISCUSSION

6. DISCUSSION

The primary objective of this Thesis is to design, develop, and characterize innovative polymeric nanomaterials that incorporate antimicrobial agents to combat bacterial and viral pathogens effectively. This goal responds to the critical need for versatile, effective materials that address the growing challenges posed by infectious diseases, particularly in light of ARB and emerging viral pathogens. Each chapter of the Thesis contributes to this overarching aim, presenting a systematic exploration of both natural and synthetic approaches to antimicrobial nanomaterials, each with distinct applications, methods, and outcomes that advance the field.

Fish Skin Mucus Extracts: An Underexplored Source of Antimicrobial Agents

The fight against infectious diseases is hindered by a significant decline in new antimicrobial agents being introduced to the market over the past several decades. With the persistent rise of drug-resistant pathogens, this shortage highlights an urgent need for alternative sources of antimicrobials. Marine environments, with their immense biodiversity and unique ecological pressures, offer an untapped reservoir of potentially powerful antimicrobial agents [663]. Recent studies have emphasized the ability of marine-derived compounds to combat various pathogens; however, despite these promising findings, substantial gaps remain in fully understanding and exploiting these resources. Specifically, fish skin mucus emerges as a highly promising source due to its role in fish innate immunity, where it plays a crucial part in defending against infection. Fish skin, as their largest organ, is constantly exposed to pathogen-rich environments, and its mucus provides a first line of defense containing various antimicrobial factors [197]. Notably, fish mucus can be obtained non-invasively, making it an ethical and sustainable choice for antimicrobial applications. This initial chapter of the Thesis focuses on this unique resource, revealing fish skin mucus as a valuable antimicrobial source and identifying the need for further systematic exploration of its properties and applications.

The main findings in this review paper reveal that fish skin mucus across different species generally exhibits broad-spectrum antibacterial activity. However, its effectiveness against various bacterial species is highly dependent on several factors, including the species of fish, composition of the mucus, extraction methods, and external variables such as seasonal, housing, and dietary conditions of the fish. These findings emphasize the complexity of utilizing fish skin mucus as a consistent antimicrobial source. The challenges in isolating and characterizing bioactive compounds from such complex, variable sources are significant and underscore the need for standardized protocols in future studies.

Among the bioactive compounds identified in fish skin mucus, AMPs stand out for their potent microbicidal properties. AMPs are a vital component of the innate immune system of fish, offering a direct antimicrobial effect on pathogens. Their mechanism of action typically involves binding to the anionic surface membrane of the target microorganism, leading to destabilization through pore formation or membrane disruption [664]. Research has shown that AMPs in fish mucus are effective against a wide range of bacteria, underscoring their potential as a source of natural antimicrobial agents. However, few studies have explored the incorporation of these AMPs into polymeric matrices to improve their stability, controlled release, and applicability in antimicrobial-related products. For example, pleurocidin has been incorporated into electrospun PVA NFs for applications in food systems [665]. This study found that antimicrobial activity of pleurocidin against *E. coli* and *S. aureus* remained effective after incorporation into the NFs. In a separate study by Ramos et al., (2024) pleurocidin was also integrated into PVA NFs, this time for wound infection treatment applications [666]. Its antimicrobial activity against pathogens, including *Acinetobacter baumannii, E. coli, Klebsiella pneumoniae, P. aeruginosa,* and *S. aureus*—both sensitive and resistant strains—was preserved post-incorporation into the NFs.

These approaches suggest that AMPs like pleurocidin could be utilized in diverse settings where bacterial contamination is a concern.

A particular group of AMPs, piscidins, has gained attention for their promising characteristics, including a unique α-helical structure, low molecular weight, and cationic charge at physiological pH. These properties enable piscidins to exhibit broad-spectrum activity against both Gram-negative and Gram-positive bacteria [667]. However, despite their activity, piscidins remain underexplored for practical applications. Their incorporation into polymeric protective matrices, such as nanofibrous mats, could be transformative, as it would allow for enhanced stability, protecting the activity of piscidins from environmental factors that might otherwise degrade their efficacy.

Protein nanofibers as versatile platforms for preserving loaded bioactive compounds

The development of an effective platform for encapsulating bioactive compounds is essential in the fight against infectious diseases. Chapter 2 of this Thesis addresses this need by investigating the use of proteins as natural polymers in synthesizing NFs to deliver antimicrobial agents. Proteins offer distinct advantages in NF applications, including biocompatibility, biodegradability, and inherent structural and functional properties [668]. These qualities make proteins promising candidates for encapsulating and preserving bioactive compounds in nanofibrous matrices. However, proteins alone often face limitations in forming NFs due to factors such as batch-to-batch variability, degradation under certain physicochemical conditions, and a lack of the necessary viscoelasticity required for electrospinning processes [669]. Consequently, blending proteins with other natural or synthetic polymers becomes necessary to enhance these mechanical and processing properties.

In this chapter, the protein-based nanofibrous platform was developed using PEO as a copolymer. PEO was chosen due to its biocompatibility and water solubility, allowing compatibility with proteins and the electrospinning process [670]. To explore the effects of molecular weight on activity retention, proteins with varying molecular weights were selected. These included HRP-IgG (200 kDa), BSA (~66 kDa), chicken LYZ (14.3 kDa), and PIS (2.6 kDa), an AMP derived from fish skin mucus (as discussed in Chapter 1).

Initial trials focused on optimizing electrospinning parameters with BSA NFs, as BSA provides structural support. Using these parameters, NFs were then fabricated with LYZ to compare characteristics and determine the impact of molecular weight on fiber formation and stability. The results showed that the viscosity of protein solutions increased with protein concentration. Moreover, protein solutions with a viscosity comparable to that of polymer solutions were capable of forming NFs through electrospinning, while PEO-only solutions were not. This indicates that the addition of proteins can significantly enhance the electrospinnability of PEO solutions, probably due to a higher electrical conductivity [671].

Further studies in this chapter included incorporating the antimicrobial agents PIS and HRP-IgG within the NFs, particularly in BSA-LYZ/PIS and BSA/PIS composites. For PIS, encapsulation within LYZ fibers was also evaluated to assess potential changes in activity and stability. The results showed that the structural integrity of both BSA and LYZ NFs was preserved through the electrospinning process, with bioactivity of the incorporated compounds largely retained. However, the full activity of some agents was not fully preserved post-incorporation, probably due to factors like low incorporation concentrations, delayed release from the matrix, or partial degradation during processing.

Interestingly, findings revealed that LYZ NFs containing PIS exhibited greater antimicrobial efficacy against specific bacterial strains than free PIS alone, even against bacteria that LYZ alone could not inhibit. This suggests a synergistic effect, where PIS activity is enhanced when

encapsulated within a LYZ-based nanofibrous matrix, highlighting a unique benefit of this protein-based delivery system.

This chapter contributes to the primary objective of the Thesis by establishing protein-based NFs as a promising encapsulation and delivery platform for antimicrobial agents derived from natural sources. The findings build upon those of Chapter 1 by providing a feasible and functional strategy for the encapsulation of natural antimicrobials, offering promising applications in infection prevention and control.

Viricidal Activity of Thermoplastic Polyurethane Materials with Silver Nanoparticles

The ultimate goal of this Thesis, as with any scientific investigation, is to achieve practical, industrial applicability that serves a meaningful societal purpose. In line with this aim, Chapter 3 of this Thesis focuses on developing TPU materials with embedded AgNPs, a project undertaken in collaboration with a local materials company. TPU is widely used in various industries due to its desirable properties, including high damping capacity, resistance to deformation, and recyclability [672]. These qualities make TPU a versatile material for use in sectors ranging from textile coatings and automotive interiors to sports equipment and consumer electronics. By integrating an antimicrobial agent like AgNPs into TPU, this platform becomes especially valuable in preventing the spread of infectious agents via surfaces—a timely focus in light of the recent pandemic, where surface transmission emerged as a potential route for viral spread. Such a material has broad promising applications in high-contact surface environments, providing a proactive approach to controlling the spread of pathogens in settings such as hospitals, public transportation, and community spaces.

The study developed in Chapter 3 first characterized the physical and chemical properties of AgNP-TPU materials, employing EDX spectroscopy to determine the elemental composition. In addition to carbon and oxygen (components of the TPU), the primary elements detected were phosphorus, magnesium, and aluminum. These elements were attributed to a ceramic material used to encapsulate the AgNPs, enhancing their stability and controlled release.

Release assays provided insight into the safety profile of material by measuring the release rates of magnesium, aluminum, and silver ions. Magnesium exhibited the highest release rate, followed by aluminum and, lastly, silver. This controlled release pattern is crucial for maintaining a balance between effective antimicrobial action and minimizing potential cytotoxicity associated with silver ions. Subsequent cytotoxicity assays were performed using EPC and Vero E6/TMPRSS2 cell lines, chosen for their relevance to viral studies. The results indicated no cytotoxic effects from the AgNP-TPU material exudates, measured at around 100 ppm after 24 hours, which is consistent with previous studies that determined the cytotoxicity of AgNPs at similar concentrations [429,430]. In this case, the controlled release mechanism likely plays a key role in maintaining the biocompatibility of the material.

Following confirmation of low cytotoxicity, antiviral efficacy tests were conducted to evaluate the applicability of AgNP-TPU for real-world antiviral settings. The initial antiviral assessment involved incubating the material with a model virus, SVCV, at 20 °C for 24 hours, resulting in approximately a 75% reduction in viral titer. Further experiments demonstrated that extending the incubation time and adjusting the temperature (with trials at 2, 8, and 24 hours and temperatures of 5, 10, and 20 °C) enhanced viral inactivation. This temperature-dependent increase in efficacy suggests a promising flexibility of AgNP-TPU materials under different environmental conditions. Finally, to validate the effectiveness of the material against a relevant human pathogen, the AgNP-TPU material was tested against SARS-CoV-2 at 30 °C for 24 hours. This experiment yielded an 81 % reduction in viral infectivity compared to the control, underscoring the potential of the material in limiting and controlling viral transmission in high-

contact areas. This chapter advances the Thesis' central objective by translating antimicrobial efficacy into a practical format, bridging the gap between laboratory research and real-world application in the battle against infectious agents.

Phytochemical-Based Nanomaterials against Antibiotic-Resistant Bacteria

Following the completion of Chapter 3, an idea emerged to use AgNPs for antibacterial purposes, this time focusing on synthesizing the NPs ourselves rather than obtaining them commercially. Chapter 4 builds on the synthetic NP work established in Chapter 3 but pivots toward a greener, more environmentally conscious synthesis approach. After exploring various synthesis methods, green synthesis stood out as the most suitable choice, not only for its minimal environmental impact but also for aligning with sustainable scientific practices. Thus, this chapter became an endeavor to both learn and apply green synthesis, creating NPs with potent antibacterial activity through eco-friendly means.

The shift in this chapter emphasizes eco-friendly strategies for creating antibacterial nanomaterials using plants, both as antimicrobial agents and as natural reducing agents for synthesizing MNPs. This approach was particularly relevant in targeting bacterial infections, with a focus on ARB—a growing global health threat. Plants were selected as a source of reducing agents due to their wealth of phytochemicals, including polyphenols, alkaloids, and terpenoids, which not only offer natural antibacterial properties but also facilitate the reduction of metal salts to form NPs. This dual functionality of plants, enabling both NP synthesis and antibacterial action, presents a significant advantage.

An added benefit of using plant-based phytochemicals lies in their "molecular promiscuity", or ability to interact with multiple bacterial targets simultaneously, although generally with lower affinity than traditional antibiotics [673]. While conventional antibiotics often target a specific bacterial molecular structure with high precision, leading to rapid resistance development, phytochemicals' multitarget approach makes it more challenging for bacteria to develop resistance mechanisms. This broad-spectrum action is particularly valuable against ARB, as it may extend the effective lifespan of antimicrobial materials derived from phytochemicals.

The review in Chapter 4 also explores various plant-based compounds, including extracts, pure compounds, and oils, that have been successfully integrated into nanomaterials for antimicrobial purposes. Notably, NFs incorporating phytochemicals have shown promising efficacy against ARB. The morphology of NFs alone enhances antimicrobial action, as the fibrous structure can physically trap bacteria, limiting their movement and multiplication. Furthermore, the surface chemistry of NFs can be tailored to interact effectively with bacteria. For example, positively charged NFs can attract and disrupt negatively charged bacterial membranes, while hydrophobic NFs may inhibit the growth of hydrophilic bacteria, offering a versatile platform for antibacterial applications.

The chapter also addresses polymeric NPs encapsulating phytochemicals. While there are fewer studies in this area compared to NFs, research involving essential oils and plant extracts incorporated into polymeric NPs shows promising antibacterial activity against ARB.

Finally, Chapter 4 discusses the synthesis of MNPs, particularly AgNPs, using phytochemicals. These plant-based reducing agents offer distinct advantages over traditional chemical synthesis methods, including enhanced biocompatibility, safety, and reduced environmental impact [117]. Various plant parts, such as leaves, flowers, and peels extracts, have been used to successfully reduce metal salts into NPs, resulting in antimicrobial materials effective against a range of resistant bacterial species, including MRSA, *K. pneumoniae*, *P. aeruginosa*, *A. baumannii*, and vancomycin-resistant *S. aureus*.

Notably, MRSA was the most frequently tested bacterium in the studies included in this chapter, likely due to its high prevalence and the broad range of infections it can cause. This pathogen is a leading cause of hospital-acquired infections, associated with serious complications such as pneumonia, sepsis, and even mortality [674]. Its prevalence in both healthcare and community settings underscores the need for effective antimicrobial strategies, making MRSA an ideal model organism for evaluating new antibacterial agents.

In general, Chapter 4 advances the Thesis towards eco-friendly synthesis methods, prioritizing environmental responsibility while achieving robust antibacterial effects. This chapter illustrates the potential of phytochemicals as sustainable alternatives to conventional antimicrobial compounds and synthetic chemicals to produce MNPs.

Innovative green synthesis of silver nanoparticles using pomegranate extract

Building on the exploration of green synthesis methods from Chapter 4, Chapter 5 centers on optimizing the synthesis of AgNPs using PGE, using insights from previous chapters to achieve a sustainable and potent antimicrobial solution. PGE was chosen not only for its natural antimicrobial properties but also for its high availability in the Mediterranean region, where large-scale pomegranate production generates considerable quantities of byproducts, particularly pomegranate peel [675]. Rich in bioactive compounds, pomegranate peel offers a cost-effective, eco-friendly source for NP synthesis, aligning with the Thesis' goal of antimicrobial material development while minimizing environmental impact.

The laboratory-prepared PGE was analyzed to determine its phytochemical composition. The primary compound identified was punicalagin, a polyphenol with notable antioxidant activity. Compared to other plant extracts used in similar studies, this extract exhibited a significantly high antioxidant capacity, which has advantages in stabilizing NPs and enhancing their bioactivity. Punicalagin, alongside other phytochemicals in the extract, facilitates the reduction of silver ions, eliminating the need for harsh chemical reducing agents.

To refine the synthesis process, a BBD was employed, allowing for a systematic approach to optimize conditions, including minimizing HDD, PDI, and ZP responses. Characterization techniques confirmed the formation of AgNPs, revealing their anisotropic shapes and crystalline structure. These findings emphasize the importance of controlled synthesis parameters to achieve NPs with optimal physical properties for antimicrobial applications.

The antimicrobial efficacy of the PGE-synthesized AgNPs was tested against common pathogens *E. coli* and *S. aureus*. Remarkably, the AgNPs exhibited strong antibacterial activity, with effective concentrations as low as 2.5 to 10 µg/mL, placing them among the most potent antibacterial agents documented in current literature. Observations of bacterial cell morphology post-treatment provided further insight into the mechanism of action. In *E. coli*, hollowed and wrinkled surfaces were observed, while *S. aureus* exhibited vesicles and membrane invaginations, suggesting that AgNPs disrupt bacterial membranes and can even penetrate the cells. This interaction damages bacterial cell integrity, likely contributing to the observed efficacy, particularly relevant in future studies against ARB.

Further advancing the goals established in Chapter 2, the AgNPs were incorporated into BSA-PEO NFs to develop a platform for antimicrobial release. By embedding AgNPs into these protein-based NFs, the study achieved a practical application of green-synthesized NPs in sustained antibacterial release systems. The combination of AgNPs and BSA-PEO NFs not only enhances the biocompatibility of the material but also allows for extended antimicrobial effects, potentially applicable in medical settings, packaging, or high-contact surfaces to prevent bacterial contamination.

Thesis contributions to the research field

This Thesis makes meaningful contributions to the field of antimicrobial nanomaterials by integrating innovative antimicrobial sources, advancing eco-friendly synthesis techniques, and developing practical, versatile delivery platforms.

The initial chapter focus on exploring underutilized natural sources for antimicrobial agents, with the aim of diversifying current materials used against infectious agents. Specifically, the research examines fish skin mucus, shedding light on marine byproducts as promising reservoirs of bioactive compounds. Fish skin mucus, in particular, offers a unique source of AMPs and various bioactive substances with considerable potential against resistant pathogens. This Thesis not only assesses the inherent antimicrobial properties of these compounds but also investigates their broader applicability by incorporating them into delivery systems suitable for diverse fields. Such integration broadens their future uses across applications in healthcare, biomedicine or food packaging, advancing the development of multifunctional antimicrobial materials that align with sustainable practices and innovative solutions.

A central contribution of this Thesis lies in emphasizing the role of natural compounds in constructing nanostructures, as demonstrated by using proteins as base materials for NF synthesis and plant extracts for NP formation. The adoption of green synthesis methods using plant-based compounds, in contrast to conventional approaches, allows NPs to form without relying on toxic chemicals or energy-intensive processes, promoting a more sustainable route. The selection of pomegranate peel, a common Mediterranean agricultural byproduct, for synthesizing AgNPs illustrates a resourceful strategy that repurposes agricultural waste into valuable antimicrobial materials. Additionally, through thorough characterization of its composition, this research clarifies the relationship between specific extract components and the resulting physicochemical properties of NPs. This often-overlooked correlation in green synthesis literature provides deeper insights into how certain phytochemicals shape NP morphology, stability, and antimicrobial potency. Such understanding allows for more targeted NP synthesis, optimizing both the environmental footprint and functional properties of antimicrobial materials derived from renewable natural sources.

The use of advanced statistical tools, particularly the BBD response surface model, further strengthens the rigor and efficiency of the AgNP synthesis process. This design allows precise optimization of synthesis conditions, enabling the production of NPs with desirable, controlled characteristics. By reducing the need for extensive trial-and-error experimentation, the model conserves experimental resources, minimizes waste, and cuts down on time and energy, aligning with sustainable research practices while producing reproducible NPs with consistent properties.

This Thesis advances the field of antimicrobial nanomaterials by promoting sustainable synthesis techniques, utilizing novel biological sources, and developing multifunctional delivery platforms with practical, scalable potential in industries such as healthcare, surface coating and food packaging. The work demonstrates that integrating environmental responsibility with scientific innovation can provide effective solutions to the critical challenge of microbial resistance while minimizing ecological impact.

Thesis potential socioeconomic impact

The global threat of antibiotic-resistant infections has intensified, underscoring the urgent need for innovative antimicrobial therapies. According to the WHO, antibiotic resistance ranks among the top ten global health threats, with drug-resistant infections projected to cause over 10 million deaths annually by 2050 if left unchecked. The economic toll is equally dire: within the EU alone, AMR costs approximately EUR 1.5 billion each year in healthcare expenses and lost productivity, and by mid-century, AMR is anticipated to drain up to $100 trillion from the global economy,

with a financial impact comparable to the 2008 economic crisis [676]. This Thesis, by developing eco-friendly, potent antimicrobial nanomaterials, is well-aligned with the global priority of curbing AMR and holds significant potential for alleviating these socioeconomic burdens.

Viral outbreaks, whether regional or global, have also historically caused widespread disruptions to societies, economies, and healthcare systems, amplifying existing vulnerabilities and inequalities The COVID-19 pandemic, as the most far-reaching viral outbreak in recent history, exemplified these effects on an unprecedented scale. Beyond its staggering death toll, it disrupted global supply chains, triggered soaring unemployment rates, and forced school closures, undoing decades of advancements in poverty reduction [677]. These challenges have disproportionately impacted marginalized populations, deepening inequalities both within and between nations. This intersection of public health crises and socioeconomic instability underscores the critical need for innovative solutions to mitigate the impacts of such outbreaks, such as those developed in this Thesis.

In parallel, this Thesis contributes directly to the burgeoning field of antimicrobial nanomaterials, which was valued at approximately USD 930.5 million in 2022 and is projected to reach USD 5.9 billion by 2032 [678]. The demand for antimicrobial nanocoatings is expected to grow, driven by the increase in resistant bacterial infections and expanding applications across various industries, particularly healthcare, where they are used in high-contact settings such as drop-in centers, surgical rooms, and home care. The automotive, food, and packaging sectors are also increasingly adopting these materials. Rising investment in research and development and the growing focus of companies on sustainable practices further bolster the potential of this market. Projects like the Horizon Europe Programme-funded initiatives Next Generation BiOactiVe NAnocoatings (NOVA) and Surface Transfer of Pathogens (STOP) illustrate the high-priority placed on combatting infectious agents with nanomaterials.

On a social impact level, this research supports seven United Nations Sustainable Development Goals (SDGs) (Figure 43). The Thesis aligns with **SDG 3** by addressing the challenge of antibiotic resistance and enhancing public health through alternative antimicrobial solutions. It contributes to **SDG 6** by leveraging the potential of nanofibrous mats to serve as pathogen-preventive filters, thereby improving water quality and sanitation. Additionally, **SDG 8** is supported through the possible industrial applications of green synthesis technologies, which promote sustainable economic growth. **SDG 9** is advanced by the practical industrial applications of all synthesized materials, which have potential use across various sectors. The eco-friendly production of NPs also resonates with **SDG 12**, minimizing environmental impact through green synthesis practices. By sustainably utilizing marine resources, particularly non-invasive harvesting of antimicrobial compounds from fish skin mucus, this research aligns with **SDG 14**. Finally, **SDG 17** is addressed through collaborations with local businesses, showcasing the importance of academic-industry partnerships in driving sustainable innovation.

Figure 43. United Nations Sustainable Development Goals addressed by this Thesis.

This Thesis also aligns with the strategic goals of the Smart Specialisation Strategy of the Valencian Community (S3-CV, 2021-2027), particularly in advancing the fields of sustainable innovation and health-related technology. The research supports the focus of the region on creating knowledge-intensive, eco-friendly technologies by developing polymeric nanocomposites with antimicrobial properties through green synthesis and natural resources. The

partnership with industrial sectors, particularly in antiviral materials, underscores the alignment of the Thesis with the S3-CV aim of enhancing public-private collaboration in applied R&D, vital for fostering competitiveness and resilience in strategic sectors.

Translationality

While laboratory-scale research is undeniably crucial in establishing foundational knowledge, one of the primary goals of translational research is to bridge the gap between these findings and real-world applications, creating future benefits for society. In this Thesis, the development of nanomaterials from natural sources, alongside green synthesis methods, lays the groundwork for scaling these materials for industrial use.

Transitioning from laboratory to industrial production necessitates the optimization of synthesis protocols to ensure high yields, reproducibility, and cost-effectiveness. In the field of NFs, several industries are already offering products for a range of applications. For instance, Nonwovens Ibérica S.L. provides Spanish-made NF solutions primarily aimed at filtration applications. Similarly, BIOINICIA, based in Valencia, develops micro- and nanostructured products for various uses. Their portfolio includes a cosmetic line and pharmaceutical products currently on the market, such as transdermal and mucoadhesive patches. Scaling up NF production often involves the use of electrospinning machinery capable of supporting larger volumes. An example is the Nanospider™ technology, patented by Elmarco, which produces high-quality NFs at an industrial scale for a broad spectrum of applications.

For green synthesis processes, however, there is limited information available on scalability. Large-scale NP production demands a deep understanding of production costs, resource availability, downstream processing requirements, and scalability forecasts [679]. One particular challenge lies in the purification and separation of AgNPs produced, as commercialization requires high-quality NPs. Substantial work remains to model these processes and enable scalable biosynthesis until large-scale production can be achieved. Nevertheless, studies like the one developed in this Thesis help pave the way by shedding light on the optimal conditions necessary to achieve desired NPs.

Successful commercialization of antimicrobial nanomaterials hinges on regulatory approval, especially since these materials are intended for environments involving direct human contact. In the European Union, the European Union Observatory for Nanomaterials (EUON) provides insights into existing nanomaterials on the EU market. According to EUON, nanomaterials are subject to the same stringent regulatory frameworks that govern all chemicals and mixtures, specifically under the REACH (Registration, Evaluation, Authorisation, and Restriction of Chemicals) and CLP (Classification, Labelling, and Packaging of Substances and Mixtures) regulations [680]. This means that the hazardous properties of nanoforms must be thoroughly assessed, and their safe use must be assured. For a substance to be legally manufactured or imported within the EU, it must be registered under REACH, with registration information detailing effects on human health and the environment, as well as exposure estimates for hazardous nanoforms throughout the life cycle of the material. Beyond REACH and CLP, there are also specific regulatory frameworks for certain product categories, covering biocides, plant protection products, cosmetics, pharmaceuticals, toys, food, and electronics.

Open science and transparency

This Thesis is rooted in the principles of Open Science and transparency, values that are essential for making research accessible, reproducible, and impactful. All the papers published as part of this Thesis are open access, meaning that anyone—scientists, industry experts, or the general public—can read and build on these findings without needing a subscription or paying a fee. Open access is especially crucial in the field of antimicrobial nanomaterials, where sharing insights

quickly and widely can accelerate progress in addressing challenges like antibiotic resistance and developing sustainable health solutions.

Throughout the course of this research, results have been shared at both national and international conferences, allowing for direct engagement with the scientific community. These presentations provided opportunities to receive valuable feedback, connect with other researchers, and encourage discussions that might lead to further collaborations. By presenting findings in these public forums, this Thesis has contributed to ongoing conversations in the field, and this openness reinforces scientific rigor by inviting others to question, evaluate, and expand on the research.

CONCLUSIONS

7. CONCLUSIONS

1. Fish mucus represents an unexplored and promising source of antimicrobial compounds, including antimicrobial peptides, proteins and other metabolites. They can be extracted using various solvents, particularly acidic, organic, and aqueous solvents.

2. Nanofiber synthesis using proteins such as bovine serum albumin and lysozyme offers enhanced biocompatibility, biodegradability, biosafety and intrinsic functions compared to conventional synthetic polymers.

3. Nanofibers synthesized using electrospinning with high concentrations of the proteins bovine serum albumin and lysozyme yielded fibers with diameters ranging from 300 to 750 nm, with the proteins retaining their function after electrospinning.

4. The bioactive compounds piscidin, an antimicrobial peptide with inherent antibacterial properties, and horseradish peroxidase-conjugated goat anti-mouse IgG, an antibody exhibiting peroxidase and antigen-recognition activities, retained their respective functionalities after being incorporated into protein-based nanofibers. These results demonstrate that protein-based nanofibers are strong contenders for applications requiring drug delivery and protection, such as antimicrobial therapies.

5. Thermoplastic polyurethane materials with silver nanoparticles demonstrated significant antiviral activity against Spring Viraemia of Carp Virus and Severe acute respiratory syndrome coronavirus-2, with this efficacy shown to be both time- and temperature-dependent, likely due to the gradual release of Ag ions over time. Importantly, these materials exhibited no cytotoxicity, highlighting their potential as promising candidates for viricidal applications aimed at reducing viral transmission.

6. The incorporation of phytochemicals into nanofibers and nanoparticles is a viable strategy to produce antibacterial nanomaterials using an eco-friendly and sustainable approach, while benefiting from their multitargeted character against bacteria.

7. Phytochemicals are effective in reducing metal salts to metal nanoparticles, providing a more sustainable alternative to conventional physical and chemical methods.

8. Silver nanoparticles were synthesized via green synthesis using punicalagin extract rich in punicalagin. The process was optimized through a Box-Behnken desgign to achieve nanoparticles with the smallest hydrodynamic diameter, polydispersity index, and zeta potential possible within the tested conditions.

9. The synthesized silver nanoparticles exhibited strong antimicrobial activity against *Escherichia coli* and *Staphylococcus aureus* bacteria, with minimum inhibitory concentrations ranging 2.5-10 µg/mL. The mode of action appeared to differ between the species: *E. coli* showed significant membrane disruption, whereas *S. aureus* exhibited vesicle formation and membrane invaginations, indicating a likely intracellular action mechanism for the silver nanoparticles.

10. Silver nanoparticles incorporated into protein nanofibers retained their antimicrobial activity, indicating that this platform holds significant promise for antimicrobial applications.

7. CONCLUSIONES

1. El moco de pez representa una fuente inexplorada y prometedora de compuestos antimicrobianos, incluidos péptidos antimicrobianos, proteínas y otros metabolitos. Estos pueden extraerse utilizando diversos solventes, especialmente solventes ácidos, orgánicos y acuosos.

2. La síntesis de nanofibras utilizando proteínas como la albúmina de suero bovina y lisozima ofrece mayor biocompatibilidad, biodegradabilidad, bioseguridad y funciones intrínsecas en comparación con los polímeros sintéticos convencionales.

3. Las nanofibras sintetizadas mediante electrohilado con altas concentraciones de las proteínas albúmina de suero bovina y lisozima dieron lugar a fibras con diámetros que oscilan entre 300 y 750 nm, conservando las proteínas su funcionalidad tras el proceso de electrohilado.

4. Los compuestos bioactivos piscidina, un péptido antimicrobiano con propiedades antibacterianas inherentes, y IgG de cabra anti-ratón conjugada con peroxidasa de rábano, un anticuerpo con actividad peroxidasa y de reconocimiento de antígenos, conservaron sus respectivas funcionalidades después de ser incorporados en las nanofibras proteicas. Estos resultados demuestran que las nanofibras basadas en proteínas son candidatas sólidas para aplicaciones que requieren liberación y protección de fármacos, como terapias antimicrobianas.

5. Los materiales de poliuretano termoplástico con nanopartículas de plata demostraron una actividad antiviral significativa contra el virus de la viremia primaveral de la carpa y el *severe acute respiratory syndrome* coronavirus de tipo 2, mostrando que esta eficacia depende tanto del tiempo como de la temperatura, probablemente debido a la liberación gradual de iones de plata. Es importante destacar que estos materiales no presentaron citotoxicidad, lo que subraya su potencial como candidatos prometedores para aplicaciones viricidas destinadas a reducir la transmisión viral.

6. La incorporación de fitoquímicos en nanofibras y nanopartículas es una estrategia viable para producir nanomateriales antibacterianos mediante un enfoque ecológico y sostenible, aprovechando además su carácter multiobjetivo contra bacterias.

7. Los fitoquímicos son eficaces para reducir sales metálicas a nanopartículas metálicas, proporcionando una alternativa más sostenible a los métodos físicos y químicos convencionales.

8. Se sintetizaron nanopartículas de plata mediante un proceso de síntesis verde utilizando extracto de granada rico en punicalagina. El proceso fue optimizado mediante un diseño de Box-Behnken para obtener nanopartículas con el menor tamaño hidrodinámico, índice de polidispersidad y potencial zeta posibles dentro de las condiciones evaluadas.

9. Las nanopartículas de plata sintetizadas mostraron una fuerte actividad antimicrobiana contra las bacterias *Escherichia coli* y *Staphylococcus aureus*, con concentraciones inhibitorias mínimas que oscilaron entre 2.5 y 10 µg/mL. El modo de acción pareció diferir entre las especies: *E. coli* mostró una rotura significativa de la membrana, mientras que *S. aureus* exhibió formación de vesículas e invaginaciones de la membrana, lo que sugiere un probable mecanismo de acción intracelular de las nanopartículas de plata.

10. Las nanopartículas de plata incorporadas en nanofibras a base de proteínas conservaron su actividad antimicrobiana, indicando que esta plataforma tiene un gran potencial para aplicaciones antimicrobianas.

FUTURE

8. LIMITATIONS AND FUTURE RESEARCH

While this Thesis presents significant advancements in the field of antimicrobial nanomaterials, some challenges and directions for future research remain to fully harness their potential. One of the main challenges is the extraction of antimicrobial compounds from fish mucus. This process requires advanced and often costly techniques, as isolating specific bioactive peptides from mucus demands specialized equipment and reagents that can limit scalability and accessibility. Future research should focus on optimizing these isolation methods to make them more cost-effective and efficient without sacrificing the yield or activity of these promising compounds.

Protein-based NFs show excellent aptitudes as a biocompatible, biodegradable alternative to traditional synthetic polymers, especially in medical applications. However, to maximize their efficacy, it is essential to investigate the stability of these NFs over time, the release rates of embedded bioactive compounds, and their effectiveness in specific applications, such as wound dressings. For instance, studies focused on controlled release profiles, as well as dermal penetration in skin models or animal testing, would help clarify their suitability for wound care, ensuring both safety and functionality over prolonged use.

The AgNP-TPU materials demonstrated strong antiviral activity, yet further work is required to ensure their safety and environmental compatibility. Additional cytotoxicity testing with diverse cell lines and over extended exposure periods will provide a more comprehensive understanding of their biocompatibility. Environmental impact studies are also crucial to assess the possible ecological risks associated with these materials, especially if they are to be used widely in medical or environmental applications. Long-term stability studies would further support their potential for real-world applications.

The green synthesis of NPs represents a sustainable alternative to traditional chemical methods, but variability in plant extract composition presents a challenge. Different plant extracts have unique chemical profiles, which can affect the size, stability, and efficacy of synthesized NPs. To address this, future studies should prioritize the development of standardized extraction protocols and conduct thorough profiling of plant extract constituents. This approach would enhance reproducibility and allow researchers to optimize synthesis conditions. Expanding the range of tested synthesis conditions, incorporating different plant sources, and evaluating the addition of stabilizers are also essential to improve NP stability and longevity. Furthermore, it is important to assess cytotoxicity across different cell lines to establish safe concentration limits without compromising antimicrobial efficacy.

The practical applications of all these nanomaterials hold significant promise, yet further testing is required to meet application-specific needs. For example, wound healing applications would benefit from *in vivo* studies that examine the safety and effectiveness of these materials in living organisms. Surface coatings and filtration membranes are additional applications that require compatibility testing with different substrates and evaluations of their performance under conditions that mimic real-world use.

Scaling up the synthesis of NFs and NPs for commercial production presents its own set of challenges. In particular, producing large quantities of green-synthesized NPs requires careful optimization to ensure consistent size, stability, and efficacy. Industrial-scale production of protein NFs would similarly require advanced electrospinning equipment capable of high-volume output while maintaining the beneficial properties of the material observed in laboratory settings. Future research should focus on developing scalable synthesis methods and protocols tailored to large-scale production needs.

BIBLIOGRAPHY

9. BIBLIOGRAPHY

1. Xiaoli, F.; Longquan, S. Chapter 20 - Neurotoxicity of nanomaterials. In *Emerging Nanotechnologies in Dentistry (Second Edition)*, Subramani, K., Ahmed, W., Eds.; William Andrew Publishing: 2018; pp. 421-444.
2. Ahire, S.A.; Bachhav, A.A.; Pawar, T.B.; Jagdale, B.S.; Patil, A.V.; Koli, P.B. The Augmentation of nanotechnology era: A concise review on fundamental concepts of nanotechnology and applications in material science and technology. *Results in Chemistry* **2022**, *4*, 100633.
3. Navya, P.N.; Daima, H.K. Rational engineering of physicochemical properties of nanomaterials for biomedical applications with nanotoxicological perspectives. *Nano Convergence* **2016**, *3*, 1.
4. Pithawalla, Y.B.; El-Shall, M.S.; Deevi, S.C.; Ström, V.; Rao, K.V. Synthesis of Magnetic Intermetallic FeAl Nanoparticles from a Non-Magnetic Bulk Alloy. *The Journal of Physical Chemistry B* **2001**, *105*, 2085-2090.
5. Adewuyi, A.; Lau, W.J. Chapter 3 - Nanomaterial development and its applications for emerging pollutant removal in water. In *Handbook of Nanotechnology Applications*, Lau, W.J., Faungnawakij, K., Piyachomkwan, K., Ruktanonchai, U.R., Eds.; Elsevier: 2021; pp. 67-97.
6. Khan, I.; Saeed, K.; Khan, I. Nanoparticles: Properties, applications and toxicities. *Arabian Journal of Chemistry* **2019**, *12*, 908-931.
7. Joudeh, N.; Linke, D. Nanoparticle classification, physicochemical properties, characterization, and applications: a comprehensive review for biologists. *Journal of Nanobiotechnology* **2022**, *20*, 262.
8. Taylor, A.C. 7 - Advances in nanoparticle reinforcement in structural adhesives. In *Advances in Structural Adhesive Bonding*, Dillard, D.A., Ed.; Woodhead Publishing: 2010; pp. 151-182.
9. Deshmukh, K. Nanotechnology in Ancient Era. In *Biotechnology Products in Everyday Life*, Khoobchandani, M., Saxena, A., Eds.; Springer International Publishing: Cham, 2019; pp. 3-14.
10. Byakodi, M.; Shrikrishna, N.S.; Sharma, R.; Bhansali, S.; Mishra, Y.; Kaushik, A.; Gandhi, S. Emerging 0D, 1D, 2D, and 3D nanostructures for efficient point-of-care biosensing. *Biosensors and Bioelectronics: X* **2022**, *12*, 100284.
11. Zhang, C.; Ma, Y.; Zhang, X.; Abdolhosseinzadeh, S.; Sheng, H.; Lan, W.; Pakdel, A.; Heier, J.; Nüesch, F. Two-Dimensional Transition Metal Carbides and Nitrides (MXenes): Synthesis, Properties, and Electrochemical Energy Storage Applications. *Energy & Environmental Materials* **2020**, *3*, 29-55.
12. Paras; Yadav, K.; Kumar, P.; Teja, D.R.; Chakraborty, S.; Chakraborty, M.; Mohapatra, S.S.; Sahoo, A.; Chou, M.M.C.; Liang, C.-T.; et al. A Review on Low-Dimensional Nanomaterials: Nanofabrication, Characterization and Applications. *Nanomaterials* **2023**, *13*, 160.
13. Saleh, T.A. Chapter 3 - Polymer science and polymerization methods toward hybrid materials. In *Polymer Hybrid Materials and Nanocomposites*, Saleh, T.A., Ed.; William Andrew Publishing: 2021; pp. 59-103.
14. Shi, J.; Votruba, A.R.; Farokhzad, O.C.; Langer, R. Nanotechnology in Drug Delivery and Tissue Engineering: From Discovery to Applications. *Nano Letters* **2010**, *10*, 3223-3230.
15. Azani, M.-R.; Hassanpour, A. Nanotechnology in the Fabrication of Advanced Paints and Coatings: Dispersion and Stabilization Mechanisms for Enhanced Performance. *ChemistrySelect* **2024**, *9*, e202400844.
16. Kumar, P.; Channi, H.K.; Babbar, A.; Kumar, R.; Bhutto, J.K.; Khan, T.M.Y.; Bhowmik, A.; Razak, A.; Wodajo, A.W. A systematic review of nanotechnology for electric vehicles battery. *International Journal of Low-Carbon Technologies* **2024**, *19*, 747-765.
17. Chhipa, H. Nanofertilizers and nanopesticides for agriculture. *Environmental Chemistry Letters* **2017**, *15*, 15-22.
18. Brandelli, A. Nanocomposites and their application in antimicrobial packaging. *Frontiers in Chemistry* **2024**, *12*, 1356304.
19. Cai, Y.; Wei, Q.; Huang, F. 3 - Processing of composite functional nanofibers. In *Functional Nanofibers and their Applications*, Wei, Q., Ed.; Woodhead Publishing: 2012; pp. 38-54.
20. Khorsandi, D.; Jenson, S.; Zarepour, A.; Khosravi, A.; Rabiee, N.; Iravani, S.; Zarrabi, A. Catalytic and biomedical applications of nanocelluloses: A review of recent developments. *International Journal of Biological Macromolecules* **2024**, *268*, 131829.
21. Ameer, J.M.; Pr, A.K.; Kasoju, N. Strategies to Tune Electrospun Scaffold Porosity for Effective Cell Response in Tissue Engineering. *Journal of Functional Biomaterials* **2019**, *10*, 30.
22. Farzan, M.; Roth, R.; Schoelkopf, J.; Huwyler, J.; Puchkov, M. The processes behind drug loading and release in porous drug delivery systems. *European Journal of Pharmaceutics and Biopharmaceutics* **2023**, *189*, 133-151.

23. Arifeen, W.U.; Kim, M.; Choi, J.; Yoo, K.; Kurniawan, R.; Ko, T.J. Optimization of porosity and tensile strength of electrospun polyacrylonitrile nanofibrous membranes. *Materials Chemistry and Physics* **2019**, *229*, 310-318.
24. Manawi, Y.M.; Ihsanullah; Samara, A.; Al-Ansari, T.; Atieh, M.A. A Review of Carbon Nanomaterials' Synthesis via the Chemical Vapor Deposition (CVD) Method. *Materials* **2018**, *11*, 822.
25. Al-Abduljabbar, A.; Farooq, I. Electrospun Polymer Nanofibers: Processing, Properties, and Applications. *Polymers* **2023**, *15*, 65.
26. Sahoo, B.; Panda, P.K.; Ramakrishna, S. Electrospinning of functional ceramic nanofibers. *Open Ceramics* **2022**, *11*, 100291.
27. Guo, B.; Ma, P.X. Synthetic biodegradable functional polymers for tissue engineering: a brief review. *Science China Chemistry* **2014**, *57*, 490-500.
28. Pakravan, M.; Heuzey, M.-C.; Ajji, A. A fundamental study of chitosan/PEO electrospinning. *Polymer* **2011**, *52*, 4813-4824.
29. Li, W.; Li, X.; Chen, Y.; Li, X.; Deng, H.; Wang, T.; Huang, R.; Fan, G. Poly(vinyl alcohol)/sodium alginate/layered silicate based nanofibrous mats for bacterial inhibition. *Carbohydrate Polymers* **2013**, *92*, 2232-2238.
30. Mokhena, T.C.; Mochane, M.J.; Mtibe, A.; John, M.J.; Sadiku, E.R.; Sefadi, J.S. Electrospun Alginate Nanofibers Toward Various Applications: A Review. *Materials* **2020**, *13*, 934.
31. Rostami, M.; Beheshtizadeh, N.; Ranjbar, F.E.; Najafi, N.; Ahmadi, A.; Ahmadi, P.; Rostamabadi, H.; Pazhouhnia, Z.; Assadpour, E.; Mirzanajafi-Zanjani, M.; et al. Recent advances in electrospun protein fibers/nanofibers for the food and biomedical applications. *Advances in Colloid and Interface Science* **2023**, *311*, 102827.
32. Taemeh, M.A.; Shiravandi, A.; Korayem, M.A.; Daemi, H. Fabrication challenges and trends in biomedical applications of alginate electrospun nanofibers. *Carbohydrate Polymers* **2020**, *228*, 115419.
33. Lencova, S.; Svarcova, V.; Stiborova, H.; Demnerova, K.; Jencova, V.; Hozdova, K.; Zdenkova, K. Bacterial Biofilms on Polyamide Nanofibers: Factors Influencing Biofilm Formation and Evaluation. *ACS Applied Materials & Interfaces* **2021**, *13*, 2277-2288.
34. Bagheri, H.; Aghakhani, A.; Baghernejad, M.; Akbarinejad, A. Novel polyamide-based nanofibers prepared by electrospinning technique for headspace solid-phase microextraction of phenol and chlorophenols from environmental samples. *Analytica Chimica Acta* **2012**, *716*, 34-39.
35. Lencova, S.; Stiborova, H.; Munzarova, M.; Demnerova, K.; Zdenkova, K. Potential of Polyamide Nanofibers With Natamycin, Rosemary Extract, and Green Tea Extract in Active Food Packaging Development: Interactions With Food Pathogens and Assessment of Microbial Risks Elimination. *Frontiers in Microbiology* **2022**, *13*, 857423.
36. Maccaferri, E.; Dalle Donne, M.; Mazzocchetti, L.; Benelli, T.; Brugo, T.M.; Zucchelli, A.; Giorgini, L. Rubber-enhanced polyamide nanofibers for a significant improvement of CFRP interlaminar fracture toughness. *Scientific Reports* **2022**, *12*, 21426.
37. Guibo, Y.; Qing, Z.; Yahong, Z.; Yin, Y.; Yumin, Y. The electrospun polyamide 6 nanofiber membranes used as high efficiency filter materials: Filtration potential, thermal treatment, and their continuous production. *Journal of Applied Polymer Science* **2013**, *128*, 1061-1069.
38. Ince Yardimci, A.; Yagmurcukardes, N.; Yagmurcukardes, M.; Capan, I.; Erdogan, M.; Capan, R.; Tarhan, O.; Acikbas, Y. Electrospun polyacrylonitrile (PAN) nanofiber: preparation, experimental characterization, organic vapor sensing ability and theoretical simulations of binding energies. *Applied Physics A* **2022**, *128*, 173.
39. Bortolassi, A.C.C.; Nagarajan, S.; de Araújo Lima, B.; Guerra, V.G.; Aguiar, M.L.; Huon, V.; Soussan, L.; Cornu, D.; Miele, P.; Bechelany, M. Efficient nanoparticles removal and bactericidal action of electrospun nanofibers membranes for air filtration. *Materials Science and Engineering: C* **2019**, *102*, 718-729.
40. Gu, S.Y.; Ren, J.; Wu, Q.L. Preparation and structures of electrospun PAN nanofibers as a precursor of carbon nanofibers. *Synthetic Metals* **2005**, *155*, 157-161.
41. Khandaker, M.; Nomhwange, H.; Progri, H.; Nikfarjam, S.; Vaughan, M.B. Evaluation of Polycaprolactone Electrospun Nanofiber-Composites for Artificial Skin Based on Dermal Fibroblast Culture. *Bioengineering* **2022**, *9*, 19.
42. singhal, P. Preparation and characterization of poly (E-CAPROLACTONE) nano fibers by electrospinning technique for tissue enginerring applications. *Materials Today: Proceedings* **2021**, *37*, 2997-3001.
43. Kamath, S.M.; Sridhar, K.; Jaison, D.; Gopinath, V.; Ibrahim, B.K.M.; Gupta, N.; Sundaram, A.; Sivaperumal, P.; Padmapriya, S.; Patil, S.S. Fabrication of tri-layered electrospun

polycaprolactone mats with improved sustained drug release profile. *Scientific Reports* **2020**, *10*, 18179.

44. El-Naggar, M.E.; Abdelgawad, A.M.; Salas, C.; Rojas, O.J. Curdlan in fibers as carriers of tetracycline hydrochloride: Controlled release and antibacterial activity. *Carbohydrate Polymers* **2016**, *154*, 194-203.
45. Lin, S.-H.; Ou, S.-L.; Hsu, H.-M.; Wu, J.-Y. Preparation and Characteristics of Polyethylene Oxide/Curdlan Nanofiber Films by Electrospinning for Biomedical Applications. *Materials* **2023**, *16*, 3863.
46. Javadi, B.; Mohsenzadeh, M. Electrospun PEO/WPI Nanofibers with Vanillin for Food Applications. *Food Biophysics* **2024**, *19*, 425-438.
47. Min, T.; Sun, X.; Yuan, Z.; Zhou, L.; Jiao, X.; Zha, J.; Zhu, Z.; Wen, Y. Novel antimicrobial packaging film based on porous poly(lactic acid) nanofiber and polymeric coating for humidity-controlled release of thyme essential oil. *LWT* **2021**, *135*, 110034.
48. Salaris, V.; San Félix García-Obregón, I.; López, D.; Peponi, L. Fabrication of PLA-Based Electrospun Nanofibers Reinforced with ZnO Nanoparticles and In Vitro Degradation Study. *Nanomaterials* **2023**, *13*, 2236.
49. Kumar, R.; Singh, R. On electrospun PLA nanofibers for bio-sensing applications. *Manufacturing Letters* **2023**, *37*, 7-11.
50. Xing, Z.-C.; Han, S.-J.; Shin, Y.-S.; Koo, T.-H.; Moon, S.; Jeong, Y.; Kang, I.-K. Enhanced Osteoblast Responses to Poly(Methyl Methacrylate)/Hydroxyapatite Electrospun Nanocomposites for Bone Tissue Engineering. *Journal of Biomaterials Science, Polymer Edition* **2013**, *24*, 61-76.
51. Taghiyar, H.; Yadollahi, B.; Kajani, A.A. Controlled drug delivery and cell adhesion for bone tissue regeneration by Keplerate polyoxometalate (Mo132)/metronidazole/PMMA scaffolds. *Scientific Reports* **2022**, *12*, 14443.
52. Ji, S.; Li, Y.; Yang, M. Gas sensing properties of a composite composed of electrospun poly(methyl methacrylate) nanofibers and in situ polymerized polyaniline. *Sensors and Actuators B: Chemical* **2008**, *133*, 644-649.
53. Cao, L.; An, P.; Xu, Z.; Huang, J. Performance evaluation of electrospun polyimide non-woven separators for high power lithium-ion batteries. *Journal of Electroanalytical Chemistry* **2016**, *767*, 34-39.
54. Lv, Y.-Y.; Xu, W.; Lin, F.-W.; Wu, J.; Xu, Z.-K. Electrospun nanofibers of porphyrinated polyimide for the ultra-sensitive detection of trace TNT. *Sensors and Actuators B: Chemical* **2013**, *184*, 205-211.
55. Xuyen, N.T.; Ra, E.J.; Geng, H.-Z.; Kim, K.K.; An, K.H.; Lee, Y.H. Enhancement of Conductivity by Diameter Control of Polyimide-Based Electrospun Carbon Nanofibers. *The Journal of Physical Chemistry B* **2007**, *111*, 11350-11353.
56. Fan, L.; Yu, Z.; Wei, X.; Dong, Z.; An, J. Polystyrene electrospun nanofibers as effective sorbents for the removal of atypical antipsychotics: Kinetic and thermodynamic studies. *Arabian Journal of Chemistry* **2022**, *15*, 104222.
57. Lee, M.W.; An, S.; Latthe, S.S.; Lee, C.; Hong, S.; Yoon, S.S. Electrospun Polystyrene Nanofiber Membrane with Superhydrophobicity and Superoleophilicity for Selective Separation of Water and Low Viscous Oil. *ACS Applied Materials & Interfaces* **2013**, *5*, 10597-10604.
58. An, J.; Wang, X.; Li, Y.; Kang, W.; Lian, K. Polystyrene nanofibers as an effective sorbent for the adsorption of clonazepam: kinetic and thermodynamic studies. *RSC Advances* **2022**, *12*, 3394-3401.
59. Akduman, C.; Özgüney, I.; Kumbasar, E.P.A. Preparation and characterization of naproxen-loaded electrospun thermoplastic polyurethane nanofibers as a drug delivery system. *Materials Science and Engineering: C* **2016**, *64*, 383-390.
60. Sambaer, W.; Zatloukal, M.; Kimmer, D. 3D modeling of filtration process via polyurethane nanofiber based nonwoven filters prepared by electrospinning process. *Chemical Engineering Science* **2011**, *66*, 613-623.
61. Ungur, G.; Hrůza, J. Modified polyurethane nanofibers as antibacterial filters for air and water purification. *RSC Advances* **2017**, *7*, 49177-49187.
62. Xu, S.; Lu, T.; Yang, L.; Luo, S.; Wang, Z.; Ye, C. In situ cell electrospun using a portable handheld electrospinning apparatus for the repair of wound healing in rats. *International Wound Journal* **2022**, *19*, 1693-1704.
63. Ghalei, S.; Asadi, H.; Ghalei, B. Zein nanoparticle-embedded electrospun PVA nanofibers as wound dressing for topical delivery of anti-inflammatory diclofenac. *Journal of Applied Polymer Science* **2018**, *135*, 46643.

64. Lee, S.Y.; Kim, J.T.; Chathuranga, K.; Lee, J.S.; Park, S.W.; Park, W.H. Tannic-Acid-Enriched Poly(vinyl alcohol) Nanofibrous Membrane as a UV-Shie lding and Antibacterial Face Mask Filter Material. *ACS Applied Materials & Interfaces* **2023**, *15*, 20435-20443.
65. Penton, K.E.; Kinler, Z.; Davis, A.; Spiva, J.A.; Hamilton, S.K. Electrospinning Drug-Loaded Alginate-Based Nanofibers towards Developing a Drug Release Rate Catalog. *Polymers* **2022**, *14*, 2773.
66. Najafiasl, M.; Osfouri, S.; Azin, R.; Zaeri, S. Alginate-based electrospun core/shell nanofibers containing dexpanthenol: A good candidate for wound dressing. *Journal of Drug Delivery Science and Technology* **2020**, *57*, 101708.
67. Mokhena, T.C.; Jacobs, N.V.; Luyt, A.S. Nanofibrous alginate membrane coated with cellulose nanowhiskers for water purification. *Cellulose* **2018**, *25*, 417-427.
68. Jayani, T.; Sanjeev, B.; Marimuthu, S.; Uthandi, S. Bacterial Cellulose Nano Fiber (BCNF) as carrier support for the immobilization of probiotic, Lactobacillus acidophilus 016. *Carbohydrate Polymers* **2020**, *250*, 116965.
69. Shu, D.; Xi, P.; Cheng, B.; Wang, Y.; Yang, L.; Wang, X.; Yan, X. One-step electrospinning cellulose nanofibers with superhydrophilicity and superoleophobicity underwater for high-efficiency oil-water separation. *International Journal of Biological Macromolecules* **2020**, *162*, 1536-1545.
70. Farahani, H.; Barati, A.; Arjomandzadegan, M.; Vatankhah, E. Nanofibrous cellulose acetate/gelatin wound dressing endowed with antibacterial and healing efficacy using nanoemulsion of Zataria multiflora. *International Journal of Biological Macromolecules* **2020**, *162*, 762-773.
71. Arkoun, M.; Daigle, F.; Heuzey, M.-C.; Ajji, A. Mechanism of Action of Electrospun Chitosan-Based Nanofibers against Meat Spoilage and Pathogenic Bacteria. *Molecules* **2017**, *22*, 585.
72. Kalalinia, F.; Taherzadeh, Z.; Jirofti, N.; Amiri, N.; Foroghinia, N.; Beheshti, M.; Bazzaz, B.S.F.; Hashemi, M.; Shahroodi, A.; Pishavar, E.; et al. Evaluation of wound healing efficiency of vancomycin-loaded electrospun chitosan/poly ethylene oxide nanofibers in full thickness wound model of rat. *International Journal of Biological Macromolecules* **2021**, *177*, 100-110.
73. Alhosseini, S.N.; Moztarzadeh, F.; Mozafari, M.; Asgari, S.; Dodel, M.; Samadikuchaksaraei, A.; Kargozar, S.; Kargozar S Fau - Jalali, N.; Jalali, N. Synthesis and characterization of electrospun polyvinyl alcohol nanofibrous scaffolds modified by blending with chitosan for neural tissue engineering. *International Journal of Nanomedicine* **2012**, *7*, 25-34.
74. Lee, C.-H.; Chang, S.-H.; Chen, W.-J.; Hung, K.-C.; Lin, Y.-H.; Liu, S.-J.; Hsieh, M.-J.; Pang, J.-H.S.; Juang, J.-H. Augmentation of diabetic wound healing and enhancement of collagen content using nanofibrous glucophage-loaded collagen/PLGA scaffold membranes. *Journal of Colloid and Interface Science* **2015**, *439*, 88-97.
75. Rho, K.S.; Jeong, L.; Lee, G.; Seo, B.-M.; Park, Y.J.; Hong, S.-D.; Roh, S.; Cho, J.J.; Park, W.H.; Min, B.-M. Electrospinning of collagen nanofibers: Effects on the behavior of normal human keratinocytes and early-stage wound healing. *Biomaterials* **2006**, *27*, 1452-1461.
76. Ba Linh, N.T.; Lee, K.-H.; Lee, B.-T. Functional nanofiber mat of polyvinyl alcohol/gelatin containing nanoparticles of biphasic calcium phosphate for bone regeneration in rat calvaria defects. *Journal of Biomedical Materials Research Part A* **2013**, *101A*, 2412-2423.
77. Sang, Q.; Williams, G.R.; Wu, H.; Liu, K.; Li, H.; Zhu, L.-M. Electrospun gelatin/sodium bicarbonate and poly(lactide-co-ε-caprolactone)/sodium bicarbonate nanofibers as drug delivery systems. *Materials Science and Engineering: C* **2017**, *81*, 359-365.
78. Min, B.-M.; Lee, G.; Kim, S.H.; Nam, Y.S.; Lee, T.S.; Park, W.H. Electrospinning of silk fibroin nanofibers and its effect on the adhesion and spreading of normal human keratinocytes and fibroblasts in vitro. *Biomaterials* **2004**, *25*, 1289-1297.
79. Ju, H.W.; Lee, O.J.; Lee, J.M.; Moon, B.M.; Park, H.J.; Park, Y.R.; Lee, M.C.; Kim, S.H.; Chao, J.R.; Ki, C.S.; et al. Wound healing effect of electrospun silk fibroin nanomatrix in burn-model. *International Journal of Biological Macromolecules* **2016**, *85*, 29-39.
80. Hadisi, Z.; Farokhi, M.; Bakhsheshi-Rad, H.R.; Jahanshahi, M.; Hasanpour, S.; Pagan, E.; Dolatshahi-Pirouz, A.; Zhang, Y.S.; Kundu, S.C.; Akbari, M. Hyaluronic Acid (HA)-Based Silk Fibroin/Zinc Oxide Core–Shell Electrospun Dressing for Burn Wound Management. *Macromolecular Bioscience* **2020**, *20*, 1900328.
81. Anusiya, G.; Jaiganesh, R. A review on fabrication methods of nanofibers and a special focus on application of cellulose nanofibers. *Carbohydrate Polymer Technologies and Applications* **2022**, *4*, 100262.
82. Ahmadi Bonakdar, M.; Rodrigue, D. Electrospinning: Processes, Structures, and Materials. *Macromol* **2024**, *4*, 58-103.

83. Keirouz, A.; Wang, Z.; Reddy, V.S.; Nagy, Z.K.; Vass, P.; Buzgo, M.; Ramakrishna, S.; Radacsi, N. The History of Electrospinning: Past, Present, and Future Developments. *Advanced Materials Technologies* **2023**, *8*, 2201723.
84. Xue, J.; Wu, T.; Dai, Y.; Xia, Y. Electrospinning and Electrospun Nanofibers: Methods, Materials, and Applications. *Chemical Reviews* **2019**, *119*, 5298-5415.
85. Angel, N.; Li, S.; Kong, L. Emerging applications of nanofibers electrospun from carbohydrate polymers. *Journal of Future Foods* **2024**, *4*, 289-299.
86. Ramalingam, M.; Ramakrishna, S. 1 - Introduction to nanofiber composites. In *Nanofiber Composites for Biomedical Applications*, Ramalingam, M., Ramakrishna, S., Eds.; Woodhead Publishing: 2017; pp. 3-29.
87. Murray, C.J.L.; Ikuta, K.S.; Sharara, F.; Swetschinski, L.; Robles Aguilar, G.; Gray, A.; Han, C.; Bisignano, C.; Rao, P.; Wool, E.; et al. Global burden of bacterial antimicrobial resistance in 2019: a systematic analysis. *The Lancet* **2022**, *399*, 629-655.
88. Manesh, A.; Varghese, G.M. Rising antimicrobial resistance: an evolving epidemic in a pandemic. *The Lancet Microbe* **2021**, *2*, e419-e420.
89. O'Neill, J. *Tackling drug-resistant infections globally: Final report and recommendations*; HM Government and Wellcome Trust: London, 2016.
90. Rasouli, R.; Barhoum, A. Advances in Nanofibers for Antimicrobial Drug Delivery. In *Handbook of Nanofibers*, Barhoum, A., Bechelany, M., Makhlouf, A.S.H., Eds.; Springer International Publishing: Cham, 2019; pp. 733-774.
91. Buzgo, M.; Mickova, A.; Rampichova, M.; Doupnik, M. 11 - Blend electrospinning, coaxial electrospinning, and emulsion electrospinning techniques. In *Core-Shell Nanostructures for Drug Delivery and Theranostics*, Focarete, M.L., Tampieri, A., Eds.; Woodhead Publishing: 2018; pp. 325-347.
92. Zhang, C.; Feng, F.; Zhang, H. Emulsion electrospinning: Fundamentals, food applications and prospects. *Trends in Food Science & Technology* **2018**, *80*, 175-186.
93. Hutchings, M.I.; Truman, A.W.; Wilkinson, B. Antibiotics: past, present and future. *Current Opinion in Microbiology* **2019**, *51*, 72-80.
94. Mujahid, M.H.; Upadhyay, T.K.; Khan, F.; Pandey, P.; Park, M.N.; Sharangi, A.B.; Saeed, M.; Upadhye, V.J.; Kim, B. Metallic and metal oxide-derived nanohybrid as a tool for biomedical applications. *Biomedicine & Pharmacotherapy* **2022**, *155*, 113791.
95. Huan, Y.; Kong, Q.; Mou, H.; Yi, H. Antimicrobial Peptides: Classification, Design, Application and Research Progress in Multiple Fields. *Frontiers in Microbiology* **2020**, *11*, 582779.
96. AlSheikh, H.M.; Sultan, I.; Kumar, V.; Rather, I.A.; Al-Sheikh, H.; Tasleem Jan, A.; Haq, Q.M. Plant-Based Phytochemicals as Possible Alternative to Antibiotics in Combating Bacterial Drug Resistance. *Antibiotics* **2020**, *9*, 480.
97. Ajalloueian, F.; Asgari, S.; Guerra, P.R.; Chamorro, C.I.; Ilchenco, O.; Piqueras, S.; Fossum, M.; Boisen, A. Amoxicillin-loaded multilayer pullulan-based nanofibers maintain long-term antibacterial properties with tunable release profile for topical skin delivery applications. *International Journal of Biological Macromolecules* **2022**, *215*, 413-423.
98. Ju, T.; Gaisford, S.; Williams, G.R. Ciprofloxacin-loaded electrospun nanofibres for antibacterial wound dressings. *Journal of Drug Delivery Science and Technology* **2024**, *91*, 105264.
99. Bakhsheshi-Rad, H.R.; Hadisi, Z.; Ismail, A.F.; Aziz, M.; Akbari, M.; Berto, F.; Chen, X.B. In vitro and in vivo evaluation of chitosan-alginate/gentamicin wound dressing nanofibrous with high antibacterial performance. *Polymer Testing* **2020**, *82*, 106298.
100. Song, D.W.; Kim, S.H.; Kim, H.H.; Lee, K.H.; Ki, C.S.; Park, Y.H. Multi-biofunction of antimicrobial peptide-immobilized silk fibroin nanofiber membrane: Implications for wound healing. *Acta Biomaterialia* **2016**, *39*, 146-155.
101. Heunis Tiaan, D.J.; Smith, C.; Dicks Leon, M.T. Evaluation of a Nisin-Eluting Nanofiber Scaffold To Treat Staphylococcus aureus-Induced Skin Infections in Mice. *Antimicrobial Agents and Chemotherapy* **2013**, *57*, 3928-3935.
102. Amariei, G.; Kokol, V.; Vivod, V.; Boltes, K.; Letón, P.; Rosal, R. Biocompatible antimicrobial electrospun nanofibers functionalized with ε-poly-l-lysine. *International Journal of Pharmaceutics* **2018**, *553*, 141-148.
103. Haider, A.; Kwak, S.; Gupta, K.C.; Kang, I.-K. Antibacterial Activity and Cytocompatibility of PLGA/CuO Hybrid Nanofiber Scaffolds Prepared by Electrospinning. *Journal of Nanomaterials* **2015**, *2015*, 832762.
104. Cai, N.; Li, C.; Han, C.; Luo, X.; Shen, L.; Xue, Y.; Yu, F. Tailoring mechanical and antibacterial properties of chitosan/gelatin nanofiber membranes with Fe3O4 nanoparticles for potential wound dressing application. *Applied Surface Science* **2016**, *369*, 492-500.

105. Augustine, R.; Malik, H.N.; Singhal, D.K.; Mukherjee, A.; Malakar, D.; Kalarikkal, N.; Thomas, S. Electrospun polycaprolactone/ZnO nanocomposite membranes as biomaterials with antibacterial and cell adhesion properties. *Journal of Polymer Research* **2014**, *21*, 347.
106. He, C.; Liu, X.; Zhou, Z.; Liu, N.; Ning, X.; Miao, Y.; Long, Y.; Wu, T.; Leng, X. Harnessing biocompatible nanofibers and silver nanoparticles for wound healing: Sandwich wound dressing versus commercial silver sulfadiazine dressing. *Materials Science and Engineering: C* **2021**, *128*, 112342.
107. Zhang, C.; Li, C.; Bai, J.; Wang, J.; Li, H. Synthesis, characterization, and antibacterial activity of Cu NPs embedded electrospun composite nanofibers. *Colloid and Polymer Science* **2015**, *293*, 2525-2530.
108. Silva, L.P.C.; de Oliveira, N.A.; Valotto, R.S.; Monteiro, F.C.; Alvarez, L.A.C.; Cesário, L.M.; Zanardo, T.É.C.; Nilo, A.P.M.C.; Schuenck, R.P.; de Oliveira, J.P.; et al. Cellulose nanofibers infused with pomegranate gold nanoparticles display antibacterial activity. *Nano-Structures & Nano-Objects* **2023**, *36*, 101045.
109. Miguel, S.P.; Ribeiro, M.P.; Coutinho, P.; Correia, I.J. Electrospun Polycaprolactone/Aloe Vera_Chitosan Nanofibrous Asymmetric Membranes Aimed for Wound Healing Applications. *Polymers* **2017**, *9*, 183.
110. Hasanpour Ardekani-Zadeh, A.; Hosseini, S.F. Electrospun essential oil-doped chitosan/poly(ε-caprolactone) hybrid nanofibrous mats for antimicrobial food biopackaging exploits. *Carbohydrate Polymers* **2019**, *223*, 115108.
111. Karamat-Iradmousa, M.; Karimi, H.; Mahboubi, A.; Rabbani, S.; Kamalinejad, M.; Haeri, A. Bi-layered nanofibers loaded with pomegranate flowers extract as a novel wound dressing: Fabrication, characterization, and in vivo healing promotion. *Industrial Crops and Products* **2023**, *202*, 117042.
112. Yaqoob, A.A.; Ahmad, H.; Parveen, T.; Ahmad, A.; Oves, M.; Ismail, I.M.I.; Qari, H.A.; Umar, K.; Mohamad Ibrahim, M.N. Recent Advances in Metal Decorated Nanomaterials and Their Various Biological Applications: A Review. *Frontiers in Chemistry* **2020**, *8*, 341.
113. Rai, M.; Kon, K.; Ingle, A.; Duran, N.; Galdiero, S.; Galdiero, M. Broad-spectrum bioactivities of silver nanoparticles: the emerging trends and future prospects. *Applied Microbiology and Biotechnology* **2014**, *98*, 1951-1961.
114. Chudobova, D.; Cihalova, K.; Kopel, P.; Melichar, L.; Ruttkay-Nedecky, B.; Vaculovicova, M.; Adam, V.; Kizek, R. Chapter 13 - Complexes of Metal-Based Nanoparticles with Chitosan Suppressing the Risk of Staphylococcus aureus and Escherichia coli Infections. In *Nanotechnology in Diagnosis, Treatment and Prophylaxis of Infectious Diseases*, Rai, M., Kon, K., Eds.; Academic Press: Boston, 2015; pp. 217-232.
115. Mohammed, Y.H.; Holmes, A.; Haridass, I.N.; Sanchez, W.Y.; Studier, H.; Grice, J.E.; Benson, H.A.E.; Roberts, M.S. Support for the Safe Use of Zinc Oxide Nanoparticle Sunscreens: Lack of Skin Penetration or Cellular Toxicity after Repeated Application in Volunteers. *Journal of Investigative Dermatology* **2019**, *139*, 308-315.
116. Dhaka, A.; Chand Mali, S.; Sharma, S.; Trivedi, R. A review on biological synthesis of silver nanoparticles and their potential applications. *Results in Chemistry* **2023**, *6*, 101108.
117. Osman, A.I.; Zhang, Y.; Farghali, M.; Rashwan, A.K.; Eltaweil, A.S.; Abd El-Monaem, E.M.; Mohamed, I.M.A.; Badr, M.M.; Ihara, I.; Rooney, D.W.; et al. Synthesis of green nanoparticles for energy, biomedical, environmental, agricultural, and food applications: A review. *Environmental Chemistry Letters* **2024**, *22*, 841-887.
118. Zhang, L.; Sathiyaseelan, A.; Zhang, X.; Lu, Y.; Wang, M.-H. Development and Analysis of Silver Nitroprusside Nanoparticle-Incorporated Sodium Alginate Films for Banana Browning Prevention. *Nanomaterials* **2024**, *14*, 292.
119. Singh, S.; Chunglok, W.; Nwabor, O.F.; Ushir, Y.V.; Singh, S.; Panpipat, W. Hydrophilic Biopolymer Matrix Antibacterial Peel-off Facial Mask Functionalized with Biogenic Nanostructured Material for Cosmeceutical Applications. *Journal of Polymers and the Environment* **2022**, *30*, 938-953.
120. Brzeziński, S.; Jasiorski, M.; Maruszewski, K.; Ornat, M.; Malinowska, G.; Borak, B.; Karbownik, I. Bacteriostatic textile-polymeric coat materials modified with nanoparticles. *Polimery* **2022**, *52*, 362-366.
121. Sharma, P.; Fialho, L.; Figueiredo, N.M.; Serra, R.; Cavaleiro, A.; Carvalho, S. Antimicrobial Polymeric Surfaces Using Embedded Silver Nanoparticles. *Antibiotics* **2023**, *12*, 207.
122. Roe, D.; Karandikar, B.; Bonn-Savage, N.; Gibbins, B.; Roullet, J.-B. Antimicrobial surface functionalization of plastic catheters by silver nanoparticles. *Journal of Antimicrobial Chemotherapy* **2008**, *61*, 869-876.

123. More, P.R.; Pandit, S.; Filippis, A.D.; Franci, G.; Mijakovic, I.; Galdiero, M. Silver Nanoparticles: Bactericidal and Mechanistic Approach against Drug Resistant Pathogens. *Microorganisms* **2023**, *11*, 369.
124. Mondal, S.K.; Chakraborty, S.; Manna, S.; Mandal, S.M. Antimicrobial nanoparticles: current landscape and future challenges. *RSC Pharmaceutics* **2024**, *1*, 388-402.
125. Jiang, H.; Li, L.; Li, Z.; Chu, X. Metal-based nanoparticles in antibacterial application in biomedical field: Current development and potential mechanisms. *Biomedical Microdevices* **2024**, *26*, 12.
126. Alavi, M.; Kamarasu, P.; McClements, D.J.; Moore, M.D. Metal and metal oxide-based antiviral nanoparticles: Properties, mechanisms of action, and applications. *Advances in Colloid and Interface Science* **2022**, *306*, 102726.
127. Ashokkumar, S.; Kaushik, N.K.; Han, I.; Uhm, H.S.; Park, J.S.; Cho, G.S.; Oh, Y.-J.; Shin, Y.O.; Choi, E.H. Persistence of Coronavirus on Surface Materials and Its Control Measures Using Nonthermal Plasma and Other Agents. *International Journal of Molecular Sciences* **2023**, *24*, 14106.
128. Maduray, K.; Parboosing, R. Metal Nanoparticles: a Promising Treatment for Viral and Arboviral Infections. *Biological Trace Element Research* **2021**, *199*, 3159-3176.
129. Gurunathan, S.; Qasim, M.; Choi, Y.; Do, J.T.; Park, C.; Hong, K.; Kim, J.-H.; Song, H. Antiviral Potential of Nanoparticles—Can Nanoparticles Fight Against Coronaviruses? *Nanomaterials* **2020**, *10*, 1645.
130. Luceri, A.; Francese, R.; Lembo, D.; Ferraris, M.; Balagna, C. Silver Nanoparticles: Review of Antiviral Properties, Mechanism of Action and Applications. *Microorganisms* **2023**, *11*, 629.
131. Singleton, V.L.; Orthofer, R.; Lamuela-Raventós, R.M. Analysis of total phenols and other oxidation substrates and antioxidants by means of folin-ciocalteu reagent. In *Methods in Enzymology*; Academic Press: 1999; Volume 299, pp. 152-178.
132. Pérez, M.; Dominguez-López, I.; Lamuela-Raventós, R.M. The Chemistry Behind the Folin–Ciocalteu Method for the Estimation of (Poly)phenol Content in Food: Total Phenolic Intake in a Mediterranean Dietary Pattern. *Journal of Agricultural and Food Chemistry* **2023**, *71*, 17543-17553.
133. Abualzulof, G.W.A.; Scandar, S.; Varfaj, I.; Dalla Costa, V.; Sardella, R.; Filippini, R.; Piovan, A.; Marcotullio, M.C. The Effect of Maturity Stage on Polyphenolic Composition, Antioxidant and Anti-Tyrosinase Activities of Ficus rubiginosa Desf. ex Vent. Extracts. *Antioxidants* **2024**, *13*, 1129.
134. Álvarez-Martínez, F.J.; Rodríguez, J.C.; Borrás-Rocher, F.; Barrajón-Catalán, E.; Micol, V. The antimicrobial capacity of Cistus salviifolius and Punica granatum plant extracts against clinical pathogens is related to their polyphenolic composition. *Scientific Reports* **2021**, *11*, 588.
135. Re, R.; Pellegrini, N.; Proteggente, A.; Pannala, A.; Yang, M.; Rice-Evans, C. Antioxidant activity applying an improved ABTS radical cation decolorization assay. *Free Radical Biology and Medicine* **1999**, *26*, 1231-1237.
136. Bradford, M.M. A rapid and sensitive method for the quantitation of microgram quantities of protein utilizing the principle of protein-dye binding. *Analytical Biochemistry* **1976**, *72*, 248-254.
137. Miller, G.L. Use of Dinitrosalicylic Acid Reagent for Determination of Reducing Sugar. *Analytical Chemistry* **1959**, *31*, 426-428.
138. Alzoubi, F.Y.; Ahmad, A.A.; Aljarrah, I.A.; Migdadi, A.B.; Al-Bataineh, Q.M. Localize surface plasmon resonance of silver nanoparticles using Mie theory. *Journal of Materials Science: Materials in Electronics* **2023**, *34*, 2128.
139. Pulingam, T.; Thong, K.L.; Ali, M.E.; Appaturi, J.N.; Dinshaw, I.J.; Ong, Z.Y.; Leo, B.F. Graphene oxide exhibits differential mechanistic action towards Gram-positive and Gram-negative bacteria. *Colloids and Surfaces B: Biointerfaces* **2019**, *181*, 6-15.
140. Spellberg, B.; Guidos, R.; Gilbert, D.; Bradley, J.; Boucher, H.W.; Scheld, W.M.; Bartlett, J.G.; Edwards, J., Jr.; the Infectious Diseases Society of, A. The Epidemic of Antibiotic-Resistant Infections: A Call to Action for the Medical Community from the Infectious Diseases Society of America. *Clinical Infectious Diseases* **2008**, *46*, 155-164.
141. Perlin, D.S.; Rautemaa-Richardson, R.; Alastruey-Izquierdo, A. The global problem of antifungal resistance: prevalence, mechanisms, and management. *The Lancet Infectious Diseases* **2017**, *17*, e383-e392.
142. Mason, S.; Devincenzo, J.P.; Toovey, S.; Wu, J.Z.; Whitley, R.J. Comparison of antiviral resistance across acute and chronic viral infections. *Antiviral Research* **2018**, *158*, 103-112.
143. Butler, M.S.; Paterson, D.L. Antibiotics in the clinical pipeline in October 2019. *The Journal of Antibiotics* **2020**, *73*, 329-364.

144. Bassetti, M.; Merelli, M.; Temperoni, C.; Astilean, A. New antibiotics for bad bugs: where are we? *Annals of Clinical Microbiology and Antimicrobials* **2013**, *12*, 22.
145. Ivanov, M.; Ćirić, A.; Stojković, D. Emerging Antifungal Targets and Strategies. *International Journal of Molecular Sciences* **2022**, *23*, 2756.
146. Tompa, D.R.; Immanuel, A.; Srikanth, S.; Kadhirvel, S. Trends and strategies to combat viral infections: A review on FDA approved antiviral drugs. *International Journal of Biological Macromolecules* **2021**, *172*, 524-541.
147. Baker, R.E.; Mahmud, A.S.; Miller, I.F.; Rajeev, M.; Rasambainarivo, F.; Rice, B.L.; Takahashi, S.; Tatem, A.J.; Wagner, C.E.; Wang, L.-F.; et al. Infectious disease in an era of global change. *Nature Reviews Microbiology* **2022**, *20*, 193-205.
148. Pawlowski, A.C.; Johnson, J.W.; Wright, G.D. Evolving medicinal chemistry strategies in antibiotic discovery. *Current Opinion in Biotechnology* **2016**, *42*, 108-117.
149. Miethke, M.; Pieroni, M.; Weber, T.; Brönstrup, M.; Hammann, P.; Halby, L.; Arimondo, P.B.; Glaser, P.; Aigle, B.; Bode, H.B.; et al. Towards the sustainable discovery and development of new antibiotics. *Nature Reviews Chemistry* **2021**, *5*, 726-749.
150. Falco, A.; Adamek, M.; Pereiro, P.; Hoole, D.; Encinar, J.A.; Novoa, B.; Mallavia, R. The Immune System of Marine Organisms as Source for Drugs against Infectious Diseases. *Marine Drugs* **2022**, *20*, 363.
151. Breitbart, M.; Rohwer, F. Here a virus, there a virus, everywhere the same virus? *Trends in Microbiology* **2005**, *13*, 278-284.
152. Hawksworth David, L.; Lücking, R. Fungal Diversity Revisited: 2.2 to 3.8 Million Species. *Microbiology Spectrum* **2017**, *5*, 10.
153. Flemming, H.-C.; Wuertz, S. Bacteria and archaea on Earth and their abundance in biofilms. *Nature Reviews Microbiology* **2019**, *17*, 247-260.
154. Durand, G.A.; Raoult, D.; Dubourg, G. Antibiotic discovery: history, methods and perspectives. *International Journal of Antimicrobial Agents* **2019**, *53*, 371-382.
155. Spížek, J.; Sigler, K.; Řezanka, T.; Demain, A. Biogenesis of antibiotics—viewing its history and glimpses of the future. *Folia Microbiologica* **2016**, *61*, 347-358.
156. Oloke, J.K. Activity pattern of natural and synthetic antibacterial agents among hospital isolates. *Microbios* **2000**, *102*, 175-181.
157. Pancu, D.F.; Scurtu, A.; Macasoi, I.G.; Marti, D.; Mioc, M.; Soica, C.; Coricovac, D.; Horhat, D.; Poenaru, M.; Dehelean, C. Antibiotics: Conventional Therapy and Natural Compounds with Antibacterial Activity—A Pharmaco-Toxicological Screening. *Antibiotics* **2021**, *10*, 401.
158. Bar-On, Y.M.; Phillips, R.; Milo, R. The biomass distribution on Earth. *Proceedings of the National Academy of Sciences* **2018**, *115*, 6506-6511.
159. Forterre, P.; Prangishvili, D. The origin of viruses. *Research in Microbiology* **2009**, *160*, 466-472.
160. Mojzsis, S.J.; Arrhenius, G.; McKeegan, K.D.; Harrison, T.M.; Nutman, A.P.; Friend, C.R.L. Evidence for life on Earth before 3,800 million years ago. *Nature* **1996**, *384*, 55-59.
161. Wang, D.Y.C.; Kumar, S.; Hedges, S.B. Divergence time estimates for the early history of animal phyla and the origin of plants, animals and fungi. *Proceedings of the Royal Society of London. Series B: Biological Sciences* **1999**, *266*, 163-171.
162. Richter, D.; Grün, R.; Joannes-Boyau, R.; Steele, T.E.; Amani, F.; Rué, M.; Fernandes, P.; Raynal, J.-P.; Geraads, D.; Ben-Ncer, A.; et al. The age of the hominin fossils from Jebel Irhoud, Morocco, and the origins of the Middle Stone Age. *Nature* **2017**, *546*, 293-296.
163. Murphy, W.J.; Eizirik, E.; Johnson, W.E.; Zhang, Y.P.; Ryder, O.A.; O'Brien, S.J. Molecular phylogenetics and the origins of placental mammals. *Nature* **2001**, *409*, 614-618.
164. Sallan, L.C. Major issues in the origins of ray-finned fish (Actinopterygii) biodiversity. *Biological Reviews* **2014**, *89*, 950-971.
165. Suttle, C.A. Marine viruses — major players in the global ecosystem. *Nature Reviews Microbiology* **2007**, *5*, 801-812.
166. Madsen, E.L. Microorganisms and their roles in fundamental biogeochemical cycles. *Current Opinion in Biotechnology* **2011**, *22*, 456-464.
167. Hagström, Å.; Pommier, T.; Rohwer, F.; Simu, K.; Stolte, W.; Svensson, D.; Zweifel Ulla, L. Use of 16S Ribosomal DNA for Delineation of Marine Bacterioplankton Species. *Applied and Environmental Microbiology* **2002**, *68*, 3628-3633.
168. Margulis, L.; Chapman, M.J. *Kingdoms and domains: an illustrated guide to the phyla of life on Earth*; Academic Press: 2009.
169. Kong, D.-X.; Jiang, Y.-Y.; Zhang, H.-Y. Marine natural products as sources of novel scaffolds: achievement and concern. *Drug Discovery Today* **2010**, *15*, 884-886.

170. Harizani, M.; Ioannou, E.; Roussis, V. The Laurencia Paradox: An Endless Source of Chemodiversity. In *Progress in the Chemistry of Organic Natural Products 102*, Kinghorn, A.D., Falk, H., Gibbons, S., Kobayashi, J.i., Eds.; Springer International Publishing: Cham, 2016; pp. 91-252.
171. Carroll, A.R.; Copp, B.R.; Davis, R.A.; Keyzers, R.A.; Prinsep, M.R. Marine natural products. *Natural Product Reports* **2019**, *36*, 122-173.
172. Ntie-Kang, F.; Svozil, D. An enumeration of natural products from microbial, marine and terrestrial sources. **2020**, *5*, 20180121.
173. Principe, P.P.; Fisher, W.S. Spatial Distribution of Collections Yielding Marine Natural Products. *Journal of Natural Products* **2018**, *81*, 2307-2320.
174. Agrawal, S.; Adholeya, A.; Deshmukh, S.K. The Pharmacological Potential of Non-ribosomal Peptides from Marine Sponge and Tunicates. *Frontiers in Pharmacology* **2016**, *7*, 333.
175. Brinchmann, M.F. Immune relevant molecules identified in the skin mucus of fish using -omics technologies. *Molecular BioSystems* **2016**, *12*, 2056-2063.
176. Tiralongo, F.; Messina, G.; Lombardo, B.M.; Longhitano, L.; Li Volti, G.; Tibullo, D. Skin Mucus of Marine Fish as a Source for the Development of Antimicrobial Agents. *Frontiers in Marine Science* **2020**, *7*, 541853.
177. Reverter, M.; Tapissier-Bontemps, N.; Lecchini, D.; Banaigs, B.; Sasal, P. Biological and Ecological Roles of External Fish Mucus: A Review. *Fishes* **2018**, *3*, 41.
178. Nelson, J.S.; Grande, T.C.; Wilson, M.V.H. *Fishes of the World*; John Wiley & Sons: 2016.
179. Martin, A.P. Increasing Genomic Complexity by Gene Duplication and the Origin of Vertebrates. *The American Naturalist* **1999**, *154*, 111-128.
180. Hurley, I.A.; Mueller, R.L.; Dunn, K.A.; Schmidt, E.J.; Friedman, M.; Ho, R.K.; Prince, V.E.; Yang, Z.; Thomas, M.G.; Coates, M.I. A new time-scale for ray-finned fish evolution. *Proceedings of the Royal Society B: Biological Sciences* **2006**, *274*, 489-498.
181. Ravi, V.; Venkatesh, B. Rapidly evolving fish genomes and teleost diversity. *Current Opinion in Genetics & Development* **2008**, *18*, 544-550.
182. Azam, F.; Malfatti, F. Erratum: Microbial structuring of marine ecosystems. *Nature Reviews Microbiology* **2007**, *5*, 966-966.
183. Bergh, Ø.; BØrsheim, K.Y.; Bratbak, G.; Heldal, M. High abundance of viruses found in aquatic environments. *Nature* **1989**, *340*, 467-468.
184. Ducklow, H.; Kirchman, D. Bacterial Production and Biomass in the Oceans. *In Microbial Ecology of the Ocean*, Kirchman, D., Ed.; John Wiley & Sons: 2000; pp. 85-120.
185. Grossart, H.-P.; Van den Wyngaert, S.; Kagami, M.; Wurzbacher, C.; Cunliffe, M.; Rojas-Jimenez, K. Fungi in aquatic ecosystems. *Nature Reviews Microbiology* **2019**, *17*, 339-354.
186. Castro, R.; Tafalla, C. Overview of fish immunity. In *Mucosal Health in Aquaculture*, Beck, B.H., Peatman, E., Eds.; Academic Press: San Diego, 2015; pp. 3-54.
187. Ponnappan, N.; Budagavi, D.P.; Yadav, B.K.; Chugh, A. Membrane-Active Peptides from Marine Organisms—Antimicrobials, Cell-Penetrating Peptides and Peptide Toxins: Applications and Prospects. *Probiotics and Antimicrobial Proteins* **2015**, *7*, 75-89.
188. Litman, G.W.; Rast, J.P.; Fugmann, S.D. The origins of vertebrate adaptive immunity. *Nature Reviews Immunology* **2010**, *10*, 543-553.
189. Ángeles Esteban, M.; Cerezuela, R. 4 - Fish mucosal immunity: skin. In *Mucosal Health in Aquaculture*, Beck, B.H., Peatman, E., Eds.; Academic Press: San Diego, 2015; pp. 67-92.
190. Salinas, I. The Mucosal Immune System of Teleost Fish. *Biology* **2015**, *4*, 525-539.
191. Ellis, A.E. Innate host defense mechanisms of fish against viruses and bacteria. *Developmental & Comparative Immunology* **2001**, *25*, 827-839.
192. Gomez, D.; Sunyer, J.O.; Salinas, I. The mucosal immune system of fish: The evolution of tolerating commensals while fighting pathogens. *Fish & Shellfish Immunology* **2013**, *35*, 1729-1739.
193. Otero-Gonzáiez, A.J.; Magalhães, B.S.; Garcia-Villarino, M.; López-Abarrategui, C.; Sousa, D.A.; Dias, S.C.; Franco, O.L. Antimicrobial peptides from marine invertebrates as a new frontier for microbial infection control. *The FASEB Journal* **2010**, *24*, 1320-1334.
194. Abdelmohsen, U.R.; Balasubramanian, S.; Oelschlaeger, T.A.; Grkovic, T.; Pham, N.B.; Quinn, R.J.; Hentschel, U. Potential of marine natural products against drug-resistant fungal, viral, and parasitic infections. *The Lancet Infectious Diseases* **2017**, *17*, e30-e41.
195. Tassanakajon, A.; Rimphanitchayakit, V.; Visetnan, S.; Amparyup, P.; Somboonwiwat, K.; Charoensapsri, W.; Tang, S. Shrimp humoral responses against pathogens: antimicrobial peptides and melanization. *Developmental & Comparative Immunology* **2018**, *80*, 81-93.

196. Shephard, K.L. Functions for fish mucus. *Reviews in Fish Biology and Fisheries* **1994**, *4*, 401-429.
197. Ángeles Esteban, M. An Overview of the Immunological Defenses in Fish Skin. *International Scholarly Research Notices* **2012**, *2012*, 853470.
198. Shephard, K.L. Mucus on the epidermis of fish and its influence on drug delivery. *Advanced Drug Delivery Reviews* **1993**, *11*, 403-417.
199. Liu, X.; Wu, H.; Liu, Q.; Wang, Q.; Xiao, J.; Zhang, Y. Skin-injured Zebrafish, Danio rerio, are more Susceptible to Vibrio anguillarum Infection. *Journal of the World Aquaculture Society* **2015**, *46*, 301-310.
200. Adamek, M.; Matras, M.; Rebl, A.; Stachnik, M.; Falco, A.; Bauer, J.; Miebach, A.-C.; Teitge, F.; Jung-Schroers, V.; Abdullah, M.; et al. Don't Let It Get Under Your Skin! – Vaccination Protects the Skin Barrier of Common Carp From Disruption Caused by Cyprinid Herpesvirus 3. *Frontiers in Immunology* **2022**, *13*, 787021.
201. Dash, S.; Das, S.K.; Samal, J.; Thatoi, H. Epidermal mucus, a major determinant in fish health: A review. *Iranian Journal of Veterinary Research* **2018**, *19*, 72-81.
202. Hussain, A.; Sachan, S.G. Fish Epidermal Mucus as a Source of Diverse Therapeutical Compounds. *International Journal of Peptide Research and Therapeutics* **2023**, *29*, 36.
203. Rakers, S.; Niklasson, L.; Steinhagen, D.; Kruse, C.; Schauber, J.; Sundell, K.; Paus, R. Antimicrobial Peptides (AMPs) from Fish Epidermis: Perspectives for Investigative Dermatology. *Journal of Investigative Dermatology* **2013**, *133*, 1140-1149.
204. Mahlapuu, M.; Håkansson, J.; Ringstad, L.; Björn, C. Antimicrobial Peptides: An Emerging Category of Therapeutic Agents. *Frontiers in Cellular and Infection Microbiology* **2016**, *6*, 194.
205. Hancock, R.E.W.; Haney, E.F.; Gill, E.E. The immunology of host defence peptides: beyond antimicrobial activity. *Nature Reviews Immunology* **2016**, *16*, 321-334.
206. Schroeder, B.O.; Wu, Z.; Nuding, S.; Groscurth, S.; Marcinowski, M.; Beisner, J.; Buchner, J.; Schaller, M.; Stange, E.F.; Wehkamp, J. Reduction of disulphide bonds unmasks potent antimicrobial activity of human β-defensin 1. *Nature* **2011**, *469*, 419-423.
207. Haag, A.F.; Kerscher, B.; Dall'Angelo, S.; Sani, M.; Longhi, R.; Baloban, M.; Wilson, H.M.; Mergaert, P.; Zanda, M.; Ferguson, G.P. Role of Cysteine Residues and Disulfide Bonds in the Activity of a Legume Root Nodule-specific, Cysteine-rich Peptide. *Journal of Biological Chemistry* **2012**, *287*, 10791-10798.
208. Falco, A.; Ortega-Villaizan, M.; Chico, V.; Brocal, I.; Perez, L.; Coll, J.M.; Estepa, A. Antimicrobial Peptides as Model Molecules for the Development of Novel Antiviral Agents in Aquaculture. *Mini-Reviews in Medicinal Chemistry* **2009**, *9*, 1159-1164.
209. Masso-Silva, J.A.; Diamond, G. Antimicrobial Peptides from Fish. *Pharmaceuticals* **2014**, *7*, 265-310.
210. Fernandes, J.M.O.; Kemp, G.D.; Molle, M.G.; Smith, V.J. Anti-microbial properties of histone H2A from skin secretions of rainbow trout, Oncorhynchus mykiss. *Biochemical Journal* **2002**, *368*, 611-620.
211. Birkemo, G.A.; Lüders, T.; Andersen, Ø.; Nes, I.F.; Nissen-Meyer, J. Hipposin, a histone-derived antimicrobial peptide in Atlantic halibut (Hippoglossus hippoglossus L.). *Biochimica et Biophysica Acta (BBA) - Proteins and Proteomics* **2003**, *1646*, 207-215.
212. Park, I.Y.; Park, C.B.; Kim, M.S.; Kim, S.C. Parasin I, an antimicrobial peptide derived from histone H2A in the catfish, Parasilurus asotus. *FEBS Letters* **1998**, *437*, 258-262.
213. Cho, J.H.; Park, I.Y.; Kim, H.S.; Lee, W.T.; Kim, M.S.; Kim, S.C. Cathepsin D produces antimicrobial peptide parasin I from histone H2A in the skin mucosa of fish. *The FASEB Journal* **2002**, *16*, 429-431.
214. Bergsson, G.; Agerberth, B.; Jörnvall, H.; Gudmundsson, G.H. Isolation and identification of antimicrobial components from the epidermal mucus of Atlantic cod (Gadus morhua). *The FEBS Journal* **2005**, *272*, 4960-4969.
215. Fernandes, J.M.O.; Molle, G.; Kemp, G.D.; Smith, V.J. Isolation and characterisation of oncorhyncin II, a histone H1-derived antimicrobial peptide from skin secretions of rainbow trout, Oncorhynchus mykiss. *Developmental & Comparative Immunology* **2004**, *28*, 127-138.
216. Lüders, T.; Birkemo Gunn, A.; Nissen-Meyer, J.; Andersen, Ø.; Nes Ingolf, F. Proline Conformation-Dependent Antimicrobial Activity of a Proline-Rich Histone H1 N-Terminal Peptide Fragment Isolated from the Skin Mucus of Atlantic Salmon. *Antimicrobial Agents and Chemotherapy* **2005**, *49*, 2399-2406.
217. Subramanian, S.; Ross, N.W.; MacKinnon, S.L. Myxinidin, A Novel Antimicrobial Peptide from the Epidermal Mucus of Hagfish, Myxine glutinosa L. *Marine Biotechnology* **2009**, *11*, 748-757.

218. Fernandes, J.M.O.; Saint, N.; Kemp, G.D.; Smith, V.J. Oncorhyncin III: a potent antimicrobial peptide derived from the non-histone chromosomal protein H6 of rainbow trout, Oncorhynchus mykiss. *Biochemical Journal* **2003**, *373*, 621-628.
219. Su, Y. Isolation and identification of pelteobagrin, a novel antimicrobial peptide from the skin mucus of yellow catfish (Pelteobagrus fulvidraco). *Comparative Biochemistry and Physiology Part B: Biochemistry and Molecular Biology* **2011**, *158*, 149-154.
220. Lazarovici, P.; Primor, N.; Loew, L.M. Purification and pore-forming activity of two hydrophobic polypeptides from the secretion of the Red Sea Moses sole (Pardachirus marmoratus). *Journal of Biological Chemistry* **1986**, *261*, 16704-16713.
221. Ruangsri, J.; Salger, S.A.; Caipang, C.M.A.; Kiron, V.; Fernandes, J.M.O. Differential expression and biological activity of two piscidin paralogues and a novel splice variant in Atlantic cod (Gadus morhua L.). *Fish & Shellfish Immunology* **2012**, *32*, 396-406.
222. Cole, A.M.; Weis, P.; Diamond, G. Isolation and Characterization of Pleurocidin, an Antimicrobial Peptide in the Skin Secretions of Winter Flounder. *Journal of Biological Chemistry* **1997**, *272*, 12008-12013.
223. Fernandes, J.M.O.; Smith, V.J. A novel antimicrobial function for a ribosomal peptide from rainbow trout skin. *Biochemical and Biophysical Research Communications* **2002**, *296*, 167-171.
224. Robinette, D.; Wada, S.; Arroll, T.; Levy, M.G.; Miller, W.L.; Noga, E.J. Antimicrobial activity in the skin of the channel catfish Ictalurus punctatus: characterization of broad-spectrum histone-like antimicrobial proteins. *Cellular and Molecular Life Sciences CMLS* **1998**, *54*, 467-475.
225. Kim, H.S.; Park, C.B.; Kim, M.S.; Kim, S.C. cDNA Cloning and Characterization of Buforin I, an Antimicrobial Peptide: A Cleavage Product of Histone H2A. *Biochemical and Biophysical Research Communications* **1996**, *229*, 381-387.
226. Valero, Y.; Chaves-Pozo, E.; Meseguer, J.; Esteban, M.; Cuesta, A. Biologial Role of Fish Antimicrobial Peptides. In *Antimicrobial Peptides*, Seong, M.D.; Hak, Y.I., Eds.; Nova Science Publishers, Inc.: 2013; pp. 31-60.
227. Oren, Z.; Shai, Y. A Class of Highly Potent Antibacterial Peptides Derived from Pardaxin, A Pore-Forming Peptide Isolated from Moses Sole Fish Pardachirus marmoratus. *European Journal of Biochemistry* **1996**, *237*, 303-310.
228. Bae, J.-S.; Jung, J.-M.; An, C.M.; Kim, J.-W.; Hwang, S.D.; Kwon, M.-G.; Park, M.-A.; Kim, M.-C.; Park, C.-I. Piscidin: Antimicrobial peptide of rock bream, Oplegnathus fasciatus. *Fish & Shellfish Immunology* **2016**, *51*, 136-142.
229. Ebran, N.; Julien, S.; Orange, N.; Auperin, B.; Molle, G. Isolation and characterization of novel glycoproteins from fish epidermal mucus: correlation between their pore-forming properties and their antibacterial activities. *Biochimica et Biophysica Acta (BBA) - Biomembranes* **2000**, *1467*, 271-280.
230. Easy, R.H.; Trippel, E.A.; Burt, M.D.B.; Cone, D.K. Identification of transferrin in Atlantic cod Gadus morhua epidermal mucus. *Journal of Fish Biology* **2012**, *81*, 2059-2063.
231. Uttakleiv Ræder, I.L.; Paulsen, S.M.; Smalås, A.O.; Willassen, N.P. Effect of fish skin mucus on the soluble proteome of Vibrio salmonicida analysed by 2-D gel electrophoresis and tandem mass spectrometry. *Microbial Pathogenesis* **2007**, *42*, 36-45.
232. B. Santoso, H.; Suhartono, E.; Yunita, R.; Biyatmoko, D. Epidermal mucus as a potential biological matrix for fish health analysis. *Egyptian Journal of Aquatic Biology and Fisheries* **2020**, *24*, 361-382.
233. Raposo, C.D.; Canelas, A.B.; Barros, M.T. Human Lectins, Their Carbohydrate Affinities and Where to Find Them. *Biomolecules* **2021**, *11*, 188.
234. Suzuki, Y.; Tasumi, S.; Tsutsui, S.; Okamoto, M.; Suetake, H. Molecular diversity of skin mucus lectins in fish. *Comparative Biochemistry and Physiology Part B: Biochemistry and Molecular Biology* **2003**, *136*, 723-730.
235. Chong, K.; Joshi, S.; Jin, L.T.; Shu-Chien, A.C. Proteomics profiling of epidermal mucus secretion of a cichlid () demonstrating parental care behavior. *Proteomics* **2006**, *6*, 2251-2258.
236. Cordero, H.; Brinchmann, M.F.; Cuesta, A.; Meseguer, J.; Esteban, M.A. Skin mucus proteome map of European sea bass (Dicentrarchus labrax). *Proteomics* **2015**, *15*, 4007-4020.
237. Rajan, B.; Fernandes, J.M.O.; Caipang, C.M.A.; Kiron, V.; Rombout, J.H.W.M.; Brinchmann, M.F. Proteome reference map of the skin mucus of Atlantic cod (Gadus morhua) revealing immune competent molecules. *Fish & Shellfish Immunology* **2011**, *31*, 224-231.
238. Tsutsui, S.; Tasumi, S.; Suetake, H.; Suzuki, Y. Lectins Homologous to Those of Monocotyledonous Plants in the Skin Mucus and Intestine of Pufferfish, Fugu rubripes. *Journal of Biological Chemistry* **2003**, *278*, 20882-20889.

239. Tsutsui, S.; Yamaguchi, M.; Hirasawa, A.; Nakamura, O.; Watanabe, T. Common Skate (Raja kenojei) Secretes Pentraxin into the Cutaneous Secretion: The First Skin Mucus Lectin in Cartilaginous Fish. *The Journal of Biochemistry* **2009**, *146*, 295-306.
240. Patel, D.M.; Brinchmann, M.F. Skin mucus proteins of lumpsucker (Cyclopterus lumpus). *Biochemistry and Biophysics Reports* **2017**, *9*, 217-225
241. Gewurz, H.; Zhang, X.-H.; Lint, T.F. Structure and function of the pentraxins. *Current Opinion in Immunology* **1995**, *7*, 54-64.
242. Ramos, F.; Smith, A.C. The C-reactive protein (CRP) test for the detection of early disease in fishes. *Aquaculture* **1978**, *14*, 261-266.
243. Lazado, C.; Skov, P.V. Secretory Proteins in the Skin Mucus of Nile Tilapia (Oreochromis niloticus) are Modulated Temporally by Photoperiod and Bacterial Endotoxin Cues. *Fishes* **2019**, *4*, 57.
244. Nigam, A.K.; Kumari, U.; Mittal, S.; Mittal, A.K. Comparative analysis of innate immune parameters of the skin mucous secretions from certain freshwater teleosts, inhabiting different ecological niches. *Fish Physiology and Biochemistry* **2012**, *38*, 1245-1256.
245. Ren, T.; Koshio, S.; Ishikawa, M.; Yokoyama, S.; Micheal, F.R.; Uyan, O.; Tung, H.T. Influence of dietary vitamin C and bovine lactoferrin on blood chemistry and non-specific immune responses of Japanese eel, Anguilla japonica. *Aquaculture* **2007**, *267*, 31-37.
246. Subramanian, S.; MacKinnon, S.L.; Ross, N.W. A comparative study on innate immune parameters in the epidermal mucus of various fish species. *Comparative Biochemistry and Physiology Part B: Biochemistry and Molecular Biology* **2007**, *148*, 256-263.
247. Hjelmeland, K.; Christie, M.; Raa, J. Skin mucus protease from rainbow trout, Salmo gairdneri Richardson, and its biological significance. *Journal of Fish Biology* **1983**, *23*, 13-22.
248. Aranishi, F.; Nakane, M. Epidermal proteases of the Japanese eel. *Fish Physiology and Biochemistry* **1997**, *16*, 471-478.
249. Aranishi, F.; Nakane, M. Epidermal Proteinases in the European Eel. *Physiological Zoology* **1997**, *70*, 563-570.
250. Firth, K.J.; Johnson, S.C.; Ross, N.W. Characterization of proteases in the skin mucus of Atlantic Salmon (Salmo salar) infected with the Salmon Louse (Lepeophtheirus salmonis) and in whole-body louse homogenate. *The Journal of Parasitology* **2000**, *86*, 1199-1205.
251. Jurado, J.; Fuentes-Almagro, C.A.; Guardiola, F.A.; Cuesta, A.; Esteban, M.Á.; Prieto-Álamo, M.-J. Proteomic profile of the skin mucus of farmed gilthead seabream (Sparus aurata). *Journal of Proteomics* **2015**, *120*, 21-34.
252. Molle, V.; Campagna, S.; Bessin, Y.; Ebran, N.; Saint, N.; Molle, G. First evidence of the pore-forming properties of a keratin from skin mucus of rainbow trout (Oncorhynchus mykiss, formerly Salmo gairdneri). *Biochemical Journal* **2008**, *411*, 33-40.
253. Hayes, M.J.; Rescher, U.; Gerke, V.; Moss, S.E. Annexin–Actin Interactions. *Traffic* **2004**, *5*, 571-576.
254. Cordero, H.; Brinchmann, M.F.; Cuesta, A.; Esteban, M.A. Chronic wounds alter the proteome profile in skin mucus of farmed gilthead seabream. *BMC Genomics* **2017**, *18*, 939.
255. Easy, R.H.; Ross, N.W. Changes in Atlantic salmon Salmo salar mucus components following short- and long-term handling stress. *Journal of Fish Biology* **2010**, *77*, 1616-1631.
256. Balasubramanian, S.; Gunasekaran, G. Fatty acids and amino acids composition in skin epidermal mucus of selected fresh water fish mugil cephalus. *World Journal of Pharmacy and Pharmaceutical Sciences* **2015**, *4*, 1275–1287.
257. Torrecillas, S.; Montero, D.; Domínguez, D.; Robaina, L.; Izquierdo, M. Skin Mucus Fatty Acid Composition of Gilthead Sea Bream (Sparus Aurata): A Descriptive Study in Fish Fed Low and High Fish Meal Diets. *Fishes* **2019**, *4*, 15.
258. Lewis, R.W. Fish cutaneous mucus: A new source of skin surface lipid. *Lipids* **1970**, *5*, 947-949.
259. Ekman, D.R.; Skelton, D.M.; Davis, J.M.; Villeneuve, D.L.; Cavallin, J.E.; Schroeder, A.; Jensen, K.M.; Ankley, G.T.; Collette, T.W. Metabolite Profiling of Fish Skin Mucus: A Novel Approach for Minimally-Invasive Environmental Exposure Monitoring and Surveillance. *Environmental Science & Technology* **2015**, *49*, 3091-3100.
260. Holland, K.; Bojar, R. Antimicrobial effects of azelaic acid. *Journal of Dermatological Treatment* **1993**, *4*, 8-11.
261. Sakko, M.; Moore, C.; Novak-Frazer, L.; Rautemaa, V.; Sorsa, T.; Hietala, P.; Järvinen, A.; Bowyer, P.; Tjäderhane, L.; Rautemaa, R. 2-hydroxyisocaproic acid is fungicidal for Candida and Aspergillus species. *Mycoses* **2014**, *57*, 214-221.
262. Patel, M.; Ashraf, M.S.; Siddiqui, A.J.; Ashraf, S.A.; Sachidanandan, M.; Snoussi, M.; Adnan, M.; Hadi, S. Profiling and Role of Bioactive Molecules from Puntius sophore (Freshwater/Brackish

Fish) Skin Mucus with Its Potent Antibacterial, Antiadhesion, and Antibiofilm Activities. *Biomolecules* **2020**, *10*, 920.

263. Lee, Y.; Bilung, L.M.; Sulaiman, B.; Chong, Y.L. The antibacterial activity of fish skin mucus with various extraction solvents and their in-vitro evaluation methods. *International Aquatic Research* **2020**, *12*, 1-21.
264. Wang, H.; Tang, W.; Zhang, R.; Ding, S. Analysis of enzyme activity, antibacterial activity, antiparasitic activity and physico-chemical stability of skin mucus derived from Amphiprion clarkii. *Fish & Shellfish Immunology* **2019**, *86*, 653-661.
265. Al-Rasheed, A.; Handool, K.O.; Garba, B.; Noordin, M.M.; Bejo, S.K.; Kamal, F.M.; Daud, H.H.M. Crude extracts of epidermal mucus and epidermis of climbing perch Anabas testudineus and its antibacterial and hemolytic activities. *Egyptian Journal of Aquatic Research* **2018**, *44*, 125-129.
266. Sanahuja, I.; Fernández-Alacid, L.; Ordóñez-Grande, B.; Sánchez-Nuño, S.; Ramos, A.; Araujo, R.M.; Ibarz, A. Comparison of several non-specific skin mucus immune defences in three piscine species of aquaculture interest. *Fish & Shellfish Immunology* **2019**, *89*, 428-436.
267. Leng, W.; Wu, X.; Xiong, Z.; Shi, T.; Sun, Q.; Yuan, L.; Gao, R. Study on antibacterial properties of mucus extract of snakehead (Channa argus) against Escherichia coli and its application in chilled fish fillets preservation. *LWT* **2022**, *167*, 113840.
268. Dhanaraj, M.; Haniffa, M.A.; Singh, S.V.A.; Ramakrishnan, C.M.; Manikandaraja, D.; Milton, M.J. Antibacterial Activity of Skin and Intestinal Mucus of Five Different Freshwater Fish Species Viz., *Channa striatus*, *C. micropeltes*, *C. marulius*, *C. punctatus* and *C. gachua*. *Malaysian Journal of Science* **2009**, *28*, 257-262.
269. Yeong, O.; Xavier, R.; Marimuthu, K. Wei OY, Xavier R, Marimuthu KScreening of antibacterial activity of mucus extract of snakehead fish, Channa striatus (Bloch). Eur Rev Med Pharmacol Sci 14:675-681. *European review for medical and pharmacological sciences* **2010**, *14*, 675-681.
270. Ramesh, B. Assessment of Antimicrobial peptides from mucus of fish. *International Journal of Current Biotechnology* **2013**, *1*, 5-8.
271. Haniffa, M.A.; Viswanathan, S.; Jancy, D.; Poomari, K.; Manikandan, S. Antibacterial studies of fish mucus from two marketed air-breathing fishes – *Channa striatus* and *Heteropneustes fossilis*. *International Research Journal of Microbiology* **2014**, *5*, 22-27.
272. Guardiola, F.A.; Cuesta, A.; Abellán, E.; Meseguer, J.; Esteban, M.A. Comparative analysis of the humoral immunity of skin mucus from several marine teleost fish. *Fish & Shellfish Immunology* **2014**, *40*, 24-31.
273. Caruso, G.; Maricchiolo, G.; Genovese, L.; Pasquale, F.; Caruso, R.; Denaro, M.G.; Delia, S.; Laganà, P. Comparative Study of Antibacterial and Haemolytic Activities in Sea Bass, European Eel and Blackspot Seabream. *The Open Marine Biology Journal* **2014**, *8*, 10-16.
274. Magarinos, B.; Pazos, F.; Santos, Y.; Romalde, J.L.; Toranzo, A.E. Response of Pasteurella piscicida and Flexibacter maritimus to skin mucus of marine fish. *Diseases of Aquatic Organisms* **1995**, *21*, 103-108.
275. Manikantan, G.; Lyla, S.; Khan, S.; Vijayanand, P.; George, E.G.J. Bioactive potency of epidermal mucus extracts from greasy grouper, Epinephelus tauvina (Forsskal, 1775). *Journal of Coastal Life Medicine* **2016**, *4*, 510-520.
276. Hellio, C.; Pons, A.M.; Beaupoil, C.; Bourgougnon, N.; Gal, d.s.Y.L. Antibacterial, antifungal and cytotoxic activities of extracts from fish epidermis and epidermal mucus. *International Journal of Antimicrobial Agents* **2002**, *20*, 214-219.
277. Katra, N.; Hisar, O.; Karatas, S.; Turgay, E.; Sarvan, C. In vitro antimicrobial activities of extracts from ballan wrasse (Labrus bergylta) skin mucus. *Marine Science and Technology Bulletin* **2016**, *5*, 13-15.
278. Subramanian, S.; Ross, N.W.; MacKinnon, S.L. Comparison of antimicrobial activity in the epidermal mucus extracts of fish. *Comparative Biochemistry and Physiology Part B: Biochemistry and Molecular Biology* **2008**, *150*, 85-92.
279. García-Marciano, M.; Apún-Molina, J.P.; Sainz-Hernández, J.C.; Santamaría-Miranda, A.; Medina-Godoy, S.; Aguiñaga-Cruz, J.A. Antibacterial activity evaluation of the Nile tilapia Oreochromis niloticus (Linnaeus, 1758) skin mucus, against Vibrio bacteria affecting the white shrimp Penaeus vannamei. *Latin American Journal of Aquatic Research* **2019**, *47, 580-585*.
280. Lirio, G.A.C.; De Leon, J.A.A.; Villafuerte, A.G. Antimicrobial Activity of Epidermal Mucus from Top Aquaculture Fish Species against Medically-Important Pathogens. *Walailak Journal of Science and Technology* **2018**, *16*, 329-340.
281. Wibowo, A.; Fadjar, M.; Maftuch. Utilization of Tilapia Mucus to Inhibit *Vibrio harveyi* on Vannamei (*Litopenaeus vannamei*). *Journal of Life Science and Biomedicine* **2015**, *5*, 141-148.

282. Elavarasi, K.; Ranjini, S.; Rajagopal, T.; Rameshkumar, G.; Ponmanickam, P. Bactericidal proteins of skin mucus and skin extracts from fresh water fishes, Clarias batrachus and Tilapia mossambicus. *Thai Journal of Pharmaceutical Sciences* **2013**, *37*, 194-200.
283. Mahadevan, G.; Mohan, K.; Vinoth, J.; Ravi, V. Biotic potential of mucus extracts of giant mudskipper Periophthalmodon schlosseri (Pallas, 1770) from Pichavaram, southeast coast of India. *The Journal of Basic and Applied Zoology* **2019**, *80*, 13.
284. Pethkar, M.R.L., M.V. . Antifungal activity of skin mucus of three cultivable fish species. *International Journal of Zoology Studies* **2017**, *2*, 1-3.
285. Manivasagan, P.; Annamalai, N.; Ashokkumar, S.; Sampathkumar, P. Studies on the proteinaceous gel secretion from the skin of the catfish, *Arius maculatus* (Thunberg, 1792). *African Journal of Biotechnology* **2009**, *8*, 7125-7129.
286. Patil, R.N.; Kadam, J.S.; Ingole, J.R.; Sathe, T.V.; Jadhav, A.D. Antibacterial activity of fish mucus from *Clarias batrachus* (Linn.) against selected microbes. *Biolife* **2015**, *3*, 788-791.
287. Loganathan, K.; Muniyan, M.; Prakash, A.A.; Raja, P.S.; Prakash, M. Studies on the Role of Mucus From C*larias batrachus* (Linn) Against Selected Microbes. *International Journal of Pharmaceutical Applications* **2011**, *2*, 202-206.
288. Kumari, U.; Nigam, A.; Mittal, S.; Mittal, A. Antibacterial properties of the skin mucus of the freshwater fishes, Rita rita and Channa punctatus. *European review for medical and pharmacological sciences* **2011**, *15*, 781-786.
289. Subhashini, S.; Lavanya, J.; Jain, S.; Agihotri, T. Screening of Antibacterial and Cytotoxic Activity of Extracts From Epidermis and Epidermal Mucus of B*arbonymus Schwanenfeldii* (Tinfoil Barb Fish). *International Journal of Research in Engineering and Technology* **2013**, *2*, 492-497.
290. Islam, M.M.; Hossain, M.M.M.; Islam, M.S.; Shoumo; Khondoker; Khatun, M.A. Competitive antibacterial activity of two Indian majorcarps and two Chinese carps fish mucus against common pathogenic bacteria at aquaculture pond. *International Journal of Fisheries and Aquatic Studies* **2014**, *2*, 158-162.
291. Balasubramanian, S.; Rani, P.B.; Prakash, A.A.; Prakash, M.; Senthilraja, P.; Gunasekaran, G. Antimicrobial properties of skin mucus from four freshwater cultivable Fishes (*Catla catla*, *Hypophthalmichthys molitrix*, *Labeo rohita* and *Ctenopharyngodon idella*). *African Journal of Microbiology Research* **2011**, *6*, 5110-5120.
292. Nigam, A.K.; Kumari, U.; Mittal, S.; Mittal, A.K. Evaluation of antibacterial activity and innate immune components in skin mucus of Indian major carp, *Cirrhinus mrigala*. *Aquaculture Research* **2015**, *48*, 407-418.
293. Kuppulakshmi, C.; Prakash, M.; Gunasekaran, G.; Manimegalai, G.; Sarojini, S. Antibacterial properties of fish mucus from Channa punctatus and Cirrhinus mrigala. *European Review of Medical Pharmacological Science* **2008**, *12*, 149-153.
294. Kumari, S.; Tyor, A.K.; Bhatnagar, A. Evaluation of the antibacterial activity of skin mucus of three carp species. *International Aquatic Research* **2019**, *11*, 225-239.
295. Tyor, A.K.; Kumari, S. Biochemical characterization and antibacterial properties of fish skin mucus of fresh water fish, *Hypophthalmichthys nobilis*. *International Journal of Pharmacy and Pharmaceutical Sciences* **2016**, *8*, 132-136.
296. Fuochi, V.; Volti, G.L.; Camiolo, G.; Tiralongo, F.; Giallongo, C.; Distefano, A.; Petronio, G.P.; Barbagallo, I.; Viola, M.; Furneri, P.M.; et al. Antimicrobial and Anti-Proliferative Effects of Skin Mucus Derived from *Dasyatis pastinaca*. *Marine drugs* **2017**, *15*, 342.
297. Hisar, O.; Hisar, S.A.; Uyanik, M.H.; Sahin, T.; Cakir, F.; Yilmaz, S. *In vitro* antimicrobial and antifungal activities of aqueous skin mucus from rainbow trout (*Oncorhynchus mykiss*) on human pathogens. *Marine Science and Technology Bulletin* **2014**, *3*, 19-22.
298. Guardiola, F.A.; Cuartero, M.; Collado-González, M.d.M.; Díaz-Baños, F.G.; Cuesta, A.; Moriñigo, M.Á.; Esteban, M.Á. Terminal carbohydrates abundance, immune related enzymes, bactericidal activity and physico-chemical parameters of the Senegalese sole (S*olea senegalensis*, Kaup) skin mucus. *Fish & Shellfish Immunology* **2017**, *60*, 483-491.
299. Wei, O.Y.; Xavier, R.; Marimuthu, K. Screening of antibacterial activity of mucus extract of snakehead fish, *Channa striatus*. *European Review for Medical and Pharmacological Sciences* **2010**, *14*, 675-681.
300. Yount, N.Y.; Bayer, A.S.; Xiong, Y.Q.; Yeaman, M.R. Advances in antimicrobial peptide immunobiology. *Peptide Science* **2006**, *84*, 435-458.
301. Afkarian, M.; Bhasin, M.; Dillon, S.T.; Guerrero, M.C.; Nelson, R.G.; Knowler, W.C.; Thadhani, R.; Libermann, T.A. Optimizing a Proteomics Platform for Urine Biomarker Discovery*. *Molecular & Cellular Proteomics* **2010**, *9*, 2195-2204.

302. Ming, L.; Xiaoling, P.; Yan, L.; Lili, W.; Qi, W.; Xiyong, Y.; Boyao, W.; Ning, H. Purification of antimicrobial factors from human cervical mucus. *Human Reproduction* **2007**, *22*, 1810-1815.
303. Fischer, C.L. Antimicrobial Activity of Host-Derived Lipids. *Antibiotics* **2020**, *9*, 75.
304. Al-Arifa, N.; Batool, A.; Hanif, A. Effects of alkaline pH on protein and fatty acid profiles of epidermal mucus from Labeo rohita. *Journal of Animal and Plant Sciences* **2013**, *23*, 1045-1051.
305. Ikram, M.; Ridzwan, B.H. A preliminary screening of antifungal activities from skin mucus extract of Malaysian local swamp eel (Monopterus albus). *International research journal of pharmacy* **2013**, *3*, 1-8.
306. Nishiyama, Y.; Nakaoka, C.; Hiratani, T.; Abe, S.; Uchida, K.; Yamaguchi, H. Synergy of lysozyme and lanoconazole on the morphology of Candida albicans. *Journal of Electron Microscopy* **2001**, *50*, 41-49.
307. Sowa-Jasiłek, A.; Zdybicka-Barabas, A.; Stączek, S.; Wydrych, J.; Skrzypiec, K.; Mak, P.; Deryło, K.; Tchórzewski, M.; Cytryńska, M. Galleria mellonella lysozyme induces apoptotic changes in Candida albicans cells. *Microbiological Research* **2016**, *193*, 121-131.
308. Zarei, M.; Aminzadeh, S.; Zolgharnein, H.; Safahieh, A.; Daliri, M.; Noghabi, K.; Ghoroghi, A.; Motallebi, A. Characterization of a chitinase with antifungal activity from a native Serratia marcescens B4A. *Brazilian journal of microbiology : [publication of the Brazilian Society for Microbiology]* **2011**, *42*, 1017-1029.
309. Raj, V.S.; Fournier, G.; Rakus, K.; Ronsmans, M.; Ouyang, P.; Michel, B.; Delforges, C.; Costes, B.; Farnir, F.; Leroy, B.; et al. Skin mucus of Cyprinus carpio inhibits cyprinid herpesvirus 3 binding to epidermal cells. *Veterinary Research* **2011**, *42*, 92.
310. Valero, Y.; Arizcun, M.; Cortés, J.; Ramírez-Cepeda, F.; Guzmán, F.; Mercado, L.; Esteban, M.Á.; Chaves-Pozo, E.; Cuesta, A. NK-lysin, dicentracin and hepcidin antimicrobial peptides in European sea bass. Ontogenetic development and modulation in juveniles by nodavirus. *Developmental & Comparative Immunology* **2020**, *103*, 103516.
311. Falco, A.; Medina-Gali, R.M.; Poveda, J.A.; Bello-Perez, M.; Novoa, B.; Encinar, J.A. Antiviral Activity of a Turbot (Scophthalmus maximus) NK-Lysin Peptide by Inhibition of Low-pH Virus-Induced Membrane Fusion. *Marine Drugs* **2019**, *17*, 87.
312. Casadei, E.; Wang, T.; Zou, J.; González Vecino, J.L.; Wadsworth, S.; Secombes, C.J. Characterization of three novel β-defensin antimicrobial peptides in rainbow trout (Oncorhynchus mykiss). *Molecular Immunology* **2009**, *46*, 3358-3366.
313. Falco, A.; Chico, V.; Marroquí, L.; Perez, L.; Coll, J.M.; Estepa, A. Expression and antiviral activity of a β-defensin-like peptide identified in the rainbow trout (Oncorhynchus mykiss) EST sequences. *Molecular Immunology* **2008**, *45*, 757-765.
314. Mai, W.-j.; Wang, W.-n. Protection of blue shrimp (Litopenaeus stylirostris) against the White Spot Syndrome Virus (WSSV) when injected with shrimp lysozyme. *Fish & Shellfish Immunology* **2010**, *28*, 727-733.
315. Hu, H.; Guo, N.; Chen, S.; Guo, X.; Liu, X.; Ye, S.; Chai, Q.; Wang, Y.; Liu, B.; He, Q. Antiviral activity of Piscidin 1 against pseudorabies virus both in vitro and in vivo. *Virology Journal* **2019**, *16*, 95.
316. Rodrigues, P.M.; Silva, T.S.; Dias, J.; Jessen, F. PROTEOMICS in aquaculture: Applications and trends. *Journal of Proteomics* **2012**, *75*, 4325-4345.
317. Ao, J.; Mu, Y.; Xiang, L.-X.; Fan, D.; Feng, M.; Zhang, S.; Shi, Q.; Zhu, L.-Y.; Li, T.; Ding, Y.; et al. Genome Sequencing of the Perciform Fish Larimichthys crocea Provides Insights into Molecular and Genetic Mechanisms of Stress Adaptation. *PLOS Genetics* **2015**, *11*, e1005118.
318. Carda-Diéguez, M.; Ghai, R.; Rodríguez-Valera, F.; Amaro, C. Wild eel microbiome reveals that skin mucus of fish could be a natural niche for aquatic mucosal pathogen evolution. *Microbiome* **2017**, *5*, 162.
319. Greer, J.B.; Andrzejczyk, N.E.; Mager, E.M.; Stieglitz, J.D.; Benetti, D.; Grosell, M.; Schlenk, D. Whole-Transcriptome Sequencing of Epidermal Mucus as a Novel Method for Oil Exposure Assessment in Juvenile Mahi-Mahi (Coryphaena hippurus). *Environmental Science & Technology Letters* **2019**, *6*, 538-544.
320. Parida, S.; Mohapatra, A.; Kar, B.; Mohanty, J.; Sahoo, P.K. Transcriptional analysis of immune-relevant genes in the mucus of Labeo rohita, experimentally infected with Argulus siamensis. **2018**, *63*, 125-133.
321. Nissa, M.U.; Pinto, N.; Parkar, H.; Goswami, M.; Srivastava, S. Proteomics in fisheries and aquaculture: An approach for food security. *Food Control* **2021**, *127*, 108125.
322. Minniti, G.; Rød Sandve, S.; Padra, J.T.; Heldal Hagen, L.; Lindén, S.; Pope, P.B.; Ø. Arntzen, M.; Vaaje-Kolstad, G. The Farmed Atlantic Salmon (Salmo salar) Skin–Mucus Proteome and Its Nutrient Potential for the Resident Bacterial Community. *Genes* **2019**, *10*, 515.

323. Liu, H.-h.; Sun, Q.; Jiang, Y.-t.; Fan, M.-h.; Wang, J.-x.; Liao, Z. In-depth proteomic analysis of Boleophthalmus pectinirostris skin mucus. *Journal of Proteomics* **2019**, *200*, 74-89.
324. Chong, K.; Sock Ying, T.; Foo, J.; Toong Jin, L.; Chong, A. Characterisation of proteins in epidermal mucus of discus fish (Symphysodon spp.) during parental phase. *Aquaculture* **2005**, *249*, 469-476.
325. Xiong, Y.; Dan, C.; Ren, F.; Su, Z.; Zhang, Y.; Mei, J. Proteomic profiling of yellow catfish (Pelteobagrus fulvidraco) skin mucus identifies differentially-expressed proteins in response to Edwardsiella ictaluri infection. *Fish & Shellfish Immunology* **2020**, *100*, 98-108.
326. Fernández-Montero, Á.; Torrecillas, S.; Montero, D.; Acosta, F.; Prieto-Álamo, M.-J.; Abril, N.; Jurado, J. Proteomic profile and protease activity in the skin mucus of greater amberjack (Seriola dumerili) infected with the ectoparasite Neobenedenia girellae — An immunological approach. *Fish & Shellfish Immunology* **2021**, *110*, 100-115.
327. Pérez-Sánchez, J.; Terova, G.; Simó-Mirabet, P.; Rimoldi, S.; Folkedal, O.; Calduch-Giner, J.A.; Olsen, R.E.; Sitjà-Bobadilla, A. Skin Mucus of Gilthead Sea Bream (Sparus aurata L.). Protein Mapping and Regulation in Chronically Stressed Fish. *Frontiers in Physiology* **2017**, *8*, 34.
328. Fæste, C.K.; Tartor, H.; Moen, A.; Kristoffersen, A.B.; Dhanasiri, A.K.S.; Anonsen, J.H.; Furmanek, T.; Grove, S. Proteomic profiling of salmon skin mucus for the comparison of sampling methods. *Journal of Chromatography B* **2020**, *1138*, 121965.
329. Goodacre, R.; Vaidyanathan, S.; Dunn, W.B.; Harrigan, G.G.; Kell, D.B. Metabolomics by numbers: acquiring and understanding global metabolite data. *Trends in Biotechnology* **2004**, *22*, 245-252.
330. Samuelsson, L.M.; Larsson, D.G.J. Contributions from metabolomics to fish research. *Molecular BioSystems* **2008**, *4*, 974-979.
331. Wen, B.; Zhou, J.-Q.; Gao, J.-Z.; Chen, H.-R.; Shen, Y.-Q.; Chen, Z.-Z. Sex-dependent changes in the skin mucus metabolome of discus fish (Symphysodon haraldi) during biparental care. *Journal of Proteomics* **2020**, *221*, 103784.
332. Ivanova, L.; Tartor, H.; Grove, S.; Kristoffersen, A.B.; Uhlig, S. Workflow for the Targeted and Untargeted Detection of Small Metabolites in Fish Skin Mucus. *Fishes* **2018**, *3*, 21.
333. Reyes-López, F.E.; Ibarz, A.; Ordóñez-Grande, B.; Vallejos-Vidal, E.; Andree, K.B.; Balasch, J.C.; Fernández-Alacid, L.; Sanahuja, I.; Sánchez-Nuño, S.; Firmino, J.P.; et al. Skin Multi-Omics-Based Interactome Analysis: Integrating the Tissue and Mucus Exuded Layer for a Comprehensive Understanding of the Teleost Mucosa Functionality as Model of Study. *Frontiers in Immunology* **2021**, *11*, 7054-7062.
334. Zhang, L.; Parente, J.; Harris Scott, M.; Woods Donald, E.; Hancock Robert, E.W.; Falla Timothy, J. Antimicrobial Peptide Therapeutics for Cystic Fibrosis. *Antimicrobial Agents and Chemotherapy* **2005**, *49*, 2921-2927.
335. Rai, M.; Pandit, R.; Gaikwad, S.; Kövics, G. Antimicrobial peptides as natural bio-preservative to enhance the shelf-life of food. *Journal of Food Science and Technology* **2016**, *53*, 3381-3394.
336. Al-Rasheed, A.; Handool, K.O.; Garba, B.; Noordin, M.M.; Bejo, S.K.; Kamal, F.M.; Daud, H.H.M. Crude extracts of epidermal mucus and epidermis of climbing perch *Anabas testudineus* and its antibacterial and hemolytic activities. *The Egyptian Journal of Aquatic Research* **2018**, *44*, 125-129.
337. Caruso, G.; Maricchiolo, G.; Genovese, L.; Pasquale, F.D.; Rosalba; Caruso; Denaro, M.G.; Delia, S.; Laganà, P. Comparative Study of Antibacterial and Haemolytic Activities in Sea Bass, European Eel and Blackspot Seabream. *The Open Marine Biology Journal* **2014**, *8*, 10-16.
338. Kumari, U.; Nigam, A.K.; Mittal, S.; Mittal, A.K. Antibacterial properties of the skin mucus of the freshwater fishes, *Rita rita* and *Channa punctatus*. *European Review for Medical and Pharmacological Sciences* **2011**, *15*, 781-786.
339. Elavarasi, K.; Ranjini, S.; Rajagopal, T.; Rameshkumar, G.; Ponmanickam, P. Bactericidal proteins of skin mucus and skin extracts from fresh water fishes, C*larias batrachus* and T*ilapia mossambicus Thai Journal of Pharmaceutical Sciences* **2013**, *37*, 194-200.
340. Magarinos, B.; Pazos, F.; Santos, Y.; Romalde, J.L.; Toranzo, A.E. Response of *Pasteurella piscicida* and *Flexibacter maritimus* to skin mucus of marine fish. *Diseases of Aquatic Organisms* **1995**, *21*, 103-108.
341. Manikantan, G.; Lyla, S.; Khan, S.A.; Vijayanand, P.; Jothi, G.E.G. Bioactive potency of epidermal mucus extracts from greasy grouper, Epinephelus tauvina (Forsskal, 1775). *Journal of Coastal Life Medicine* **2016**, *4*, 510-520.
342. Katra, N.; Hisar, O.; Yilmaz, S.; Turgay, E.; Sarvan, C.; Suheyla; Karatas. *In vitro* antimicrobial activities of extracts from ballan wrasse (*Labrus bergylta*) skin mucus. *Marine Science and Technology Bulletin* **2016**, *5*, 13-15.

343. García-Marciano, M.; Apún-Molina, J.P.; Sainz-Hernández, J.C.; Santamaría-Miranda, A.; Medina-Godoy, S.; Aguiñaga-Cruz, J.A. Antibacterial activity evaluation of the Nile tilapia O*reochromis niloticus* (Linnaeus, 1758) skin mucus, against V*ibrio* bacteria affecting the white shrimp P*enaeus vannamei*. *Latin American Journal of Aquatic Research* **2019**, *47*, 580-585.
344. Bergsson, G.; Agerberth, B.; Jörnvall, H.; Gudmundsson, G.H. Isolation and identification of antimicrobial components from the epidermal mucus of Atlantic cod (*Gadus morhua*). *The FEBS Journal* **2005**, *272*, 4960–4969.
345. Lirio, G.A.C.; Leon, J.A.A.D.; Villafuerte, A.G. Antimicrobial Activity of Epidermal Mucus from Top Aquaculture Fish Species against Medically-Important Pathogens. *Walailak Journal* **2018**, *16*, 329-340.
346. Patel, M.; Ashraf, M.S.; Siddiqui, A.J.; Ashraf, S.A.; Sachidanandan, M.; Snoussi, M.; Adnan, M.; Hadi, S. Profiling and Role of Bioactive Molecules from P*untius sophore (*Freshwater/Brackish Fish) Skin Mucus with Its Potent Antibacterial, Antiadhesion, and Antibiofilm Activities. *Biomolecules* **2020**, *10*, 920.
347. Jain, S.; Gupta, S.; Patiyal, S.; Raghava, G.P.S. THPdb2: compilation of FDA approved therapeutic peptides and proteins. *Drug Discovery Today* **2024**, *29*, 104047.
348. Usmani, S.S.; Bedi, G.; Samuel, J.S.; Singh, S.; Kalra, S.; Kumar, P.; Ahuja, A.A.; Sharma, M.; Gautam, A.; Raghava, G.P.S. THPdb: Database of FDA-approved peptide and protein therapeutics. *PLOS ONE* **2017**, *12*, e0181748.
349. Bhawani, S.A.; Husaini, A.; Ahmad, F.B.; Asaruddin, M.R. Polymer based protein therapeutics. *Current Protein and Peptide Science* **2018**, *19*, 972-982.
350. Iliopoulos, F.; Sil, B.C.; Evans, C.L. The role of excipients in promoting topical and transdermal delivery: Current limitations and future perspectives. *Frontiers in Drug Delivery* **2022**, *2*, 1049848.
351. Raina, N.; Rani, R.; Thakur, V.K.; Gupta, M. New Insights in Topical Drug Delivery for Skin Disorders: From a Nanotechnological Perspective. *ACS Omega* **2023**, *8*, 19145-19167.
352. Ji, Y.; Song, W.; Xu, L.; Yu, D.-G.; Annie Bligh, S.W. A Review on Electrospun Poly(amino acid) Nanofibers and Their Applications of Hemostasis and Wound Healing. *Biomolecules* **2022**, *12*, 794.
353. Law, J.X.; Liau, L.L.; Saim, A.; Yang, Y.; Idrus, R. Electrospun Collagen Nanofibers and Their Applications in Skin Tissue Engineering. *Tissue Engineering and Regenerative Medicine* **2017**, *14*, 699-718.
354. González de Torre, I.; Ibáñez-Fonseca, A.; Quintanilla, L.; Alonso, M.; Rodríguez-Cabello, J.-C. Random and oriented electrospun fibers based on a multicomponent, in situ clickable elastin-like recombinamer system for dermal tissue engineering. *Acta Biomaterialia* **2018**, *72*, 137-149.
355. Samadian, H.; Zamiri, S.; Ehterami, A.; Farzamfar, S.; Vaez, A.; Khastar, H.; Alam, M.; Ai, A.; Derakhshankhah, H.; Allahyari, Z.; et al. Electrospun cellulose acetate/gelatin nanofibrous wound dressing containing berberine for diabetic foot ulcer healing: in vitro and in vivo studies. *Scientific Reports* **2020**, *10*, 8312.
356. Serag, E.; El-Aziz, A.M.A.; El-Maghraby, A.; Taha, N.A. Electrospun non-wovens potential wound dressing material based on polyacrylonitrile/chicken feathers keratin nanofiber. *Scientific Reports* **2022**, *12*, 15460.
357. Bayazidi, P.; Almasi, H.; Asl, A.K. Immobilization of lysozyme on bacterial cellulose nanofibers: Characteristics, antimicrobial activity and morphological properties. *International Journal of Biological Macromolecules* **2018**, *107*, 2544-2551.
358. Park, J.-M.; Kim, M.; Park, H.-S.; Jang, A.; Min, J.; Kim, Y.-H. Immobilization of lysozyme-CLEA onto electrospun chitosan nanofiber for effective antibacterial applications. *International Journal of Biological Macromolecules* **2013**, *54*, 37-43.
359. Li, S.-F.; Chen, J.-P.; Wu, W.-T. Electrospun polyacrylonitrile nanofibrous membranes for lipase immobilization. *Journal of Molecular Catalysis B: Enzymatic* **2007**, *47*, 117-124.
360. Fazel, R.; Torabi, S.-F.; Naseri-Nosar, P.; Ghasempur, S.; Ranaei-Siadat, S.-O.; Khajeh, K. Electrospun polyvinyl alcohol/bovine serum albumin biocomposite membranes for horseradish peroxidase immobilization. *Enzyme and Microbial Technology* **2016**, *93-94*, 1-10.
361. Atik, G.; Kilic, N.M.; Horzum, N.; Odaci, D.; Timur, S. Antibody-Conjugated Electrospun Nanofibers for Electrochemical Detection of Methamphetamine. *ACS Applied Materials & Interfaces* **2023**, *15*, 24109-24119.
362. Homaeigohar, S.; Monavari, M.; Koenen, B.; Boccaccini, A.R. Biomimetic biohybrid nanofibers containing bovine serum albumin as a bioactive moiety for wound dressing. *Materials Science and Engineering: C* **2021**, *123*, 111965.

363. Ramprasath, R.; Jolius, G.; Praveen, R.; Balu, R.; Samala Murali Mohan, R.; Ganesh, S. Effect of Solution Properties and Operating Parameters on Needleless Electrospinning of Poly(Ethylene Oxide) Nanofibers Loaded with Bovine Serum Albumin. *Current Drug Delivery* **2019**, *16*, 913-922.
364. Chipman, D.M.; Sharon, N. Mechanism of Lysozyme Action. *Science* **1969**, *165*, 454-465.
365. Briggs, T.; Arinzeh, T.L. Examining the formulation of emulsion electrospinning for improving the release of bioactive proteins from electrospun fibers. *Journal of Biomedical Materials Research Part A* **2014**, *102*, 674-684.
366. Zalipsky, S.; Harris, J.M. Introduction to Chemistry and Biological Applications of Poly(ethylene glycol). In *Poly(ethylene glycol)*; ACS Symposium Series; American Chemical Society: 1997.
367. Graessley, W.W. The entanglement concept in polymer rheology. In *The Entanglement Concept in Polymer Rheology*; Springer Berlin Heidelberg: Berlin, Heidelberg, 1974; pp. 1-179.
368. Nie, H.; He, A.; Wu, W.; Zheng, J.; Xu, S.; Li, J.; Han, C.C. Effect of poly(ethylene oxide) with different molecular weights on the electrospinnability of sodium alginate. *Polymer* **2009**, *50*, 4926-4934.
369. Liu, S.L.; Shao, L.; Chua, M.L.; Lau, C.H.; Wang, H.; Quan, S. Recent progress in the design of advanced PEO-containing membranes for CO_2 removal. *Progress in Polymer Science* **2013**, *38*, 1089-1120.
370. Mira, A.; Mateo, C.R.; Mallavia, R.; Falco, A. Poly(methyl vinyl ether-alt-maleic acid) and ethyl monoester as building polymers for drug-loadable electrospun nanofibers. *Scientific Reports* **2017**, *7*, 17205.
371. Mira, A.; Sainz-Urruela, C.; Codina, H.; Jenkins, S.I.; Rodriguez-Diaz, J.C.; Mallavia, R.; Falco, A. Physico-Chemically Distinct Nanomaterials Synthesized from Derivates of a Poly(Anhydride) Diversify the Spectrum of Loadable Antibiotics. *Nanomaterials* **2020**, *10*, 486.
372. Jiang, H.; Hu, Y.; Li, Y.; Zhao, P.; Zhu, K.; Chen, W. A facile technique to prepare biodegradable coaxial electrospun nanofibers for controlled release of bioactive agents. *Journal of Controlled Release* **2005**, *108*, 237-243.
373. Schönfeld, A.; Constantinescu, M.; Peters, K.; Frenz, M. Electrospinning of highly concentrated albumin patches by using auxiliary polymers for laser-assisted vascular anastomosis. *Biomedical Materials* **2018**, *13*, 055001.
374. Fong, H.; Chun, I.; Reneker, D.H. Beaded nanofibers formed during electrospinning. *Polymer* **1999**, *40*, 4585-4592.
375. Panić, J.; Vraneš, M.; Mirtič, J.; Cerc Korošec, R.; Zupančič, Š.; Gadžurić, S.; Kristl, J.; Bešter-Rogač, M. Preparation and characterization of innovative electrospun nanofibers loaded with pharmaceutically applicable ionic liquids. *International Journal of Pharmaceutics* **2022**, *615*, 121510.
376. Serôdio, R.; Schickert, S.L.; Costa-Pinto, A.R.; Dias, J.R.; Granja, P.L.; Yang, F.; Oliveira, A.L. Ultrasound sonication prior to electrospinning tailors silk fibroin/PEO membranes for periodontal regeneration. *Materials Science and Engineering: C* **2019**, *98*, 969-981.
377. Bloustine, J.; Virmani, T.; Thurston, G.M.; Fraden, S. Light Scattering and Phase Behavior of Lysozyme-Poly(Ethylene Glycol) Mixtures. *Physical Review Letters* **2006**, *96*, 087803.
378. Zaman, A.A.; Moudgil, B.M. Role of Electrostatic Repulsion on the Viscosity of Bidisperse Silica Suspensions. *Journal of Colloid and Interface Science* **1999**, *212*, 167-175.
379. Zhang, H.; Xi, S.; Han, Y.; Liu, L.; Dong, B.; Zhang, Z.; Chen, Q.; Min, W.; Huang, Q.; Li, Y.; et al. Determining electrospun morphology from the properties of protein–polymer solutions. *Soft Matter* **2018**, *14*, 3455-3462.
380. Angammana, C.J.; Jayaram, S.H. Analysis of the Effects of Solution Conductivity on Electrospinning Process and Fiber Morphology. *IEEE Transactions on Industry Applications* **2011**, *47*, 1109-1117.
381. Ewaldz, E.; Randrup, J.; Brettmann, B. Solvent Effects on the Elasticity of Electrospinnable Polymer Solutions. *ACS Polymers Au* **2022**, *2*, 108-117.
382. Brown, C.E. Coefficient of Variation. In *Applied Multivariate Statistics in Geohydrology and Related Sciences*, Brown, C.E., Ed.; Springer Berlin Heidelberg: Berlin, Heidelberg, 1998; pp. 155-157.
383. Kowalczyk, T.; Nowicka, A.; Elbaum, D.; Kowalewski, T.A. Electrospinning of Bovine Serum Albumin. Optimization and the Use for Production of Biosensors. *Biomacromolecules* **2008**, *9*, 2087-2090.
384. Al-Shamari, A.A.; Abdelghany, A.M.; Alnattar, H.; Oraby, A.H. Structural and optical properties of PEO/CMC polymer blend modified with gold nanoparticles synthesized by laser ablation in water. *Journal of Materials Research and Technology* **2021**, *12*, 1597-1605.

385. Pan, C.-Y.; Chen, J.-C.; Chen, T.-L.; Wu, J.-L.; Hui, C.-F.; Chen, J.-Y. Piscidin is Highly Active against Carbapenem-Resistant Acinetobacter baumannii and NDM-1-Producing Klebsiella pneumonia in a Systemic Septicaemia Infection Mouse Model. *Marine Drugs* **2015**, *13*, 2287-2305.
386. Valmikinathan, C.M.; Defroda, S.; Yu, X. Polycaprolactone and Bovine Serum Albumin Based Nanofibers for Controlled Release of Nerve Growth Factor. *Biomacromolecules* **2009**, *10*, 1084-1089.
387. Xu, X.; Yu, H.; Gao, S.; Mao, H.-Q.; Leong, K.W.; Wang, S. Polyphosphoester microspheres for sustained release of biologically active nerve growth factor. *Biomaterials* **2002**, *23*, 3765-3772.
388. Montalbano, G.; Tomasina, C.; Fiorilli, S.; Camarero-Espinosa, S.; Vitale-Brovarone, C.; Moroni, L. Biomimetic Scaffolds Obtained by Electrospinning of Collagen-Based Materials: Strategies to Hinder the Protein Denaturation. *Materials* **2021**, *14*, 4360.
389. Cao, E.; Chen, Y.; Cui, Z.; Foster, P.R. Effect of freezing and thawing rates on denaturation of proteins in aqueous solutions. *Biotechnology and Bioengineering* **2003**, *82*, 684-690.
390. Bs, C.; Rr, M. Enzyme thermostabilization by bovine serum albumin and other proteins: evidence for hydrophobic interactions. *Biotechnology and Applied Biochemistry* **1995**, *22*, 203-214.
391. Duskey, J.T.; da Ros, F.; Ottonelli, I.; Zambelli, B.; Vandelli, M.A.; Tosi, G.; Ruozi, B. Enzyme Stability in Nanoparticle Preparations Part 1: Bovine Serum Albumin Improves Enzyme Function. *Molecules* **2020**, *25*, 4593.
392. Gulati, B.K.; Sharma, S.; Vardhana Rao, M.V. Analyzing the Changes in Certain Infectious and Parasitic Diseases in Urban Population of India By Using Medical Certification of Cause of Death Data. *Indian Journal of Community Medicine* **2021**, *46*, 20-23.
393. Deeks, S.G.; Overbaugh, J.; Phillips, A.; Buchbinder, S. HIV infection. *Nature Reviews Disease Primers* **2015**, *1*, 15035.
394. Jacob, S.T.; Crozier, I.; Fischer, W.A.; Hewlett, A.; Kraft, C.S.; Vega, M.-A.d.L.; Soka, M.J.; Wahl, V.; Griffiths, A.; Bollinger, L.; et al. Ebola virus disease. *Nature Reviews Disease Primers* **2020**, *6*, 13.
395. Mohsen, M.O.; Rothen, D.; Balke, I.; Martina, B.; Zeltina, V.; Inchakalody, V.; Gharailoo, Z.; Nasrallah, G.; Dermime, S.; Tars, K.; et al. Neutralization of MERS coronavirus through a scalable nanoparticle vaccine. *npj Vaccines* **2021**, *6*, 107.
396. Andersen, K.G.; Rambaut, A.; Lipkin, W.I.; Holmes, E.C.; Garry, R.F. The proximal origin of SARS-CoV-2. *Nature Medicine* **2020**, *26*, 450-452.
397. WHO. WHO Coronavirus (COVID-19) Dashboard. Available online: https://covid19.who.int/ (accessed on 5 October 2022).
398. Leung, N.H.L. Transmissibility and transmission of respiratory viruses. *Nature Reviews Microbiology* **2021**, *19*, 528-545.
399. Castaño, N.; Cordts, S.C.; Kurosu Jalil, M.; Zhang, K.S.; Koppaka, S.; Bick, A.D.; Paul, R.; Tang, S.K.Y. Fomite Transmission, Physicochemical Origin of Virus–Surface Interactions, and Disinfection Strategies for Enveloped Viruses with Applications to SARS-CoV-2. *ACS Omega* **2021**, *6*, 6509-6527.
400. Ganime, A.C.; Carvalho-Costa, F.A.; Santos, M.; Costa Filho, R.; Leite, J.P.G.; Miagostovich, M.P. Viability of human adenovirus from hospital fomites. *Journal of Medical Virology* **2014**, *86*, 2065-2069.
401. Ganime, A.C.; Leite, J.P.G.; Figueiredo, C.E.d.S.; Carvalho-Costa, F.A.; Melgaço, F.G.; Malta, F.C.; Fumian, T.M.; Miagostovich, M.P. Dissemination of human adenoviruses and rotavirus species A on fomites of hospital pediatric units. *American Journal of Infection Control* **2016**, *44*, 1411-1413.
402. Gralton, J.; McLaws, M.-L.; Rawlinson, W.D. Personal clothing as a potential vector of respiratory virus transmission in childcare settings. *Journal of Medical Virology* **2015**, *87*, 925-930.
403. Canales, R.A.; Reynolds, K.A.; Wilson, A.M.; Fankem, S.L.M.; Weir, M.H.; Rose, J.B.; Abd-Elmaksoud, S.; Gerba, C.P. Modeling the role of fomites in a norovirus outbreak. *Journal of Occupational and Environmental Hygiene* **2019**, *16*, 16-26.
404. Asadi, S.; Gaaloul ben Hnia, N.; Barre, R.S.; Wexler, A.S.; Ristenpart, W.D.; Bouvier, N.M. Influenza A virus is transmissible via aerosolized fomites. *Nature Communications* **2020**, *11*, 4062.
405. Dowell, S.F.; Simmerman, J.M.; Erdman, D.D.; Wu, J.-S.J.; Chaovavanich, A.; Javadi, M.; Yang, J.-Y.; Anderson, L.J.; Tong, S.; Ho, M.S. Severe Acute Respiratory Syndrome Coronavirus on Hospital Surfaces. *Clinical Infectious Diseases* **2004**, *39*, 652-657.

406. Otter, J.A.; Donskey, C.; Yezli, S.; Douthwaite, S.; Goldenberg, S.D.; Weber, D.J. Transmission of SARS and MERS coronaviruses and influenza virus in healthcare settings: the possible role of dry surface contamination. *Journal of Hospital Infection* **2016**, *92*, 235-250.
407. Kraay, A.N.M.; Hayashi, M.A.L.; Berendes, D.M.; Sobolik, J.S.; Leon, J.S.; Lopman, B.A. Risk of fomite-mediated transmission of SARS-CoV-2 in child daycares, schools, and offices: a modeling study. *medRxiv* **2020**, *27*, 1229-1231.
408. Bushman, F.D.; McCormick, K.; Sherrill-Mix, S. Virus structures constrain transmission modes. *Nature Microbiology* **2019**, *4*, 1778-1780.
409. Leclercq, L.; Nardello-Rataj, V. A New Synergistic Strategy for Virus and Bacteria Eradication: Towards Universal Disinfectants. *Pharmaceutics* **2022**, *14*, doi:10.3390/pharmaceutics14122791.
410. Kasloff, S.B.; Leung, A.; Strong, J.E.; Funk, D.; Cutts, T. Stability of SARS-CoV-2 on critical personal protective equipment. *Scientific Reports* **2021**, *11*, 984.
411. Bello-Perez, M.; Esparza, I.; De la Encina, A.; Bartolome, T.; Molina, T.; Sanjuan, E.; Falco, A.; Enjuanes, L.; Sola, I.; Usera, F. Pulsed-Xenon Ultraviolet Light Highly Inactivates Human Coronaviruses on Solid Surfaces, Particularly SARS-CoV-2. *International Journal of Environmental Research and Public Health* **2022**, *19*, 13780.
412. Alizadeh, F.; Khodavandi, A. Systematic Review and Meta-Analysis of the Efficacy of Nanoscale Materials Against Coronaviruses—Possible Potential Antiviral Agents for SARS-CoV-2. *IEEE Transactions on NanoBioscience* **2020**, *19*, 485-497.
413. Weiss, C.; Carriere, M.; Fusco, L.; Capua, I.; Regla-Nava, J.A.; Pasquali, M.; Scott, J.A.; Vitale, F.; Unal, M.A.; Mattevi, C.; et al. Toward Nanotechnology-Enabled Approaches against the COVID-19 Pandemic. *ACS Nano* **2020**, *14*, 6383-6406.
414. Galdiero, S.; Falanga, A.; Vitiello, M.; Cantisani, M.; Marra, V.; Galdiero, M. Silver Nanoparticles as Potential Antiviral Agents. *Molecules* **2011**, *16*, 8894-8918, doi:10.3390/molecules16108894.
415. Morris, D.; Ansar, M.; Speshock, J.; Ivanciuc, T.; Qu, Y.; Casola, A.; Garofalo, R.P. Antiviral and Immunomodulatory Activity of Silver Nanoparticles in Experimental RSV Infection. *Viruses* **2019**, *11*, 732.
416. Jeremiah, S.S.; Miyakawa, K.; Morita, T.; Yamaoka, Y.; Ryo, A. Potent antiviral effect of silver nanoparticles on SARS-CoV-2. *Biochemical and Biophysical Research Communications* **2020**, *533*, 195-200.
417. Almanza-Reyes, H.; Moreno, S.; Plascencia-López, I.; Alvarado-Vera, M.; Patrón-Romero, L.; Borrego, B.; Reyes-Escamilla, A.; Valencia-Manzo, D.; Brun, A.; Pestryakov, A.; et al. Evaluation of silver nanoparticles for the prevention of SARS-CoV-2 infection in health workers: In vitro and in vivo. *PLOS ONE* **2021**, *16*, e0256401.
418. Chen, L.; Liang, J. An overview of functional nanoparticles as novel emerging antiviral therapeutic agents. *Materials Science and Engineering: C* **2020**, *112*, 110924.
419. Alshabanah, L.A.; Hagar, M.; Al-Mutabagani, L.A.; Abozaid, G.M.; Abdallah, S.M.; Shehata, N.; Ahmed, H.; Hassanin, A.H. Hybrid Nanofibrous Membranes as a Promising Functional Layer for Personal Protection Equipment: Manufacturing and Antiviral/Antibacterial Assessments. *Polymers* **2021**, *13*, 1776.
420. Xu, T.; Shen, W.; Lin, X.; Xie, Y.M. Mechanical Properties of Additively Manufactured Thermoplastic Polyurethane (TPU) Material Affected by Various Processing Parameters. *Polymers* **2020**, *12*, 3010.
421. Bello-Perez, M.; Pereiro, P.; Coll, J.; Novoa, B.; Perez, L.; Falco, A. Zebrafish C-reactive protein isoforms inhibit SVCV replication by blocking autophagy through interactions with cell membrane cholesterol. *Scientific Reports* **2020**, *10*, 566.
422. Danaei, M.; Dehghankhold, M.; Ataei, S.; Hasanzadeh Davarani, F.; Javanmard, R.; Dokhani, A.; Khorasani, S.; Mozafari, M.R. Impact of Particle Size and Polydispersity Index on the Clinical Applications of Lipidic Nanocarrier Systems. *Pharmaceutics* **2018**, *10*, 57.
423. Leo, B.F.; Chen, S.; Kyo, Y.; Herpoldt, K.-L.; Terrill, N.J.; Dunlop, I.E.; McPhail, D.S.; Shaffer, M.S.; Schwander, S.; Gow, A.; et al. The Stability of Silver Nanoparticles in a Model of Pulmonary Surfactant. *Environmental Science & Technology* **2013**, *47*, 11232-11240.
424. Römer, I.; White, T.A.; Baalousha, M.; Chipman, K.; Viant, M.R.; Lead, J.R. Aggregation and dispersion of silver nanoparticles in exposure media for aquatic toxicity tests. *Journal of Chromatography A* **2011**, *1218*, 4226-4233.
425. Lukina, Y.; Kotov, S.; Bionyshev-Abramov, L.; Serejnikova, N.; Chelmodeev, R.; Fadeev, R.; Toshev, O.; Tavtorkin, A.; Ryndyk, M.; Smolentsev, D.; et al. Low-Temperature Magnesium Calcium Phosphate Ceramics with Adjustable Resorption Rate. *Ceramics* **2023**, *6*, 168-194.

426. Kumar, V.; Sarkar, K.; Bavya Devi, K.; Ghosh, D.; Nandi, S.K.; Roy, M. Quantitative assessment of degradation, cytocompatibility, and in vivo bone regeneration of silicon-incorporated magnesium phosphate bioceramics. *Journal of Materials Research* **2019**, *34*, 4024-4036.
427. Akter, M.; Sikder, M.T.; Rahman, M.M.; Ullah, A.K.M.A.; Hossain, K.F.B.; Banik, S.; Hosokawa, T.; Saito, T.; Kurasaki, M. A systematic review on silver nanoparticles-induced cytotoxicity: Physicochemical properties and perspectives. *Journal of Advanced Research* **2018**, *9*, 1-16.
428. Samberg, M.E.; Loboa, E.G.; Oldenburg, S.J.; Monteiro-Riviere, N.A. Silver Nanoparticles Do Not Influence Stem Cell Differentiation But Cause Minimal Toxicity. *Nanomedicine* **2012**, *7*, 1197-1209.
429. Carrola, J.; Bastos, V.; Jarak, I.; Oliveira-Silva, R.; Malheiro, E.; Daniel-da-Silva, A.L.; Oliveira, H.; Santos, C.; Gil, A.M.; Duarte, I.F. Metabolomics of silver nanoparticles toxicity in HaCaT cells: structure–activity relationships and role of ionic silver and oxidative stress. *Nanotoxicology* **2016**, *10*, 1105-1117.
430. Rogers, J.V.; Parkinson, C.V.; Choi, Y.W.; Speshock, J.L.; Hussain, S.M. A Preliminary Assessment of Silver Nanoparticle Inhibition of Monkeypox Virus Plaque Formation. *Nanoscale Research Letters* **2008**, *3*, 129.
431. Feng, D.; Zhang, R.; Zhang, M.; Fang, A.; Shi, F. Synthesis of Eco-Friendly Silver Nanoparticles Using Glycyrrhizin and Evaluation of Their Antibacterial Ability. *Nanomaterials* **2022**, *12*, 2636.
432. Chang, X.; Wang, X.; Li, J.; Shang, M.; Niu, S.; Zhang, W.; Li, Y.; Sun, Z.; Gan, J.; Li, W.; et al. Silver nanoparticles induced cytotoxicity in HT22 cells through autophagy and apoptosis via PI3K/AKT/mTOR signaling pathway. *Ecotoxicology and Environmental Safety* **2021**, *208*, 111696.
433. Tortella, G.R.; Rubilar, O.; Durán, N.; Diez, M.C.; Martínez, M.; Parada, J.; Seabra, A.B. Silver nanoparticles: Toxicity in model organisms as an overview of its hazard for human health and the environment. *Journal of Hazardous Materials* **2020**, *390*, 121974.
434. Szymańska, E.; Orłowski, P.; Winnicka, K.; Tomaszewska, E.; Bąska, P.; Celichowski, G.; Grobelny, J.; Basa, A.; Krzyżowska, M. Multifunctional Tannic Acid/Silver Nanoparticle-Based Mucoadhesive Hydrogel for Improved Local Treatment of HSV Infection: In Vitro and In Vivo Studies. *International Journal of Molecular Sciences* **2018**, *19*, 387.
435. Elechiguerra, J.L.; Burt, J.L.; Morones, J.R.; Camacho-Bragado, A.; Gao, X.; Lara, H.H.; Yacaman, M.J. Interaction of silver nanoparticles with HIV-1. *Journal of Nanobiotechnology* **2005**, *3*, 6.
436. Mori, Y.; Ono, T.; Miyahira, Y.; Nguyen, V.Q.; Matsui, T.; Ishihara, M. Antiviral activity of silver nanoparticle/chitosan composites against H1N1 influenza A virus. *Nanoscale Research Letters* **2013**, *8*, 93.
437. Saadh, M. Potent antiviral effect of green synthesis silver nanoparticles on Newcastle disease virus. *Arabian Journal of Chemistry* **2022**, *15*, 103899.
438. Kittler, S.; Greulich, C.; Diendorf, J.; Köller, M.; Epple, M. Toxicity of Silver Nanoparticles Increases during Storage Because of Slow Dissolution under Release of Silver Ions. *Chemistry of Materials* **2010**, *22*, 4548-4554.
439. Liu, J.; Sonshine, D.A.; Shervani, S.; Hurt, R.H. Controlled Release of Biologically Active Silver from Nanosilver Surfaces. *ACS Nano* **2010**, *4*, 6903-6913.
440. Zhang, W.; Yao, Y.; Sullivan, N.; Chen, Y. Modeling the Primary Size Effects of Citrate-Coated Silver Nanoparticles on Their Ion Release Kinetics. *Environmental Science & Technology* **2011**, *45*, 4422-4428.
441. Huemer, M.; Mairpady Shambat, S.; Brugger, S.D.; Zinkernagel, A.S. Antibiotic resistance and persistence—Implications for human health and treatment perspectives. *EMBO reports* **2020**, *21*, e51034.
442. Malik, B.; Bhattacharyya, S. Antibiotic drug-resistance as a complex system driven by socio-economic growth and antibiotic misuse. *Scientific Reports* **2019**, *9*, 9788.
443. Hays, J.P.; Ruiz-Alvarez, M.J.; Roson-Calero, N.; Amin, R.; Murugaiyan, J.; van Dongen, M.B.M.; the Global, A.M.R.I.A.N. Perspectives on the Ethics of Antibiotic Overuse and on the Implementation of (New) Antibiotics. *Infectious Diseases and Therapy* **2022**, *11*, 1315-1326.
444. Avershina, E.; Shapovalova, V.; Shipulin, G. Fighting Antibiotic Resistance in Hospital-Acquired Infections: Current State and Emerging Technologies in Disease Prevention, Diagnostics and Therapy. *Frontiers in Microbiology* **2021**, *12*, 707330.
445. Larsson, D.G.J.; Flach, C.-F. Antibiotic resistance in the environment. *Nature Reviews Microbiology* **2022**, *20*, 257-269.
446. van Vuuren, S.; Viljoen, A. Plant-based antimicrobial studies–methods and approaches to study the interaction between natural products. *Planta medica* **2011**, *77*, 1168-1182.

447. Jubair, N.; Rajagopal, M.; Chinnappan, S.; Abdullah, N.B.; Fatima, A. Review on the Antibacterial Mechanism of Plant-Derived Compounds against Multidrug-Resistant Bacteria (MDR). *Evidence-Based Complementary and Alternative Medicine* **2021**, *2021*, 3663315.
448. Tapsell, L.C.; Hemphill, I.; Cobiac, L.; Sullivan, D.R.; Fenech, M.; Patch, C.S.; Roodenrys, S.; Keogh, J.B.; Clifton, P.M.; Williams, P.G.; et al. Health benefits of herbs and spices: the past, the present, the future. *Medical Journal of Australia* **2006**, *185*, 1-24.
449. Barani, M.; Zeeshan, M.; Kalantar-Neyestanaki, D.; Farooq, M.A.; Rahdar, A.; Jha, N.K.; Sargazi, S.; Gupta, P.K.; Thakur, V.K. Nanomaterials in the Management of Gram-Negative Bacterial Infections. *Nanomaterials* **2021**, *11*, 2535.
450. Hamdan, N.; Yamin, A.; Hamid, S.A.; Khodir, W.K.; Guarino, V. Functionalized Antimicrobial Nanofibers: Design Criteria and Recent Advances. *Journal of Functional Biomaterials* **2021**, *12*, 59.
451. Spizzirri, U.G.; Aiello, F.; Carullo, G.; Facente, A.; Restuccia, D. Nanotechnologies: An Innovative Tool to Release Natural Extracts with Antimicrobial Properties. *Pharmaceutics* **2021**, *13*, 230.
452. Zielińska, A.; Carreiró, F.; Oliveira, A.M.; Neves, A.; Pires, B.; Venkatesh, D.N.; Durazzo, A.; Lucarini, M.; Eder, P.; Silva, A.M.; et al. Polymeric Nanoparticles: Production, Characterization, Toxicology and Ecotoxicology. *Molecules* **2020**, *25*, 3731.
453. Mira, A.; Rubio-Camacho, M.; Alarcón, D.; Rodríguez-Cañas, E.; Fernández-Carvajal, A.; Falco, A.; Mallavia, R. L-Menthol-Loadable Electrospun Fibers of PMVEMA Anhydride for Topical Administration. *Pharmaceutics* **2021**, *13*, 1845.
454. Vaou, N.; Stavropoulou, E.; Voidarou, C.; Tsigalou, C.; Bezirtzoglou, E. Towards Advances in Medicinal Plant Antimicrobial Activity: A Review Study on Challenges and Future Perspectives. *Microorganisms* **2021**, *9*, doi:10.3390/microorganisms9102041.
455. Francisco Javier, Á.-M.; Enrique, B.-C.; José Antonio, E.; Juan Carlos, R.-D.; Vicente, M. Antimicrobial Capacity of Plant Polyphenols against Gram-positive Bacteria: A Comprehensive Review. *Current Medicinal Chemistry* **2020**, *27*, 2576-2606.
456. Dimech, G.S.; Soares, L.A.L.; Ferreira, M.A.; de Oliveira, A.G.V.; Carvalho, M.d.C.; Ximenes, E.A. Phytochemical and Antibacterial Investigations of the Extracts and Fractions from the Stem Bark of Hymenaea stigonocarpa Mart. ex Hayne and Effect on Ultrastructure of Staphylococcus aureus Induced by Hydroalcoholic Extract. *The Scientific World Journal* **2013**, *2013*, 862763.
457. Meng, X.; Li, D.; Zhou, D.; Wang, D.; Liu, Q.; Fan, S. Chemical composition, antibacterial activity and related mechanism of the essential oil from the leaves of Juniperus rigida Sieb. et Zucc against Klebsiella pneumoniae. *Journal of Ethnopharmacology* **2016**, *194*, 698-705.
458. Tiwari, V. Molecular insight into the therapeutic potential of phytoconstituents targeting protein conformation and their expression. *Phytomedicine* **2019**, *52*, 225-237.
459. Kim, G.; Xu, Y.; Zhang, J.; Sui, Z.; Corke, H. Antibacterial Activity and Multi-Targeting Mechanism of Dehydrocorydaline From Corydalis turtschaninovii Bess. Against Listeria monocytogenes. *Frontiers in Microbiology* **2022**, *12*, 799094.
460. Hatano, T.; Kusuda, M.; Inada, K.; Ogawa, T.-o.; Shiota, S.; Tsuchiya, T.; Yoshida, T. Effects of tannins and related polyphenols on methicillin-resistant Staphylococcus aureus. *Phytochemistry* **2005**, *66*, 2047-2055.
461. Sousa, V.; Luís, Â.; Oleastro, M.; Domingues, F.; Ferreira, S. Polyphenols as resistance modulators in Arcobacter butzleri. *Folia Microbiologica* **2019**, *64*, 547-554.
462. Wright, G.D. Antibiotic Adjuvants: Rescuing Antibiotics from Resistance. *Trends in Microbiology* **2016**, *24*, 862-871.
463. Khameneh, B.; Eskin, N.A.M.; Iranshahy, M.; Fazly Bazzaz, B.S. Phytochemicals: A Promising Weapon in the Arsenal against Antibiotic-Resistant Bacteria. *Antibiotics* **2021**, *10*, 1044.
464. Kumar, M.; Jaiswal, S.; Sodhi, K.K.; Shree, P.; Singh, D.K.; Agrawal, P.K.; Shukla, P. Antibiotics bioremediation: Perspectives on its ecotoxicity and resistance. *Environment International* **2019**, *124*, 448-461.
465. Bhattacharya, S.; Paul, S.M.N. Efficacy of phytochemicals as immunomodulators in managing COVID-19: a comprehensive view. *VirusDisease* **2021**, *32*, 435-445.
466. Ait-Ouazzou, A.; Espina, L.; Gelaw, T.K.; de Lamo-Castellví, S.; Pagán, R.; García-Gonzalo, D. New insights in mechanisms of bacterial inactivation by carvacrol. *Journal of Applied Microbiology* **2013**, *114*, 173-185.
467. Brooker, J.D.; O'Donovan, L.A.; Skene, I.; Clarke, K.; Blackall, L.; Muslera, P. Streptococcus caprinus sp.nov., a tannin-resistant ruminal bacterium from feral goats. *Letters in Applied Microbiology* **1994**, *18*, 313-318.

468. Butler, L.G. Antinutritional Effects of Condensed and Hydrolyzable Tannins. In *Plant Polyphenols: Synthesis, Properties, Significance*, Hemingway, R.W., Laks, P.E., Eds.; Springer US: Boston, MA, 1992; pp. 693-698.
469. Smith, A.H.; Zoetendal, E.; Mackie, R.I. Bacterial Mechanisms to Overcome Inhibitory Effects of Dietary Tannins. *Microbial Ecology* **2005**, *50*, 197-205.
470. Monagas, M.; Urpi-Sarda, M.; Sánchez-Patán, F.; Llorach, R.; Garrido, I.; Gómez-Cordovés, C.; Andres-Lacueva, C.; Bartolomé, B. Insights into the metabolism and microbial biotransformation of dietary flavan-3-ols and the bioactivity of their metabolites. *Food & Function* **2010**, *1*, 233-253.
471. Gupta, P.D.; Birdi, T.J. Development of botanicals to combat antibiotic resistance. *Journal of Ayurveda and Integrative Medicine* **2017**, *8*, 266-275.
472. Warnke, P.H.; Becker, S.T.; Podschun, R.; Sivananthan, S.; Springer, I.N.; Russo, P.A.J.; Wiltfang, J.; Fickenscher, H.; Sherry, E. The battle against multi-resistant strains: Renaissance of antimicrobial essential oils as a promising force to fight hospital-acquired infections. *Journal of Cranio-Maxillofacial Surgery* **2009**, *37*, 392-397.
473. Álvarez-Martínez, F.J.; Barrajón-Catalán, E.; Micol, V. Tackling Antibiotic Resistance with Compounds of Natural Origin: A Comprehensive Review. *Biomedicines* **2020**, *8*, 405.
474. Di Lorenzo, C.; Colombo, F.; Biella, S.; Stockley, C.; Restani, P. Polyphenols and Human Health: The Role of Bioavailability. *Nutrients* **2021**, *13*, 273.
475. Hassanzadeh, K.; Buccarello, L.; Dragotto, J.; Mohammadi, A.; Corbo, M.; Feligioni, M. Obstacles against the Marketing of Curcumin as a Drug. *International Journal of Molecular Sciences* **2020**, *21*, 6619.
476. Manjula, V.; Akhilendra, K.M. Quercetin Loaded Nanoparticles in Targeting Cancer: Recent Development. *Anti-Cancer Agents in Medicinal Chemistry* **2019**, *19*, 1560-1576.
477. Erick José, T.-M.; José Manuel Cornejo, B.; Aracely Serrano, M.; Graciela Lizeth Pérez, G.; Luis Jesús Villarreal, G. A Summary of Electrospun Nanofibers as Drug Delivery System: Drugs Loaded and Biopolymers Used as Matrices. *Current Drug Delivery* **2018**, *15*, 1360-1374.
478. Martínez-Ortega, L.; Mira, A.; Fernandez-Carvajal, A.; Mateo, C.R.; Mallavia, R.; Falco, A. Development of A New Delivery System Based on Drug-Loadable Electrospun Nanofibers for Psoriasis Treatment. *Pharmaceutics* **2019**, *11*, 14.
479. Nemati, S.; Kim, S.-j.; Shin, Y.M.; Shin, H. Current progress in application of polymeric nanofibers to tissue engineering. *Nano Convergence* **2019**, *6*, 36.
480. Sundarrajan, S.; Tan, K.L.; Lim, S.H.; Ramakrishna, S. Electrospun Nanofibers for Air Filtration Applications. *Procedia Engineering* **2014**, *75*, 159-163.
481. Wei, J.; Geng, S.; Pitkänen, O.; Järvinen, T.; Kordas, K.; Oksman, K. Green Carbon Nanofiber Networks for Advanced Energy Storage. *ACS Applied Energy Materials* **2020**, *3*, 3530-3540.
482. Baji, A.; Agarwal, K.; Oopath, S.V. Emerging Developments in the Use of Electrospun Fibers and Membranes for Protective Clothing Applications. *Polymers* **2020**, *12*, 492.
483. Asgari, S.; Mohammadi Ziarani, G.; Badiei, A.; Ajalloueian, F.; Vasseghian, Y. Electrospun composite nanofibers as novel high-performance and visible-light photocatalysts for removal of environmental pollutants: A review. *Environmental Research* **2022**, *215*, 114296.
484. Lou, L.; Osemwegie, O.; Ramkumar, S.S. Functional Nanofibers and Their Applications. *Industrial & Engineering Chemistry Research* **2020**, *59*, 5439-5455.
485. Falco, A.; Mallavia, R. Electrospun Nanomaterials: Applications in Food, Environmental Remediation, and Bioengineering. *Nanomaterials* **2020**, *10*, 1714.
486. Bharathi, S.K.V.; Murugesan, P.; Moses, J.A.; Anandharamakrishnan, C. Recent trends in nanocomposite packaging materials. In *Reference Module in Food Science*, Knoerzer, K.; Muthukumarappan, K.; Eds., Elsevier: 2021; pp. 731-755.
487. Choi, H.-J.; Kumita, M.; Hayashi, S.; Yuasa, H.; Kamiyama, M.; Seto, T.; Tsai, C.-J.; Otani, Y. Filtration Properties of Nanofiber/Microfiber Mixed Filter and Prediction of its Performance. *Aerosol and Air Quality Research* **2017**, *17*, 1052-1062.
488. Sista, D. New perspective of nano fibers: synthesis and applications. In *Nanofibers-Synthesis, Properties and Applications*, Kumar, B., Ed., Intechopen: 2021.
489. Hoang Thi, T.T.; Pilkington, E.H.; Nguyen, D.H.; Lee, J.S.; Park, K.D.; Truong, N.P. The Importance of Poly(ethylene glycol) Alternatives for Overcoming PEG Immunogenicity in Drug Delivery and Bioconjugation. *Polymers* **2020**, *12*, 298.
490. Singh, R.; Mehrotra, T.; Bisaria, K.; Sinha, S. Environmental hazards and biodegradation of plastic waste: Challenges and future prospects. *Bioremediation for environmental sustainability* **2021**, 193-214.

491. Zeka, K.; Coppa, P.; Corsi, L.; Pajewski, L.A.; Vegliò, F.; Continenza, M.A. In vitro biocompatibility of a new PVP-Hydrogel. *Italian Journal of Anatomy and Embryology* **2012**, *117*, 202.
492. Malikmammadov, E.; Tanir, T.E.; Kiziltay, A.; Hasirci, V.; Hasirci, N. PCL and PCL-based materials in biomedical applications. *Journal of Biomaterials Science, Polymer Edition* **2018**, *29*, 863-893.
493. Singhvi, M.S.; Zinjarde, S.S.; Gokhale, D.V. Polylactic acid: synthesis and biomedical applications. *Journal of Applied Microbiology* **2019**, *127*, 1612-1626, doi:10.1111/jam.14290.
494. Xia, W.; Dechao, N.; Chen, H.; Pei, L. Polyethyleneimine-Based Nanocarriers for Gene Delivery. *Current Pharmaceutical Design* **2015**, *21*, 6140-6156.
495. Jiménez-Gómez, C.P.; Cecilia, J.A. Chitosan: A Natural Biopolymer with a Wide and Varied Range of Applications. *Molecules* **2020**, *25*, 3981.
496. Ul Rehman, W.; Majeed, A.; Mehra, R.; Bhushan, S.; Rani, P.; Saini, K.C.; Bast, F. Gelatin: A comprehensive report covering its indispensable aspects. Nova Science Publishers, Inc.: 2016.
497. Dhalendra, K.; Utsav, V.; Nagesh, D.; Partha, J.; Ankit, J.; Dharmendra, J. Alginate as Promising Natural Polymer for Pharmaceutical, Food, and Biomedical Applications. *Current Drug Delivery* **2020**, *17*, 755-775.
498. Sionkowska, A.; Gadomska, M.; Musiał, K.; Piątek, J. Hyaluronic Acid as a Component of Natural Polymer Blends for Biomedical Applications: A Review. *Molecules* **2020**, *25*, 35.
499. Zarrintaj, P.; Saeb, M.R.; Jafari, S.H.; Mozafari, M. Application of compatibilized polymer blends in biomedical fields. In *Compatibilization of polymer blends*, Ajitha, A.R.; Thomas, S., Eds., Elsevier: 2020; pp. 511-537.
500. Nunes, C.S.; Philipps-Wiemann, P. Formulation of enzymes. In *Enzymes in Human and Animal Nutrition*, Nunes, C.S.; Kumar, V., Eds.; Elsevier: 2018; pp. 429-440.
501. Begines, B.; Ortiz, T.; Pérez-Aranda, M.; Martínez, G.; Merinero, M.; Argüelles-Arias, F.; Alcudia, A. Polymeric Nanoparticles for Drug Delivery: Recent Developments and Future Prospects. *Nanomaterials* **2020**, *10*, 1403.
502. Luraghi, A.; Peri, F.; Moroni, L. Electrospinning for drug delivery applications: A review. *Journal of Controlled Release* **2021**, *334*, 463-484.
503. Lee, K.Y.; Jeong, L.; Kang, Y.O.; Lee, S.J.; Park, W.H. Electrospinning of polysaccharides for regenerative medicine. *Advanced Drug Delivery Reviews* **2009**, *61*, 1020-1032.
504. John, J.V.; McCarthy, A.; Xie, J. Electrospun nanofiber matrix for tissue repair and regeneration. In *Tissue Engineering*, Sharma, C.P.; Chandy, T.; Thomas, V.; Thankam, F.G.; Eds..; Elsevier: 2022; pp. 175-191.
505. Davoodi, P.; Gill, E.L.; Wang, W.; Huang, Y.Y.S. Advances and innovations in electrospinning technology. In *Biomedical Applications of Electrospinning and Electrospraying*, Kasoju, N.; Ye, H.; Eds.; Elsevier: 2021; pp. 45-81.
506. Nikmaram, N.; Roohinejad, S.; Hashemi, S.; Koubaa, M.; Barba, F.J.; Abbaspourrad, A.; Greiner, R. Emulsion-based systems for fabrication of electrospun nanofibers: food, pharmaceutical and biomedical applications. *RSC Advances* **2017**, *7*, 28951-28964.
507. Singh, B.; Kim, K.; Park, M.-H. On-Demand Drug Delivery Systems Using Nanofibers. *Nanomaterials* **2021**, *11*, 3411.
508. Lindner, H.B.; Zhang, A.; Eldridge, J.; Demcheva, M.; Tsichilis, P.; Seth, A.; Vournakis, J.; Muise-Helmericks, R.C. Correction: Anti-Bacterial Effects of Poly-N-Acetyl-Glucosamine Nanofibers in Cutaneous Wound Healing: Requirement for Akt1. *PLOS ONE* **2011**, *6*, e18996.
509. Confederat, L.G.; Tuchilus, C.G.; Dragan, M.; Sha'at, M.; Dragostin, O.M. Preparation and Antimicrobial Activity of Chitosan and Its Derivatives: A Concise Review. *Molecules* **2021**, *26*, 3694.
510. Rather, A.H.; Wani, T.U.; Khan, R.S.; Pant, B.; Park, M.; Sheikh, F.A. Prospects of Polymeric Nanofibers Loaded with Essential Oils for Biomedical and Food-Packaging Applications. *International Journal of Molecular Sciences* **2021**, *22*, 4017.
511. Kwak, H.W.; Kang, M.J.; Bae, J.H.; Hur, S.B.; Kim, I.-S.; Park, Y.H.; Lee, K.H. Fabrication of Phaeodactylum tricornutum extract-loaded gelatin nanofibrous mats exhibiting antimicrobial activity. *International Journal of Biological Macromolecules* **2014**, *63*, 198-204.
512. Ramalingam, R.; Dhand, C.; Mayandi, V.; Leung, C.M.; Ezhilarasu, H.; Karuppannan, S.K.; Prasannan, P.; Ong, S.T.; Sunderasan, N.; Kaliappan, I. Core–shell structured antimicrobial nanofiber dressings containing herbal extract and antibiotics combination for the prevention of biofilms and promotion of cutaneous wound healing. *ACS applied materials & interfaces* **2021**, *13*, 24356-24369.

513. Karuppannan, S.K.; Bushion, J.; Ramalingam, R.; Swaminathan, S.; Arunachalam, K.D.; Kadam, A.A.; Rajagopal, R.; Sathya, R.; Chinnappan, S. Fabrication, characterization and in vitro evaluation of Melia dubia extract infused nanofibers for wound dressing. *Journal of King Saud University - Science* **2022**, *34*, 101931.
514. Wang, Q.; Liu, S.; Lu, W.; Zhang, P. Fabrication of Curcumin@Ag Loaded Core/Shell Nanofiber Membrane and its Synergistic Antibacterial Properties. *Frontiers in Chemistry* **2022**, *10*, 870666.
515. Thamer, B.M.; Al-Sabri, A.E.; Almansob, A.; El-Newehy, M.H. Fabrication of Biohybrid Nanofibers by the Green Electrospinning Technique and Their Antibacterial Activity. *ACS Omega* **2022**, *7*, 7311-7319.
516. Serbezeanu, D.; Bargan, A.; Homocianu, M.; Aflori, M.; Rîmbu, C.M.; Enache, A.A.; Vlad-Bubulac, T. Electrospun Polyvinyl Alcohol Loaded with Phytotherapeutic Agents for Wound Healing Applications. *Nanomaterials* **2021**, *11*, 3336.
517. Sedghi, R.; Shaabani, A. Electrospun biocompatible core/shell polymer-free core structure nanofibers with superior antimicrobial potency against multi drug resistance organisms. *Polymer* **2016**, *101*, 151-157.
518. Ye, P.; Wei, S.; Luo, C.; Wang, Q.; Li, A.; Wei, F. Long-Term Effect against Methicillin-Resistant Staphylococcus aureus of Emodin Released from Coaxial Electrospinning Nanofiber Membranes with a Biphasic Profile. *Biomolecules* **2020**, *10*, 362.
519. Ramalingam, N.; Natarajan, T.S.; Rajiv, S. Preparation and characterization of electrospun curcumin loaded poly(2-hydroxyethyl methacrylate) nanofiber—A biomaterial for multidrug resistant organisms. *Journal of Biomedical Materials Research Part A* **2015**, *103*, 16-24.
520. Yang, X.; Fan, L.; Ma, L.; Wang, Y.; Lin, S.; Yu, F.; Pan, X.; Luo, G.; Zhang, D.; Wang, H. Green electrospun Manuka honey/silk fibroin fibrous matrices as potential wound dressing. *Materials & Design* **2017**, *119*, 76-84.
521. Kurakula, M.; Koteswara Rao, G.S.N. Moving polyvinyl pyrrolidone electrospun nanofibers and bioprinted scaffolds toward multidisciplinary biomedical applications. *European Polymer Journal* **2020**, *136*, 109919.
522. Zare, M.; Dziemidowicz, K.; Williams, G.R.; Ramakrishna, S. Encapsulation of Pharmaceutical and Nutraceutical Active Ingredients Using Electrospinning Processes. *Nanomaterials* **2021**, *11*, 1968.
523. Zhang, L.; Liang, E.; Cheng, Y.; Mahmood, T.; Ge, F.; Zhou, K.; Bao, M.; Lv, L.; Li, L.; Yi, J.; et al. Is combined medication with natural medicine a promising therapy for bacterial biofilm infection? *Biomedicine & Pharmacotherapy* **2020**, *128*, 110184.
524. Dai, C.; Lin, J.; Li, H.; Shen, Z.; Wang, Y.; Velkov, T.; Shen, J. The Natural Product Curcumin as an Antibacterial Agent: Current Achievements and Problems. *Antioxidants* **2022**, *11*, 459.
525. Stanger, J.; Tucker, N.; Kirwan, K.; Staiger, M.P. Effect of charge density on the taylor cone in electrospinning. *International Journal of Modern Physics B* **2009**, *23*, 1956-1961.
526. Abrigo, M.; Kingshott, P.; McArthur, S.L. Electrospun Polystyrene Fiber Diameter Influencing Bacterial Attachment, Proliferation, and Growth. *ACS Applied Materials & Interfaces* **2015**, *7*, 7644-7652.
527. Liu, F.; Rajabi, S.; Shi, C.; Afifirad, G.; Omidi, N.; Kouhsari, E.; Khoshnood, S.; Azizian, K. Antibacterial activity of recently approved antibiotics against methicillin-resistant Staphylococcus aureus (MRSA) strains: A systematic review and meta-analysis. *Annals of Clinical Microbiology and Antimicrobials* **2022**, *21*, 37.
528. Patel, K.; Bunachita, S.; Agarwal, A.A.; Bhamidipati, A.; Patel, U.K. A comprehensive overview of antibiotic selection and the factors affecting it. *Cureus* **2021**, *13*, e13925.
529. Gumaste, M.R.; Kulkarni, G.A. High mobility and size dependent carrier concentration in CdTe nanoparticles synthesized by single injection hydrothermal method for device applications. *Materials Today: Proceedings* **2021**, *45*, 3927-3930.
530. Neikov, O.D. Nanopowders. In *Handbook of non-ferrous metal powders*; 2009; pp. 80-101.
531. Dorfs, D.; Krahne, R.; Falqui, A.; Manna, L.; Giannini, C.; Zanchet, D. Quantum dots: synthesis and characterization. In *Comprehensive Nanoscience and Technology. 1: Nanomaterials*, Andrews, D.L.; Scholes, G.D.; Wiederrecht, G.P., Eds; Elsevier: 2011; pp. 219-270.
532. Kamaly, N.; Yameen, B.; Wu, J.; Farokhzad, O.C. Degradable Controlled-Release Polymers and Polymeric Nanoparticles: Mechanisms of Controlling Drug Release. *Chemical Reviews* **2016**, *116*, 2602-2663.
533. Calzoni, E.; Cesaretti, A.; Polchi, A.; Di Michele, A.; Tancini, B.; Emiliani, C. Biocompatible Polymer Nanoparticles for Drug Delivery Applications in Cancer and Neurodegenerative Disorder Therapies. *Journal of Functional Biomaterials* **2019**, *10*, 4.

534. Umerska, A.; Gaucher, C.; Oyarzun-Ampuero, F.; Fries-Raeth, I.; Colin, F.; Villamizar-Sarmiento, M.G.; Maincent, P.; Sapin-Minet, A. Polymeric Nanoparticles for Increasing Oral Bioavailability of Curcumin. *Antioxidants* **2018**, *7*, 46.
535. Feczkó, T. Polymeric nanotherapeutics acting at special regions of body. *Journal of Drug Delivery Science and Technology* **2021**, *64*, 102597.
536. Skourtis, D.; Stavroulaki, D.; Athanasiou, V.; Fragouli, P.G.; Iatrou, H. Nanostructured Polymeric, Liposomal and Other Materials to Control the Drug Delivery for Cardiovascular Diseases. *Pharmaceutics* **2020**, *12*, 1160.
537. Mitchell, M.J.; Billingsley, M.M.; Haley, R.M.; Wechsler, M.E.; Peppas, N.A.; Langer, R. Engineering precision nanoparticles for drug delivery. *Nature Reviews Drug Discovery* **2021**, *20*, 101-124.
538. Pal, G.; Rai, P.; Pandey, A. Chapter 1 - Green synthesis of nanoparticles: A greener approach for a cleaner future. In *Green Synthesis, Characterization and Applications of Nanoparticles*, Shukla, A.K., Iravani, S., Eds.; Elsevier: 2019; pp. 1-26.
539. Idrees, H.; Zaidi, S.Z.; Sabir, A.; Khan, R.U.; Zhang, X.; Hassan, S.-u. A Review of Biodegradable Natural Polymer-Based Nanoparticles for Drug Delivery Applications. *Nanomaterials* **2020**, *10*, 1970.
540. Spirescu, V.A.; Chircov, C.; Grumezescu, A.M.; Andronescu, E. Polymeric Nanoparticles for Antimicrobial Therapies: An up-to-date Overview. *Polymers* **2021**, *13*, 724.
541. Verma, G.; Rajagopalan, M.D.; Valluru, R.; Sridhar, K.A. Chapter 7 - Nanoparticles: A Novel Approach to Target Tumors. In *Nano- and Microscale Drug Delivery Systems*, Grumezescu, A.M., Ed.; Elsevier: 2017; pp. 113-129.
542. Rao, J.P.; Geckeler, K.E. Polymer nanoparticles: Preparation techniques and size-control parameters. *Progress in Polymer Science* **2011**, *36*, 887-913.
543. Nagavarma, B.V.N.; Yadav, H.K.S.; Ayaz, A.; Vasudha, L.S.; Shivakumar, H.G. Different techniques for preparation of polymeric nanoparticles-a review. *Asian J. Pharm. Clin. Res* **2012**, *5*, 16-23.
544. El-Naggar, N.E.-A.; Saber, W.I.A.; Zweil, A.M.; Bashir, S.I. An innovative green synthesis approach of chitosan nanoparticles and their inhibitory activity against phytopathogenic Botrytis cinerea on strawberry leaves. *Scientific Reports* **2022**, *12*, 3515.
545. Cano, A.; Ettcheto, M.; Espina, M.; López-Machado, A.; Cajal, Y.; Rabanal, F.; Sánchez-López, E.; Camins, A.; García, M.L.; Souto, E.B. State-of-the-art polymeric nanoparticles as promising therapeutic tools against human bacterial infections. *Journal of Nanobiotechnology* **2020**, *18*, 156.
546. Makabenta, J.M.V.; Park, J.; Li, C.-H.; Chattopadhyay, A.N.; Nabawy, A.; Landis, R.F.; Gupta, A.; Schmidt-Malan, S.; Patel, R.; Rotello, V.M. Polymeric Nanoparticles Active against Dual-Species Bacterial Biofilms. *Molecules* **2021**, *26*, 4958.
547. Conte, C.; Maiolino, S.; Pellosi, D.S.; Miro, A.; Ungaro, F.; Quaglia, F. Polymeric Nanoparticles for Cancer Photodynamic Therapy. In *Light-Responsive Nanostructured Systems for Applications in Nanomedicine*, Sortino, S., Ed.; Springer International Publishing: Cham, 2016; pp. 61-112.
548. Lam, S.J.; Wong, E.H.H.; Boyer, C.; Qiao, G.G. Antimicrobial polymeric nanoparticles. *Progress in Polymer Science* **2018**, *76*, 40-64.
549. Ndayishimiye, J.; Kumeria, T.; Popat, A.; Falconer, J.R.; Blaskovich, M.A.T. Nanomaterials: The New Antimicrobial Magic Bullet. *ACS Infectious Diseases* **2022**, *8*, 693-712.
550. Barani, M.; Fathizadeh, H.; Arkaban, H.; Kalantar-Neyestanaki, D.; Akbarizadeh, M.R.; Turki Jalil, A.; Akhavan-Sigari, R. Recent Advances in Nanotechnology for the Management of Klebsiella pneumoniae–Related Infections. *Biosensors* **2022**, *12*, 1155.
551. Jonassen, H.; Kjøniksen, A.-L.; Hiorth, M. Stability of Chitosan Nanoparticles Cross-Linked with Tripolyphosphate. *Biomacromolecules* **2012**, *13*, 3747-3756.
552. Waschinski, C.J.; Herdes, V.; Schueler, F.; Tiller, J.C. Influence of Satellite Groups on Telechelic Antimicrobial Functions of Polyoxazolines. *Macromolecular Bioscience* **2005**, *5*, 149-156.
553. Qiao, Y.; Yang, C.; Coady, D.J.; Ong, Z.Y.; Hedrick, J.L.; Yang, Y.-Y. Highly dynamic biodegradable micelles capable of lysing Gram-positive and Gram-negative bacterial membrane. *Biomaterials* **2012**, *33*, 1146-1153..
554. Haktaniyan, M.; Bradley, M. Polymers showing intrinsic antimicrobial activity. *Chemical Society Reviews* **2022**, *51*, 8584-8611.
555. Song, J.; Jung, Y.; Lee, I.; Jang, J. Fabrication of pDMAEMA-coated silica nanoparticles and their enhanced antibacterial activity. *Journal of Colloid and Interface Science* **2013**, *407*, 205-209.
556. Hazra, C.; Kundu, D.; Chatterjee, A.; Chaudhari, A.; Mishra, S. Poly(methyl methacrylate) (core)–biosurfactant (shell) nanoparticles: Size controlled sub-100nm synthesis, characterization,

antibacterial activity, cytotoxicity and sustained drug release behavior. *Colloids and Surfaces A: Physicochemical and Engineering Aspects* **2014**, *449*, 96-113.

557. Lalloz, A.; Bolzinger, M.-A.; Faivre, J.; Latreille, P.-L.; Garcia Ac, A.; Rakotovao, C.; Rabanel, J.-M.; Hildgen, P.; Banquy, X.; Briançon, S. Effect of surface chemistry of polymeric nanoparticles on cutaneous penetration of cholecalciferol. *International Journal of Pharmaceutics* **2018**, *553*, 120-131.
558. Vigliotta, G.; Mella, M.; Rega, D.; Izzo, L. Modulating Antimicrobial Activity by Synthesis: Dendritic Copolymers Based on Nonquaternized 2-(Dimethylamino)ethyl Methacrylate by Cu-Mediated ATRP. *Biomacromolecules* **2012**, *13*, 833-841.
559. Jamil, B.; Abbasi, R.; Abbasi, S.; Imran, M.; Khan, S.U.; Ihsan, A.; Javed, S.; Bokhari, H.; Imran, M. Encapsulation of Cardamom Essential Oil in Chitosan Nano-composites: In-vitro Efficacy on Antibiotic-Resistant Bacterial Pathogens and Cytotoxicity Studies. *Frontiers in Microbiology* **2016**, *7*, 1580.
560. El-Naggar, N.E.-A.; Shiha, A.M.; Mahrous, H.; Mohammed, A.B.A. Green synthesis of chitosan nanoparticles, optimization, characterization and antibacterial efficacy against multi drug resistant biofilm-forming Acinetobacter baumannii. *Scientific Reports* **2022**, *12*, 19869.
561. de Oliveira, M.S.; Oshiro-Junior, J.A.; Sato, M.R.; Conceição, M.M.; Medeiros, A.C. Polymeric Nanoparticle Associated with Ceftriaxone and Extract of Schinopsis Brasiliensis Engler against Multiresistant Enterobacteria. *Pharmaceutics* **2020**, *12*, 695.
562. Vrouvaki, I.; Koutra, E.; Kornaros, M.; Avgoustakis, K.; Lamari, F.N.; Hatziantoniou, S. Polymeric Nanoparticles of Pistacia lentiscus var. chia Essential Oil for Cutaneous Applications. *Pharmaceutics* **2020**, *12*, 353.
563. Maliki, S.; Sharma, G.; Kumar, A.; Moral-Zamorano, M.; Moradi, O.; Baselga, J.; Stadler, F.J.; García-Peñas, A. Chitosan as a Tool for Sustainable Development: A Mini Review. *Polymers* **2022**, *14*, 1475.
564. Mikušová, V.; Mikuš, P. Advances in Chitosan-Based Nanoparticles for Drug Delivery. *International Journal of Molecular Sciences* **2021**, *22*, 9652.
565. Kołodziejska, M.; Jankowska, K.; Klak, M.; Wszoła, M. Chitosan as an Underrated Polymer in Modern Tissue Engineering. *Nanomaterials* **2021**, *11*, 3019.
566. Mabrouk, M.; Das, D.B.; Salem, Z.A.; Beherei, H.H. Nanomaterials for Biomedical Applications: Production, Characterisations, Recent Trends and Difficulties. *Molecules* **2021**, *26*, 77.
567. Ramanathan, S.; Gopinath, S.C.B.; Arshad, M.K.M.; Poopalan, P.; Perumal, V. 2 - Nanoparticle synthetic methods: strength and limitations. In *Nanoparticles in Analytical and Medical Devices*, Gopinath, S.C.B., Gang, F., Eds.; Elsevier: 2021; pp. 31-43.
568. Singh, J.; Dutta, T.; Kim, K.-H.; Rawat, M.; Samddar, P.; Kumar, P. 'Green' synthesis of metals and their oxide nanoparticles: applications for environmental remediation. *Journal of Nanobiotechnology* **2018**, *16*, 84.
569. Marchiol, L. Synthesis of metal nanoparticles in living plants. *Italian Journal of Agronomy* **2012**, *7*, e37.
570. Wang, L.; Hu, C.; Shao, L. The antimicrobial activity of nanoparticles: present situation and prospects for the future. *International Journal of Nanomedicine* **2017**, *12*, 1227-1249.
571. Mammari, N.; Lamouroux, E.; Boudier, A.; Duval, R.E. Current Knowledge on the Oxidative-Stress-Mediated Antimicrobial Properties of Metal-Based Nanoparticles. *Microorganisms* **2022**, *10*, 437.
572. Nisar, P.; Ali, N.; Rahman, L.; Ali, M.; Shinwari, Z.K. Antimicrobial activities of biologically synthesized metal nanoparticles: an insight into the mechanism of action. *JBIC Journal of Biological Inorganic Chemistry* **2019**, *24*, 929-941.
573. Raza, M.A.; Kanwal, Z.; Rauf, A.; Sabri, A.N.; Riaz, S.; Naseem, S. Size- and Shape-Dependent Antibacterial Studies of Silver Nanoparticles Synthesized by Wet Chemical Routes. *Nanomaterials* **2016**, *6*, 74.
574. Cui, Y.; Zhao, Y.; Tian, Y.; Zhang, W.; Lü, X.; Jiang, X. The molecular mechanism of action of bactericidal gold nanoparticles on Escherichia coli. *Biomaterials* **2012**, *33*, 2327-2333.
575. Li, W.-R.; Xie, X.-B.; Shi, Q.-S.; Duan, S.-S.; Ouyang, Y.-S.; Chen, Y.-B. Antibacterial effect of silver nanoparticles on Staphylococcus aureus. *BioMetals* **2011**, *24*, 135-141.
576. Jadoun, S.; Arif, R.; Jangid, N.K.; Meena, R.K. Green synthesis of nanoparticles using plant extracts: a review. *Environmental Chemistry Letters* **2021**, *19*, 355-374.
577. Chuy, G.P.; Muraro, P.C.L.; Viana, A.R.; Pavoski, G.; Espinosa, D.C.R.; Vizzotto, B.S.; da Silva, W.L. Green Nanoarchitectonics of Silver Nanoparticles for Antimicrobial Activity Against Resistant Pathogens. *Journal of Inorganic and Organometallic Polymers and Materials* **2022**, *32*, 1213-1222.

578. Dash, S.S.; Samanta, S.; Dey, S.; Giri, B.; Dash, S.K. Rapid Green Synthesis of Biogenic Silver Nanoparticles Using Cinnamomum tamala Leaf Extract and its Potential Antimicrobial Application Against Clinically Isolated Multidrug-Resistant Bacterial Strains. *Biological Trace Element Research* **2020**, *198*, 681-696.
579. Tyavambiza, C.; Elbagory, A.M.; Madiehe, A.M.; Meyer, M.; Meyer, S. The Antimicrobial and Anti-Inflammatory Effects of Silver Nanoparticles Synthesised from Cotyledon orbiculata Aqueous Extract. *Nanomaterials* **2021**, *11*,1343.
580. Alqahtani, M.A.; Al Othman, M.R.; Mohammed, A.E. Bio fabrication of silver nanoparticles with antibacterial and cytotoxic abilities using lichens. *Scientific Reports* **2020**, *10*, 16781.
581. Foroohimanjili, F.; Mirzaie, A.; Hamdi, S.M.M.; Noorbazargan, H.; Hedayati Ch, M.; Dolatabadi, A.; Rezaie, H.; Bishak, F.M. Antibacterial, antibiofilm, and antiquorum sensing activities of phytosynthesized silver nanoparticles fabricated from extract against multidrug resistance of clinical strains. *Journal of Basic Microbiology* **2020**, *60*, 216-230.
582. Moorthy, K.; Chang, K.-C.; Wu, W.-J.; Hsu, J.-Y.; Yu, P.-J.; Chiang, C.-K. Systematic Evaluation of Antioxidant Efficiency and Antibacterial Mechanism of Bitter Gourd Extract Stabilized Silver Nanoparticles. *Nanomaterials* **2021**, *11*, 2278.
583. Ali, S.; Khan, M.R.; Khan, R. Green synthesized AgNPs from Periploca hydaspidis Falc. and its biological activities. *Microscopy Research and Technique* **2021**, *84*, 2268-2285.
584. Padilla-Camberos, E.; Sanchez-Hernandez, I.M.; Torres-Gonzalez, O.R.; Ramirez-Rodriguez, P.; Diaz, E.; Wille, H.; Flores-Fernandez, J.M. Biosynthesis of Silver Nanoparticles Using Stenocereus queretaroensis Fruit Peel Extract: Study of Antimicrobial Activity. *Materials* **2021**, *14*, 4543.
585. Asghar, M.A.; Zahir, E.; Asghar, M.A.; Iqbal, J.; Rehman, A.A. Facile, one-pot biosynthesis and characterization of iron, copper and silver nanoparticles using Syzygium cumini leaf extract: As an effective antimicrobial and aflatoxin B1 adsorption agents. *PLOS ONE* **2020**, *15*, e0234964.
586. Ashour, A.; Raafat, D.; El-Gowelli, H.; El-Kamel, A. Green synthesis of silver nanoparticles using cranberry powder aqueous extract: characterization and antimicrobial properties. *International Journal of Nanomedicine* **2015**, *10*, 7207.
587. Mandhata, C.P.; Sahoo, C.R.; Mahanta, C.S.; Padhy, R.N. Isolation, biosynthesis and antimicrobial activity of gold nanoparticles produced with extracts of Anabaena spiroides. *Bioprocess and Biosystems Engineering* **2021**, *44*, 1617-1626.
588. Hussein, M.A.M.; Grinholc, M.; Dena, A.S.A.; El-Sherbiny, I.M.; Megahed, M. Boosting the antibacterial activity of chitosan–gold nanoparticles against antibiotic–resistant bacteria by Punicagranatum L. extract. *Carbohydrate Polymers* **2021**, *256*, 117498.
589. Ssekatawa, K.; Byarugaba, D.K.; Angwe, M.K.; Wampande, E.M.; Ejobi, F.; Nxumalo, E.; Maaza, M.; Sackey, J.; Kirabira, J.B. Phyto-Mediated Copper Oxide Nanoparticles for Antibacterial, Antioxidant and Photocatalytic Performances. *Frontiers in Bioengineering and Biotechnology* **2022**, *10*, 820218.
590. Sonbol, H.; Ameen, F.; AlYahya, S.; Almansob, A.; Alwakeel, S. Padina boryana mediated green synthesis of crystalline palladium nanoparticles as potential nanodrug against multidrug resistant bacteria and cancer cells. *Scientific Reports* **2021**, *11*, 5444.
591. Medina-Cruz, D.; Vernet-Crua, A.; Mostafavi, E.; González, M.U.; Martínez, L.; Iii, A.A.D.J.; Kusper, M.; Sotelo, E.; Gao, M.; Geoffrion, L.D.; et al. Aloe Vera-Mediated Te Nanostructures: Highly Potent Antibacterial Agents and Moderated Anticancer Effects. *Nanomaterials* **2021**, *11*, 514.
592. Rasha, E.; Monerah, A.; Manal, A.; Rehab, A.; Mohammed, D.; Doaa, E. Biosynthesis of Zinc Oxide Nanoparticles from Acacia nilotica (L.) Extract to Overcome Carbapenem-Resistant Klebsiella Pneumoniae. *Molecules* **2021**, *26*, 1919.
593. Ahmar Rauf, M.; Oves, M.; Ur Rehman, F.; Rauf Khan, A.; Husain, N. Bougainvillea flower extract mediated zinc oxide's nanomaterials for antimicrobial and anticancer activity. *Biomedicine & Pharmacotherapy* **2019**, *116*, 108983.
594. Abdelghany, T.M.; Al-Rajhi, A.M.H.; Al Abboud, M.A.; Alawlaqi, M.M.; Ganash Magdah, A.; Helmy, E.A.M.; Mabrouk, A.S. Recent Advances in Green Synthesis of Silver Nanoparticles and Their Applications: About Future Directions. A Review. *BioNanoScience* **2018**, *8*, 5-16.
595. Bruna, T.; Maldonado-Bravo, F.; Jara, P.; Caro, N. Silver Nanoparticles and Their Antibacterial Applications. *International Journal of Molecular Sciences* **2021**, *22*, doi:10.3390/ijms22137202.
596. Dakal, T.C.; Kumar, A.; Majumdar, R.S.; Yadav, V. Mechanistic Basis of Antimicrobial Actions of Silver Nanoparticles. *Frontiers in Microbiology* **2016**, *7*, 1831.
597. Arakha, M.; Saleem, M.; Mallick, B.C.; Jha, S. The effects of interfacial potential on antimicrobial propensity of ZnO nanoparticle. *Scientific Reports* **2015**, *5*, 9578.

598. Qamar, H.; Rehman, D.S.; Chauhan, D.K.; Tiwari, A.; Upmanyu, V. Green Synthesis, Characterization and Antimicrobial Activity of Copper Oxide Nanomaterial Derived from Momordica charantia. *International Journal of Nanomedicine* **2020**, *15*, 2541-2553.
599. Govindasamy, G.A.; Mydin, R.B.S.M.N.; Sreekantan, S.; Harun, N.H. Compositions and antimicrobial properties of binary ZnO–CuO nanocomposites encapsulated calcium and carbon from Calotropis gigantea targeted for skin pathogens. *Scientific Reports* **2021**, *11*, 99.
600. Azizi, S.; Mohamad, R.; Abdul Rahim, R.; Mohammadinejad, R.; Bin Ariff, A. Hydrogel beads bio-nanocomposite based on Kappa-Carrageenan and green synthesized silver nanoparticles for biomedical applications. *International Journal of Biological Macromolecules* **2017**, *104*, 423-431.
601. Khan, T.; Jalal, H.; Karam, K.; Khan, M. Biodegradable gum: A green source for silver nanoparticles. In *Green Synthesis of Silver Nanomaterials*, Abd-Elsalam, K.A., Ed.; Elsevier: 2022; pp. 189-217.
602. Kaushal, A.; Khurana, I.; Yadav, P.; Allawadhi, P.; Banothu, A.K.; Neeradi, D.; Thalugula, S.; Barani, P.J.; Naik, R.R.; Navik, U.; et al. Advances in therapeutic applications of silver nanoparticles. *Chemico-Biological Interactions* **2023**, *382*, 110590.
603. Nie, P.; Zhao, Y.; Xu, H. Synthesis, applications, toxicity and toxicity mechanisms of silver nanoparticles: A review. *Ecotoxicology and Environmental Safety* **2023**, *253*, 114636.
604. Varma, R.S. Greener and Sustainable Trends in Synthesis of Organics and Nanomaterials. *ACS Sustainable Chemistry & Engineering* **2016**, *4*, 5866-5878.
605. Alqarni, L.; Alghamdi, M.; Alshahrani, A.; Nassar, A. Green Nanotechnology: Recent Research on Bioresource-Based Nanoparticle Synthesis and Applications. *Journal of Chemistry* **2022**, *2022*, 1-31.
606. Díaz-Puertas, R.; Álvarez-Martínez, F.J.; Falco, A.; Barrajón-Catalán, E.; Mallavia, R. Phytochemical-Based Nanomaterials against Antibiotic-Resistant Bacteria: An Updated Review. *Polymers* **2023**, *15*, 1392.
607. Hano, C.; Abbasi, B.H. Plant-Based Green Synthesis of Nanoparticles: Production, Characterization and Applications. *Biomolecules* **2022**, *12*, 31.
608. Xu, L.; Wang, Y.-Y.; Huang, J.; Chen, C.-Y.; Wang, Z.-X.; Xie, H. Silver nanoparticles: Synthesis, medical applications and biosafety. *Theranostics* **2020**, *10*, 8996-9031.
609. Jain, S.; Mehata, M.S. Medicinal Plant Leaf Extract and Pure Flavonoid Mediated Green Synthesis of Silver Nanoparticles and their Enhanced Antibacterial Property. *Scientific Reports* **2017**, *7*, 15867.
610. Mussin, J.; Robles-Botero, V.; Casañas-Pimentel, R.; Rojas, F.; Angiolella, L.; San Martín-Martínez, E.; Giusiano, G. Antimicrobial and cytotoxic activity of green synthesis silver nanoparticles targeting skin and soft tissue infectious agents. *Scientific Reports* **2021**, *11*, 14566.
611. Liaqat, N.; Jahan, N.; Khalil ur, R.; Anwar, T.; Qureshi, H. Green synthesized silver nanoparticles: Optimization, characterization, antimicrobial activity, and cytotoxicity study by hemolysis assay. *Frontiers in Chemistry* **2022**, *10*, 952006.
612. Karimi, M.; Sadeghi, R.; Kokini, J. Pomegranate as a promising opportunity in medicine and nanotechnology. *Trends in Food Science & Technology* **2017**, *69*, 59-73.
613. Valero-Mendoza, A.G.; Meléndez-Rentería, N.P.; Chávez-González, M.L.; Flores-Gallegos, A.C.; Wong-Paz, J.E.; Govea-Salas, M.; Zugasti-Cruz, A.; Ascacio-Valdés, J.A. The whole pomegranate (Punica granatum. L), biological properties and important findings: A review. *Food Chemistry Advances* **2023**, *2*, 100153.
614. Saad, P.G.; Castelino, R.D.; Ravi, V.; Al-Amri, I.S.; Khan, S.A. Green synthesis of silver nanoparticles using Omani pomegranate peel extract and two polyphenolic natural products: characterization and comparison of their antioxidant, antibacterial, and cytotoxic activities. *Beni-Suef University Journal of Basic and Applied Sciences* **2021**, *10*, 29.
615. Ahmad, N.; Sharma; Radheshyam Rai, S. Rapid Green Synthesis Of Silver And Gold Nanoparticles Using Peels Of Punica Granatum . *Advanced Materials Letters* **2012**, *3*, 376-380.
616. Sarkar, S.; Kotteeswaran, V. Green synthesis of silver nanoparticles from aqueous leaf extract of Pomegranate (Punica granatum) and their anticancer activity on human cervical cancer cells. *Advances in Natural Sciences: Nanoscience and Nanotechnology* **2018**, *9*, 025014.
617. Chau, T.P.; Veeraragavan, G.R.; Narayanan, M.; Chinnathambi, A.; Alharbi, S.A.; Subramani, B.; Brindhadevi, K.; Pimpimon, T.; Pikulkaew, S. Green synthesis of Zirconium nanoparticles using Punica granatum (pomegranate) peel extract and their antimicrobial and antioxidant potency. *Environmental Research* **2022**, *209*, 112771.

618. Ifeanyichukwu, U.L.; Fayemi, O.E.; Ateba, C.N. Green Synthesis of Zinc Oxide Nanoparticles from Pomegranate (Punica granatum) Extracts and Characterization of Their Antibacterial Activity. *Molecules* **2020**, *25*, 4521.
619. Shaban, A.S.; Owda, M.E.; Basuoni, M.M.; Mousa, M.A.; Radwan, A.A.; Saleh, A.K. Punica granatum peel extract mediated green synthesis of zinc oxide nanoparticles: structure and evaluation of their biological applications. *Biomass Conversion and Biorefinery* **2024**, *14*, 12265-12281.
620. Ibrahim, S.; Ahmad, Z.; Manzoor, M.Z.; Mujahid, M.; Faheem, Z.; Adnan, A. Optimization for biogenic microbial synthesis of silver nanoparticles through response surface methodology, characterization, their antimicrobial, antioxidant, and catalytic potential. *Scientific Reports* **2021**, *11*, 770.
621. Ba-Abbad, M.M.; Chai, P.V.; Benamour, A.; Ewis, D.; Mohammad, A.W.; Mahmoudi, E. Optimizing and control of effective synthesize parameters for Fe3O4 nanoparticles using response surface methodology. *Chemical Papers* **2022**, *76*, 6359-6370.
622. Mohammadi, S.Z.; Lashkari, B.; Khosravan, A. Green synthesis of Co3O4 nanoparticles by using walnut green skin extract as a reducing agent by using response surface methodology. *Surfaces and Interfaces* **2021**, *23*, 100970.
623. Wyantuti, S.; Pratomo, U.; Manullang, L.A.; Hendrati, D.; Hartati, Y.W.; Bahti, H.H. Development of differential pulse voltammetric method for determining samarium (III) through electroanalytical study of the metal ion in acetonitrile using Box–Behnken design. *Heliyon* **2021**, *7*, e06602.
624. Huang, D.; Ou, B.; Prior, R.L. The Chemistry behind Antioxidant Capacity Assays. *Journal of Agricultural and Food Chemistry* **2005**, *53*, 1841-1856.
625. Cimpoiu, C.; Cristea, V.-M.; Hosu, A.; Sandru, M.; Seserman, L. Antioxidant activity prediction and classification of some teas using artificial neural networks. *Food Chemistry* **2011**, *127*, 1323-1328.
626. Díaz-Puertas, R.; Rodríguez-Cañas, E.; Lozoya-Agulló, M.J.; Badía-Hernández, P.V.; Álvarez-Martínez, F.J.; Falcó, A.; Mallavia, R. Bovine serum albumin and lysozyme nanofibers as versatile platforms for preserving loaded bioactive compounds. *International Journal of Biological Macromolecules* **2024**, *280*, 136019.
627. Kupina, S.; Fields, C.; Roman, M.; Brunelle, S. Determination of Total Phenolic Content Using the Folin-C Assay: Single-Laboratory Validation, First Action 2017.13. *Journal of AOAC International* **2018**, *101*, 1466-1472.
628. Jebabli, H.; Nsir, H.; Taamalli, A.; Abu-Reidah, I.; Álvarez-Martínez, F.J.; Losada-Echeberria, M.; Barrajón Catalán, E.; Mhamdi, R. Industrial-Scale Study of the Chemical Composition of Olive Oil Process-Derived Matrices. *Processes* **2020**, *8*, 701.
629. Tsai, T.-H.; Tsai, T.-H.; Chien, Y.-C.; Lee, C.-W.; Tsai, P.-J. In vitro antimicrobial activities against cariogenic streptococci and their antioxidant capacities: A comparative study of green tea versus different herbs. *Food Chemistry* **2008**, *110*, 859-864.
630. Cervantes-Anaya, N.; Azpilcueta-Morales, G.; Estrada-Camarena, E.; Ramírez Ortega, D.; Pérez de la Cruz, V.; González-Trujano, M.E.; López-Rubalcava, C. Pomegranate and Its Components, Punicalagin and Ellagic Acid, Promote Antidepressant, Antioxidant, and Free Radical-Scavenging Activity in Ovariectomized Rats. *Frontiers in Behavioral Neuroscience* **2022**, *16*, 836681.
631. El-Beltagi, H.S.; Eshak, N.S.; Mohamed, H.I.; Bendary, E.S.A.; Danial, A.W. Physical Characteristics, Mineral Content, and Antioxidant and Antibacterial Activities of Punica granatum or Citrus sinensis Peel Extracts and Their Applications to Improve Cake Quality. *Plants* **2022**, *11*, 1740.
632. Dewan, A.; Dawra, S.; Kaushik, N.; Singh, A.; Thakur, S.; Kaur, S.; Xavier, J.R. Process characterization for tisane development using pomegranate waste: an herbal drink optimization strategy. *Sustainable Food Technology* **2024**, *2*, 806-815, doi:10.1039/D3FB00202K.
633. Bewick, V.; Cheek, L.; Ball, J. Statistics review 7: Correlation and regression. *Critical Care* **2003**, *7*, 451.
634. Eti, M.; Cihanoğlu, A.; Hamaloğlu, K.Ö.; Altıok, E.; Güler, E.; Tuncel, A.; Kabay, N. Synthesis of Silver Nanoparticle-Immobilized Antibacterial Anion-Exchange Membranes for Salinity Gradient Energy Production by Reverse Electrodialysis. *ACS Sustainable Chemistry & Engineering* **2024**, *12*, 3977-3986.
635. Vazquez-Muñoz, R.; Bogdanchikova, N.; Huerta-Saquero, A. Beyond the Nanomaterials Approach: Influence of Culture Conditions on the Stability and Antimicrobial Activity of Silver Nanoparticles. *ACS Omega* **2020**, *5*, 28441-28451.

636. Yu, Z.; Hu, C.; Guan, L.; Zhang, W.; Gu, J. Green Synthesis of Cellulose Nanofibrils Decorated with Ag Nanoparticles and Their Application in Colorimetric Detection of l-Cysteine. *ACS Sustainable Chemistry & Engineering* **2020**, *8*, 12713-12721.
637. Ying, S.; Guan, Z.; Ofoegbu, P.C.; Clubb, P.; Rico, C.; He, F.; Hong, J. Green synthesis of nanoparticles: Current developments and limitations. *Environmental Technology & Innovation* **2022**, *26*, 102336.
638. Paramelle, D.; Sadovoy, A.; Gorelik, S.; Free, P.; Hobley, J.; Fernig, D.G. A rapid method to estimate the concentration of citrate capped silver nanoparticles from UV-visible light spectra. *Analyst* **2014**, *139*, 4855-4861.
639. Sreeja, S.; Pesala, B. Plasmonic enhancement of betanin-lawsone co-sensitized solar cells via tailored bimodal size distribution of silver nanoparticles. *Scientific Reports* **2020**, *10*, 8240.
640. Radan, M.; Ćujić Nikolić, N.; Kuzmanović Nedeljković, S.; Mutavski, Z.; Krgović, N.; Stević, T.; Marković, S.; Jovanović, A.; Živković, J.; Šavikin, K. Multifunctional Pomegranate Peel Microparticles with Health-Promoting Effects for the Sustainable Development of Novel Nutraceuticals and Pharmaceuticals. *Plants* **2024**, *13*, 281.
641. Wang, Y.; Wang, X.; Zhou, D.; Xia, X.; Zhou, H.; Wang, Y.; Ke, H. Preparation and Characterization of Polycaprolactone (PCL) Antimicrobial Wound Dressing Loaded with Pomegranate Peel Extract. *ACS Omega* **2023**, *8*, 20323-20331.
642. Anagbonu, P.; Ghali, M.; Allam, A. Low-temperature green synthesis of few-layered graphene sheets from pomegranate peels for supercapacitor applications. *Scientific Reports* **2023**, *13*, 15627.
643. Adiba, A.; Razouk, R.; Haddioui, A.; Ouaabou, R.; Hamdani, A.; Kouighat, M.; Hssaini, L. FTIR spectroscopy-based lipochemical fingerprints involved in pomegranate response to water stress. *Heliyon* **2023**, *9*, e16687.
644. Okere, E.E.; Arendse, E.; Nieuwoudt, H.; Perold, W.J.; Opara, U.L. Non-destructive Evaluation of the Quality Characteristics of Pomegranate Kernel Oil by Fourier Transform Near-Infrared and Mid-Infrared Spectroscopy. *Frontiers in Plant Science* **2022**, *13*, 867555.
645. Ghasemi, S.; Dabirian, S.; Kariminejad, F.; Koohi, D.E.; Nemattalab, M.; Majidimoghadam, S.; Zamani, E.; Yousefbeyk, F. Process optimization for green synthesis of silver nanoparticles using Rubus discolor leaves extract and its biological activities against multi-drug resistant bacteria and cancer cells. *Scientific Reports* **2024**, *14*, 4130.
646. Al-Nemrawi, N.; Hameedat, F.; El-Elimat, T. Green Synthesis of Silver Nanoparticles Using Bellevalia Flexuosa Leaves Extract. *Scientia Pharmaceutica* **2022**, *90*, 60.
647. Yousefbeyk, F.; Dabirian, S.; Ghanbarzadeh, S.; Eghbali Koohi, D.; Yazdizadeh, P.; Ghasemi, S. Green synthesis of silver nanoparticles from Stachys byzantina K. Koch: characterization, antioxidant, antibacterial, and cytotoxic activity. *Particulate Science and Technology* **2022**, *40*, 219-232.
648. Ali, M.H.; Azad, M.A.K.; Khan, K.A.; Rahman, M.O.; Chakma, U.; Kumer, A. Analysis of Crystallographic Structures and Properties of Silver Nanoparticles Synthesized Using PKL Extract and Nanoscale Characterization Techniques. *ACS Omega* **2023**, *8*, 28133-28142.
649. Ounkaew, A.; Jarensungnen, C.; Jaroenthai, N.; Boonmars, T.; Artchayasawat, A.; Narain, R.; Chindaprasirt, P.; Kasemsiri, P. Fabrication of Hydrogel-Nano Silver Based on Aloe vera/Carboxymethyl Cellulose/Tannic Acid for Antibacterial and pH-Responsive Applications. *Journal of Polymers and the Environment* **2023**, *31*, 50-63.
650. Tripathi, N.; Goshisht, M.K. Recent Advances and Mechanistic Insights into Antibacterial Activity, Antibiofilm Activity, and Cytotoxicity of Silver Nanoparticles. *ACS Applied Bio Materials* **2022**, *5*, 1391-1463.
651. Rolim, W.R.; Pelegrino, M.T.; de Araújo Lima, B.; Ferraz, L.S.; Costa, F.N.; Bernardes, J.S.; Rodigues, T.; Brocchi, M.; Seabra, A.B. Green tea extract mediated biogenic synthesis of silver nanoparticles: Characterization, cytotoxicity evaluation and antibacterial activity. *Applied Surface Science* **2019**, *463*, 66-74.
652. Loo, Y.Y.; Rukayadi, Y.; Nor-Khaizura, M.-A.-R.; Kuan, C.H.; Chieng, B.W.; Nishibuchi, M.; Radu, S. In Vitro Antimicrobial Activity of Green Synthesized Silver Nanoparticles Against Selected Gram-negative Foodborne Pathogens. *Frontiers in Microbiology* **2018**, *9*, 1555.
653. Yuan, Y.-G.; Peng, Q.-L.; Gurunathan, S. Effects of Silver Nanoparticles on Multiple Drug-Resistant Strains of Staphylococcus aureus and Pseudomonas aeruginosa from Mastitis-Infected Goats: An Alternative Approach for Antimicrobial Therapy. *International Journal of Molecular Sciences* **2017**, *18*, 569.
654. Talank, N.; Morad, H.; Barabadi, H.; Mojab, F.; Amidi, S.; Kobarfard, F.; Mahjoub, M.A.; Jounaki, K.; Mohammadi, N.; Salehi, G.; et al. Bioengineering of green-synthesized silver

nanoparticles: In vitro physicochemical, antibacterial, biofilm inhibitory, anticoagulant, and antioxidant performance. *Talanta* **2022**, *243*, 123374.

655. Ji, H.; Zhou, S.; Fu, Y.; Wang, Y.; Mi, J.; Lu, T.; Wang, X.; Lü, C. Size-controllable preparation and antibacterial mechanism of thermo-responsive copolymer-stabilized silver nanoparticles with high antimicrobial activity. *Materials Science and Engineering: C* **2020**, *110*, 110735.
656. Ferreyra Maillard, A.P.V.; Gonçalves, S.; Santos, N.C.; López de Mishima, B.A.; Dalmasso, P.R.; Hollmann, A. Studies on interaction of green silver nanoparticles with whole bacteria by surface characterization techniques. *Biochimica et Biophysica Acta (BBA) - Biomembranes* **2019**, *1861*, 1086-1092.
657. Sondi, I.; Salopek-Sondi, B. Silver nanoparticles as antimicrobial agent: a case study on E. coli as a model for Gram-negative bacteria. *Journal of Colloid and Interface Science* **2004**, *275*, 177-182.
658. Morones-Ramirez, J.; Elechiguerra, J.; Camacho, A.; Holt, K.; Kouri, J.; Tapia, J.; Yacaman, M. The Bactericidal Effect of Silver Nanoparticles. *Nanotechnology* **2005**, *16*, 2346-2353.
659. Arif, R.; Uddin, R. A review on recent developments in the biosynthesis of silver nanoparticles and its biomedical applications. *MEDICAL DEVICES & SENSORS* **2021**, *4*, e10158.
660. GhavamiNejad, A.; Rajan Unnithan, A.; Ramachandra Kurup Sasikala, A.; Samarikhalaj, M.; Thomas, R.G.; Jeong, Y.Y.; Nasseri, S.; Murugesan, P.; Wu, D.; Hee Park, C.; et al. Mussel-Inspired Electrospun Nanofibers Functionalized with Size-Controlled Silver Nanoparticles for Wound Dressing Application. *ACS Applied Materials & Interfaces* **2015**, *7*, 12176-12183.
661. Xu, L.; Zhao, K.; Miao, J.; Yang, Z.; Li, Z.; Zhao, L.; Su, H.; Lin, L.; Hu, Y. High-strength and anti-bacterial BSA/carboxymethyl chitosan/silver nanoparticles/calcium alginate composite hydrogel membrane for efficient dye/salt separation. *International Journal of Biological Macromolecules* **2022**, *220*, 267-279.
662. Sabarees, G.; Velmurugan, V.; Tamilarasi, G.P.; Alagarsamy, V.; Raja Solomon, V. Recent Advances in Silver Nanoparticles Containing Nanofibers for Chronic Wound Management. *Polymers* **2022**, *14*, 3994.
663. Giordano, D. Bioactive Molecules from Extreme Environments. *Marine Drugs* **2020**, *18*, 640.
664. Wang, X.; van Beekveld, R.A.M.; Xu, Y.; Parmar, A.; Das, S.; Singh, I.; Breukink, E. Analyzing mechanisms of action of antimicrobial peptides on bacterial membranes requires multiple complimentary assays and different bacterial strains. *Biochimica et Biophysica Acta (BBA) - Biomembranes* **2023**, *1865*, 184160.
665. Wang, X.; Yue, T.; Lee, T.-c. Development of Pleurocidin-poly(vinyl alcohol) electrospun antimicrobial nanofibers to retain antimicrobial activity in food system application. *Food Control* **2015**, *54*, 150-157.
666. Ramos, C.; Lorenz, K.; Putrinš, M.; Hind, C.K.; Meos, A.; Laidmäe, I.; Tenson, T.; Sutton, J.M.; Mason, A.J.; Kogermann, K. Fibrous matrices facilitate pleurocidin killing of wound associated bacterial pathogens. *European Journal of Pharmaceutical Sciences* **2024**, *192*, 106648.
667. Asensio-Calavia, P.; González-Acosta, S.; Otazo-Pérez, A.; López, M.R.; Morales-delaNuez, A.; Pérez de la Lastra, J.M. Teleost Piscidins—In Silico Perspective of Natural Peptide Antibiotics from Marine Sources. *Antibiotics* **2023**, *12*, 855.
668. Falsafi, S.R.; Topuz, F.; Esfandiari, Z.; Can Karaca, A.; Jafari, S.M.; Rostamabadi, H. Recent trends in the application of protein electrospun fibers for loading food bioactive compounds. *Food Chemistry: X* **2023**, *20*, 100922.
669. Syed, M.H.; Khan, M.M.R.; Zahari, M.A.K.M.; Beg, M.D.H.; Abdullah, N. Current issues and potential solutions for the electrospinning of major polysaccharides and proteins: A review. *International Journal of Biological Macromolecules* **2023**, *253*, 126735.
670. Lorente, M.Á.; González-Gaitano, G.; González-Benito, J. Preparation, Properties and Water Dissolution Behavior of Polyethylene Oxide Mats Prepared by Solution Blow Spinning. *Polymers* **2022**, *14*, 1299.
671. Kutzli, I.; Gibis, M.; Baier, S.K.; Weiss, J. Electrospinning of whey and soy protein mixed with maltodextrin – Influence of protein type and ratio on the production and morphology of fibers. *Food Hydrocolloids* **2019**, *93*, 206-214.
672. Shou, T.; Hu, S.; Wu, Y.; Tang, X.; Fu, G.; Zhao, X.; Zhang, L. Biobased and Recyclable Polyurethane for Room-Temperature Damping and Three-Dimensional Printing. *ACS Omega* **2021**, *6*, 30003-30011.
673. Tomás-Menor, L.; Barrajón-Catalán, E.; Segura-Carretero, A.; Martí, N.; Saura, D.; Menéndez, J.A.; Joven, J.; Micol, V. The Promiscuous and Synergic Molecular Interaction of Polyphenols in Bactericidal Activity: An Opportunity to Improve the Performance of Antibiotics? *Phytotherapy Research* **2015**, *29*, 466-473.

674. CDC. Methicillin-resistant *Staphylococcus aureus* (MRSA) Basics. Available online: https://www.cdc.gov/mrsa/about/index.html (accessed on 14th November 2024).
675. Cano-Lamadrid, M.; Martínez-Zamora, L.; Castillejo, N.; Artés-Hernández, F. From Pomegranate Byproducts Waste to Worth: A Review of Extraction Techniques and Potential Applications for Their Revalorization. *Foods* **2022**, *11*, 2596.
676. EU. *A European One Health Action Plan against Antimicrobial Resistance (AMR)*; European Commission: 2017.
677. UN. *Shared Responsibility, Global Solidarity: Responding to the Socio-Economic Impacts of COVID-19.*; 2020.
678. Antimicrobial Nanocoatings Market Outlook (2022 to 2032). Available online: https://www.futuremarketinsights.com/reports/anti-microbial-nanocoatings-market (accessed on 14th November 2024).
679. Gacem, M.A.; Abd-Elsalam, K.A. Chapter 27 - Strategies for scaling up of green-synthesized nanomaterials: Challenges and future trends. In *Green Synthesis of Silver Nanomaterials*, Abd-Elsalam, K.A., Ed.; Elsevier: 2022; pp. 669-698.
680. EUON. Regulation. Available online: https://euon.echa.europa.eu/regulation (accessed on 14th November 2024).